博士論文

Construction of metal ion clusters by discrete columnar stacks of polynuclear metal complexes

(多核金属錯体の有限自己集積による金属イオン三次元配列の構築)

大須賀　孝史

Contents

Chapter 1

General Introduction

Accumulation of metal ions in close proximity can induce metal-metal interactions and corresponding various properties that cannot be achieved with a single metal ion. In particular, metal ion clusters, namely discrete three-dimensional arrays of metal ions, have attracted increasing interest for understanding those properties depending on the species, number, and array of component metal ions. Meanwhile, precise regulation of metal ion arrays is not easy, especially in solution (see below). In this thesis, the author is going to propose a novel method for constructing three-dimensional arrays of metal ions with discrete stacks of multinuclear planar complexes within confined cavities. For this purpose, the author will deal with the precise control of the number of stacking component complexes and the stacking modes in the following chapters.

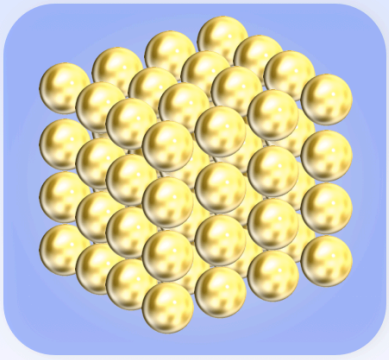

Three-Dimensional Arrays of Metal Ions

In the general introduction, the author surveys conventional methods to construct metal ion clusters from a viewpoint of coordination chemistry. Broadly speaking, there are two approaches: (1) arrangement of metal ions with multidentate organic ligands and (2) stacking of planar metal complexes. In the first approach, most of the researchers focused on the way to arrange coordination sites of rigid ligands, which made it difficult to design sterically crowded metal ion clusters, especially three-dimensional arrays. On the other hand, the infinite chains of metal ions are commonly seen in the stacks of planar metal units with square planar coordination geometries. Consequently in the second approach, researchers have been interested in the method to control the stacking number of metal units and their arrangements. In the latter part, the author focuses on discrete stacks of planar metal units by non-covalent interactions, which play important role in molecular assembly in solution.

1.1 Multidentate Ligands

Mashima and coworkers reported linear, heterometallic chains by using a tridentate ligand 6-diphenylphosphino-2-pyridonate (pyphos), in which three different coordination sites, P, N, and O are linearly laid out with a rigid framework.[1] The treatment of dinuclear Mo–Mo complex $Mo_2(pyphos)_4$ with group 10 metal sources, then following reduction resulted in the formation of M–Mo–Mo–M heterometallic chains $Mo_2M_2X_2(pyphos)_4$ (M = Pd, Pt, X = Cl, Br, I) (Figure 1).[2,3] Similar chains with group 9 metal ions M–Mo–Mo–M (M = Rh, Ir) are also synthesized in several years later.[4,5]

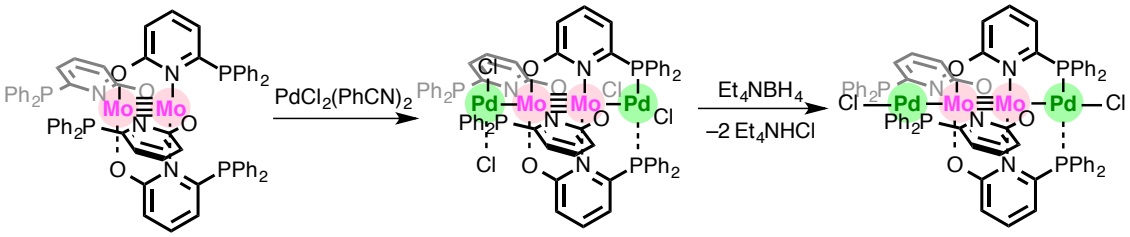

Figure 1. Preparation of a linear Pd–Mo–Mo–Pd metal chain supported with tridentate linear ligands.

In the former example, the number of metal ions in the chain was limited to four. In order to largely extend metal chains, linear multidentate ligands whose binding sites can be repeatedly multiplied were introduced. Peng's and Cotton's group constructed a pentanuclear Ni_5 chain by a simple mixing of oligo-α-pyridylamine and $NiCl_2$ under basic conditions.[6] The deprotonated ligand was fixed to a syn–syn–syn-··· conformation and aligned five Ni(II) ions on a line with the distance of ~2.2 Å. The solubility of the complex gradually decreases with extension of the Ni chains, however up to Ni_9 species was characterized by X-ray crystallography (Figure 2).[7–10] While there exist no bonds between Ni(II) ions in the chain, the magnetic measurements for each Ni chain revealed an antiferromagnetic interaction between two terminal high-spin Ni(II) ions, and the coupling constant was proportional to r^{-3} (r: distance).

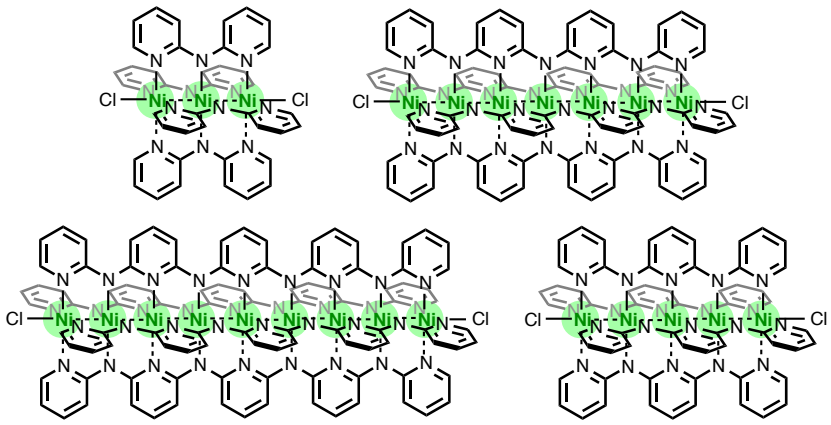

Figure 2. Linear tri-, penta, hepta-, nona- nuclear Ni(II) chains with the assistance of origo-α-pyridylamide ligands.

This system was applicable to the preparation of a similar Co and Cr chains.[10–15] The metal-metal bond orders determined by extended Hückel MO calculations for chains of Ni, Co, and Cr cores, were 0, 0.5, and 1.5, respectively. The bond order, namely coupling of the d-orbital electrons between adjacent metal ions, highly correlated with their electron conductivity of chains $[M_nL_4(NCS)_2]$ (M = Ni(II), Co(II), Cr(II); n = 3 or 5), as evidenced by single-molecular conductivity measurements using STM techniques.[16–18]

On the other hand, Murahashi and coworkers found that π-type coordination ligands are also applicable for the formation of metal ion chains.[19–24] When they combined $Pd(0)_2(dba)_3$ (dba = dibenzylideneacetone) and $[Pd(II)_2(CH_3CN)_6][BF_4]_2$ in the existence of π-conjugated polyens, one-dimensional Pd ion cluster sandwiched by two equivalents of polyens was selectively obtained. The number of Pd ions was controlled by changing the ratio of two Pd sources (i.e. by redox condensation). A variety of polycyclic aromatic hydrocarbons with one-dimensional sp^2 carbon frameworks as well as π-conjugated polyens, formed polypalladium chains (Figure 3).

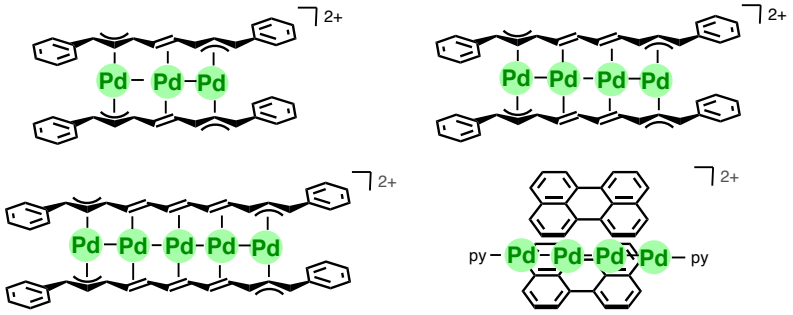

Figure 3. One-dimensional chains of Pd ions sandwiched with conjugated polyens.

They expanded this sandwich system for the construction of two-dimensional metal ion sheets. Triangular, rhomboidal, and pentagonal Pd or Pt sheets with tropylium cation, cyclooctatetraene, and tetracene are selectively obtained and fully characterized by X-ray crystallography (Figure 4).[25–31] Molecular orbital analysis of the ligand revealed that the orbital distribution of the frontier orbitals correlate significantly with the arrangement of metal ions.

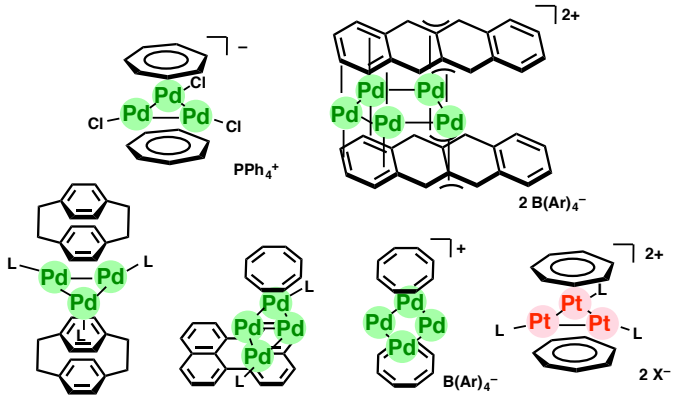

Figure 4. Two-dimensional sheets of Pd and Pt ions sandwiched with polycyclic aromatic hydrocarbons.

1.2 Infinite Stacks of Planar Complexes

One-dimensional chains of metal ions with metal-metal interaction are commonly seen in infinite stacks of square planar complexes. In 1828, Magnus found a green salt, $[Pt(NH_3)_4][PtCl_4]$.[32] This complex results from the mixing of solutions of K_2PtCl_4 and $Pt(NH_3)_4Cl_2$ and X-ray crystallographic analysis revealed that planar cations $[Pt(NH_3)_4]^{2+}$ and anions $[PtCl_4]^{2-}$ stacked in an alternating sequence and formed an infinite linear Pt(II) chain in a vertical direction.[33] Although the short contacts between the adjacent Pt(II) ions (3.25 Å) indicate the existence of weak Pt(II)–Pt(II) interactions in the chains, the electrostatic interaction is considered to be the main driving force for the spontaneous formation of the alternating stack.[34]

The attractive interaction between metal centers was strengthened by partial oxidation of a similar Pt(II) chain. For example, a Pt chain with a composition of $K_2[Pt(CN)_4]Cl_{0.32}$, has a bonding nature as partial oxidation generated the hole in the fully occupied $5d_z^2$ band structure (Figure 5a).[35] In fact, the distance between Pt(II) ions shortened to 2.88 Å, and the conductivity in the vertical direction was ~10^4 times larger than that in the horizontal direction.[36]

While in the case of planar $Pt_3(CO)_6$ complex, partial reduction forms discrete Pt chains $[Pt_3(CO)_6]_n^{2-}$ (n = 1, 2, 3, 4, 5, 6, 10~).[37,38] The dimer, trimer, and pentamers were revealed by X-ray crystallographic analysis (Figure 5b) These Pt chains have bonding character in the vertical direction, which is derived from partially occupied $6p_z$ orbitals.

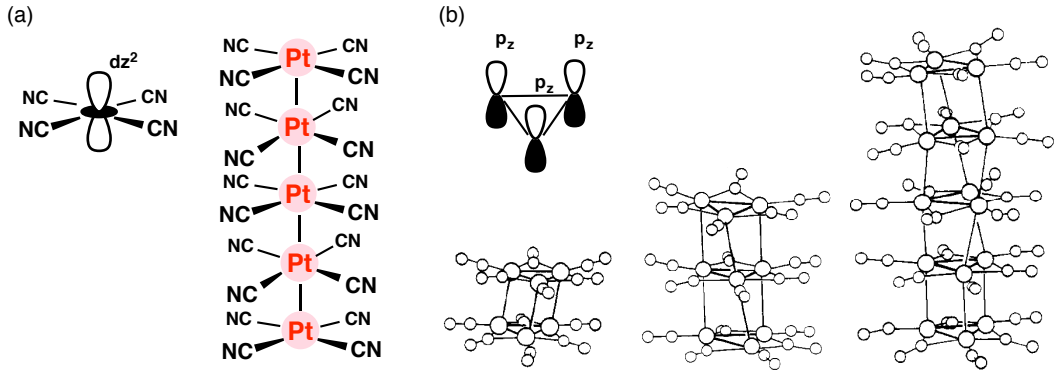

Figure 5. (a) Partially oxidized Pt(II) chain $K_2[Pt(CN)_4]Cl_{0.32}$, and (b) X-ray crystal structure of partially reduced Pt_3 chains $[Pt_3(\mu\text{-}CO)_3(CO)_3]_n^{2-}$ (n = 2, 3, 5). Adapted with permission from *J. Am. Chem. Soc.* **1976**, *98*, 7225–7231. Copyright (1976) American Chemical Society.

1.3 Discrete Stacks of Planar Complexes

1.3.1 Covalent Bonds

The control of the stacking number of Pt planes by oxidation state remains problems in accuracy and repeatability.[39–42] Che's and coworkers tethered tridentate cyclometalated Pt (II) complexes by using oligophosphine, and then obtained the dimer and trimer of cofacially stacking Pt(II) complexes (Figure 6). The stable cofacial stacking structures with Pt(II)–Pt(II) and π-π interactions were confirmed both in solution and in the solid state. The absorption and emission assigned as ^{3}MMLCT sequentially shifted long wavelengths from mono-, di-, to trinuclear Pt(II) species.

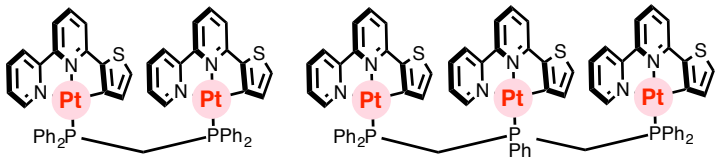

Figure 6. Di- and Trinuclear Pt(II) stacks tethered by oligophosphine auxiliaries.

Shionoya and coworkers used DNA as a hierarchical template for metal ion assembly (Figure 7a, b). Replacement of DNA natural bases by metal-mediated base pairing such as H–Cu(II)–H (H = hydroxypyridone-bearing nucleoside), produced one-dimensional metal ion chains with one to five Cu(II) ions.[43] By choosing appropriate combinations of ligand bearing nucleosides and metal ions, metal ion chains with a variety of metal species, number, and special arrangements were reported.[44–49]

Similarly, a peptide duplex worked as a template for a stepwise synthesis of metalloporphyrin stacked arrays. Tanaka and coworkers sequentially developed Pd(II) monomer, Pd(II)–Ni(II) dimer, and Pd(II)–Ni(II)–Cu(II) trimers via repetitive construction of peptide duplexes (Figure 7c).[50]

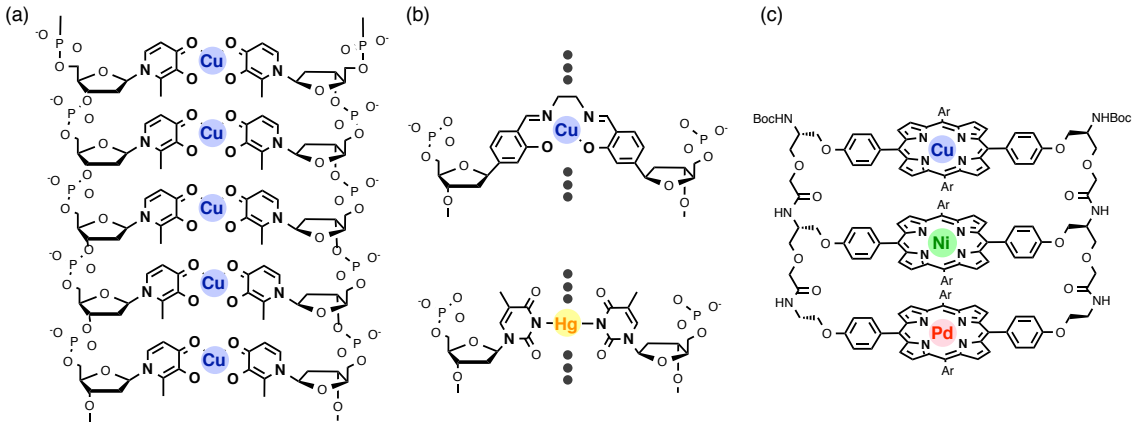

Figure 7. (a) Cu(II) mediated duplex formation between two artificial DNA strands. (b) Heterogeneous metal assembly with Cu(II) and Hg(II) mediated base paring. (c) Cofacially stacked porphyrin Cu(II)–Ni(II)–Pd(II) trimer formed via repetitive construction of a peptide duplex.

1.3.2 Electrostatic Interaction

Synthesis of a covalently linked stacking complex is often lengthy and tedious. There are several simple methods to prepare stable stacking moieties supported with non-covalent intermolecular interactions. Purrello and coworkers focused on electrostatic interactions.[51–54] One to five molecules of tetracationic porphyrins are stacked with the assistance of four equivalents of anionic calixarenes in an aqueous solution (Figure 8). The stoichiometry was tuned by charge modulation of calixarenes. For example, 3:4 complex (porphiline to calixarene) at pH 2.2 and 5:4 complex at pH 6.0, were characterized.

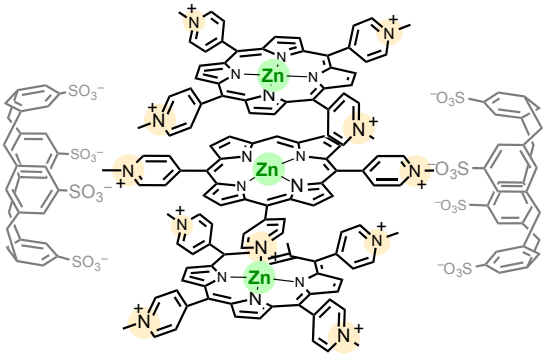

Figure 8. Discrete stacks of cationic Zn(II) complexes stabilized by anionic calixarenes. The stacking number of Zn(II) complexes are controlled with charge modulation of calixarenes.

1.3.3 Hydrogen Bond

Stoddard's group prepared a dimer of Cu porphyrin connected with rotaxane moieties.[55] Two units of the tetrafurcated tetrakisammonium cations with porphyrin core was bound with four crown ethers, [34]crown-10 (Figure 9a). The assembled complex is stabilized via hydrogen bonds between ammonium centers of the porphyrin hub and the oxygen atoms of polyether linkages. ESR spectrum revealed the spin-spin interactions between the two Cu(II) centers. Related mechanically interlocked metal complexes were synthesized by Tanaka's group. In this example, the distances between two metal units is switchable, which enabled a controllable spin-spin communication system (Figure 9b).[56–58]

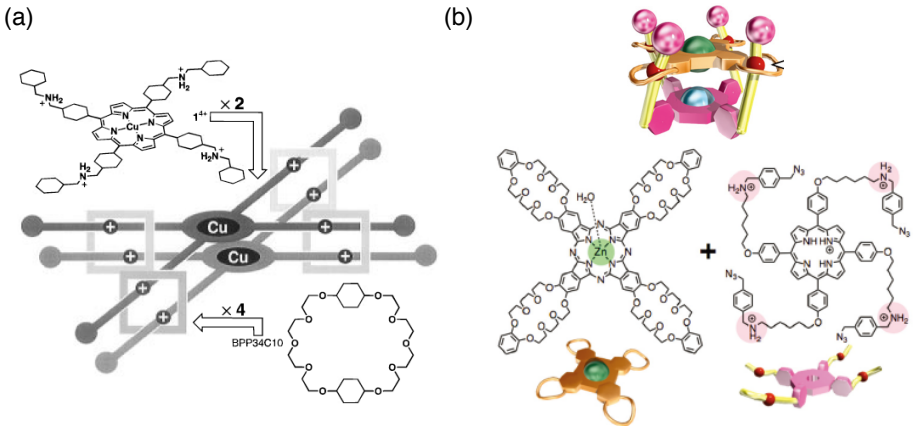

Figure 9. (a) Dimer formation of a Cu(II) porphyrin via quasi-rotaxane formation. (b) A double stacked array of Cu(II) porphyrin and Cu(II) phthalocyanine formed by a four-fold rotaxane and an ionic complex. Adapted with permission from *J. Am. Chem. Soc.* **1997**, *119*, 8119–8120. Copyright (1997) American Chemical Society. Adapted with permission from *Dalton Trans.* **2013**, *42*, 15873–15876. Copyright (2013) Royal Society of Chemistry.

1.3.4 Host-Guest System

Bosnich's group synthesized molecular receptors consisting of two parallel disposed terpy-M-Cl units (M = Pd, Pt) (Figure 10a). The receptor bound planar compounds, such as aromatic molecules, square planar Pt(II) and Au(III) complexes and formed host–guest adducts.[59–63] The binding of Pt(II) complexes produced more stable aggregates than that of Au(III) complexes because Pt(II)–Pt(II) interactions

between the host and the guest took part in the driving force of the aggregation.

Beer and coworkers assembled mixed metal [2]catenanes with dithiocarbamate (dtc) macrocycles (Figure10b).[64,65] Simple mixing of Cu(II)–Cu(II) and Au(III)–Au(III) macrocycles spontaneously formed a heteropolymetallic Cu(II)–Au(III)–Cu(II)–Au(III) chain. The authors mentioned that the lability of coordination bonds to Cu(II) centers and charge transfer effects between Cu(dtc) and Au(dtc) planes are responsible for the catenane formation.

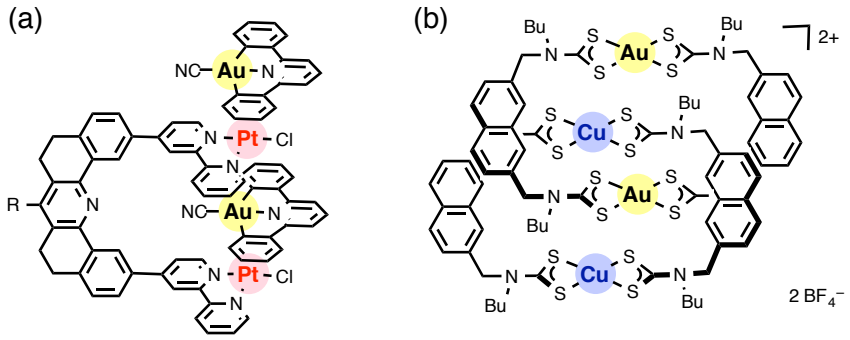

Figure 10. (a) Formation of Au–Pt–Au–Pt chain with a molecular receptor composed of two Pt panels. (b) Au–Cu–Au–Cu chain assembled as a [2]catenane.

1.4 Organic-Pillared Coordination Cage

Host molecules with a large box-shaped cavity are suitable candidates for cofacial stacks of planar molecules. Fujita's group reported an organic-pillared coordination cage composed of two equivalents of panel ligands, three pillar ligands, and six *cis*-protected Pd or Pt hinges (Figure 11).[66–68] A flat, hydrophobic cavity of the cage can accommodate planar aromatic molecules. The cage quantitatively self-assemble when these components are mixed in a 2:3:6 ratio in water with excess amount of guest aromatics as cage templates. Because hydrophobic effect is one of the main driving forces for the guest accommodation, a variety of aromatic compounds, such as triphenylene, pyrene-dione work as templates without any functionalization.[69–77] Furthermore, the number of stacking guest molecules within the cavity (n) is precisely determined by changing the height of the pillar ligands (n = 1–5).[69,75]

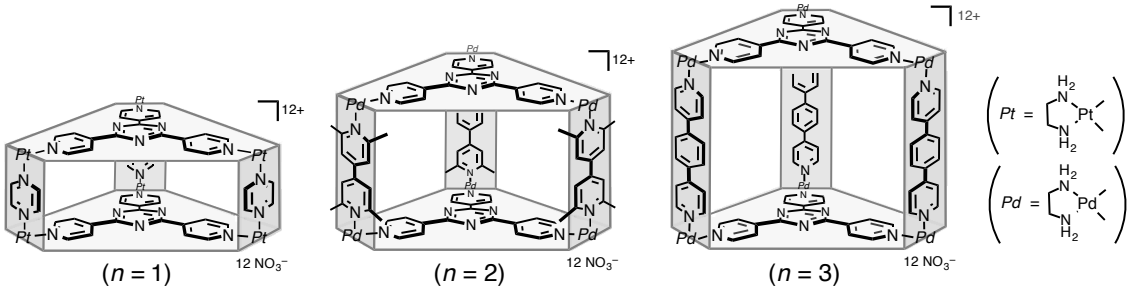

Figure 11. Organic-pillared coordination cage. These cages encapsulate and stack planar compounds within their box-shaped hydrophobic cavities. The number of stacking guests within the cages is precisely controlled by the height of the pillar ligands.

Encapsulation, and then stack formation of planar conventional complexes within the cages, is a simple and precise method to manage a number of metal ions through the molecular space. The simplest example is the formation of dinuclear M(II)–M(II) complexes (M = Pt, Pd, Cu).[78] The organic-pillared coordination cage accommodated two molecules of square planar complexes $M(acac)_2$ (acac = acetylacetonate), which have never shown to form intermolecular short M–M interactions (Figure 12). X-ray crystallographic analysis and an absorption spectrum of the $Pt(II)_2$ and $Pd(II)_2$ dimer evidenced Pt(II)–Pt(II) and Pd(II)–Pd(II) d^8–d^8 interactions, respectively. For the $Cu(II)_2$ dimer, the authors observed spin-spin interaction between two Cu(II) centers with d^9 electron configurations.

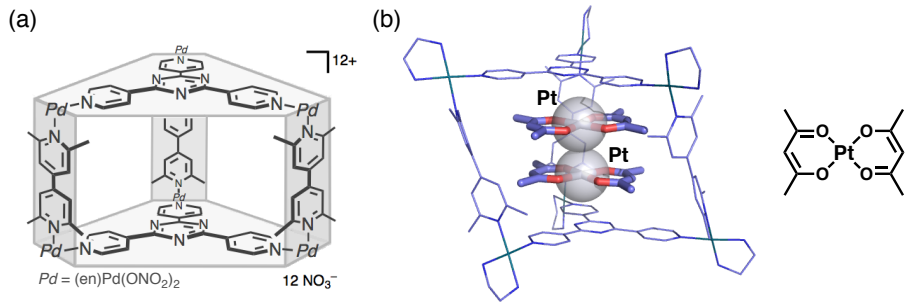

Figure 12. (a) An organic-pillared coordination cage and (b) encapsulateon of two Pt complexes within the cage. The Pt(II)–Pt(II) distance was 3.32 Å, indicating the existence of Pt(II)–Pt(II) interaction.

Because Pd coordinated triazine ligands on the top and bottom of the cage are electron-deficient (acceptor, A) aromatics, an electron-rich (donor, D) complex is an electrostatically suitable guest molecule. When two molecules of Cu(Por) (Por =

porphyrin) was encapsulated within the cage, the total stacking mode was A–D–D–A, while in the case of taller cage, two Cu complexes sandwiched a single free ligand and selectively formed an A–D–A–D–A stacking mode (Figure 13).[79] As expected, intermolecular spin-spin exchange interaction was only observed in the former case.

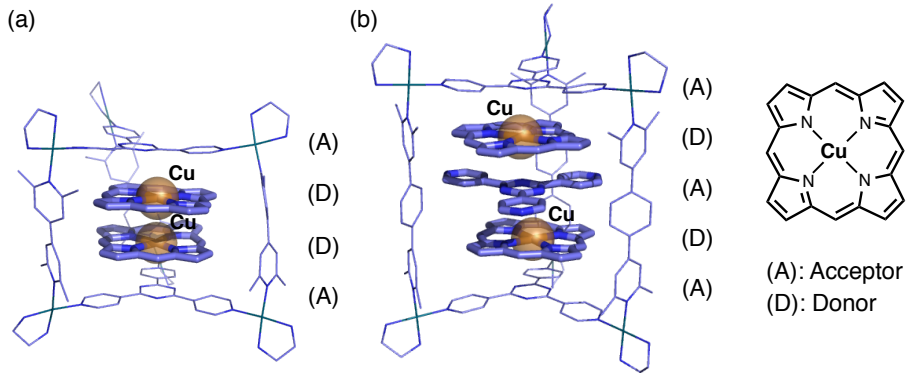

Figure 13. Accumulation of two Cu-porphyrins with organic-pillared coordination cages. (a) A–D–D–A and (b) A–D–A–D–A stacking modes.

With this result in mind, a trinuclear Cu(II)–Cu(II)–Cu(II) complex was constructed with relatively electron deficient guest complexes (Figure 14).[80] In this case, Cu(TAP) (TAP = tetraazaporphyrin) was applied for the guests in place of Cu(Por). Moreover, the combination of two types of guests (i.e. electron rich and deficient guest) was able to form hetero Cu(II)–Pd(II)–Cu(II) and Cu(II)–Co(II)–Cu(II) chains.

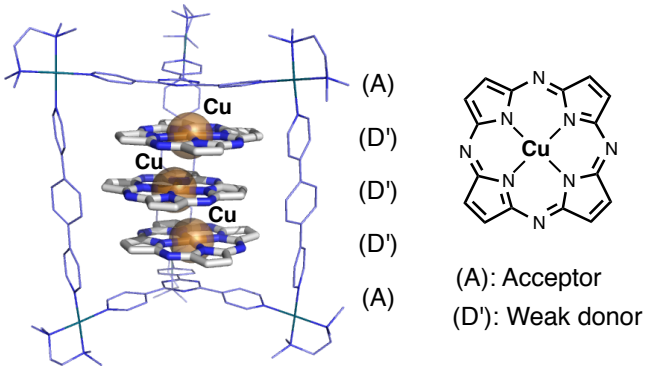

Figure 14. Accumulation and cofacial stacks of three Cu(TAP) planes within organic-pillared coordination cages.

1.5 Survey of This Thesis

In the present thesis, the author focus on the precise synthesis of metal ion clusters (i.e., three-dimensional arrays of metal ions) using a variety of self-assembly systems. The body of this thesis consists of four chapters (Figure 15). In the first three chapters, the author deals with the three different concepts concerned with the formation of metal ion clusters. Three methods of assembly of component metal complexes or ions will be discussed. The last chapter describes the electronic property of the metal ion clusters depending on the number of component metal ions.

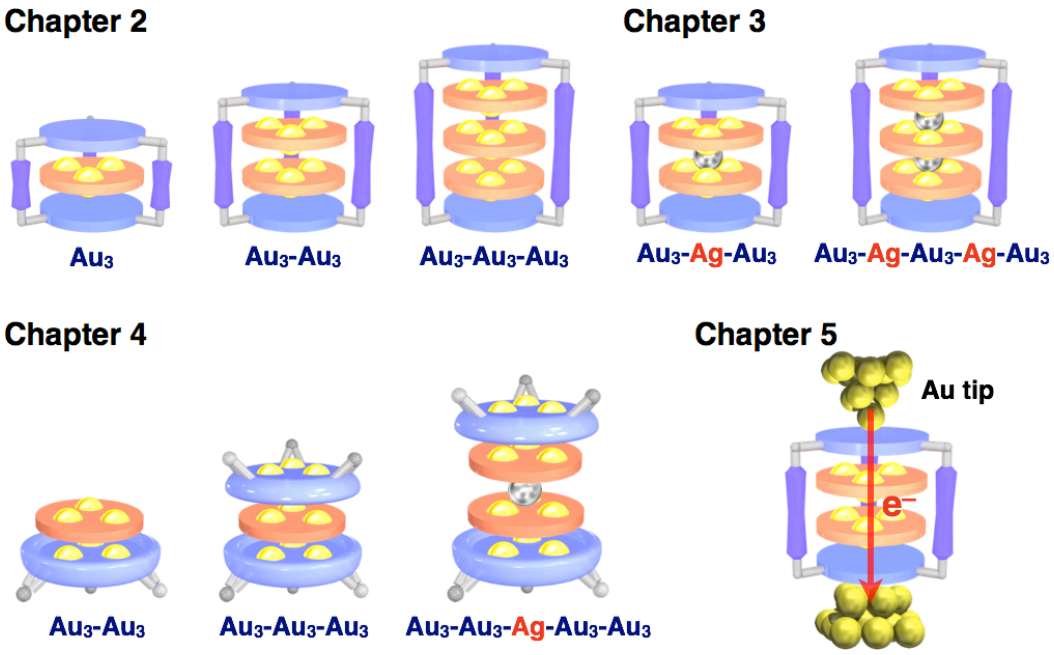

Figure 15. Survey of this thesis. Metal ion clusters prepared in this study are shown. The blue moieties represent host molecules used in this study, while planar orange subjects correspond to guest trinuclear $Au(I)_3$ complexes. Throughout this thesis, the chemical properties of well-known $Au(I)_3$ complexes[81,82] played an important role. The yellow and silver spheres indicate the accumulated Au(I) and Ag(I) ions, respectively.

In chapter 2, the author demonstrates the synthesis of metal ion clusters by staking of planar multinuclear complexes within a box-shaped cage in a [$m \times n$] fashion (Figure 16). The number of assembled metal ions ($m \times n$) is determined beforehand from employed multinuclear complexes (m) and the encapsulation number (n = 1–3) adjusted by the cage height. Because each binding site is located in the confined cavity without covalent linkage, this method circumvents steric complexity of the ligand

designs for conventional metal ion clusters. For planar guest molecules, the author selected trinuclear Au(I) complexes (m = 3). Moreover, the crystallographic analysis revealed that the cage shape defined the final cluster structures and intermolecular Au(I)–Au(I) interactions effectively worked within the cage.

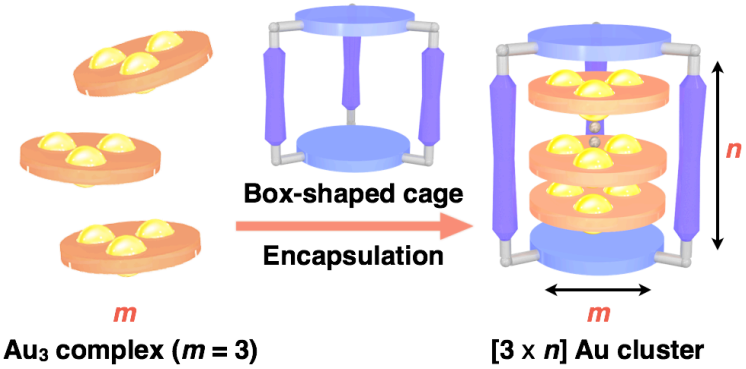

Figure 16. Schematic representation of [m × n] metal ion clusters with box-shaped coordination cages. In this study, the author used trinuclear Au(I)$_3$ complexes (m = 3) for stacking guests and encapsulation number (n = 1–3) was determined up front by the height of the cage.

Chapter 3 concerns the arrangement of metal ions through metal-metal attractive interaction and extension of the Au(I) ion cluster. In this chapter, Au(I)–Ag(I) hetero clusters were prepared using the Au(I) homo ion clusters as template molecules. Within the coordination cages, trinuclear Au(I)$_3$ complexes and Ag(I) ions piled up alternately to form Au$_3$–Ag–Au$_3$ and Au$_3$–Ag–Au$_3$–Ag–Au$_3$ clusters. In each cluster, Ag(I) ion was located at the center of six Au(I) ions through Au(I)–Ag(I) metallophilic interactions.

In chapter 4, the author notes the formation of Au(I) homo and Au(I)–Ag(I) hetero clusters without the help of conventional box-shaped cavities. A tray-shaped trinuclear Au(I)$_3$ complex acts as a molecular scaffold that systematically assembles the guest Au(I)$_3$ complexes and forms various types of clusters in a modular fashion (Figure 17). Guest Au(I)$_3$ complexes were accommodated in the tray's concave cavity and the stack number (n) of Au(I)$_3$ planes was tuned (n = 2–4) by changing the solvent conditions and addition of the Ag(I) ions. The Ag(I) ion acts as a glue connecting two Au(I)$_6$ clusters as a consequence of Au(I)–Ag(I) interactions.

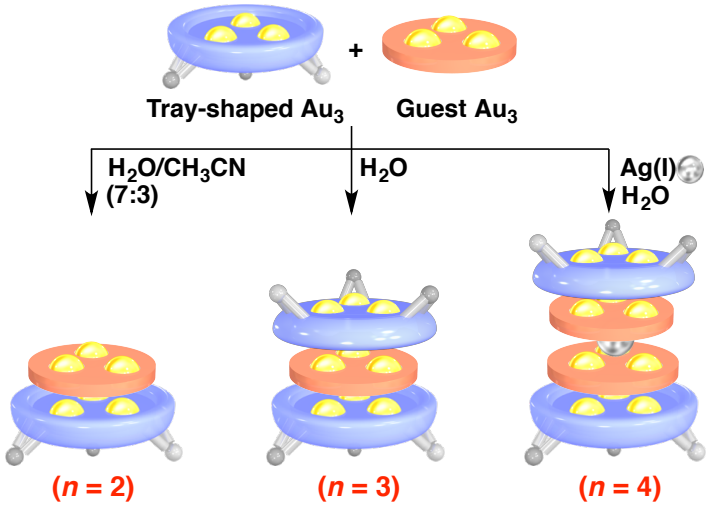

Figure 17. Formation of double-triple, and quadruple Au_3 stacks constructed from tray-shaped Au_3 molecule and the Au_3 guest.

Chapter 5 focuses on the electron transport ability of Au(I) ion clusters. The single-molecule conductance of [3 × *n*] Au(I) ion clusters (*n* = 1–3) is measured by an STM break junction technique. The large conductance values and a small attenuation factor represent a long-range electron ability of Au(I) ion clusters. The result also indicates that the self-assembled coordination cage is a suitable box-shaped platform for the measurement of single-molecular conductance inside it.

1.6 References

[1] K. Mashima, *Bull. Chem. Soc. Jpn.* **2010**, *83*, 299–312.

[2] K. Mashima, H. Nakano, A. Nakamura, *J. Am. Chem. Soc.* **1993**, *115*, 11632–11633.

[3] K. Mashima, H. Nakano, A. Nakamura, *J. Am. Chem. Soc*. **1996**, *118*, 9083–9095.

[4] T. Ruffer, M. Ohashi, A. Shima, H. Mizumoto, Y. Kaneda, K. Mashima, *J. Am. Chem. Soc*. **2004**, *126*, 12244–12245.

[5] M. Ohashi, A. Shima, T. Rüffer, H. Mizumoto, Y. Kaneda, K. Mashima, *Inorg. Chem.* **2007**, *46*, 6702–6714.

[6] S.-J. Shieh, C.-C. Chou, G.-H. Lee, C.-C. Wang, S.-M. Peng, *Angew. Chem. Int. Ed. Engl.* **1997**, *36*, 56–59.

[7] S.-Y. Lai, T.-W. Lin, Y.-H. Chen, C.-C. Wang, G.-H. Lee, M.-h. Yang, M.-k. Leung, S.-M. Peng, *J. Am. Chem. Soc.* **1999**, *121*, 250–251.

[8] S.-M. Peng, C.-C. Wang, Y.-L. Jang, Y.-H. Chen, F.-Y. Li, C.-Y. Mou, M.-K. Leung, *J. Magn. Magn. Mater.* **2000**, *209*, 80–83.

[9] J. F. Berry, F. A. Cotton, L. M. Daniels, C. A. Murillo, *J. Am. Chem. Soc*. **2002**, *124*, 3212–3213.

[10] R. H. Ismayilov, W.-Z. Wang, G.-H. Lee, C.-H. Chien, C.-H. Jiang, C.-L. Chiu, C.-Y. Yeh, S.-M. Peng, *Eur. J. Inorg. Chem*. **2009**, 2110–2120.

[11] E.-C. Yang, M.-C. Cheng, M.-S. Tsai, S.-M. Peng, *J. Chem. Soc. Chem. Commun.* **1994**, 2377–2378.

[12] Y.-H. Chen, C.-C. Lee, C.-C. Wang, G.-H. Lee, S.-Y. Lai, F.-Y. Li, C.-Y. Mou, S.-M. Peng, *Chem. Commun.* **1999**, 1667–1668.

[13] F. A. Cotton, C. A. Murillo, X. Wang, *J. Chem. Soc. Dalton Trans.* **1999**, 3327–3328.

[14] L. F. Berry, F. A. Cotton, C. S. Fewox, T. Lu, C. A. Murillo, X. Wang, *Dalton Trans*. **2004**, 2297–2302.

[15] W.-Z. Wang, R. H. Ismayilov, G.-H. Lee, I. P.-C. Liu, C.-Y. Yeh, S.-M. Peng, *Dalton Trans*. **2007**, 830–839.

[16] S.-Y. Lin, I-W. P. Chen, C.-h. Chen, M.-H. Hsieh, C.-Y. Yeh, T.-W. Lin, Y.-H. Chen, S.-M. Peng, *J. Phys. Chem. B* **2004**, *108*, 959–964.

[17] I-W. P. Chen, M.-D. Fu, W.-H. Tseng, J.-Y. Yu, S.-H. Wu, C.-J. Ku, C.-h. Chen, S.-M. Peng, *Angew. Chem. Int. Ed.* **2006**, *45*, 5814–5818.

[18] T.-W. Tsai, Q.-R. Huang, S.-M. Peng, B.-Y. Jin, *J. Phys. Chem. C* **2010**, *114*, 3641–3644.

[19] T. Murahashi, E. Mochizuki, Y. Kai, H. Kurosawa, *J. Am. Chem. Soc.* **1999**, *121*, 10660–10661.

[20] T. Murahashi, Y. Higuchi, T. Katoh, H. Kurosawa, *J. Am. Chem. Soc.* **2002**, *124*, 14288–14289.

[21] T. Murahashi, T. Uemura, H. Kurosawa, *J. Am. Chem. Soc*. **2003**, *125*, 8436–8437.

[22] Y. Tatsumi, T. Naga, H. Nakashima, T. Murahashi, H. Kurosawa, *Chem. Commun*, **2004**, 1430–1431.

[23] Y. Tatsumi, K. Shirato, T. Murahashi, S. Ogoshi, H. Kurosawa, *Angew. Chem.*

Int. Ed. **2006**, *45*, 5799–5803.

[24] T. Murahashi, K. Shirato, A. Fukushima, K. Takase, T. Suenobu, S. Fukuzumi, S. Ogoshi, H. Kurosawa, *Nature Chem*. **2012**, *4*, 52–58.

[25] T. Murahashi, M. Fujimoto, M. Oka, Y. Hashimoto, T. Uemura, Y. Tatsumi, Y. Nakao, A. Ikeda, S. Sakaki, H. Kurosawa, *Science*, **2006**, *313*, 1104–1107.

[26] T. Murahashi, M. Fujimoto, Y. Kawabata, R. Inoue, S. Ogoshi, H. Kurosawa, *Angew. Chem. Int. Ed*. **2007**, *46*, 5440–5443.

[27] T. Murahashi, N. Kato, T. Uemura, H. Kurosawa, *Angew. Chem. Int. Ed*. **2007**, *46*, 3509–3512.

[28] T. Murahashi, Y. Hashimoto, K. Chiyoda, M. Fujimoto, T. Uemura, R. Inoue, S. Ogoshi, H. Kurosawa, *J. Am. Chem. Soc*. **2008**, *130*, 8586–8587.

[29] T. Murahashi, R. Inoue, K. Usui, S. Ogoshi, *J. Am. Chem. Soc.* **2009**, *131*, 9888–9889.

[30] T. Murahashi, K. Usui, R. Inoue, S. Ogoshi, H. Kurosawa, *Chem. Sci*. **2011**, *2*, 117–122.

[31] T. Murahashi, S. Kimura, K. Takase, T. Uemura, S. Ogoshi, K. Yamamoto, *Chem. Commun.* **2014**, *50*, 820–822.

[32] G. Magnus, *Ann. Phys.* **1828**, *90*, 239–242.

[33] M. Atoji, J. W. Richardson, R. E. Rundle, *J. Am. Chem. Soc.* **1957**, *79*, 3017–3020.

[34] J. R. Miller, *J. Chem. Soc.* **1961**, 4452–4457.

[35] M.-H. Whangbo, R. Hoffmann, *J. Am. Chem. Soc.* **1978**, *100*, 6093–6098.

[36] K. Krogmann, *Angew. Chem. Int. Ed. Engl.* **1969**, *8*, 35–42.

[37] G. Longoni, P. Chini, *J. Am. Chem. Soc.* **1976**, *98*, 7225–7231.

[38] D. J. Underwood, R. Hoffmann, K. Tatsumi, A. Nakamura, Y. Yamamoto, *J. Am. Chem. Soc.* **1985**, *107*, 5968–5980.

[39] S.-W. Lai, M. C.-W. Chan, T.-C. Cheung, S.-M. Peng, C.-M. Che, *Inorg. Chem.* **1999**, *38*, 4046–4055.

[40] S.-W. Lai, T.-C. Cheung, M. C. W. Chan, K.-K. Cheung, S.-M. Peng, C.-M. Che, *Inorg. Chem.* **2000**, *39*, 255–262.

[41] W. Lu, N. Zhu, C.-M. Che, *Chem. Commun.* **2002**, 900–901.

[42] W. Lu, C. W. Chan, N. Zhu, C.-M. Che, C. Li, Z. Hui, *J. Am. Chem. Soc.* **2004**, *126*, 7639–7651.

[43] K. Tanaka, A. Tengeiji, T. Kato, N. Toyama, M. Shionoya, *Science*, **2003**, *299*, 1212–1213.

[44] K. Tnaka, G. H. Clever, Y. Takezawa, Y. Yamada, C. Kaul, M. Shionoya, T. Carell, *Nature Nanotech*, **2006**, *1*, 190–194.

[45] K. Tanaka, M. Shionoya, *Chem. Lett.* **2006**, *35*, 694–699.

[46] G. Clever, C. Kaul, T. Carell, *Angew. Chem. Int. Ed.* **2007**, *46*, 6226–6236.

[47] Y. Takezawa, W. Maeda, K. Tanaka, M. Shionoya, *Angew. Chem. Int. Ed*. **2009**, *48*, 1081–1084.

[48] G. H. Clever, M. Shionoya, *Coord. Chem. Rev.* **2010**, *254*, 2391–2402.

[49] Y. Takezawa, M. Shionoya, *Acc. Chem. Res*. **2012**, *45*, 2066–2076.

[50] Y. Yamada, T. Kubota, M. Nishio, K. Tanaka, *J. Am. Chem. Soc.* **2014**, *136*, 6505–6509.

[51] L. D. Costanzo, S. Geremia, L. Randaccio, R. Purrello, R. Lauceri, D. Sciotto, F. G. Gulino, V. Pavone, *Angew. Chem. Int. Ed.* **2001**, *40*, 4245–4247.

[52] G. Moschetto, R. Lauceri, F. G. Gulino, D. Sciotto, R. Purrello, *J. Am. Chem. Soc.* **2002**, *124*, 14536–14537.

[53] R. D. Zorzi, N. Guidolin, L. Randaccio, R. Purrello, S. Geremia, *J. Am. Chem. Soc.* **2009**, *131*, 2487–2489.

[54] F. G. Gulino, R. Lauceri, L. Frish, T. Evan-Salem, Y. Cohen, R. D. Zorzi, S. Geremia, L. D. Costanzo, L. Randaccio, D. Sciotto, R. Purrello, *Chem. Eur. J.* **2006**, *12*, 2722–2729.

[55] M. C. Feiters, M. C. T. Fyfe, M.-V. Martínez-Díaz, S. Menzer, R. J. M. Nolte, J. F. Stoddard, P. J. M. v. Kan, D. J. Williams, *J. Am. Chem. Soc.* **1997**, *119*, 8119–8120.

[56] Y. Yamada, M. Okamoto, K. Furukawa, T. Kato, K. Tanaka, *Angew. Chem. Int. Ed.* **2012**, *51*, 709–713.

[57] Y. Yamada, N. Mihara, S. Shibano, K. Sugimoto, K. Tanaka, *J. Am. Chem. Soc.* **2013**, *135*, 11505–11508.

[58] Y. Yamada, N. Mihara, K. Tanaka, *Dalton Trans.* **2013**, *42*, 15873–15876.

[59] R. D. Sommer, A. L. Rheingold, A. J. Goshe, B. Bosnich, *J. Am. Chem. Soc.* **2001**, *123*, 3940–3952.

[60] A. J. Goshe, I. M. Steele, C. Ceccarelli, A. L. Rheingold, B. Bosnich, *Proc. Natl. Acad. Sci. U. S. A.* **2002**, *99*, 4823–4829.

[61] A. J. Goshe, I. M. Steele, B. Bosnich, *J. Am. Chem. Soc.* **2003**, *125*, 444–451.

[62] J. D. Crowley, A. J. Goshe, B. Bosnich, *Chem. Commun*. **2003**, 392–393.

[63] J. D. Crowley, I. M. Steele, B. Bosnich, *Inorg. Chem.* **2005**, *44*, 2989–2991.

[64] W. W. H. Wong, J. Cookson, E. A. L. Evans, E. J. L. Mclnnes, J. Wolowska, J. P. Maher, P. Bishop, P. D. Beer, *Chem. Commun.* **2005**, 2214–2216.

[65] M. E. Padilla-Tosta, O. D. Fox, M. G. B. Drew, P. D. Beer, *Angew. Chem. Int. Ed.* **2001**, *40*, 4235–4239.

[66] K. Kumazawa, K. Biradha, T. Kusukawa, T. Okano, M. Fujita, *Angew. Chem. Int. Ed.* **2003**, *42*, 3909–3913.

[67] M. Yoshizawa, J. Nakagawa, K Kumizawa, M. Nagao, M. Kawano, T. Ozeki, M. Fujita, *Angew. Chem. Int. Ed.* **2005**, *44*, 1810–1813.

[68] M. Yoshizawa, M. Nagao, K. Kumazawa, M. Fujita, *J. Organomet. Chem.* **2005**, *690*, 5383–5388.

[69] J. K. Klosterman, Y. Yamauchi, M. Fujita, *Chem. Soc. Rev.* **2009**, *38*, 1714–1725.

[70] T. Sawada, M. Yoshizawa, S. Sato, M. Fujita, *Nature Chem.* **2009**, *1*, 53–56.

[71] Y. Yamauchi, M. Yoshizawa, M. Akita, M. Fujita, *Proc. Natl. Acad. Sci. U. S. A.* **2009**, *106*, 10435–10437.

[72] K. Ono, M. Yoshizawa, M. Akita, T. Kato, Y. Tsunobuchi, S.-i. Ohkoshi, M. Fujita, *J. Am. Chem. Soc.* **2009**, *131*, 2782–2783.

[73] K. Ono, J. K. Klosterman, M. Yoshizawa, K. Sekiguchi, T. Tahara, M. Fujita, *J. Am. Chem. Soc.* **2009**, *131*, 12526–12527.

[74] T. Sawada, M. Fujita, *J. Am. Chem. Soc.* **2010**, *132*, 7194–7201.

[75] Y. Yamauchi, M. Yoshizawa, M. Akita, M. Fujita, *J. Am. Chem. Soc.* **2010**, *132*, 960–966.

[76] T. Murase, K. Otsuka, M. Fujita, *J. Am. Chem. Soc.* **2010**, *132*, 7864–7865.

[77] Y. Yamauchi, M. Fujita, *Chem. Commun.* **2010**, *46*, 5897–5899.

[78] M. Yoshizawa, K. Ono, K. Kumazawa, T. Kato, M. Fujita, *J. Am. Chem. Soc.* **2005**, *127*, 10800–10801.

[79] K. Ono, M. Yoshizawa, T. Kato, K. Watanabe, M. Fujita, *Angew. Chem. Int. Ed.* **2007**, *46*, 1803–1806.

[80] K. Ono, M. Yoshizawa, T. Kato, M. Fujita, *Chem. Commun.* **2008**, 2328–2330.

[81] A. Burini, A. A. Mohamed, J. P. Fackler, Jr., *Comments Inorg. Chem.* **2003**, *24*, 253–280.

[82] H. E. Abdou, A. A. Mohamed, J. P. Fackler, Jr. in *Gold Chemistry: Applications and Future Directions in the Life Sciences* (Ed.: F. Mohr), Wiley-VCH, Weinheim, 2008, pp. 1–45.

Chapter 2

[3 × *n*] Gold Ion Clusters Templated by Coordination Cages

Abstract

Three-dimensional [3 × *n*] (*n* = 1–3) arrays of Au(I) clusters were precisely prepared as discrete stacks of planar cyclic trinuclear $Au(I)_3$ complexes within box-shaped coordination cages. The stack number (*n*) of the $Au(I)_3$ planes was precisely determined in advance by the height of the cage. X-ray crystallographic analysis of the [3 × 3] Au(I) cluster revealed a trigonal prismatic array of nine Au(I) atoms, whose conformation was restricted by the cage symmetry. Moreover, the short intermolecular Au···Au distances indicated the existence of attractive Au(I)–Au(I) interactions among them.

2.1 Introduction

Cyclic trinuclear complexes are potential components of metal ion clusters at the nanometer scale, since triangular arrangements of metal ions are commonly seen in part of the cluster textures.[1] For the formation of planar, cyclic trimer, the linear coordination geometry of Au(I) ions is suitable with a variety of exobidentate bridging ligands, such as pyrazolates and carbeniates.[2] In order to utilize these trinuclear $Au(I)_3$ complexes to the constituent of Au(I) clusters, I focused on the molecular motifs of the $Au(I)_3$ complexes in the crystalline states. Carbeniate $Au(I)_3$ complex, $[\mu\text{-}C(OEt)=N(C_6H_4Me)Au]_3$[3] stacks in a slipped dimeric form, and the six Au(I) ions are arranged in a chair conformation (Figure 1a). Two short intermolecular Au···Au contacts less than 3.6 Å, namely the sum of the can der Waals radii,[4] are found between the dimer. Pyridinate $Au(I)_3$ complex, $[\mu\text{-}N^1,C^2\text{-pyAu}]_3$[5] has an extended infinite stack, with a similar alignment, which is called a stair-step stacking mode (Figure 1b). Besides, pyrazolate $Au(I)_3$ complex, $[\mu\text{-}N,N\text{-pzAu}]_3$,[6] assembles into complicated network through one or two Au(I)–Au(I) contacts in close proximity for each $Au(I)_3$ complex (Figure 1c).

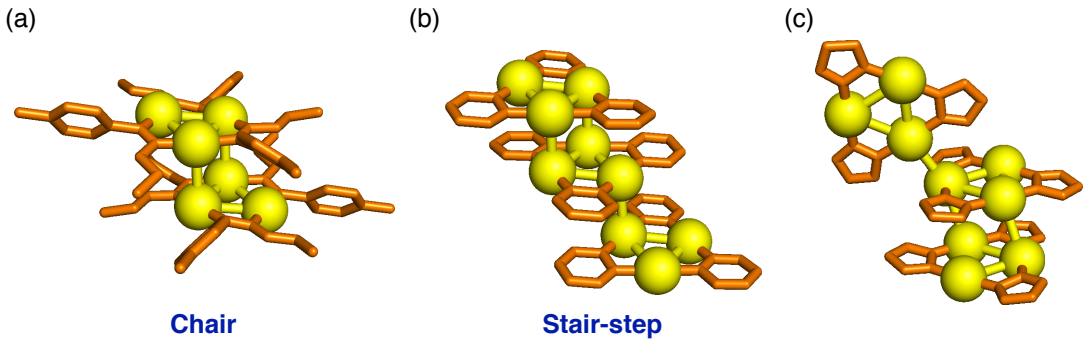

Figure 1. Crystalline motifs of trinuclear $Au(I)_3$ complexes. (a) A chair alignment of a dimer of carbeniate-bridged $Au(I)_3$ complex $[\mu\text{-}C(OEt)=N(C_6H_4Me)Au]_3$ (Au: yellow, Bridging ligands: orange). All hydrogens are omitted for clarity. The short contacts between Au atoms less than 3.6 Å are shown in the yellow lines. (b) A stair-step alignment of pyridine-bridged $Au(I)_3$ complex $[\mu\text{-}N^1,C^2\text{-pyAu}]_3$. (c) Pyrazolate-bridged $Au(I)_3$ complex $[\mu\text{-}N,N\text{-pzAu}]_3$ shows an erratic alignment.

As I have seen, the short Au···Au contacts contribute to the arrangement of Au(I) complexes in the solid state. It has been established that the short Au···Au separations

less than the sum of the van der Waals radii, are generated by weak aurophilic attractive interactions[7-11] between Au(I) ions. Theoretical studies concluded that the attraction results from a combination of correlation and relativistic effects among metal ions with d^{10} electron configurations,[12] and the strength reaches a maximum for Au(I) ions. This interaction is directional with bond energies of ca. 7–11 kcal/mol, that is similar to the hydrogen bonds. This is the reason not all of Au(I) ions in the above mentioned $Au(I)_3$ complexes take part in the short intermolecular Au···Au contacts and this relatively weak attraction usually competes with other intermolecular interactions such as ionic bonds, hydrogen bondings, and CH···π interactions.

There are a few $Au(I)_3$ complexes forming the eclipsed stacking modes. Balch and co-workers found the infinite trigonal stacks of Au(I) ions in the crystal structure of $Au(I)_3$ complex [μ-C(OMe)=N(Me)Au]$_3$ (Figure 2).[13] The intermolecular Au···Au separations are equally 3.346 Å, while the intramolecular Au···Au separations are 3.308 Å, which lie within the range of attractive Au(I)–Au(I) contacts. The aggregation with Au(I)–Au(I) interactions are thought to play a key role in producing physical properties such as luminescence and conductivity. The solid of the $Au(I)_3$ complex shows remarkable solvent-stimulated luminescence, which is triggered by a contact of a liquid with the solid that formerly have been irradiated with UV light. Indeed, introduction of bulkier bridging ligands in the carbeniate $Au(I)_3$ trimer leads to a disruption of the columnar crystal structure.[14,15]

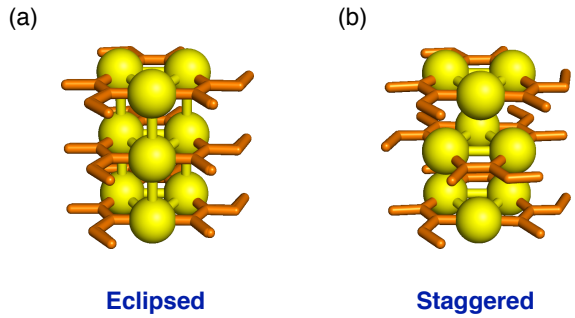

Figure 2. Crystalline motifs of trinuclear $Au(I)_3$ complexes. (a) Carbeniate-bridged $Au(I)_3$ complex [μ-C(OMe)=N(Me)Au]$_3$ crystalizes in the eclipsed motief. All hydrogens are omitted and the color codes are the same as those of Figure 1. (b) In addition to the eclipsed stacks, the staggered stack was also found in the same crystal. There are two eclipsed stacks for every staggered stack.

In order to achieve such unique properties, there are several approaches to form columnar stacks of planar $Au(I)_3$ complexes.[16,17] Serrano and Kim groups individually engineered mesophases of $Au(I)_3$ complexes substituted with long alkyl chains.[18,19] The alignment of the Au(I) ions was dynamic, so that the intermolecular Au(I)–Au(I) interactions did not effectively work. On the other hand, Aida and co-workers developed phosphorescent organogels using $Au(I)_3$ complexes substituted with alkyl chains.[20] These materials have columnar infinite stacks of $Au(I)_3$ planes and show emission derived from Au(I)–Au(I) interactions. Another example used mesoporous silica as a nanoscopic template in order to achieve the columnar stacks of $Au(I)_3$ complexes.[21]

In this work, Au(I) clusters are constructed in [3 × *n*] fashions (*n* = 1–3) as discrete stacks of trinuclear Au(I) complexes by using columnar coordination cages **1**[22] in solution (Figure 3a). As previous studies shows, a series of coordination cages **1** provides box-shaped hydrophobic cavities to encapsulate planar aromatics[23] and pile them up along the C_3 axis of the cage. Moreover, the number of stacking aromatics is determined by the height of cage **1**, namely the length of the lateral rigid pillar ligands. For stable formation of the host–guest complex, electron interactions between the cage and guest molecules are an important driving force. Triazine panel ligands at the top and the bottom of cage **1** are electron-deficient acceptor aromatics, thereby electron-rich donor aromatics (e.g., pyrene, colonene, porphine) are suitable guest molecules. In consequence, an electron-rich, imidazolate-bridged $Au(I)_3$ complex **2a**[24] is used for the first candidate of the guest multinuclear complex (Figure 3b).

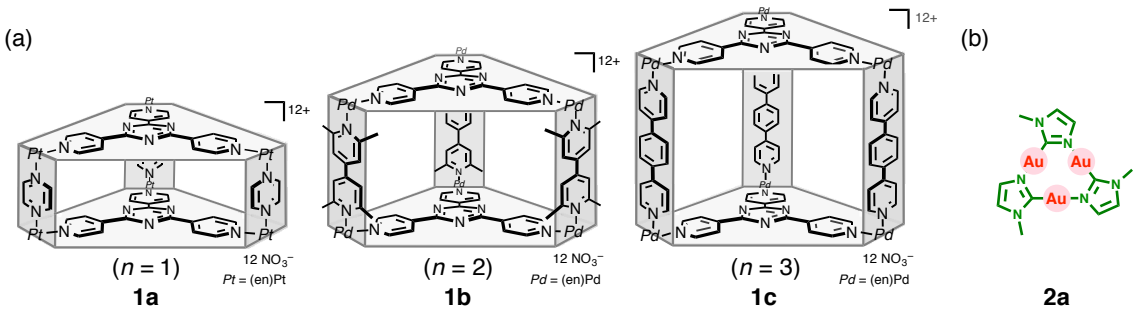

Figure 3. (a) Box-shaped coordination cages **1** and (b) imidazolate-bridged $Au(I)_3$ complex. **2a**. The number of stacking molecules in cage **1** (*n* = 1–3) is precisely controlled by the height of the cage.

2.2 [3 × 1] Au(I) Cluster 1a•2a

The smallest [3 × 1] Au(I) cluster **1a•2a** was built from self-assembled coordination cage **1a**,[22a] with pyrazines as pillar ligands, and imidazolate-bridged trinuclear $Au(I)_3$ complex **2a**.[24] $Au(I)_3$ complex **2a** (16.7 mg, 0.020 mmol) was added to an aqueous solution of cage **1a** (34.6 mg, 0.010 mmol) and the suspension was stirred at 60 ºC for 1 h (Figure 4a). After removal of the residual excess Au(I) complex **2a** by filtration, the NMR spectroscopy of the resulting orange solution revealed the quantitative encapsulation of guest **2a**, namely the formation of [3 × 1] Au(I) cluster **1a•2a**. In the ^{1}H NMR spectrum, the upfield shift of the signals of guest **2a** indicated the shielding by the aromatic panels of cage **1a** (Figure 4b). A single host–guest structure was supported by Diffusion-ordered NMR spectroscopy (DOSY), a NMR technique to separate signals according to diffusion coefficient (*D*) of molecules in

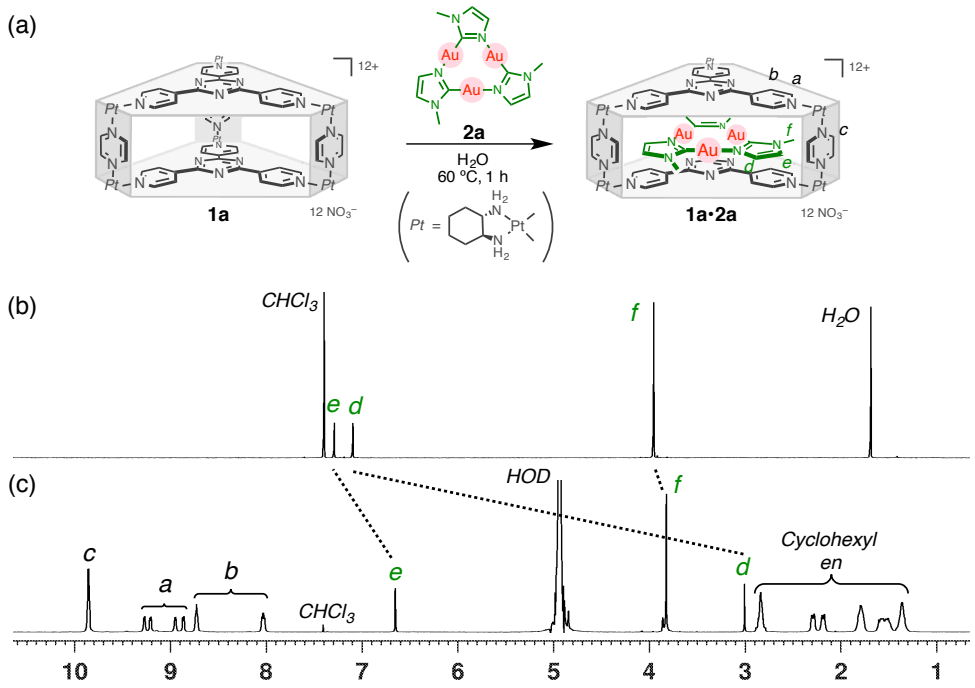

Figure 4. Synthesis of [3 × 1] Au(I) cluster 1a•2a. (a) Schematic representation of the formation of [3 × 1] Au(I) cluster **1a•2a** from empty cage **1a** with guest $Au(I)_3$ complex **2a**. (b,c) ^{1}H NMR spectra (500 MHz, 300 K) of (b) guest **2a** (in $CDCl_3$) before encapsulation and (c) obtained Au(I) cluster **1a•2a** (in D_2O). At most four sets of signals of cage protons ($H_{a,b}$) were observed that indicates the diastereotopic environment of cage **1a** derived from tight stacking of C_{3h} symmetrical guest **2a** as well as asymmetrical Pd hinges.

solution,[25–27] with a single diffusion coefficient (D = 1.5 × 10^{-10} m^2 s^{-1}). Cold-spray ionization mass spectrometry (CSI-MS) also confirmed a stable, single solution structure of 1:1 complex **1a•2a** with a molecular weight of 4298.8 Da (Figure 5).

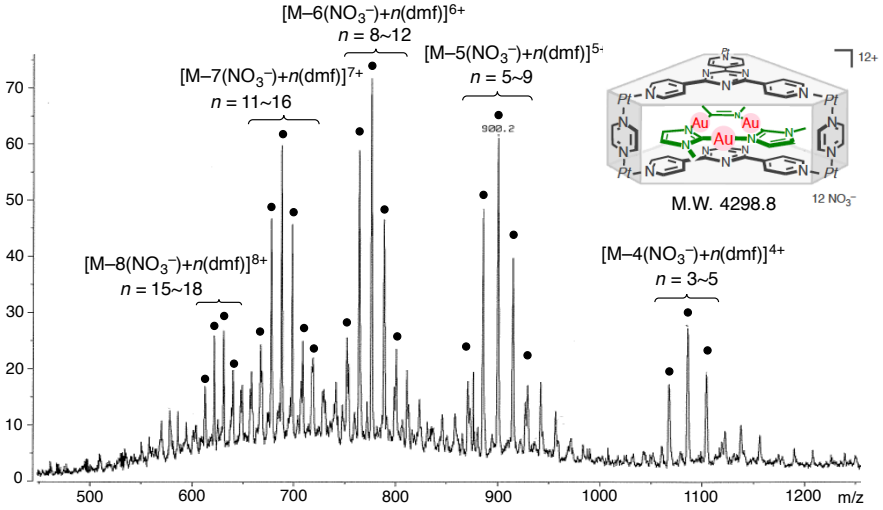

Figure 5. CSI-MS spectrum of Au(I) cluster 1a•2a (H_2O : CH_3CN : DMF = 1 :1 : 0.1). The spectra shows a series of prominent signals for [M–m(NO_3^-)+n(dmf)]$^{m+}$. Addition of DMF as an ionization-promoting matrix was quite effective for the observation of the molecular-ion peaks, see ref 28.

2.3 [3 × 2] Au(I) Cluster 1b•$(2a)_2$

Next, [3 × 2] Au(I) cluster **1b**•$(\mathbf{2a})_2$ was constructed using extended coordination cage **1b**.[22b,c] After heating an aqueous suspension of cage **1b** (10 mM, 1.0 mL, 0.010 mmol) and trinuclear $Au(I)_3$ complex **2a** (33.5 mg, 0.040 mmol) at 60 ºC for 2 h, the quantitative formation of inclusion complex **1b**•$(\mathbf{2a})_2$ was determined by NMR spectroscopy (Figure 6a). In the ^{1}H NMR spectrum, two sets of signals were observed for both cage **1b** and guest **2b** in a ~1:1 ratio. This result indicates that C_{3h} symmetrical guest **2a** can orient either clockwise (+) or counterclockwise (–), and tight stacking of two molecules of **2a** generated two diastereomers (+, +), and (+, –) (Figure 7). In the DOSY study, all the signals derived from both the cage **1b** and two guests **2a** showed the same diffusion coefficient (D = 1.5 × 10^{-10} m^2 s^{-1}) (Figure 6b).

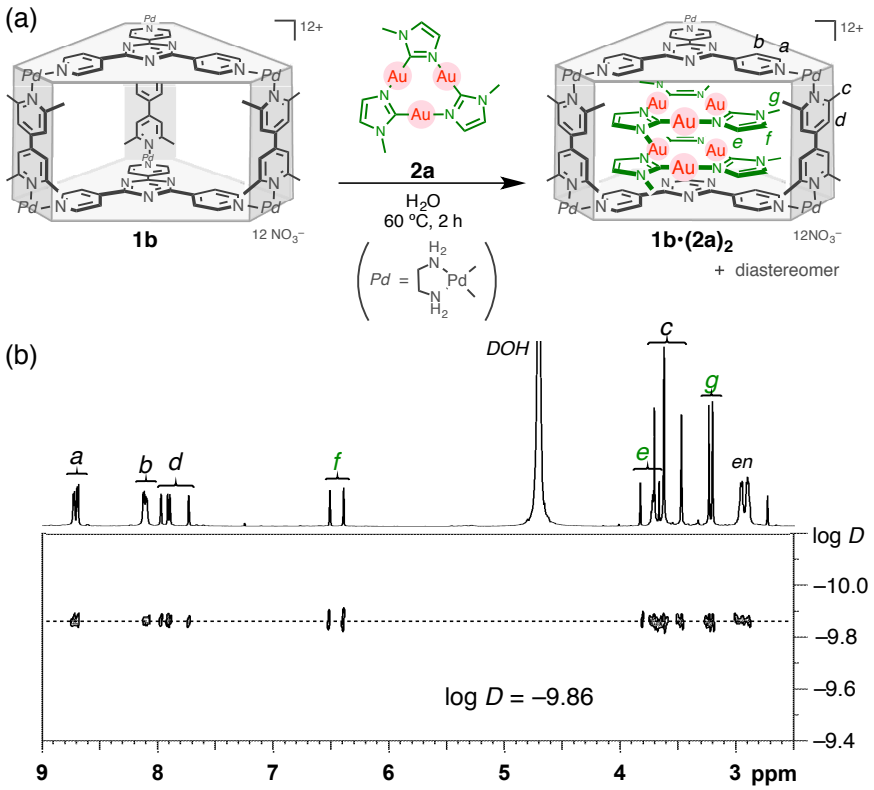

Figure 6. Synthesis of [3 × 2] Au(I) cluster 1b•(2a)$_2$. (a) Schematic representation of the formation of [3 × 2] Au(I) cluster **1b**•(**2a**)$_2$. The reaction quantitatively gave the product. (b) ^{1}H NMR (top) and DOSY (bottom) spectra of Au(I) cluster **1b**•(**2a**)$_2$ (500 MHz, 300 K, D_2O).

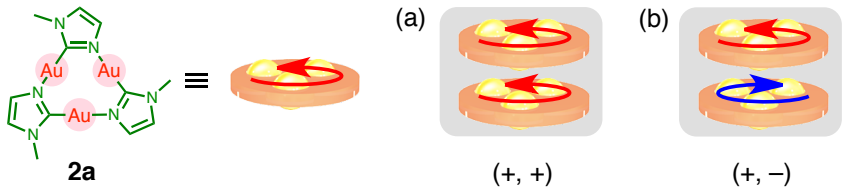

Figure 7. Two diastereomers (2a)$_2$ generated in cage 1b. Tight staking of two molecules of C_{3h} symmetrical Au(I)$_3$ complexes **2a** formed (a) the same and (b) opposite orientations as a result of relative planar chirality (meso and *dl*, rspectively).

2.4 Self-Assembled Complex 1c'•(2a•3•2a)

In my attempt to synthesize [3 × 3] Au(I) cluster i.e., inclusion complex **1c**•(**2a**)$_3$, I unexpectedly obtained the self-assembe complex **1c**•(**2a•3•2a**), in which electron-deficient panel ligand **3** was sandwiched with the pair of electron-rich Au(I) complexes **2a**, as the major product (Figure 8a). This result can be understood in the following

way. Alternate stacks of electron-rich $Au(I)_3$ complexes **2a** (donor, D) and electron-deficient triazine panel **3** (acceptor, A) of cage **1c** is favorable,[22b,23d] so that an A–D–A–D–A stack was formed during self-assembly, instead of unstable triple stacks of electron-rich guests (A–D–D–D–A). For the quantitative formation of self-assembled complex **1c'•(2a•3•2a)**, the following procedure was used: trinuclear $Au(I)_3$ complex **2a**, panel-like ligand **3**, pillar-like ligand, and $(tmeda)Pd(ONO_2)_2$ were combined in a 2:3:3:6 ratio in water and stirred at 60 ºC. Note that $(tmeda)Pd(ONO_2)_2$ was employed in cage **1c'** instead of conventional $(en)Pd(ONO_2)_2$ as metal hinges to enhance the solubility and that the conventional guest encapsulation procedure was not applied to because empty cage **1c'** is not stable enough. After heating for 12 h, I revealed the quantitative formation of inclusion complex **1c'•(2a•3•2a)** with 1D and 2D NMR studies of the yellow solution (Figure 8b).

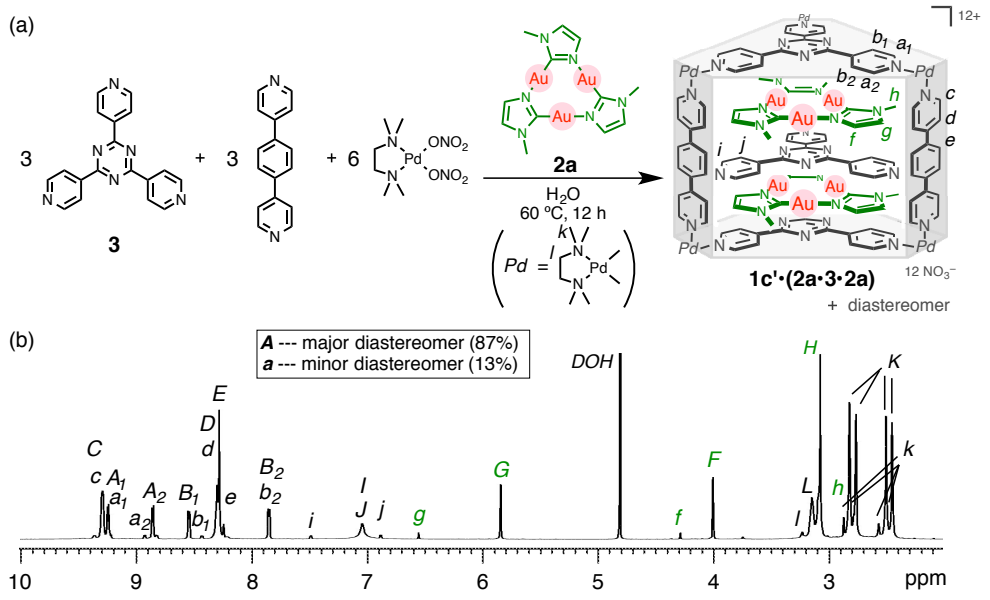

Figure 8. Synthesis of undesired complex 1c'•(2a•3•2a). (a) Schematic representation of the formation of self-assembled complex **1c'•(2a•3•2a)**. Within cage **1c'**, electron-deficient panel ligand **3** was sandwiched with two molecules of electron-rich $Au(I)_3$ complex **2a**. (b) ^1H NMR spectrum of self-assembled complex **1c'•(2a•3•2a)** (500 MHz, 300 K, D_2O). Two diastereomers were observed as in the case of [3 × 2] Au(I) cluster **1b•(2a)**$_2$ as the result of the stacking modes. The major and minor diastereomers were assigned in capital and small letters, respectively.

2.5 [3 × 3] Au(I) Cluster 1c·(2b)$_3$

To circumvent the binding of triazine panel **3** with electron-rich guests **2a**, I designed a relatively electron-deficient trinuclear Au(I)$_3$ complex. The electrostatic potential maps show that trinuclear Au(I)$_3$ complex **2b'** with pyrazolate bridging ligands is more electron deficient than Au(I)$_3$ complex **2a** with imidazoleate moieties (Figure 9).[29] In fact, when I used Au(I) complex **2b** substituted with ester groups as a guest, I obtained desired [3 × 3] Au(I) cluster **1c•(2b)**$_3$ in the same procedure (Figure 10). In the ^{1}H NMR spectrum of the pale yellow solution, the signals of three guest molecules in the cage ($H_{f,g,f',g'}$) appeared in a 2:1 ratio, as expected for the triple stacks of D_{3h} symmetrical guests **2b**.

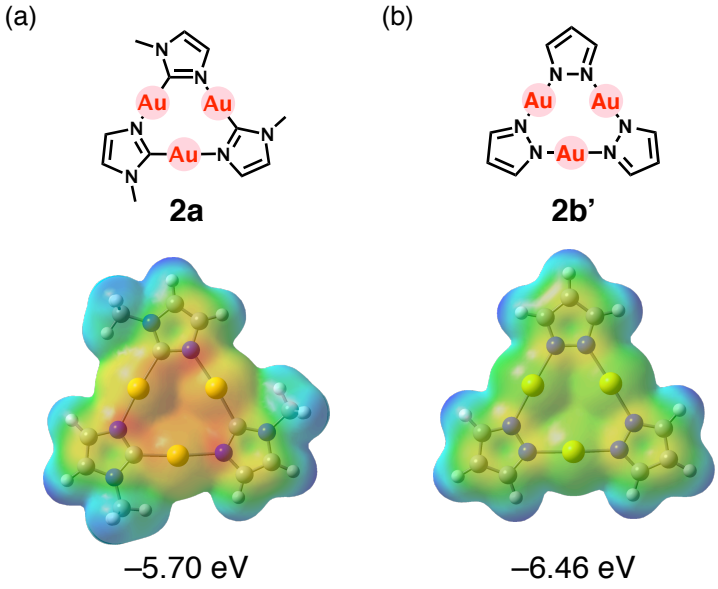

Figure 9. Relative π-basicity of Au(I)$_3$ complexes as a function of the bridging ligands. Electrostatic potential surfaces and the HOMO orbital energies of (a) imidazolate-bridged Au(I)$_3$ complex **2a** and (b) pyrazolate-bridged analogue **2b'** (electron-withdrawing substituents of compelx **2b** are omitted). The structures were optimized with the B3LYP/6-31G(d,p) level of theory,[30] which was included in the Gaussian09 code.[31] For gold atoms, the basis LANL2DZ that includes relativistic effects was used.[32] The surface maps were plotted using the GaussView program.[33] The color scale is such that basicity increases in the direction blue→green→yellow→orange.

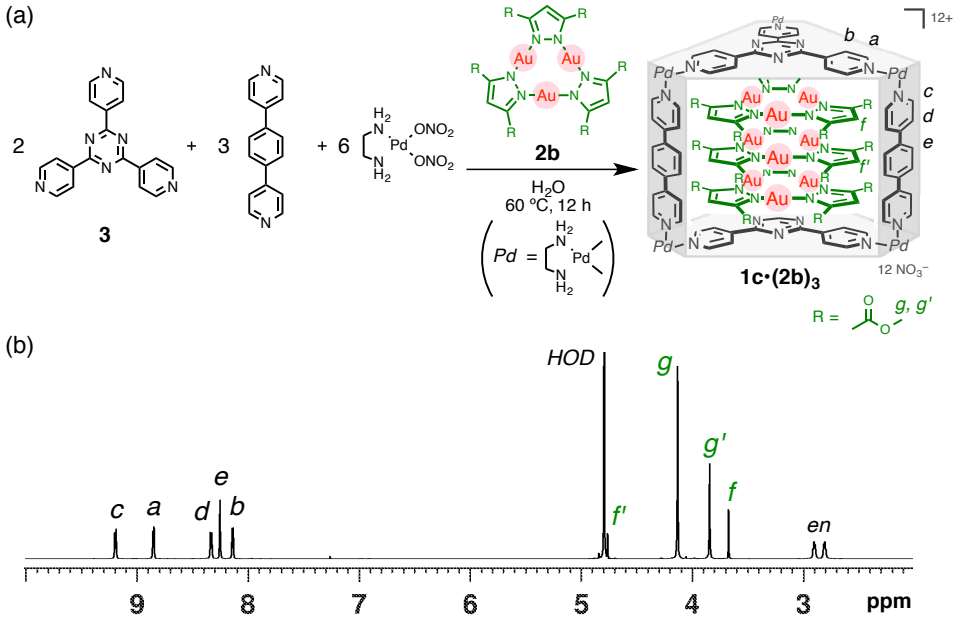

Figure 10. Synthesis of [3 × 3] Au(I) cluster 1c•(2b)$_3$. (a) Schematic representation of the formation of [3 × 3] Au(I) cluster **1c•(2b)**$_3$. A triple stack of Au(I)$_3$ complex was achieved with relatively electron-deficient Au(I)$_3$ complex **2b** bridged by pyrazole derivatives. (b) ^{1}H NMR spectrum of [3 × 3] Au(I) cluster **1c•(2b)**$_3$ (500 MHz, 300 K, D_2O).

The arrangement of the Au(I) ions within the cage was successfully determined by X-ray crystallographic analysis with analogous complex **1c'•(2b)**$_3$ (Figure 11). Cage **1c'** with (tmeda)Pd(ONO$_2$)$_2$ instead of (en)Pd(ONO$_2$)$_2$ as Pd hinges efficiently underwent crystallization when the aqueous solution was evaporated slowly for over 1 month. The result shows that three Au(I)$_3$ complexes **2b** arranged in an eclipsed rather than a staggered conformation despite the unfavorable steric hindrance between side chains. The nine gold atoms formed an extended trigonal prismatic array with the short intermolecular Au···Au distances (3.206–3.230 Å). These distances are shorter than the sum of the van der Waals radii (3.6 Å),[4] which clearly indicate the existence of Au(I)–Au(I) interactions. The columnar array of nine Au(I) ions is due not solely to the Au(I)–Au(I) interactions but also to the constrains imposed by the D_{3h} symmetry of cage **1c'**. This is because trinuclear Au(I)$_3$ complexes usually form chair or stair-step stacks in the crystalline state, with only one or two of the three Au(I) ions participating in the short Au(I)···Au(I) contacts due either to the steric demands of the bridging ligands or to the competition with other weak interactions such as CH···π, dipole-dipole interactions (Figure 1). Moreover, the two triazine panels of cage **1c'** clamp down

upon the guests, resulting in severe distortion of the pillar ligands. This result clearly shows that host–guest aromatic–aromatic stacking interactions between guest **2b** and host **1c'** are also present.

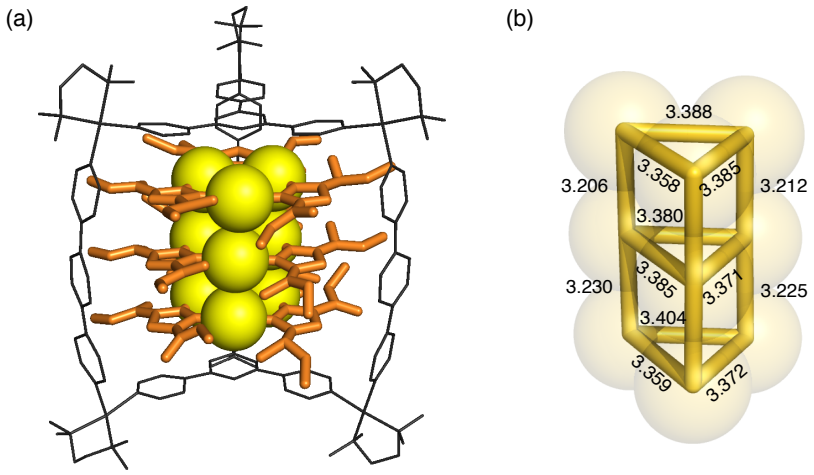

Figure 11. Trigonal prismatic array of the nine Au(I) ions within the cage. (a) X-ray crystallographic analysis of [3 × 3] Au(I) cluster **1c'**•(**2b**)$_3$. All hydrogens are omitted (the color code is the same as that of Figure 1, Box-shaped cage: black). Intermolecular Au(I)–Au(I) interactions as well as host–guest aromatic–aromatic stacking prominently distorted the pillars of the cage framework. (b) Highlight of the Au(I)$_9$ array in the cage. Intra- and intermolecular Au–Au distances are given in Å. The short contacts (< 3.6 Å) indicates the existence of Au(I)–Au(I) interactions between them. Such a trigonal prismatic array with eclipsed Au(I)$_3$ complexes was achieved with the help of steric demands of D_{3h} symmetrical coordination cage.

Polynuclear Au(I) complexes involving aurophilic attractions often display long lived phosphorescence from the Au(I)–Au(I) bonded excited states in the visible region.[2,8–12] The photophysical properties of them have been attracted interest because the emission property is highly sensitive to the environment, such as molecular arrangement, coordination geometry, and distance between Au(I) ions. Indeed, investigation of the emission property depending on the number of Au(I) ions was one of the purpose of this study, a series of [3 × n] Au(I) clusters (n = 1–3) were not emissive. This is probably because cage **1** strongly absorbs light with λ < 350 nm and host–guest charge transfer and heavy Pd atoms of the cage can efficiently quench guest emissions.[23h,34]

2.6 Conclusion

In this chapter, three-dimensional arrays of Au(I) ions were constructed in [3 × *n*] fashions (*n* = 1–3) using box-shaped coordination cages as templates for the discrete stacks of trinuclear Au(I) complexes. The number of $Au(I)_3$ stacks was able to be determined in advance by judicious choices of the rigid pillar ligands. This simple and systematic procedure is widely applicable to a variety of planar complexes, yielding a variety of homo and hetero metal ion clusters.

2.7 References

[1] a) D. M. P. Mingos, D. J. Wales, *Introduction to Cluster Chemistry*, Prentice-Hall, Englewood Cliffs, NJ, **1990**; b) F. A. Cotton, C. A. Murillo, R. A. Walton, *Multiple Bonds between Metal Atoms*, 3rd ed, Springer, New York, **2005**; c) E. J. Fernández, M. Monge in *Modern Supermolecular Gold Chemistry: Gold-Metal Interactions and Applications* (Ed.: A. Laguna), Wiley-VCH, Weinheim, **2008**, pp. 131–179.

[2] a) A. Burini, A. A. Mohamed, J. P. Fackler, Jr., *Comments Inorg. Chem.* **2003**, *24*, 253–280; b) H. E. Abdou, A. A. Mohamed, J. P. Fackler, Jr. in *Gold Chemistry: Applications and Future Directions in the Life Sciences* (Ed.: F. Mohr), Wiley-VCH, Weinheim, 2008, pp. 1–45.

[3] a) G. Minghetti, F. Bonati, *Inorg. Chem.* **1974**, *13*, 1600–1602; b) A. Tiripicchio, M. T. Camellini, G. Minghetti, *J. Organomet. Chem.* **1979**, *171*, 399–406.

[4] A. Bondi, *J. Phys. Chem.* **1964**, *68*, 441–451.

[5] a) L. G. Vaughan, *J. Am. Chem. Soc.* **1970**, *92*, 730–731; b) A. Hayashi, M. M. Olmstead, S. Attar, A. L. Balch, *J. Am. Chem. Soc.* **2002**, *124*, 5791–5795.

[6] G. Yang, R. G. Raptis, *Inorg. Chem.* **2003**, *42*, 261–263.

[7] M. Jansen, *Angew. Chem. Int. Ed. Engl.* **1987**, *26*, 1098–1110.

[8] P. Pyykkö, *Chem. Rev.* **1997**, *97*, 597–636.

[9] C.-M. Che, S.-W. Lai, *Coord. Chem. Rev.* **2005**, *249*, 1296–1309.

[10] a) H. Schmidbaur, A. Schier, *Chem. Soc. Rev.* **2008**, *37*, 1931–1951; b) H. Schmidbaur, A. Schier, *Chem. Soc. Rev.* **2012**, *41*, 370–412.

[11] M. J. Katz, K. Sakai, D. B. Leznoff, *Chem. Soc. Rev.* **2008**, *37*, 1884–1895.

[12] P. Pyykkö, *Angew. Chem. Int. Ed.* **2004**, *43*, 4412–4456.

[13] a) J. C. Vickery, M. M. Olmstead, E. Y. Fung, A. L. Balch, *Angew. Chem. Int. Ed. Engl.* **1997**, *36*, 1179–1181; b) E. Y. Fung, M. M. Olmstead, J. C. Vickery, A. L. Balch, *Coord. Chem. Rev.* **1998**, *171*, 151–159.

[14] a) R. L. White-Morris, M. M. Olmstead, S. Attar, A. L. Balch, *Inorg. Chem.* **2005**, *44*, 5021–5029; b) K. Winkler, M. Wysocka-Zolopa, K. Recko, L. Dobrzynski, J. S. Vickery, A. L. Balch, *Inorg. Chem.* **2009**, *48*, 1551–1558.

[15] R. N. McDougald, Jr., B. Chilukuri, H. Jia, M. R. Perez, H. Rabaâ, X. Wang, V. N. Nesterov, T. R. Cundari, B. E. Gnade, M. A. Omary, *Inorg. Chem.* **2014**, *53*, 7485–7499.

[16] S. Coco, P. Espinet in *Gold Chemistry: Applications and Future Directions in the Life Sciences* (Ed.: F. Mohr), Wiley-VCH, Weinheim, 2008, pp. 357–396.

[17] For recent syntheses of $M(I)_6$ clusters (M = Au, Ag, Cu) as double-stacked $M(I)_3$ complexes with bipyrazolyl ligands, see: a) T. Jozak, Y. Sun, Y. Schmitt, S. Lebedkin, M. Kappes, M. Gerhards, W. R. Thiel. *Chem. Eur. J.* **2011**, *17*, 3384–3389; b) G.-F. Gao, M. Li, S. Z. Zhan, Z. Lv, G.-h. Chen, D. Li, *Chem. Eur. J.* **2011**, *17*, 4113–4117.

[18] a) J. Barberá, A. Elduque, R. Giménez, L. A. Oro, J. L. Serrano, *Angew. Chem. Int. Ed. Engl.* **1996**, *35*, 2832–2835; b) J. Barberá, A. Elduque, R. Giménez, F. J. Lahoz, J. A. López, L. A. Oro, J. L. Serrano, *Inorg. Chem.* **1998**, *37*, 2960–2967; c) E. Beltrán, J. Barberá, J. L. Serrano, A. Elduque, R. Giménez, *Eur. J. Inorg. Chem.* **2014**, 1165–1173.

[19] S. J. Kim, S. H. Kang, K.-M. Park, H. Kim, W.-C. Zin, M.-G. Choi, K. Kim, *Chem. Mater.* **1998**, *10*, 1889–1893.

[20] M. Enomoto, A. Kishimura, T. Aida, *J. Am. Chem. Soc.* **2001**, *123*, 5608–5609.

[21] H. O. Lintang, K. Kinbara, K. Tanaka, T. Yamashita, T. Aida, *Angew. Chem. Int. Ed.* **2010**, *49*, 4241–4245.

[22] a) K. Kumazawa, K. Biradha, T. Kusukawa, T. Okano, M. Fujita, *Angew. Chem. Int. Ed.* **2003**, *42*, 3909–3913; b) M. Yoshizawa, J. Nakagawa, K. Kumazawa, M. Nagao, M. Kawano, T. Ozeki, M. Fujita, *Angew. Chem. Int. Ed.* **2005**, *44*, 1810–1813; c) M. Yoshizawa, M. Nagoa, K. Kumazawa, M. Fujita, *J. Organomet. Chem.* **2005**, *690*, 5383–5388; d) J. K. Klosterman, Y. Yamauchi, M. Fujita, *Chem. Soc. Rev.* **2009**, *38*, 1714–1725.

[23] a) M. Yoshizawa, K. Ono, K. Kumazawa, T. Kato, M. Fujita, *J. Am. Chem. Soc.*

2005, *127*, 10800–10801; b) M. Yoshizawa, K. Kumazawa, M. Fujita, *J. Am. Chem. Soc.* **2005**, *127*, 13456–13457; c) V. Maurizot, M. Yoshizawa, M. Kawano, M. Fujita, *Dalton Trans.*, **2006**, 2750–2756; d) K. Ono, M. Yoshizawa, T. Kato, K. Watanabe, M. Fujita, *Angew. Chem. Int. Ed.* **2007**, *46*, 1803–1806; e) K. Ono, M. Yoshizawa, T. Kato, M. Fujita, *Chem. Commun.* **2008**, 2328–2330; f) T. Sawada, M. Yoshizawa, S. Sato, M. Fujita, *Nature Chem.* **2009**, *1*, 53–56; g) K. Ono, M. Yoshizawa, M. Akita, T. Kato, Y. Tsunobuchi, S.-i. Ohkshi, M. Fujita, *J. Am. Chem. Soc.* **2009**, *131*, 2782–2783; h) K. Ono, J. K. Klosterman, M. Yoshizawa, K. Sekiguchi, T. Tahara, M. Fujita, *J. Am. Chem. Soc.* **2009**, *131*, 12526–12527; i) Y. Yamauchi, M. Yoshizawa, M. Akita, M. Fujita, *Proc. Natl. Acad. Sci. U. S. A.* **2009**, *106*, 10435–10437; j) T. Sawada, M. Fujita, *J. Am. Chem. Soc.* **2010**, *132*, 7194–7201; k) Y. Yamauchi, M. Yoshizawa, M. Akita, M. Fujita, *J. Am. Chem. Soc.* **2010**, *132*, 960–966; l) T. Murase, K. Otsuka, M. Fujita, *J. Am. Chem. Soc.* **2010**, *132*, 7864–7865; m) Y. Yamauchi, M. Fujita, *Chem. Commun.* **2010**, *46*, 5897–5899.

[24] F. Bonati, A. Burini, B. R. Pietroni, B. Bovio, *J. Organomet. Chem.* **1989**, *375*, 147–160.

[25] K. F. Morris, C. S. Johnson, Jr. *J. Am. Chem. Soc.* **1993**, *115*, 4291–4299.

[26] a) M. Valentini, P. S. Pregosin, H. Rüegger, *Organometallics*, **2000**, *19*, 12551–2555; b) I. Keresztes, P. G. Williard, *J. Am. Chem. Soc.* **2000**, *122*, 10228–10229.

[27] A. Hori, K. Kumazawa, T. Kusukawa, D. K. Chand, M. Fujita, S. Sakamoto, K. Yamaguchi, *Chem. Eur. J.* **2001**, *7*, 4142–4149.

[28] K. Kumazawa, M. Yoshizawa, H.-B. Liu, Y. Kamikawa, M. Moriyama, T. Kato, M. Fujita, *Chem. Eur. J.* **2005**, *11*, 2519–2524.

[29] a) M. A. Omary, M. A. Rawashdeh-Omary, M. W. A. Gonser, O. Elbjeirami, T. Grimes, T. R. Cundari, H. V. K. Diyabalanage, C. S. P. Gamage, H. V. R. Dias, *Inorg. Chem.* **2005**, *44*, 8200–8210; b) L. E. Sansores, R. Salcedo, A. Martínez, N. Mireles, *THEOCHEM* **2006**, *763*, 7–11; c) S. M. Tekarli, T. R. Cundari, M. A. Omary, *J. Am. Chem. Soc.* **2008**, *130*, 1669–1675.

[30] A. D. Becke, *J. Chem. Phys.* **1993**, *98*, 5648–5652.

[31] Gaussian 09, Revision A.02, M. J. Frisch, G. W. Trucks, H. B. Schlegel, G. E. Scuseria, M. A. Robb, J. R. Cheeseman, G. Scalmani, V. Barone, B. Mennucci,

G. A. Petersson, H. Nakatsuji, M. Caricato, X. Li, H. P. Hratchian, A. F. Izmaylov, J. Bloino, G. Zheng, J. L. Sonnenberg, M. Hada, M. Ehara, K. Toyota, R. Fukuda, J. Hasegawa, M. Ishida, T. Nakajima, Y. Honda, O. Kitao, H. Nakai, T. Vreven, J. A. Montgomery, Jr., J. E. Peralta, F. Ogliaro, M. Bearpark, J. J. Heyd, E. Brothers, K. N. Kudin, V. N. Staroverov, R. Kobayashi, J. Normand, K. Raghavachari, A. Rendell, J. C. Burant, S. S. Iyengar, J. Tomasi, M. Cossi, N. Rega, J. M. Millam, M. Klene, J. E. Knox, J. B. Cross, V. Bakken, C. Adamo, J. Jaramillo, R. Gomperts, R. E. Stratmann, O. Yazyev, A. J. Austin, R. Cammi, C. Pomelli, J. W. Ochterski, R. L. Martin, K. Morokuma, V. G. Zakrzewski, G. A. Voth, P. Salvador, J. J. Dannenberg, S. Dapprich, A. D. Daniels, Ö. Farkas, J. B. Foresman, J. V. Ortiz, J. Cioslowski, and D. J. Fox, Gaussian, Inc., Wallingford CT, 2009.

[32] P. J. Hay, W. R. Wadt, *J. Chem. Phys.* **1985**, *82*, 299–310.

[33] GaussView, Versiton 5, R. Dennington, T. Keith, and J. Millam, *Semichem Inc.*, Shawnee Mission, KS, 2009.

[34] J. K. Klosterman, M. Iwamura, T. Tahara, M. Fujita, *J. Am. Chem, Soc.* **2009**, *131*, 9478–9479.

2.8 Experimental Section

Materials and Instructions: Reagents and solvents were purchased from TCI Co., Ltd., WAKO Pure Chemical Industries Ltd., Sigma-Aldrich Co., and KANTO Chemical Co., Inc. Deuterated H_2O was used as supplied for the complexation reactions and NMR measurements. NMR spectra were recorded on Bruker DRX-500 (500 MHz) equipped with BBO gradient probe or Bruker AV-500 (500 MHz) with CP-TCI CryoProbe. TMS ($CDCl_3$ solution) in a capillary served as an external standard ($\delta = 0$ ppm). IR measurements were carried out using a DIGILAB FTS-7000 instrument. UV-visible spectral data were recorded on a SHIMADZU UV-3150. MALDI-TOF MS and CSI-MS were measured on Applied Biosystem Voyager DE-STR instruments and a four-sector (BE/BE) tandem mass spectrometer (JMS-700C, JEOL), respectively. Melting points were determined with a Yanaco MP-500P micro melting point apparatus. Elemental analyses were performed on a Yanaco MT-6. Diffraction measurements were made using a Bruker APEXII/CCD diffractometer equipped with a focusing mirror (MoKα radiation $\lambda = 0.71073$ Å). Self-assembled box-shaped cage **1a**[1] and **1b**,[2] and trinuclear gold(I) complex **2a**[3] were prepared according to the literature procedures.

References

[1] K. Kumazawa, K. Biradha, T. Kusukawa, T. Okano, M. Fujita, *Angew. Chem. Int. Ed.* **2003**, *42*, 3909–3913.

[2] M. Yoshizawa, J. Nakagawa, K. Kumazawa, M. Nagao, M. Kawano, T. Ozeki, M. Fujita, *Angew. Chem. Int. Ed.* **2005**, *44*, 1810–1813.

[3] F. Bonati, A. Burini, B. R. Pietroni, B. Bovio, *J. Organomet. Chem.* **1989**, *375*, 147–160.

Synthesis and Physical Data of [3 × 1] Au(I) Cluster 1a•2a

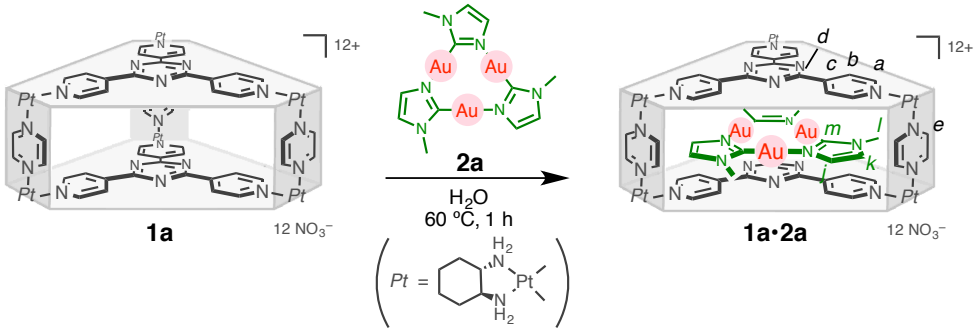

Scheme S1. Synthesis of [3 × 1] Au(I) cluster **1a•2a**.

Trinuclear Au(I) complex (**2a**; 16.7 mg, 20.0 μmol) was added to an aqueous solution (1.0 mL) of cage **1a** (34.6 mg, 10.0 μmol), and the suspended mixture was stirred at 60 ºC for 1 h. After filtration of the resulting solution, NMR spectroscopy revealed the quantitative formation of inclusion complex **1a•2a**. The solution was evaporated and dried by vacuum freeze-drying equipment to give inclusion complex **1a•2a** (34.3 mg, 7.98 μmol, 80%) as an orange solid. ^{1}H NMR (500 MHz, D_2O, 300 K) δ: 9.72 (s, 6H, **1a**, H^e), 9.71 (s, 6H, **1a**, H^e), 9.13 (d, J = 5.5 Hz, 3H, **1a**, H^a), 9.06 (d, J = 5.5 Hz, 3H, **1a**, H^a), 8.80 (d, J = 5.5 Hz, 3H, **1a**, H^a), 8.72 (d, J = 5.5 Hz, 3H, **1a**, H^a), 8.58 (br, 6H, **1a**, H^b), 7.89 (br, 6H, **1a**, H^b), 6.51 (s, 3H, **2a**, H^k), 3.68 (s, 9H, **2a**, H^l), 2.86 (s, 3H, **2a**, H^j), 2.69 (m, 12H, **1a**, cyclohexyl-H), 2.15–2.03 (m, 12H, **1a**, cyclohexyl-H), 1.65 (m, 12H, **1a**, cyclohexyl-H), 1.46–1.36 (m, 12H, **1a**, cyclohexyl-H), 1.21 (m, 12H, **1a**, cyclohexyl-H). ^{13}C NMR (125 MHz, D_2O, 300 K) δ: 168.8 (C, **1a**, C^d), 165.6 (C, **2a**, C^m), 153.2–152.3 (CH, **1a**, C^a), 151.8 (CH, **1a**, C^e), 147.2–145.8 (C, **1a**, C^c), 126.6–124.7 (CH, **1a**, C^b), 121.3 (CH, **2a**, C^j), 120.6 (CH, **2a**, C^k), 62.0 (CH, **1a**, cyclohexyl-C), 35.14 (CH_3, **2a**, C^l), 31.8 (CH_3, **1a**, cyclohexyl-C), 23.9 (CH_3, **1a**, cyclohexyl-C). ^{1}H DOSY (D_2O, 300 K) (m^2/s): D = 1.5 × 10^{-10}. IR (KBr, cm^{-1}): 3435 (br), 3052 (br), 2940, 2863, 2766, 1647 (br), 1522, 1383, 1124, 810. m.p. = ~210 ºC (decomposed). CSI-MS (H_2O : CH_3CN : DMF = 1 : 1 : 0.1): m/z = 612.5 [**1a•2a**–8·NO_3^-+15·DMF]$^{8+}$, 621.5 [**1a•2a**–8·NO_3^-+16·DMF]$^{8+}$, 630.7 [**1a•2a**–8·NO_3^-+17·DMF]$^{8+}$, 639.9 [**1a•2a**–8·NO_3^-+18·DMF]$^{8+}$, 677.5 [**1a•2a**–7·NO_3^-+12·DMF]$^{7+}$, 687.9 [**1a•2a**–7·NO_3^-+13·DMF]$^{7+}$, 698.3 [**1a•2a**–7·NO_3^-+14·DMF]$^{7+}$, 764.0 [**1a•2a**–6·NO_3^-+9·DMF]$^{6+}$, 776.2 [**1a•2a**–6·NO_3^-+10·DMF]$^{6+}$, 788.4 [**1a•2a**–6·NO_3^-+11·DMF]$^{6+}$, 885.5 [**1a•2a**–5·NO_3^-+6·DMF]$^{5+}$, 900.2 [**1a•2a**–5·NO_3^-+7·DMF]$^{5+}$, 914.8

[**1a•2a**–5·NO_3^-+8·DMF]$^{5+}$, 1067.5 [**1a•2a**–4·NO_3^-+3·DMF]$^{4+}$, 1085.7 [**1a•2a**–4·NO_3^- +4·DMF]$^{4+}$, 1104.2 [**1a•2a**–4·NO_3^-+5·DMF]$^{4+}$. E.A. Calcd. for $C_{96}H_{135}Au_3N_{48}O_{36}Pt_6$ ·$(H_2O)_{24}$: C, 24.37; H, 3.90; N, 14.21; Found: C, 24.72; H, 4.23; N, 13.87.

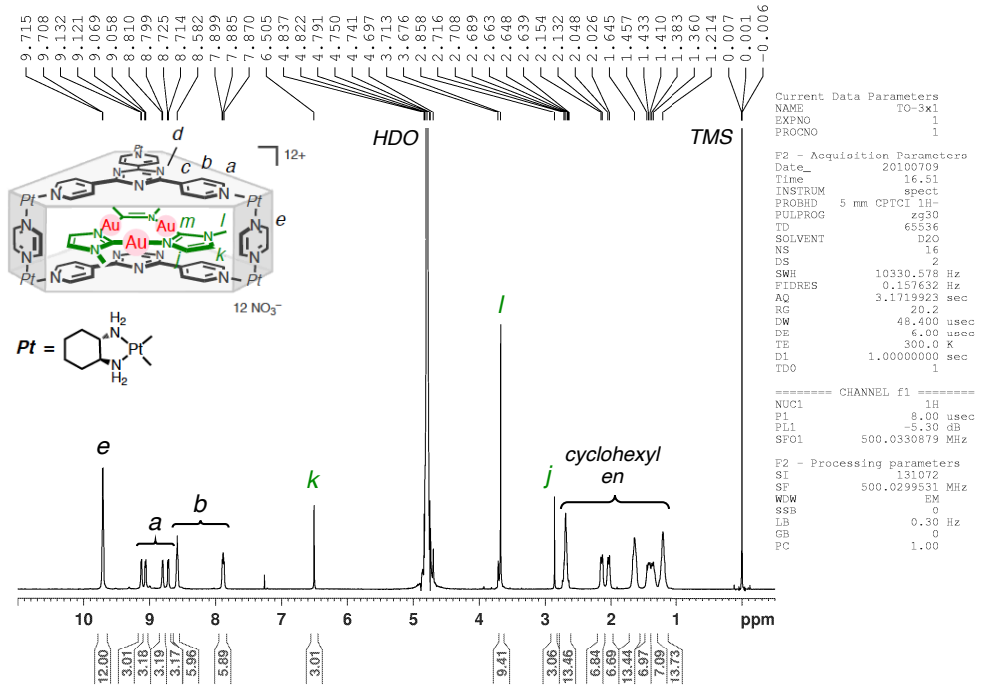

Figure S1. ^{1}H NMR (500 MHz, D_2O, 300 K) spectrum of **1a•2a**.

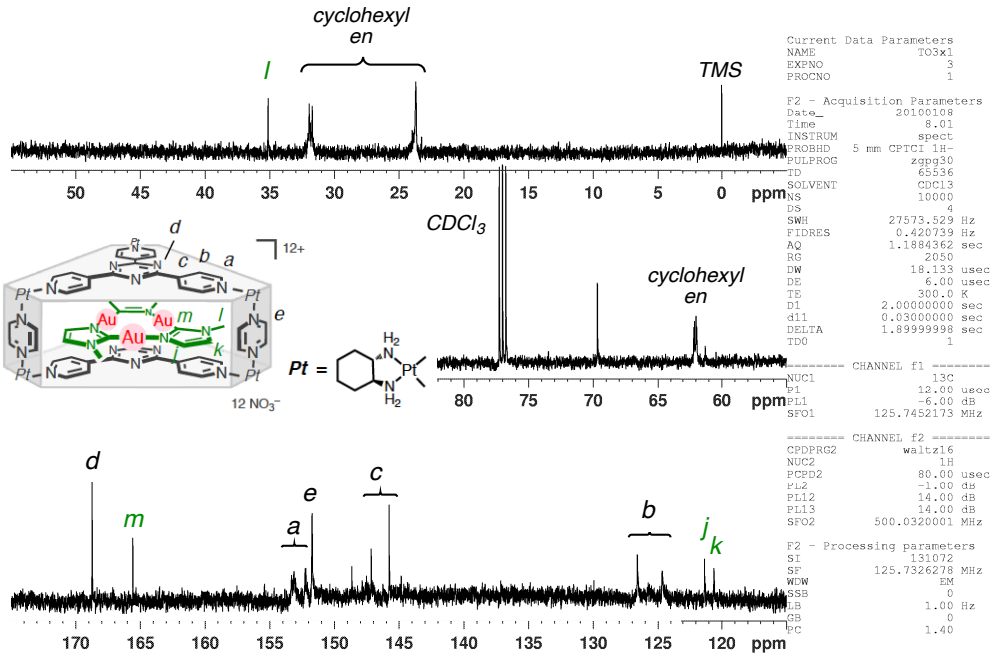

Figure S2. ^{13}C NMR (125 MHz, D_2O, 300 K) spectrum of **1a•2a**.

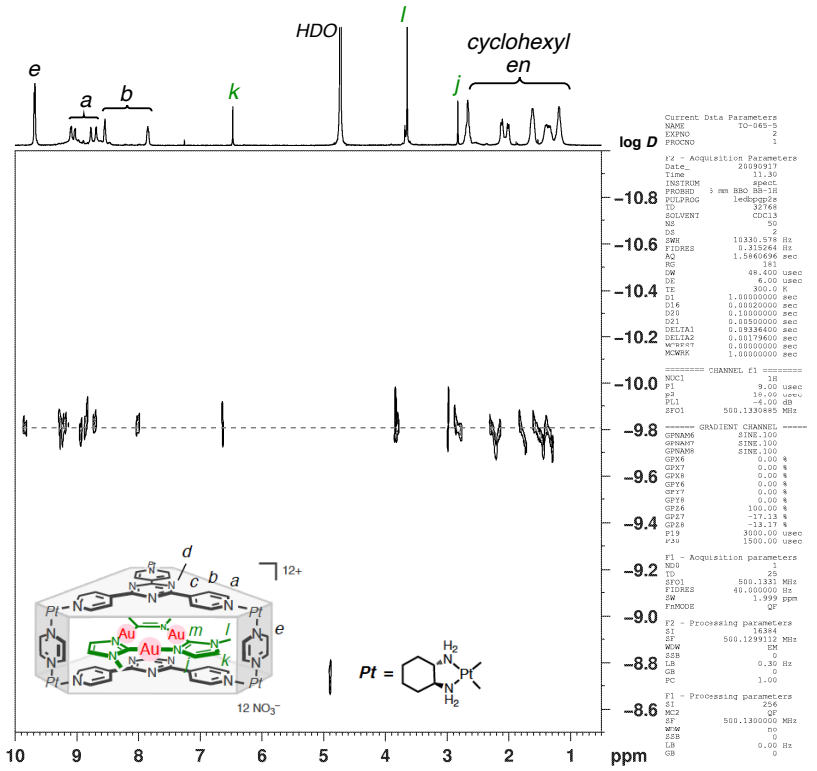

Figure S3. ^{1}H DOSY (500 MHz, D_2O, 300 K) spectrum of **1a·2a**.

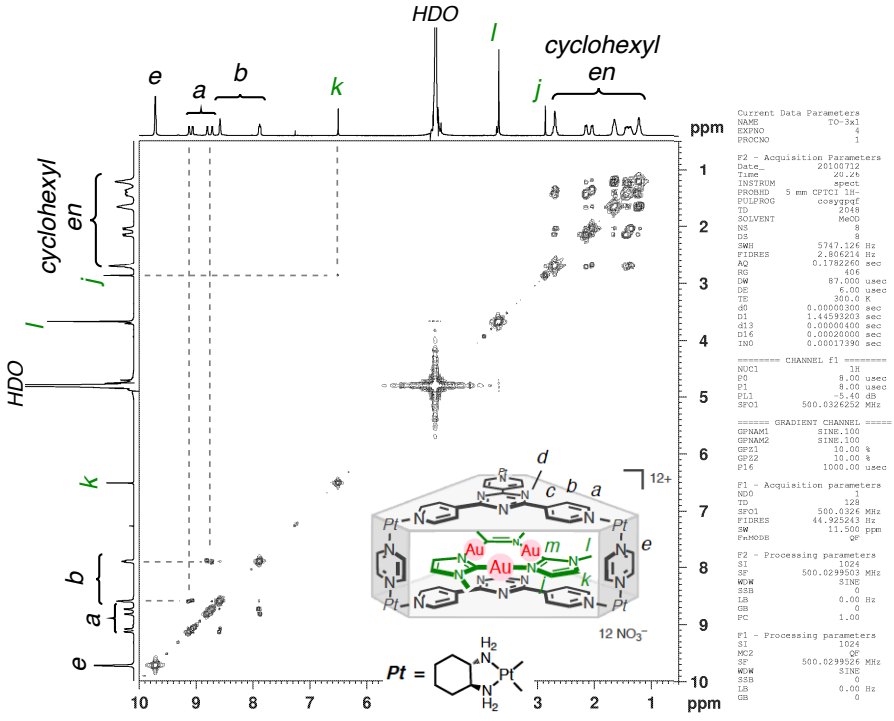

Figure S4. ^{1}H-^{1}H COSY (500 MHz, D_2O, 300 K) spectrum of **1a·2a**.

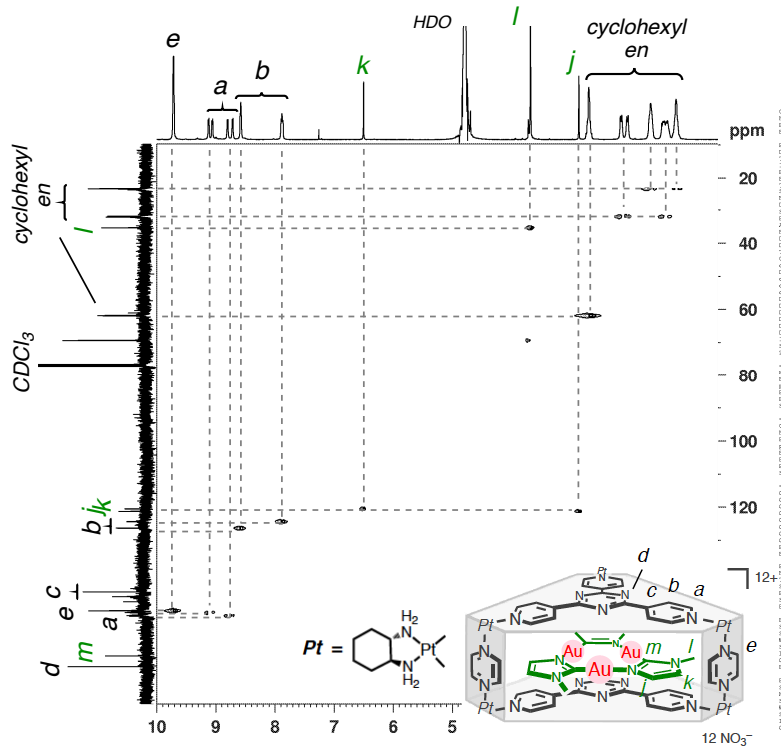

Figure S5. ^{1}H-^{13}C HSQC (500 MHz, D_2O, 300 K) spectrum of **1a·2a**.

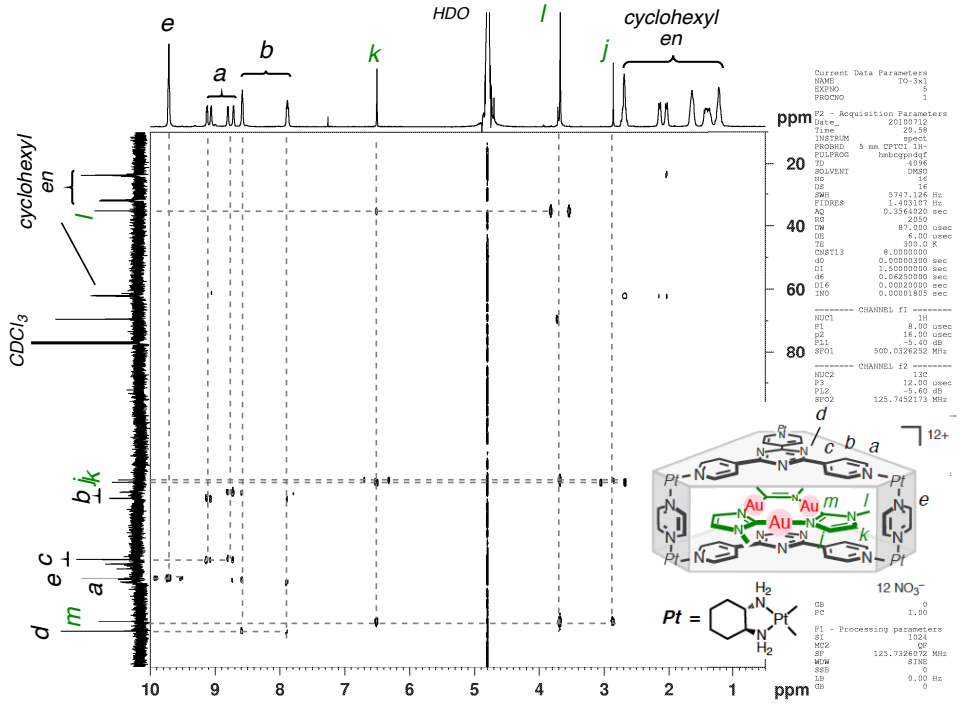

Figure S6. ^{1}H-^{13}C HMBC (500 MHz, D_2O, 300 K) spectrum of **1a·2a**.

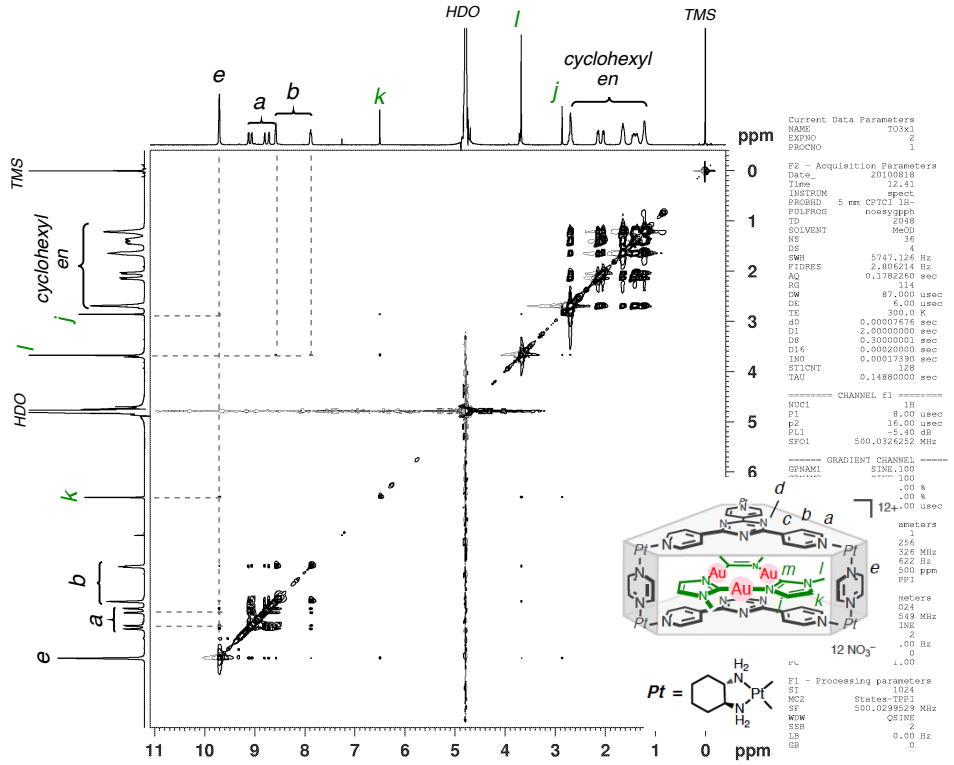

Figure S7. ^{1}H-^{1}H NOESY (500 MHz, D_2O, 300 K) spectrum of **1a•2a**.

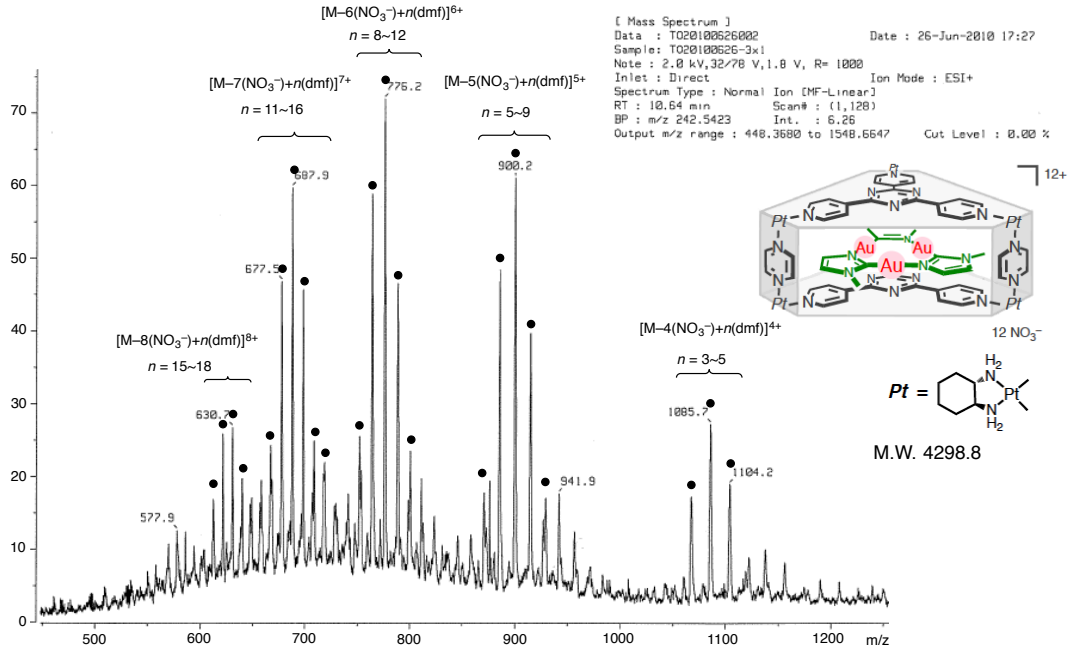

Figure S8. CSI-MS spectrum of **1a•2a** (H_2O : CH_3CN : DMF = 1 : 1 : 0.1).

Synthesis and Physical Data of [3 × 2] Au(I) Cluster 1b•(2a)$_2$

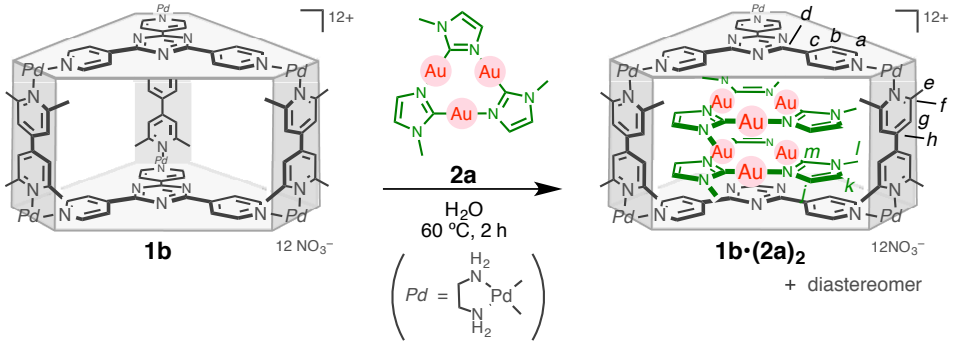

Scheme S2. Synthesis of [3 × 2] Au(I) cluster **1b•(2a)$_2$**.

Trinuclear Au(I) complex (**2a**; 33.5 mg, 40.0 μmol) was added to an aqueous solution (1.0 mL) of cage **1b** (30.0 mg, 10.0 μmol), and the suspended mixture was stirred at 60 ºC for 2 h. After filtration of the resulting solution, NMR spectroscopy revealed the quantitative formation of inclusion complex **1b•(2a)$_2$**. Two sets of signals were observed for cage **1b** and guest **2a** in almost the same ratio, indicating two stacking modes of the C_{3h} symmetrical guest **2a** within cages **1b**. The solution was evaporated and dried by vacuum freeze-drying equipment to give inclusion complex **1b•(2a)$_2$** (35.4 mg, 7.58 μmol, 76%) as an orange solid. ^{1}H NMR (500 MHz, D_2O, 300 K) δ: 8.74 (d, J = 5.5 Hz, 6H, **1b**, H^a), 8.71 (d, J = 5.5 Hz, 6H, **1b**, H^a), 8.14 (d, J = 5.5 Hz, 6H, **1b**, H^b), 8.12 (d, J = 5.5 Hz, 6H, **1b**, H^b), 7.99 (s, 3H, **1b**, H^g), 7.93 (s, 3H, **1b**, H^g), 7.91 (s, 3H, **1b**, H^g), 7.75 (s, 3H, **1b**, H^g), 6.52 (s, 3H, **2a**, H^k), 6.40 (s, 3H, **2a**, H^k), 3.83 (s, 3H, **2a**, H^j), 3.72 (s, 9H, **1b**, H^e), 3.67 (s, 3H, **2a**, H^j), 3.64 (s, 18H, **1b**, H^e), 3.49 (s, 9H, **1b**, H^e), 3.25 (s, 9H, **2a**, H^l), 3.22 (s, 9H, **2a**, H^l), 2.97 (br, 6H, **1b**, ethylenediamine-H), 2.96 (br, 6H, **1b**, ethylenediamine-H), 2.92 (br, 6H, **1b**, ethylenediamine-H), 2.91 (br, 6H, **1b**, ethylenediamine-H). ^{13}C NMR (125 MHz, D_2O, 300 K) δ: 168.9 (C, **1b**, C^d), 168.8 (C, **1b**, C^d), 168.5 (C, **2a**, C^m), 168.1 (C, **2a**, C^m), 161.4 (C, **1b**, C^f), 161.3 (C, **1b**, C^f), 151.9 (CH, **1b**, C^a), 151.8 (CH, **1b**, C^a), 147.5 (C, **1b**, C^h), 147.1 (C, **1b**, C^h), 146.0 (C, **1b**, C^c), 145.8 (C, **1b**, C^c), 125.7 (CH, **1b**, C^b), 125.5 (CH, **1b**, C^b), 124.2 (CH, **2a**, C^j), 123.9 (CH, **2a**, C^j), 122.5 (CH, **1b**, C^g), 122.3 (CH, **1b**, C^g), 118.2 (CH, **2a**, C^k), 118.0 (CH, **2a**, C^k), 47.6 (CH_2, **1b**, ethylenediamine-C), 46.5 (CH_2, **1b**, ethylenediamine-C), 34.5 (CH_3, **2a**, C^l), 34.4 (CH_3, **2a**, C^l), 26.0 (CH_3, **2a**, C^e), 25.1 (CH_3, **2a**, C^e). ^{1}H DOSY (D_2O, 300 K) (m^2/s): D = 1.5 × 10^{-10}. IR (KBr, cm^{-1}): 3435(br), 2953, 2765, 1616, 1520, 1384 (br), 1058, 806.

m.p. = ~220 ºC (decomposed). CSI-MS (H_2O : CH_3CN : DMF = 1 : 1 : 0.1): *m/z* = 650.3 $[\mathbf{1b•(2a)_2}–8·NO_3^-+14·DMF]^{8+}$, 659.3 $[\mathbf{1b•(2a)_2}–8·NO_3^-+15·DMF]^{8+}$, 668.4 $[\mathbf{1b•(2a)_2}–8·NO_3^-+16·DMF]^{8+}$, 677.9 $[\mathbf{1b•(2a)_2}–8·NO_3^-+17·DMF]^{8+}$, 730.8 $[\mathbf{1b•(2a)_2}–7·NO_3^-+12·DMF]^{7+}$, 741.2 $[\mathbf{1b•(2a)_2}–7·NO_3^-+13·DMF]^{7+}$, 777.9 $[\mathbf{1b•(2a)_2}–6·NO_3^-+5·DMF]^{6+}$, 789.7 $[\mathbf{1b•(2a)_2}–6·NO_3^-+6·DMF]^{6+}$, 802.1 $[\mathbf{1b•(2a)_2}–6·NO_3^-+7·DMF]^{6+}$, 814.4 $[\mathbf{1b•(2a)_2}–6·NO_3^-+8·DMF]^{6+}$, 916.7 $[\mathbf{1b•(2a)_2}–5·NO_3^-+3·DMF]^{5+}$, 931.1 $[\mathbf{1b•(2a)_2}–5·NO_3^-+4·DMF]^{5+}$, 945.8 $[\mathbf{1b•(2a)_2}–5·NO_3^-+5·DMF]^{5+}$. E.A. Calcd. for $C_{114}H_{150}Au_6N_{54}O_{36}Pd_6·(H_2O)_{19}$: C, 27.30; H, 3.78; N, 15.08; Found: C, 27.37; H, 3.59; N, 14.89.

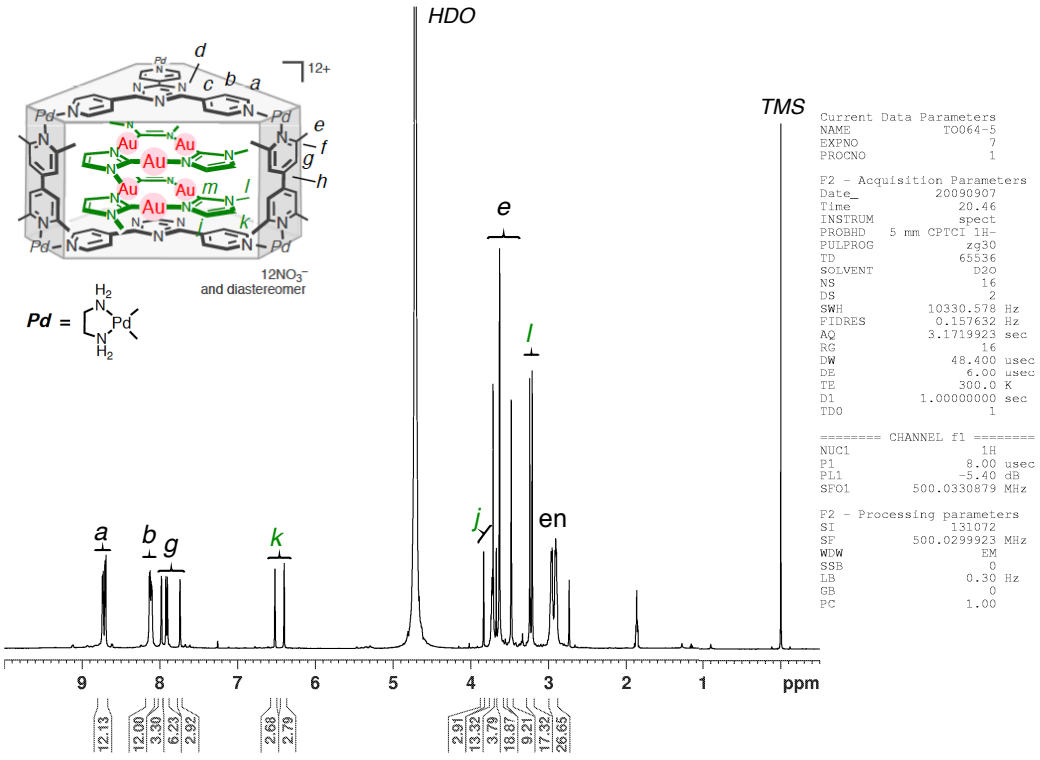

Figure S9. ^{1}H NMR (500 MHz, D_2O, 300 K) spectrum of **1b•(2a)$_2$**.

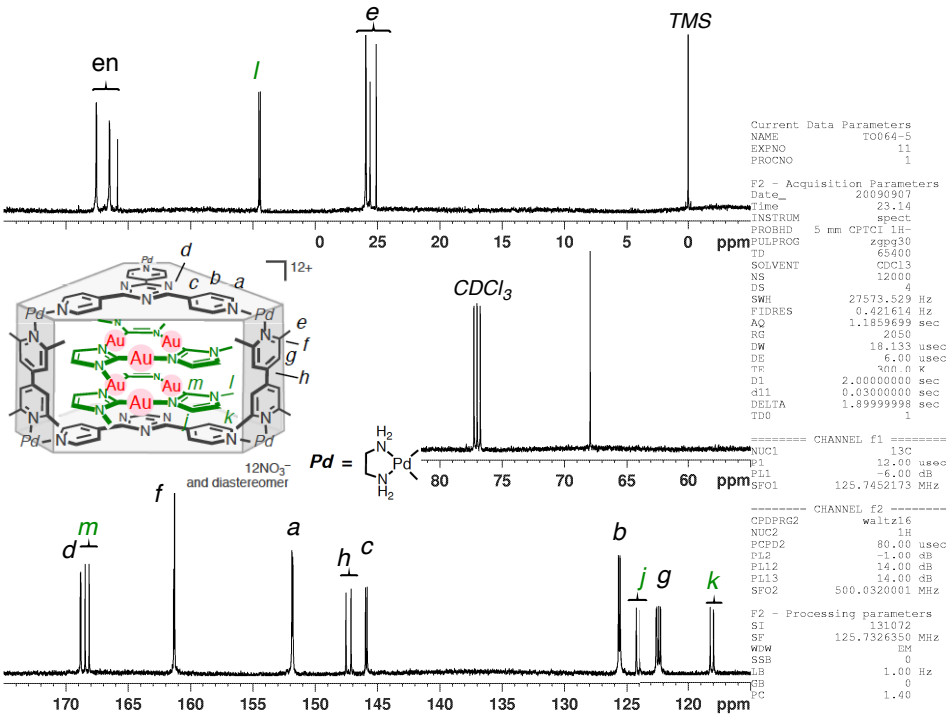

Figure S10. ^{13}C NMR (125 MHz, D_2O, 300 K) spectrum of **1b**•(**2a**)$_2$.

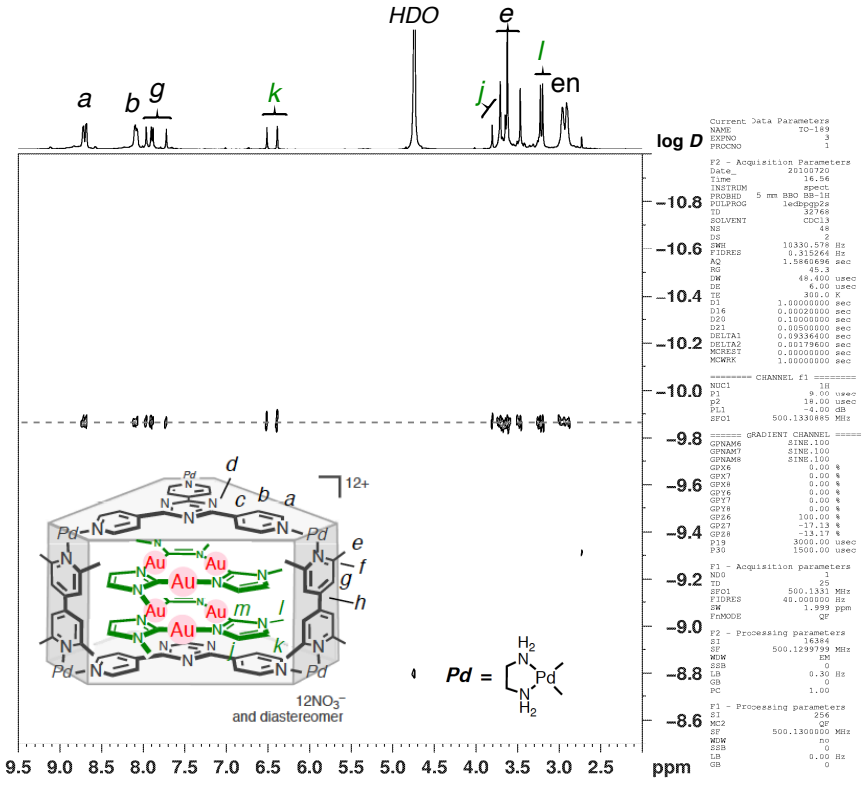

Figure S11. ^{1}H DOSY (500 MHz, D_2O, 300 K) spectrum of **1b**•(**2a**)$_2$.

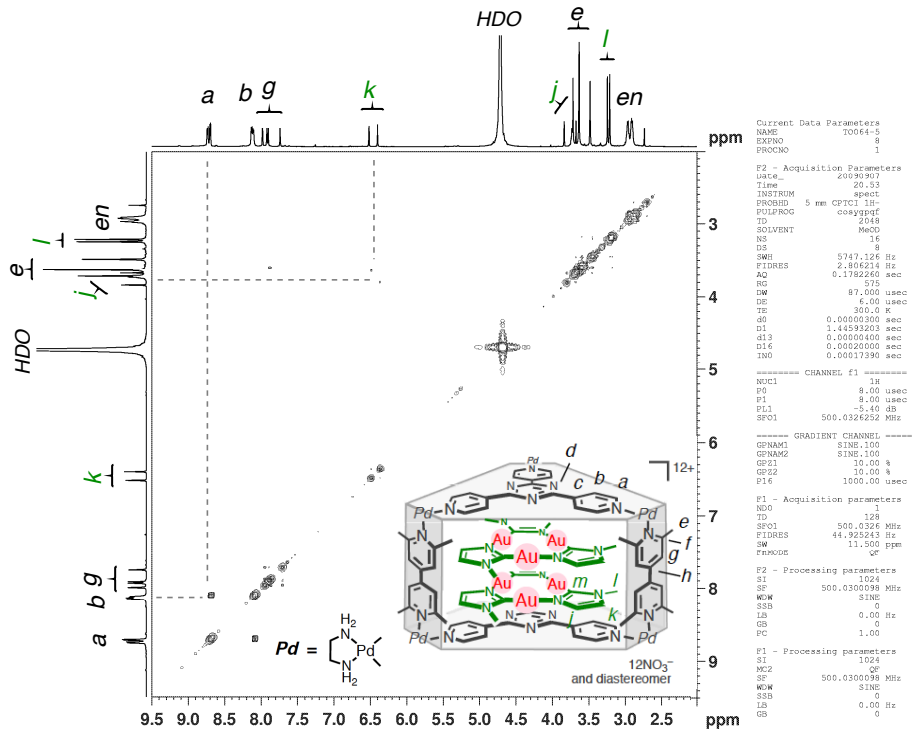

Figure S12. ^{1}H-^{1}H COSY (500 MHz, D_2O, 300 K) spectrum of **1b**•(**2a**)$_2$.

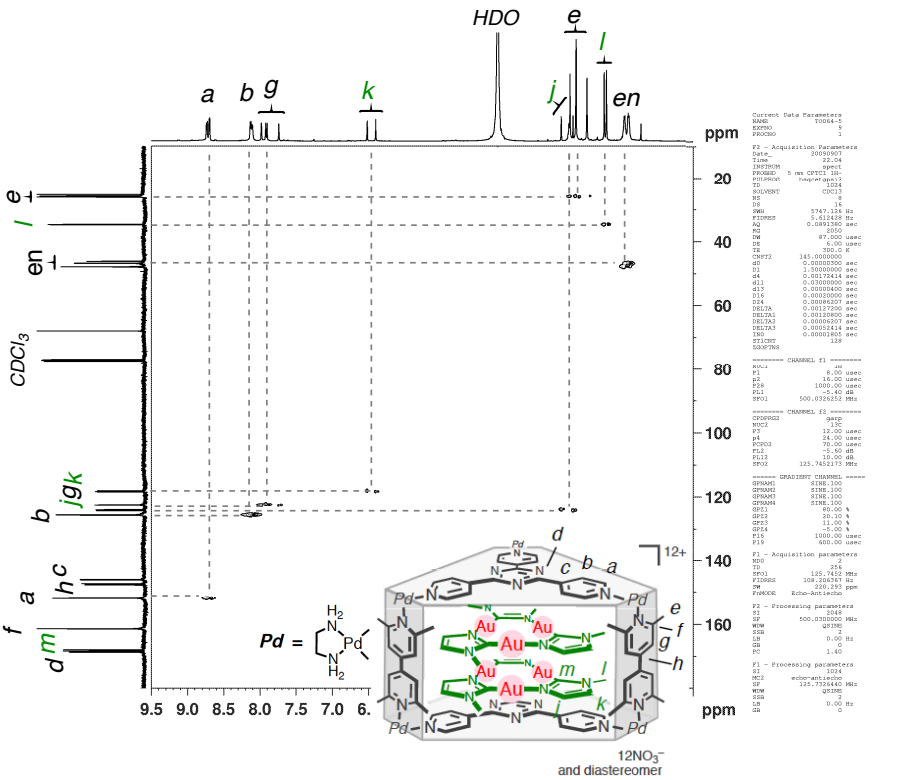

Figure S13. ^{1}H-^{13}C HSQC (500 MHz, D_2O, 300 K) spectrum of **1b**•(**2a**)$_2$.

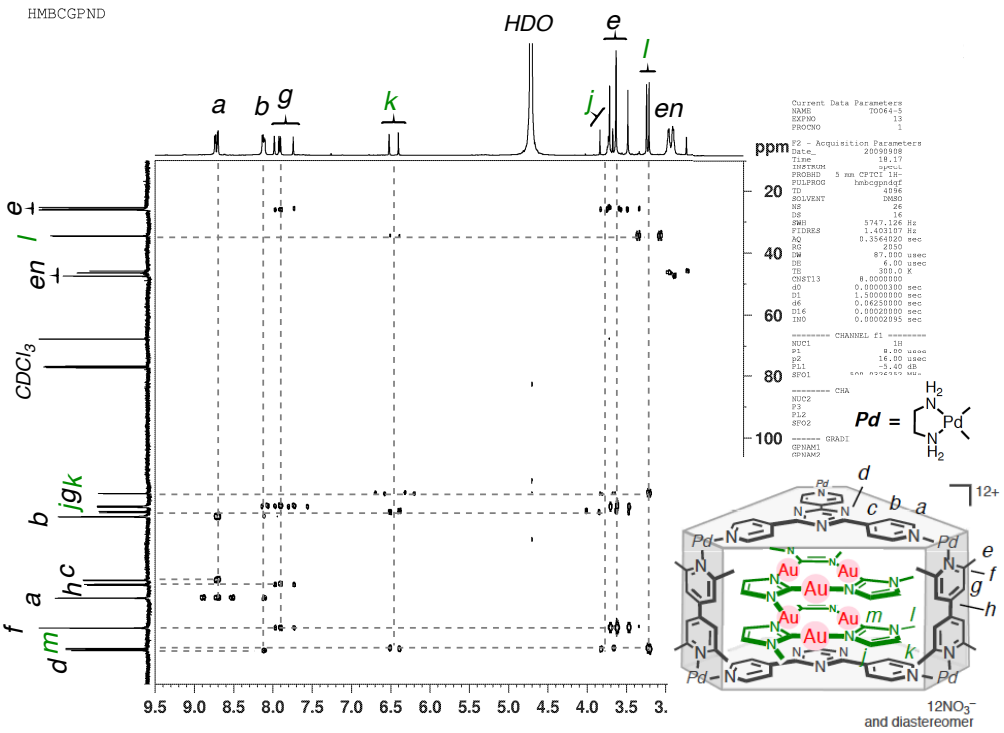

Figure S14. ^{1}H-^{13}C HMBC (500 MHz, D_2O, 300 K) spectrum of **1b**•(**2a**)$_2$.

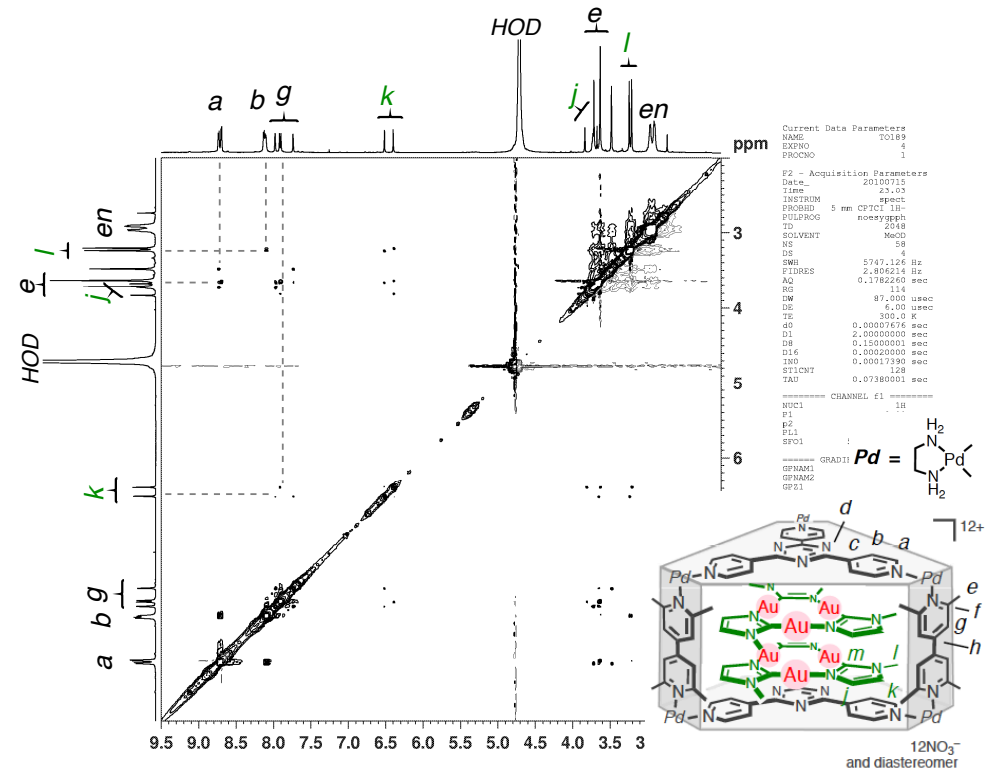

Figure S15. ^{1}H-^{1}H NOESY (500 MHz, D_2O, 300 K) spectrum of **1b**•(**2a**)$_2$.

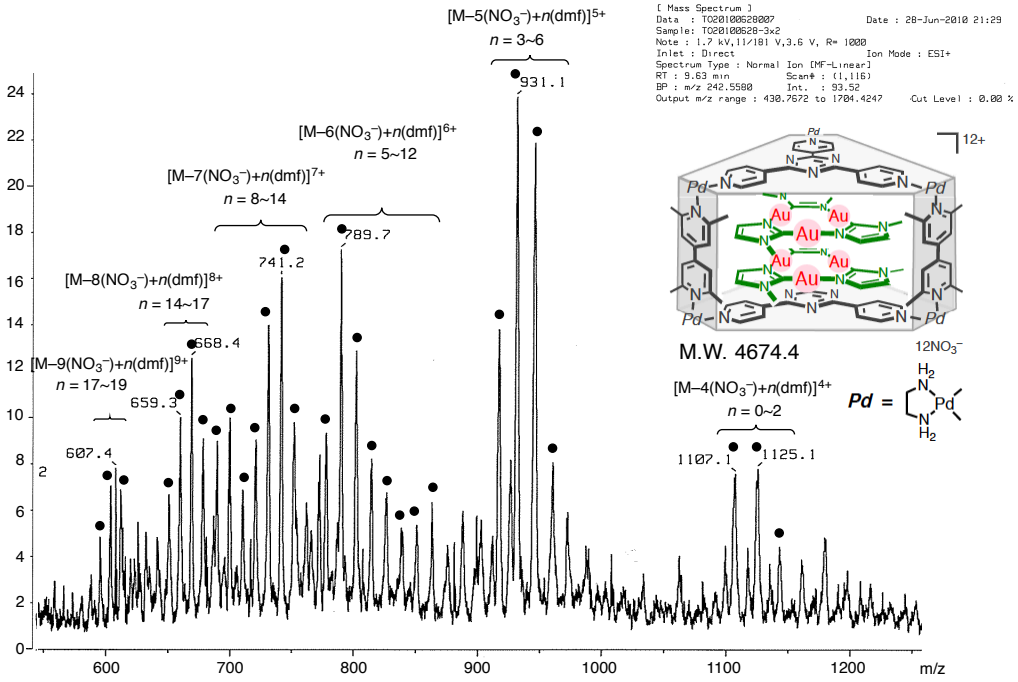

Figure S16. CSI-MS spectrum of **1b**•(**2a**)$_2$ (H_2O : CH_3CN : DMF = 1 : 1 : 0.1).

Synthesis and Physical Data of Au(I) Cluster 1c'•(2a•3•2a)

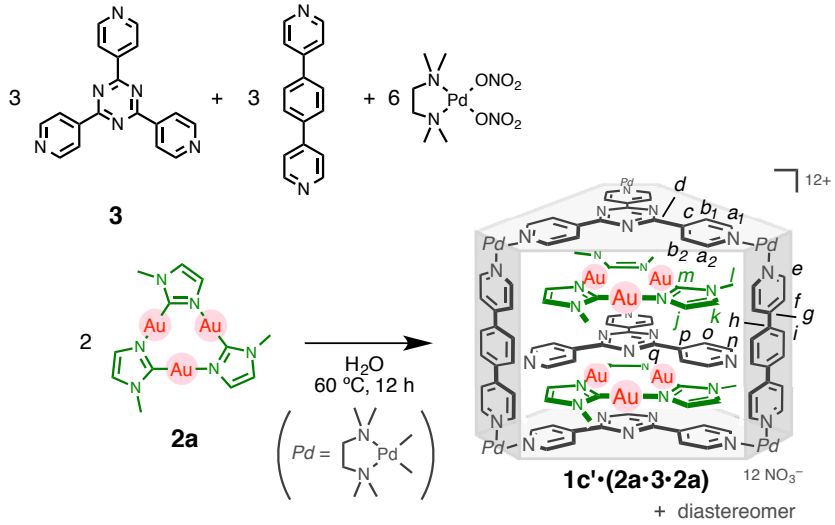

Scheme S3. Synthesis of Au(I) cluster **1c'•(2a•3•2a)**.

Panel-like ligand **3** (9.38 mg, 30.0 μmol), pillar-like ligand (8.65 mg, 30.0 μmol), (tmeda)Pd(ONO_2)$_2$ (20.80 mg, 60.0 μmol), and trinuclear Au(I) complex **2a** (33.5 mg, 40.0 μmol) were stirred in water (1.0 mL) at 60 ºC for 12 h. After filtration of the resulting solution, NMR spectroscopy revealed the quantitative formation of inclusion complex **1c'•(2a•3•2a)**. As in the case of [3 × 2] Au(I) cluster **1b•(2a)**$_2$, two sets of signals were observed for cage **1c'** and guest **2a** (~ 9 : 1 ratio at 300 K), indicating two stacking modes of the C_{3h} symmetrical guest **2a** within cages **1c'**. The solution was evaporated and dried by vacuum freeze-drying equipment to give inclusion complex **1c'•(2a•3•2a)** (44.8 mg, 8.32 μmol, 83%) as an orange yellow solid. On the following spectra, the major and minor diastereomers were assigned in capital and small letters, respectively. ^{1}H NMR (500 MHz, D_2O, 320 K) (major diastereomer) δ: 9.20 (d, J = 5.5 Hz, 12H, **1c'**, H^E), 9.15 (d, J = 5.5 Hz, 6H, **1c'**, H^A), 8.76 (d, J = 5.5 Hz, 6H, **1c'**, H^A), 8.43 (d, J = 5.5 Hz, 6H, **1c'**, H^B), 8.21 (br, 12H, **1c'**, H^F), 8.18 (s, 12H, **1c'**, H^I), 7.75 (d, J = 5.5 Hz, 6H, **1c'**, H^B), 7.06 (br, 6H, **3**, H^N), 6.94 (br, 6H, **3**, H^O), 5.84 (s, 6H, **2a**, H^K), 3.93 (s, 6H, **2a**, H^J), 3.06 (br, 12H, **1c'**, H^R), 3.01 (br, 12H, **1c'**, H^R), 2.96 (s, 18H, **2a**, H^L), 2.73 (s, 18H, **2a**, H^S), 2.68(s, 18H, **2a**, H^S), 2.42(s, 18H, **2a**, H^S), 2.38(s, 18H, **2a**, H^S), (minor diastereomer) δ: 9.20 (d, J = 5.5 Hz, 12H, **1c'**, H^e), 9.13 (d, J = 5.5 Hz, 12H, **1c'**, H^a), 8.85 (d, J = 5.5 Hz, 6H, **1c'**, H^a), 8.32 (d, J = 5.5 Hz, 6H, **1c'**, H^b), 8.21 (br, 12H, **1c'**, H^f), 8.13 (s, 12H, **1c'**, H^i), 7.75 (d, J = 5.5 Hz, 6H, **1c'**, H^b), 7.48 (d, J = 5.5 Hz, 6H, **3**, H^n), 6.79 (d, J = 5.5 Hz, 6H, **3**, H^o), 6.50 (s, 6H, **2a**, H^k), 4.24 (s, 6H,

2a, H^{j}), 3.14 (br, 12H, **1c'**, H^{r}), 3.10 (br, 12H, **1c'**, H^{r}), 2.77 (s, 18H, **2a**, H^{l}), 2.74 (s, 18H, **1c'**, H^{s}), 2.70 (s, 18H, **1c'**, H^{s}), 2.48 (s, 18H, **1c'**, H^{s}), 2.44(s, 18H, **1c'**, H^{s}). ^{13}C NMR (125 MHz, D_2O, 320 K) (major diastereomer) δ: 168.9 (C, **3**, C^{Q}), 168.9 (C, **1c'**, C^{D}), 166.7(C, **2a**, C^{M}), 151.6 (CH, **1c'**, C^{A}), 151.3 (CH, **1c'**, C^{E}), 151.3 (CH, **1c'**, C^{A}), 151.1 (C, **1c'**, C^{G}), 147.3 (CH, **3**, C^{N}), 145.8 (C, **1c'**, C^{C}), 142.7 (C, **3**, C^{P}), 137.5 (C, **1c'**, C^{H}), 128.9 (CH, **1c'**, C^{I}), 126.3 (CH, **1c'**, C^{B}), 125.4 (CH, **1c'**, C^{F}), 124.9 (CH, **1c'**, C^{B}), 123.4 (CH, **2a**, C^{J}), 121.7 (CH, **3**, C^{O}), 119.2 (CH, **2a**, C^{K}), 62.8 (CH_2, **1c'**, C^{R}), 50.6–50.2 (CH_3, **1c'**, C^{S}), 34.7 (CH_3, **2a**, C^{L}), (minor diastereomer) δ: 169.0 (C, **3**, C^{q}), 168.8 (C, **1c'**, C^{d}), 166.9 (C, **2a**, C^{m}), 151.6 (CH, **1c'**, C^{a}), 151.5 (CH, **1c'**, C^{e}), 151.3 (CH, **1c'**, C^{a}), 151.1 (C, **1c'**, C^{g}), 147.5 (CH, **3**, C^{n}), 146.0 (C, **1c'**, C^{c}), 143.4 (C, **3**, C^{p}) 137.5 (C, **1c'**, C^{h}), 128.8 (CH, **1c'**, C^{i}), 126.1 (CH, **1c'**, C^{b}), 125.6 (CH, **1c'**, C^{f}), 124.9 (CH, **1c'**, C^{b}), 124.1 (CH, **2a**, C^{j}), 121.9 (CH, **3**, C^{o}), 119.5 (CH, **2a**, C^{k}), 62.8 (CH_2, **1c'**, C^{r}), 50.6–50.2 (CH_3, **1c'**, C^{s}), 34.5 (CH_3, **2a**, C^{l}). ^{1}H DOSY (D_2O, 300 K) (m^2/s): D = 1.4×10^{-10}. E.A. Calcd. for $C_{162}H_{198}Au_6N_{60}O_{36}Pd_6{\cdot}(H_2O)_{22}$: C, 33.67; H, 4.22; N, 14.54; Found: C, 33.97; H, 4.02; N, 14.16. IR (KBr, cm^{-1}): 3420(br), 3009(br), 2919(br), 1685, 1614, 1519, 1383 (br), 1200, 808. m.p. ~205 ºC (decomposed).

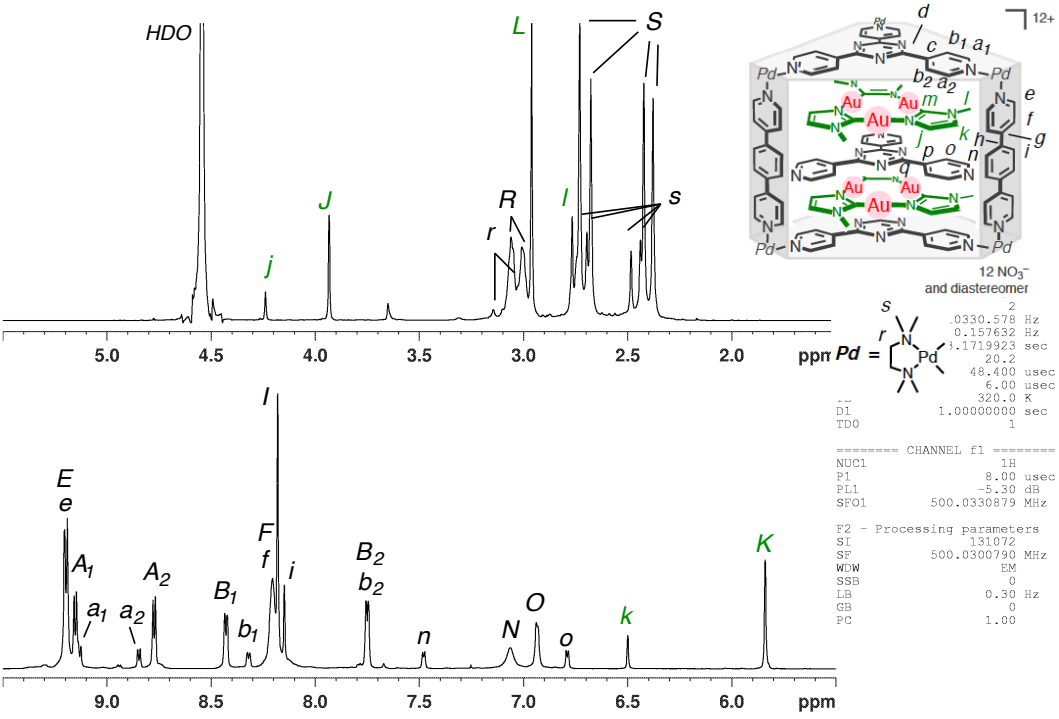

Figure S17. ^{1}H NMR (500 MHz, D_2O, 320 K) spectrum of **1c'**•(**2a**•**3**•**2a**).

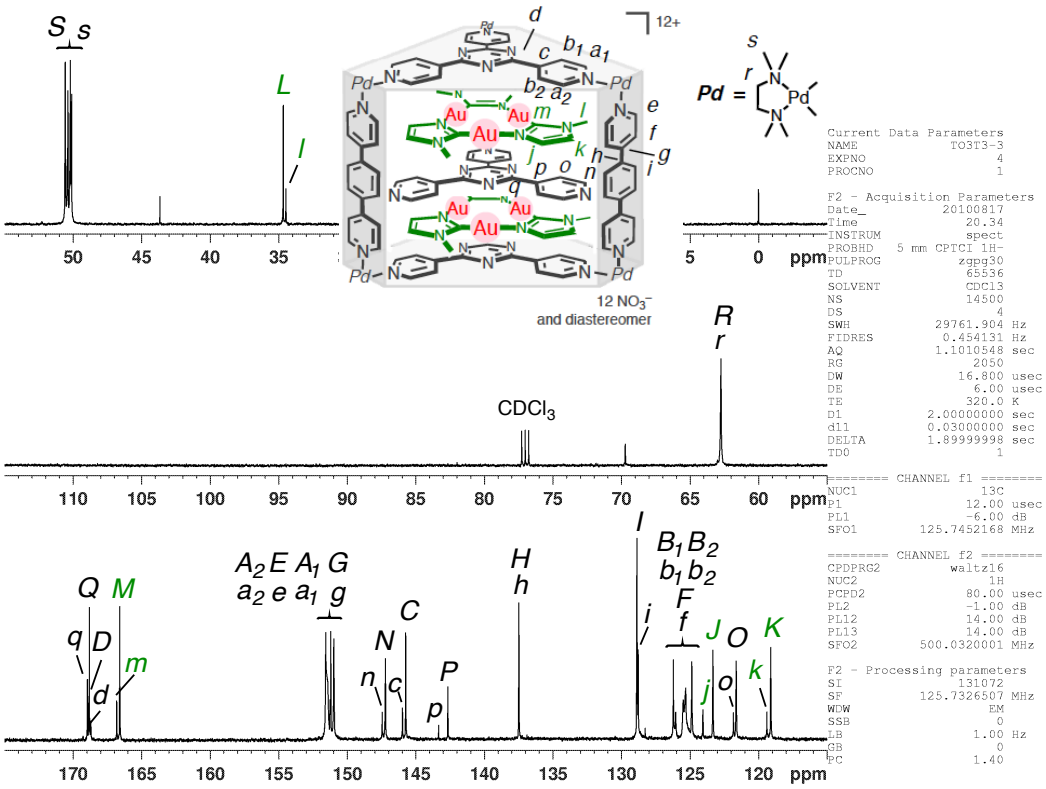

Figure S18. ^{13}C NMR (125 MHz, D_2O, 320 K) spectrum of **1c'•(2a•3•2a)**.

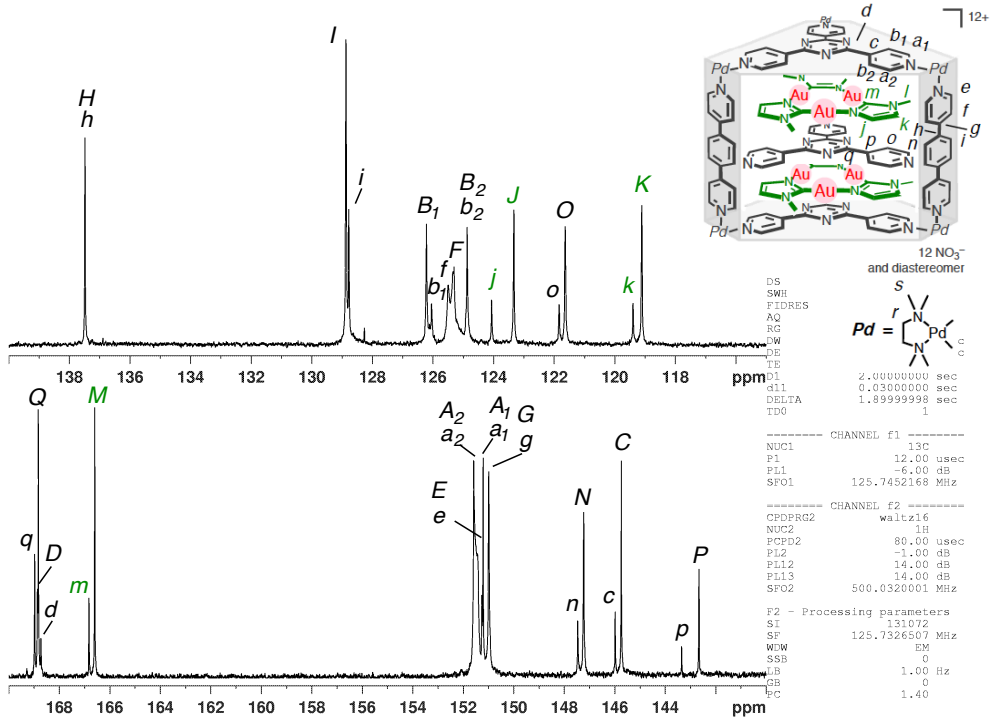

Figure S19. Enlarged ^{13}C NMR (125 MHz, D_2O, 320 K) spectrum of **1c'•(2a•3•2a)**.

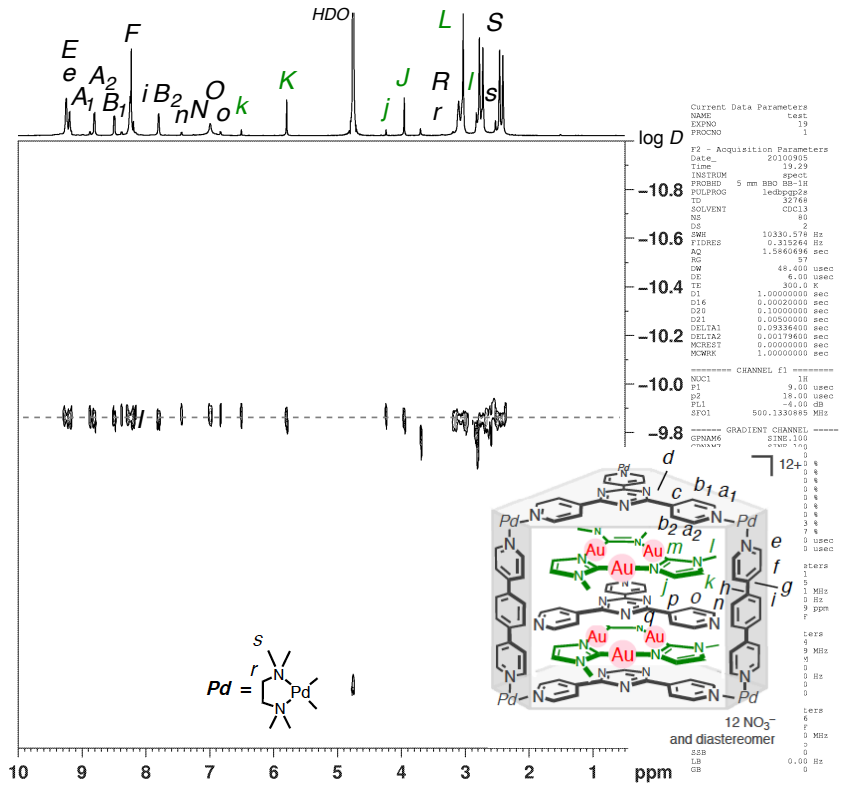

Figure S20. ^{1}H DOSY (500 MHz, D_2O, 300 K) spectrum of **1c'**•(**2a**•**3**•**2a**).

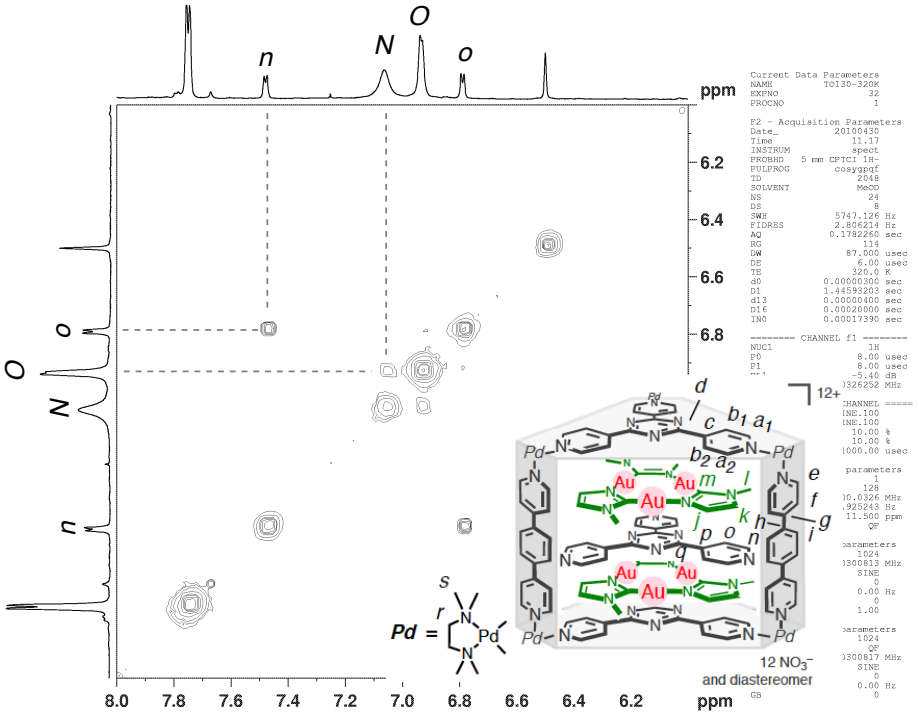

Figure S21. ^{1}H-^{1}H COSY (500 MHz, D_2O, 320 K) spectrum of **1c'**•(**2a**•**3**•**2a**).

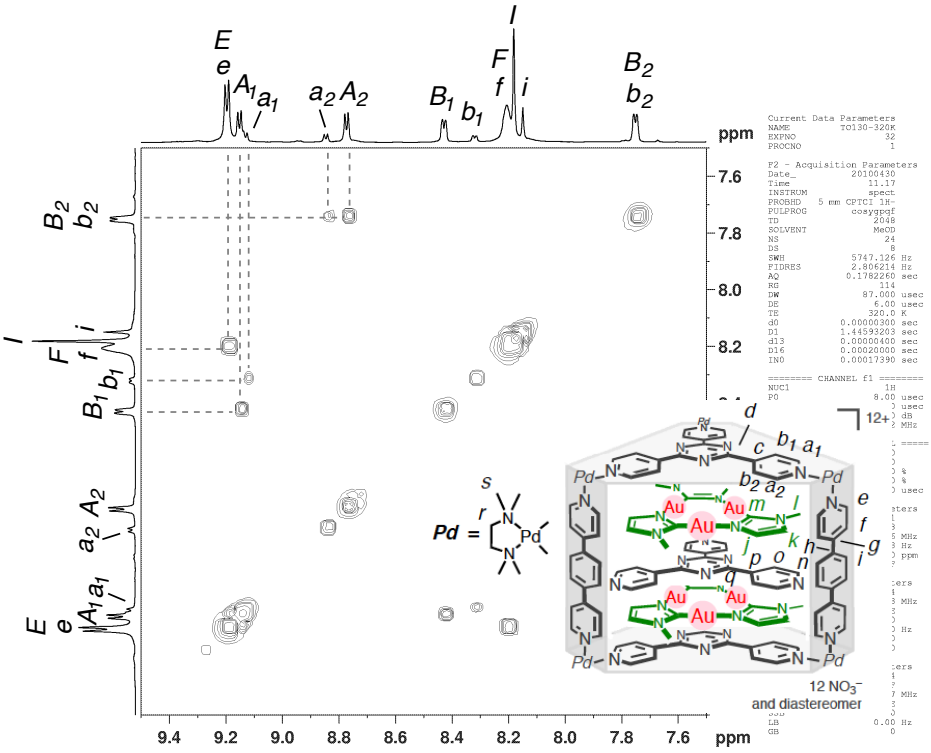

Figure S22. ^{1}H-^{1}H COSY (500 MHz, D_2O, 320 K) spectrum of **1c'**•(**2a**•**3**•**2a**).

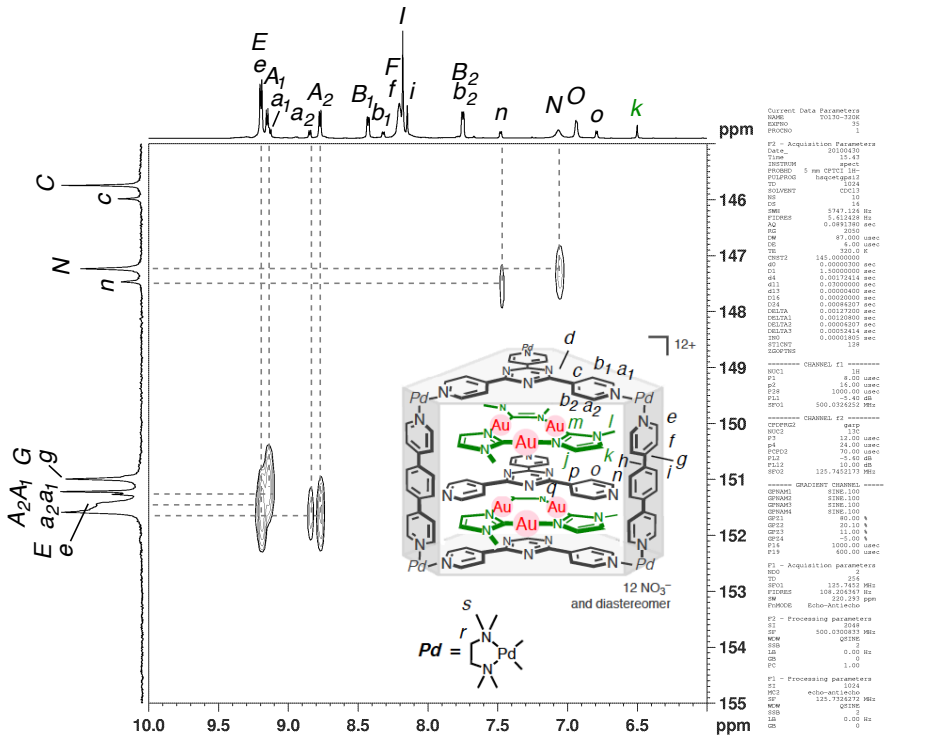

Figure S23. ^{1}H-^{13}C HSQC (500 MHz, D_2O, 320 K) spectrum of **1c'**•(**2a**•**3**•**2a**).

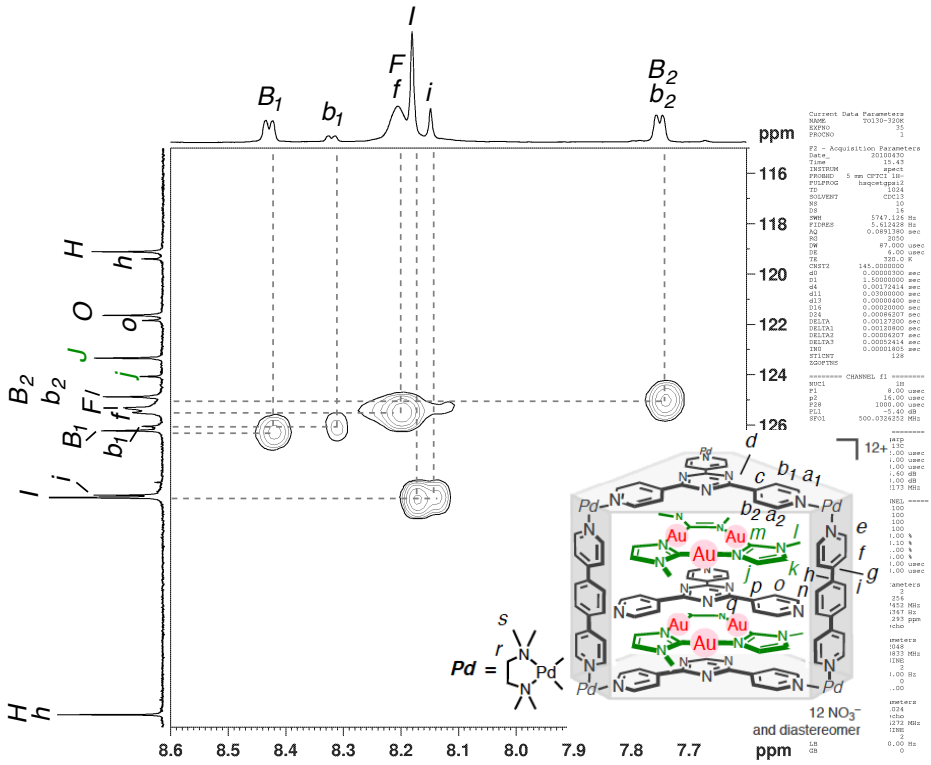

Figure S24. ^{1}H-^{13}C HSQC (500 MHz, D_2O, 320 K) spectrum of **1c'**•(**2a**•**3**•**2a**).

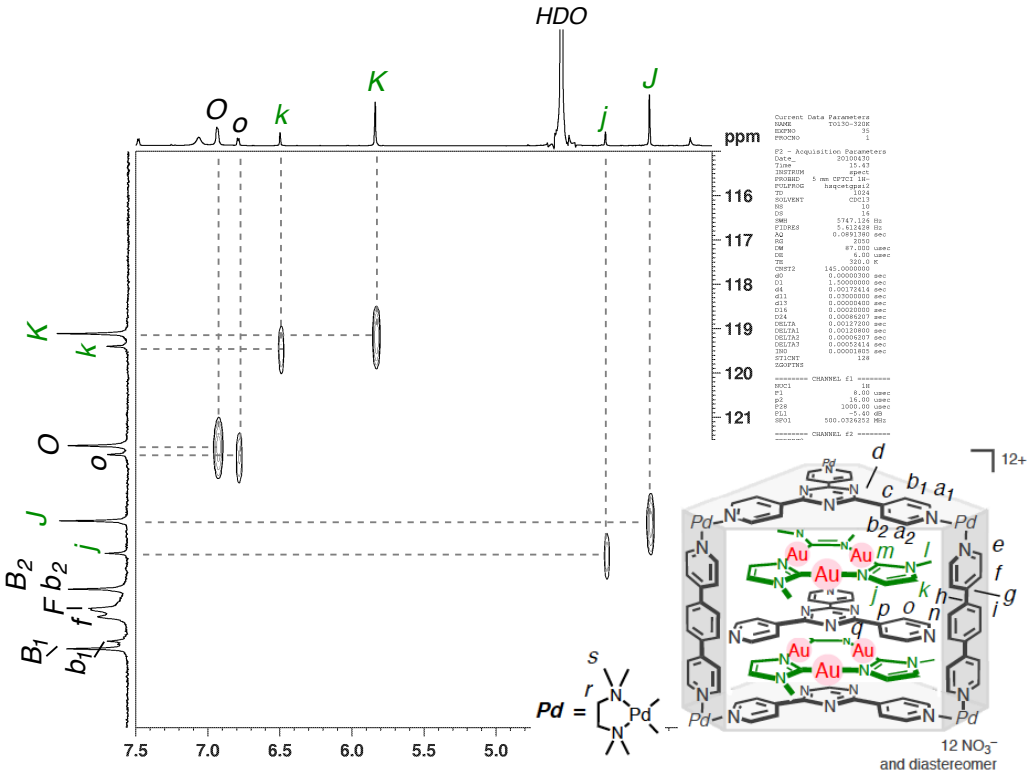

Figure S25. ^{1}H-^{13}C HSQC (500 MHz, D_2O, 320 K) spectrum of **1c'**•(**2a**•**3**•**2a**).

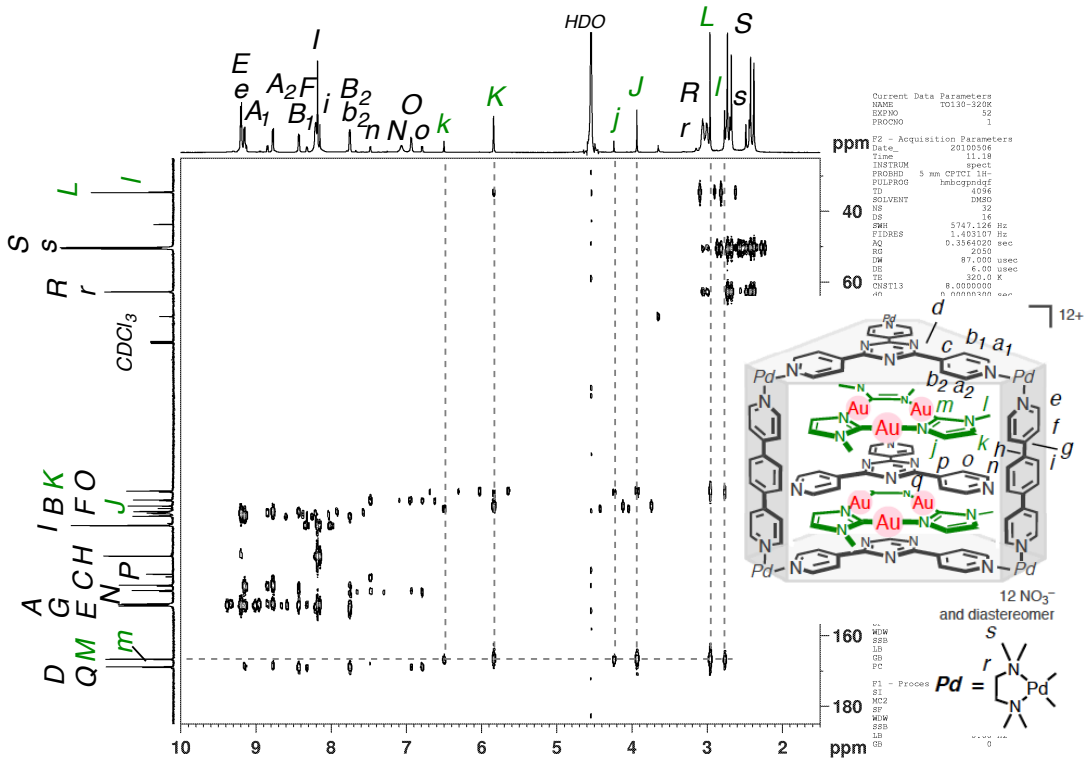

Figure S26. ^{1}H-^{13}C HMBC (500 MHz, D_2O, 320 K) spectrum of **1c'**•(**2a**•**3**•**2a**).

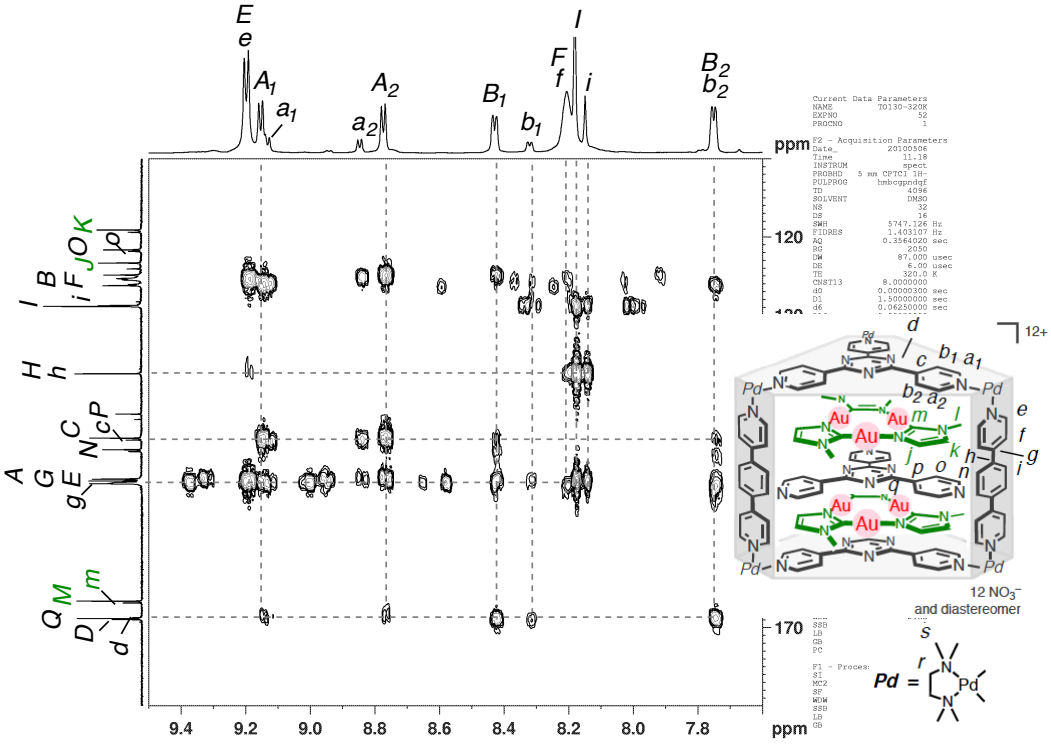

Figure S27. Enlarged ^{1}H-^{13}C HMBC (500 MHz, D_2O, 320 K) spectrum of **1c'**•(**2a**•**3**•**2a**).

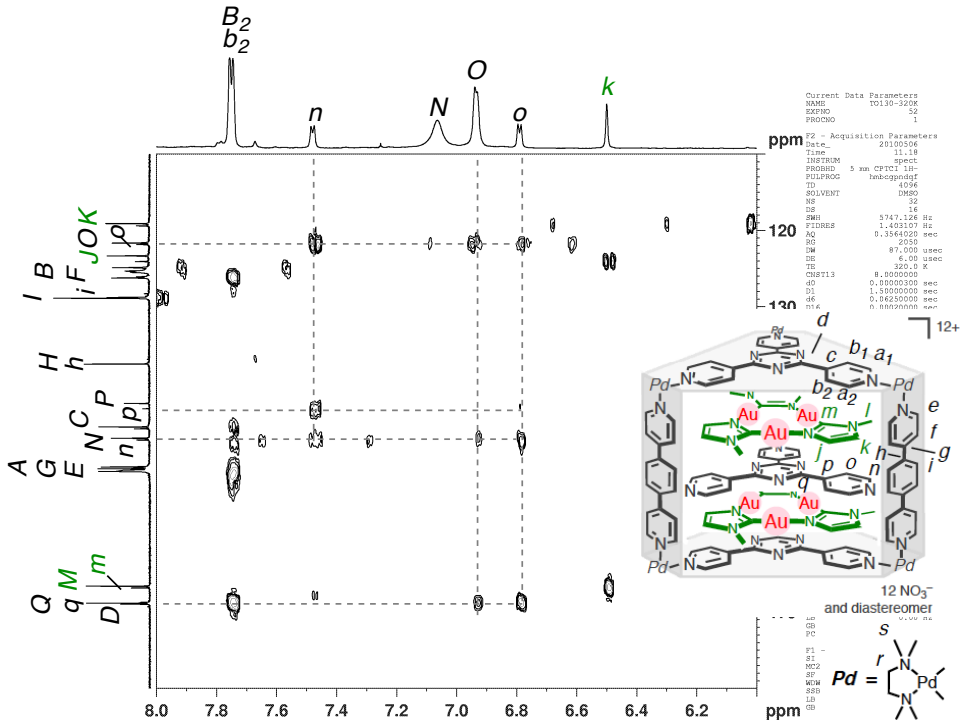

Figure S28. Enlarged ^{1}H-^{13}C HMBC (500 MHz, D_2O, 320 K) spectrum of **1c'**•(**2a**•**3**•**2a**).

Synthesis and Physical Data of Trinuclear Gold Complex 2b

Methyl pyrazole-3,5-dicarboxylate (384 mg, 2.09 mmol) and chloro(dimethylsulfide)gold(I) (615 mg, 2.09 mmol) were dissolved in MeOH–THF (1/1 (v/v), 100 mL). To the resulting clear solution, Et_3N (1mL) was added, and colorless tiny needles appeared within 10 min. Trinuclear Au(I) complex **2b** was obtained by filtration as a white solid (111 mg, 97.3 μmol, 14% yield): ^{1}H NMR (500 MHz, $CDCl_3$, 300 K) δ: 7.57 (s, 3H, pyrazole), 3.98 (s, 18H, methyl). The solubility of the product was not good enough to measure ^{13}C NMR. MALDI-TOF-MS *m/z* calcd for $[M]^+$: 1163.01; found 1162.97. IR (KBr, cm^{-1}): 3143, 2999, 2955, 1749, 1712, 1529, 1483, 1474, 1432, 1408, 1359, 1283, 1263, 1236, 1188, 1170, 1079, 1033, 959, 822, 758. E.A. Calcd. for $C_{12}H_{21}Au_3N_6O_{12}$: C, 22.12; H, 1.86; N, 7.37; Found: C, 22.11; H, 1.92; N, 7.18. m.p. = ~270 ºC (decomposed).

Synthesis and Physical Data of [3 × 3] Au(I) Cluster 1c·(2b)$_3$

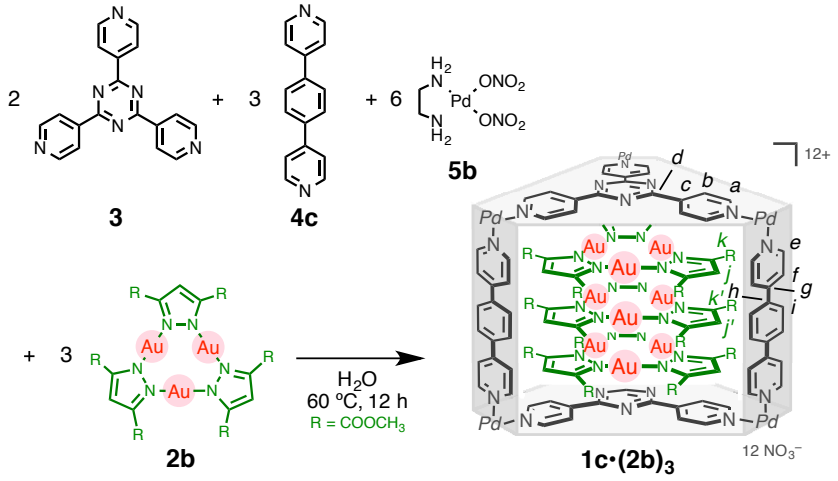

Scheme S4. Synthesis of [3 × 3] Au(I) cluster **1c·(2b)$_3$**.

Panel-like ligand **3** (6.25 mg, 20.0 μmol), pillar-like ligand **4c** (8.65 mg, 30.0 μmol), (en)Pd(ONO$_2$)$_2$ (**5b**; 17.4 mg, 60.0 μmol), and trinuclear Au(I) complex **2b** (45.7 mg, 40.0 μmol) were stirred in water (1.0 mL) at 60 ºC for 12 h. After decantation of the solution, NMR analysis of the redissolved precipitate revealed the selective formation of inclusion complex **1c•(2b)$_3$**. The solution was evaporated and dried by vacuum freeze-drying equipment to give inclusion complex **1c•(2b)$_3$** (20.2 mg, 2.11 μmol, 31%) as a pale yellow solid. ^{1}H NMR (500 MHz, D$_2$O, 300 K) δ: 9.21 (d, J = 6.5 Hz, 12H, **1c**, H^e), 8.87 (d, J = 6.5 Hz, 12H, **1c**, H^a), 8.35 (d, J = 6.5 Hz, 12H, **1c**, H^f), 8.27 (s, 12H, **1c**, H^i), 8.15 (d, J = 6.5 Hz, 12H, **1c**, H^b), 4.77 (s, 3H, **2b**, H$^{j'}$), 4.14 (s, 36H, **2b**, H^m), 3.85 (s, 18H, **2b**, H$^{m'}$), 3.68 (s, 6H, **2b**, H^j), 2.92 (br, 12H, **1c**, ethylenediamine-H), 2.81 (br, 12H, **1c**, ethylenediamine-H). ^{13}C NMR (125 MHz, D$_2$O, 300 K) δ: 169.2 (C, **1c**, C^d), 159.3 (C, **2b**, C^l), 159.1 (C, **2b**, C$^{l'}$), 152.1 (CH, **1c**, C^e), 151.8 (CH, **1c**, C^a), 149.6 (C, **1c**, C^g), 144.1 (C, **1c**, C^c), 141.2 (C, **2b**, C^k), 140.5 (C, **2b**, C$^{k'}$), 136.6 (C, **1c**, C^h), 128.5 (CH, **1c**, C^i), 124.6 (CH, **1c**, C^b), 124.4 (CH, **1c**, C^f), 112.7 (CH, **2b**, C$^{j'}$), 109.4 (CH, **2b**, C^j), 53.1 (CH$_3$, **2b**, C^m), 52.6 (CH$_3$, **2b**, C$^{m'}$), 46.8 (CH$_2$, **1c**, ethylenediamine-C), 46.6 (CH$_2$, **1c**, ethylenediamine-C). ^{1}H DOSY (D$_2$O, 300 K) (m^2/s): D = 1.4 × 10^{-10}. E.A. Calcd. for C$_{159}$H$_{171}$Au$_9$N$_{60}$O$_{72}$Pd$_6$·(D$_2$O)$_8$: C, 28.74; H, 3.08; N, 12.65; Found: C, 28.96; H, 3.22; N, 12.42. IR (KBr, cm^{-1}): 3434 (br), 3227 (br), 2954, 2766, 1717, 1615, 1518, 1383 (br), 1259 (br), 1171, 1082, 1060, 808. m.p. = ~215 ºC (decomposed).

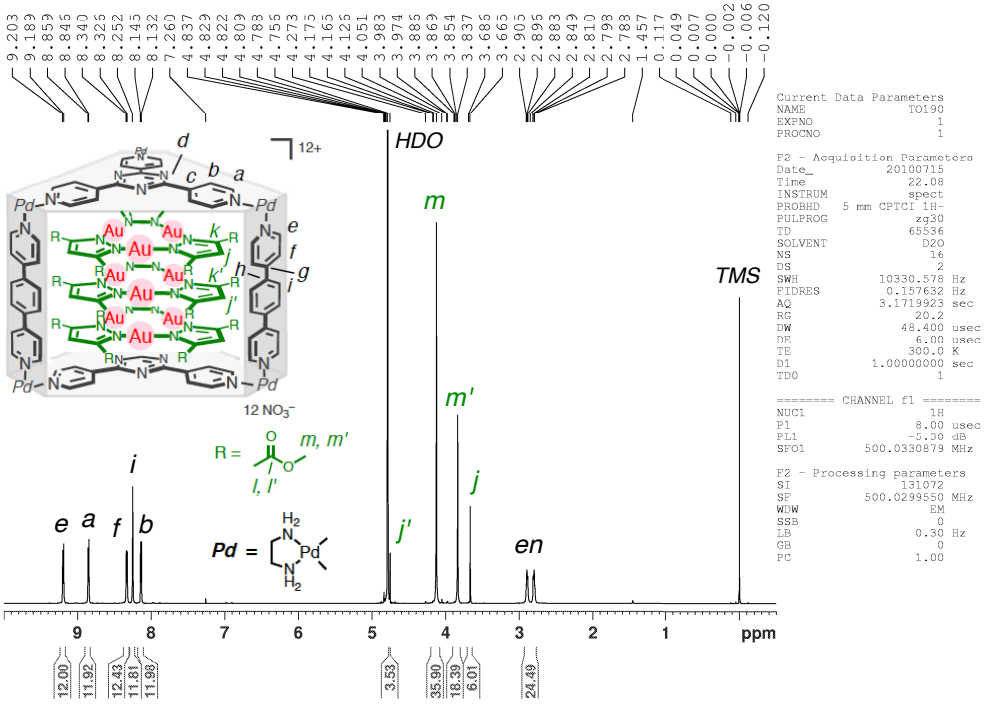

Figure S29. ^{1}H NMR (500 MHz, D_2O, 300 K) spectrum of **1c**•(**2b**)$_3$.

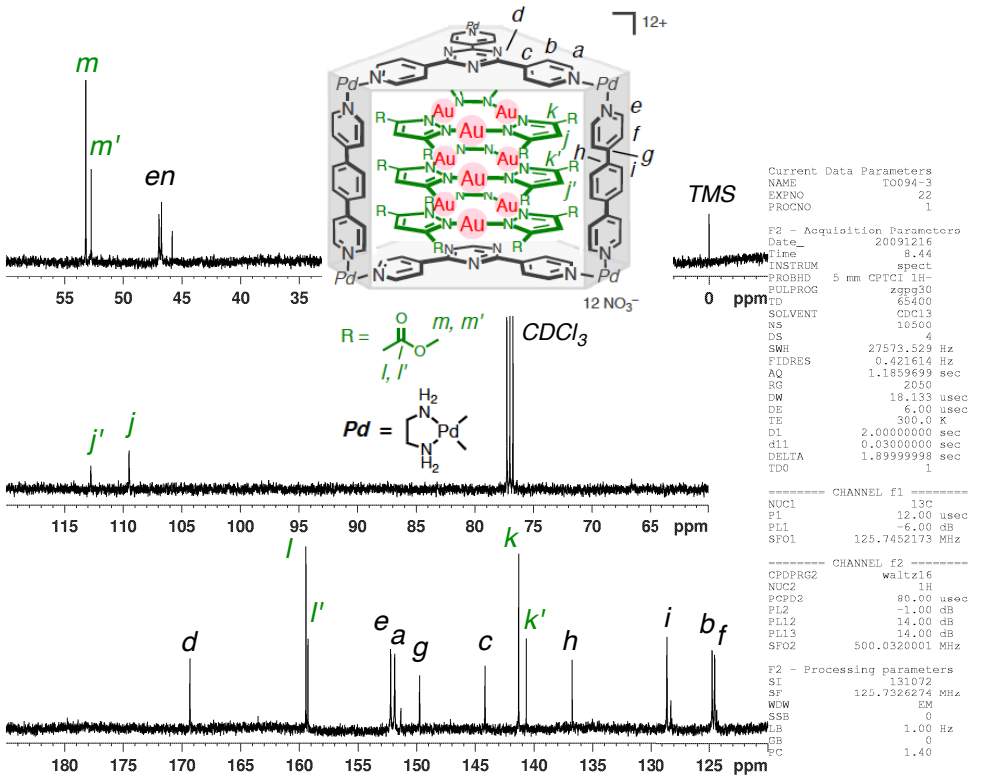

Figure S30. ^{13}C NMR (125 MHz, D_2O, 300 K) spectrum of **1c**•(**2b**)$_3$.

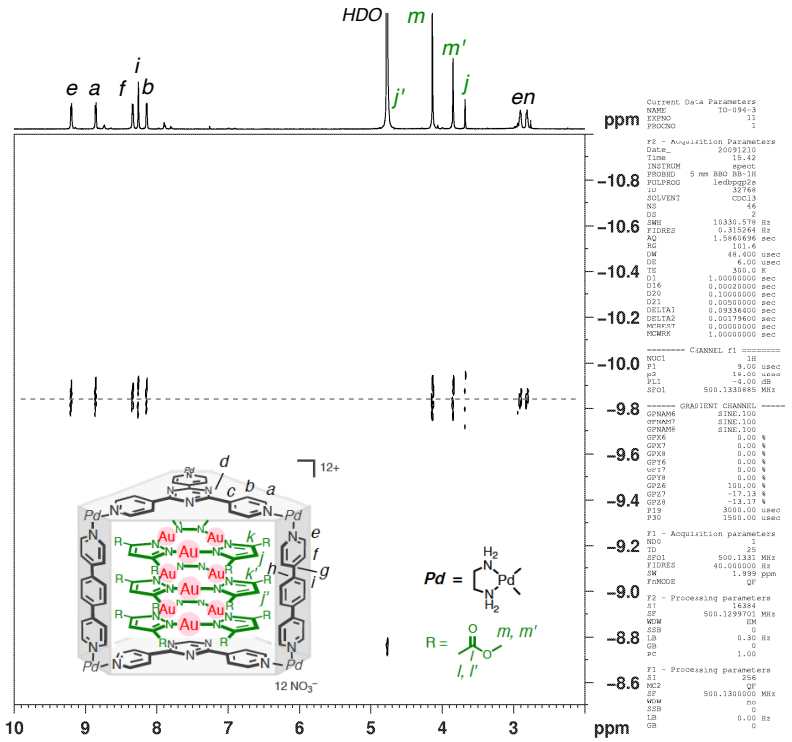

Figure S31. ^{1}H DOSY (500 MHz, D_2O, 300 K) spectrum of **1c**•(**2b**)$_3$.

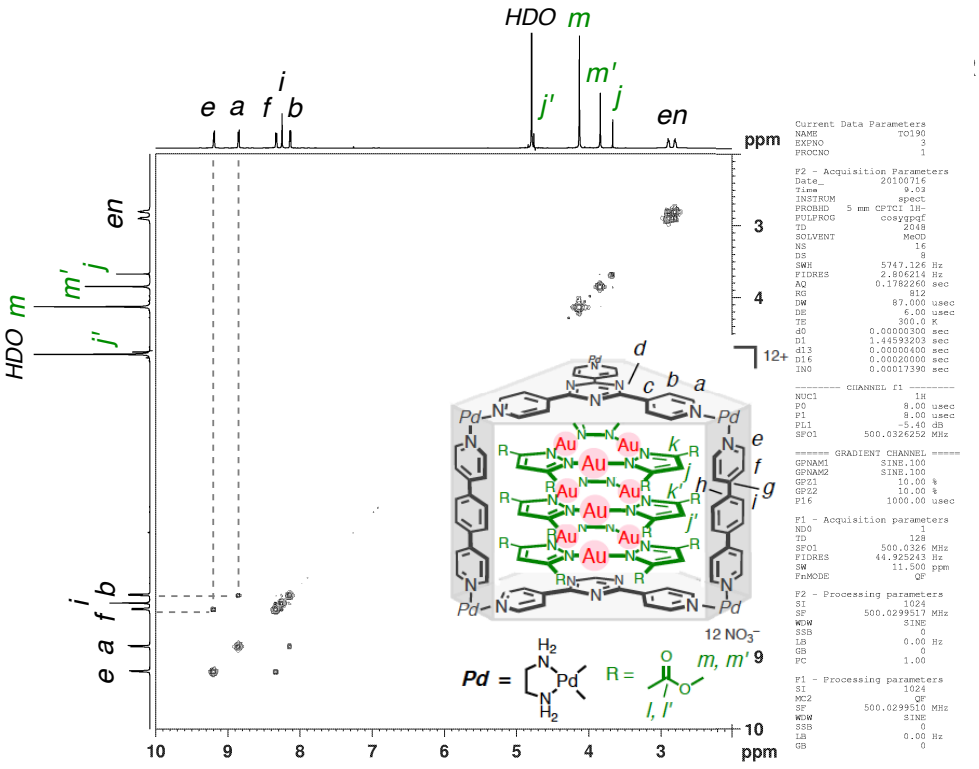

Figure S32. ^{1}H-^{1}H COSY (500 MHz, D_2O, 300 K) spectrum of **1c**•(**2b**)$_3$.

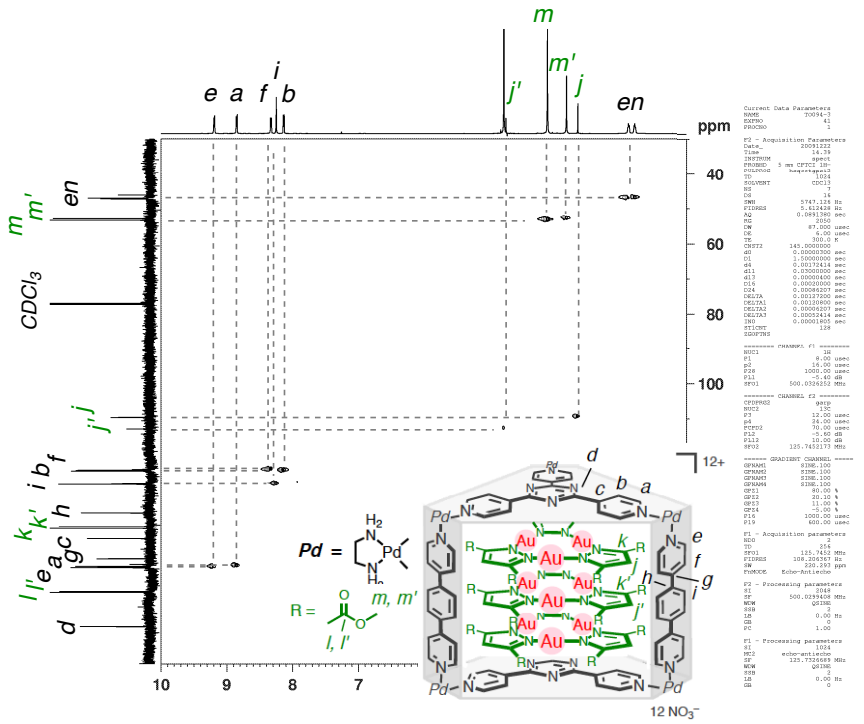

Figure S33. ^{1}H-^{13}C HSQC (500 MHz, D_2O, 300 K) spectrum of **1c**•(**2b**)$_3$.

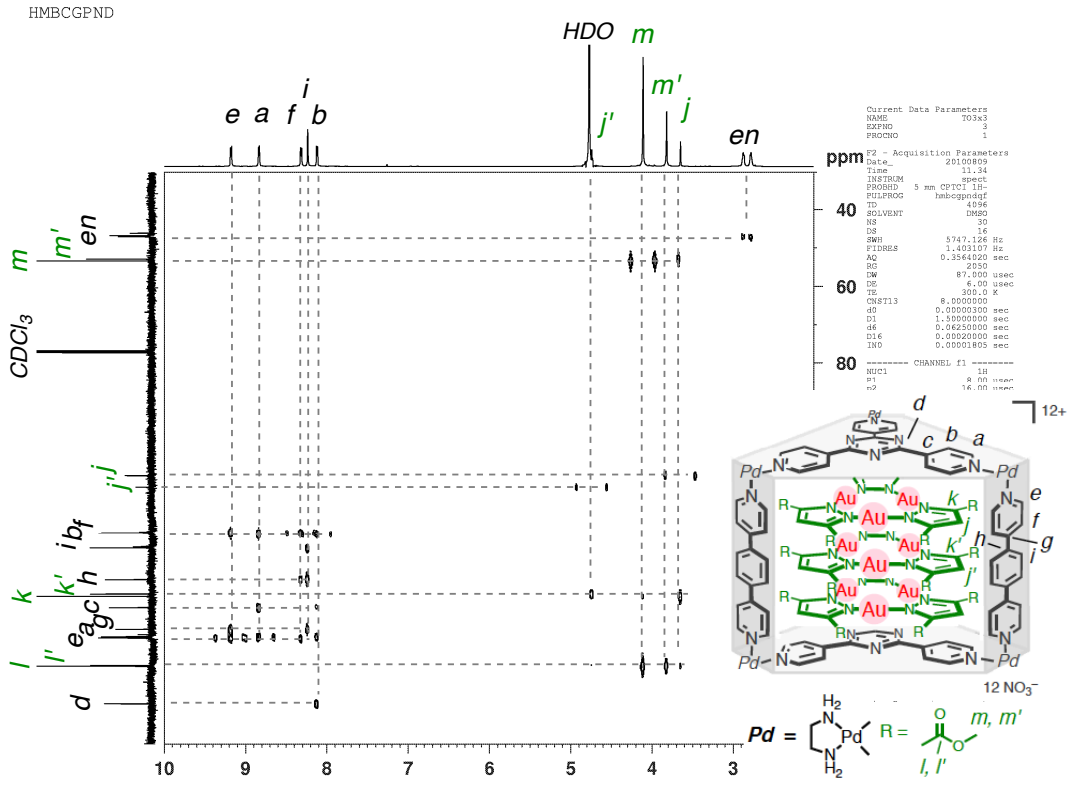

Figure S34. ^{1}H-^{13}C HMBC (500 MHz, D_2O, 300 K) spectrum of **1c**•(**2b**)$_3$.

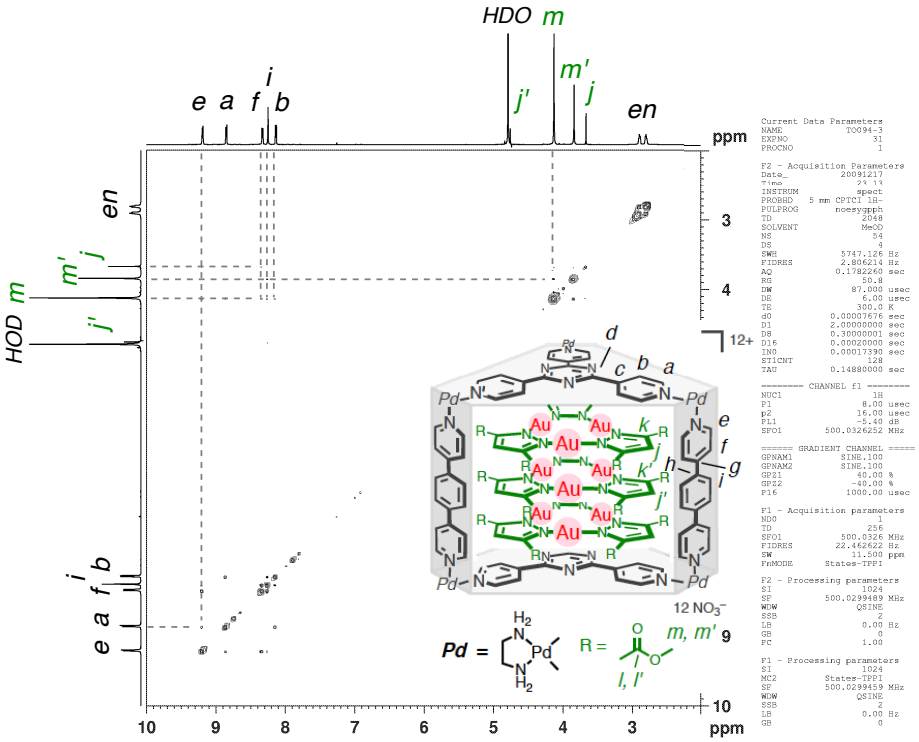

Figure S35. ^{1}H-^{1}H NOESY (500 MHz, D_2O, 300 K) spectrum of **1c**•(**2b**)$_3$.

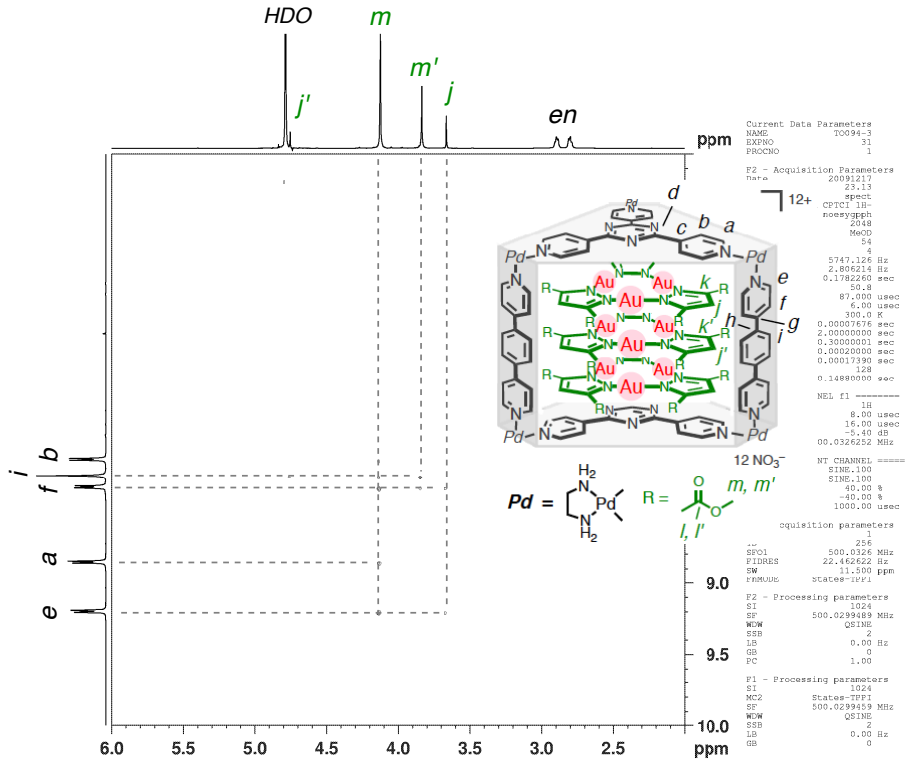

Figure S36. Enlarged ^{1}H-^{1}H NOESY (500 MHz, D_2O, 300 K) spectrum of **1c**•(**2b**)$_3$.

Table S1. Crystal data and structure refinement for **1c·(2b)$_3$**.

Identification code	p1	
Empirical formula	C366 H438 Au18 N97.50 O189.50 Pd12	
Formula weight	14057.34	
Temperature	90(2) K	
Wavelength	0.71073 Å	
Crystal system	Triclinic	
Space group	*P*-1	
Unit cell dimensions	a = 18.571(9) Å	α = 83.515(6)°.
	b = 30.944(16) Å	β = 87.051(6)°.
	c = 47.850(20) Å	γ = 89.237(6)°.
Volume	27285(24) Å^3	
Z	2	
Density (calculated)	1.711 Mg/m^3	
Absorption coefficient	5.291 mm^{-1}	
F(000)	13613	
Crystal size	0.14 x 0.08 x 0.07 mm^3	
Theta range for data collection	0.75 to 24.35°	
Index ranges	-21<=h<=21, -35<=k<=35, -55<=l<=55	
Reflections collected	243884	
Independent reflections	88380 [R(int) = 0.0849]	
Completeness to theta = 24.35°	98.9 %	
Absorption correction	Semi-empirical from equivalents	
Max. and min. transmission	0.7083 and 0.5246	
Refinement method	Full-matrix least-squares on F^2	
Data / restraints / parameters	88380 / 997 / 3139	
Goodness-of-fit on F^2	1.027	
Final R indices [I>2sigma(I)]	R_1 = 0.1331, wR_2 = 0.2875	
R indices (all data)	R_1 = 0.2410, wR_2 = 0.3523	
Largest diff. peak and hole	5.394 and -7.399 e.Å^{-3}	
CCDC reference number	792086	

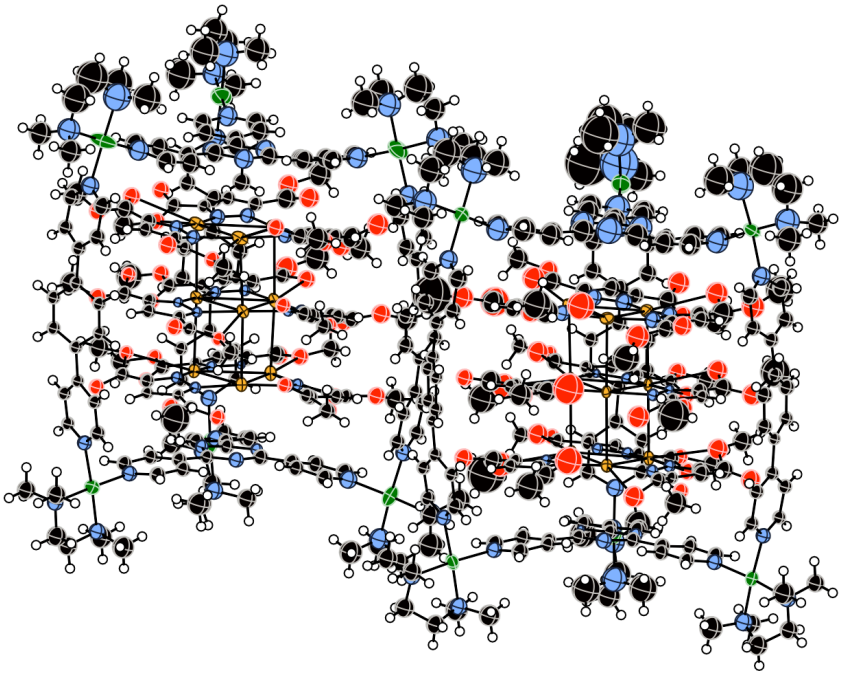

Figure S37. ORTEP drawing (30% probability ellipsoids) of [3 × 3] Au(I) cluster **1c·(2b)$_3$**. Counter anions ($NO3^-$) and solvents are omitted for clarity.

Chapter 3

Multiple-Decker Gold-Silver Ion Clusters Template by Coordination Cages

Abstract

Box-shaped coordination cages are suitable platforms for discrete stacks of trinuclear $Au(I)_3$ complexes to form [3 × *n*] Au(I) clusters (*n* = 1–3). In this study, Ag(I) ions were introduced into the Au(I) clusters, and subsequent formation of Au_3–Ag–Au_3 and Au_3–Ag–Au_3–Ag–Au_3 hetero ion clusters were confirmed by NMR and X-ray structural analysis. These double- and triple-decker alignments of metal ions are composed of alternate stacks of trinuclear $Au(I)_3$ complexes and Ag(I) ions within the cages, and X-ray analysis revealed that Au(I)-Ag(I) attractive interactions contributed to their aggregation. Interestingly, the triple-decker alignment, namely Au_3–Ag–Au_3–Ag–Au_3 ion cluster, was only available within the box-shaped confined cage.

3.1 Introduction

Precise synthesis of metal ion clusters has attracted increasing interest for understanding of their properties depending on the species, number, and array of component metal ions.[1–4] There have been several examples of the synthesis of one- and two-dimensional metal ion arrays with the help of multidentate ligands.[5–10] Metal ions are fixed in close proximity with the equally spaced binding sites through coordination bonds, while this means that elaborated and sophisticated ligand design is always demanded. In particular, precise three-dimensional arrangement of metal ion arrays is not easy owing to the steric complexity, especially in solution.

On the other hand, metal ions with a closed shell d^{10} electron configurations such as Au(I), Ag(I), and Cu(I), often aggregate through attractive metal-metal interactions and form polymeric systems in the solid states.[11,12] Since the infinity of metal ion polymers propagates one-, two-, and three-dimensions, the d^{10}–d^{10} interactions have been employed to engineer a variety of functional materials. For example, cyclic trinuclear $Au(I)_3$ complexes $[\mu\text{-}N^1,C^2\text{-bzimAu}]_3$ interact with Ag(I) ions to produce $[Au_3–Ag–Au_3]_n$ linear chains in the crystalline state (Figure 1).[13] A repeating unit of the infinite chain consists of a double-decker $Au_3–Ag–Au_3$ cluster with short Au(I)···Ag(I) contacts. On the basis of these observations, discrete metal ion arrays (i.e., metal ion clusters) seem to be efficiently prepared via d^{10}–d^{10} interactions.[14–19] However, there seems no efficient, simple method for generating metal ion clusters owing to the relative weakness of the interactions.[20–22] In fact, the stability of the foregoing $Au_3–Ag–Au_3$ repeating unit in a solution state is not clear.

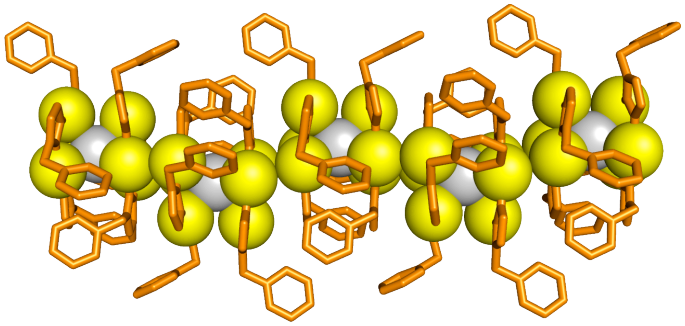

Figure 1. X-ray crystal structure of a $[Au_3–Ag–Au_3]_n$ infinite chain. Two molecules of Imidazolate-bridged $Au(I)_3$ complex $[\mu\text{-}N^1,C^2\text{-bzimAu}]_3$ sandwich an Ag(I) ion through Au(I)–Ag(I) interactions and form $[Au_3–Ag–Au_3]_n$ infinite crystalline chains. All hydrogens are omitted for clarity (Au: yellow, Ag: gray, Bridging ligands: orange).

Furthermore, precise control of the number of component metal ions in the cluster is also a matter of debate. Other types of the alignment of $Au(I)_3$ complexes and Ag(I) ions, such as triple (and higher)-decker sandwich units, are not found even in the crystalline states.[23,24]

In this chapter, I conceived an idea that a well-defined, confined cavity can stabilize weakly associated Au(I)–Ag(I) clusters. In chapter 2, I reported that [3 × *n*] Au(I) ion clusters were constructed as discrete stacks of planar trinuclear $Au(I)_3$ complexes **2**[25] within box-shaped cages **1**, in which the stack number (*n* = 1–3) was determined in advance by the height of each cage (Figure 2).[26] Within the cage, intermolecular Au(I)–Au(I) interactions contributed to the formation of trigonal prismatic array of Au(I) ions. Keeping this in mind, Ag(I) ions were added to the Au(I) clusters to form Au(I)–Ag(I) hetero clusters. Accordingly, Au_3–Ag–Au_3 and Au_3–Ag–Au_3–Ag–Au_3 multi-decker ion clusters were prepared within the cages **1** as alternate stacks of imidazolate-bridged trinuclear $Au(I)_3$ complexes **2a** and Ag(I) ions. In particular, the triple-decker alignment of $Au(I)_3$ complexes and Ag(I) ions is the first example that is only accessible with the help of the cage.

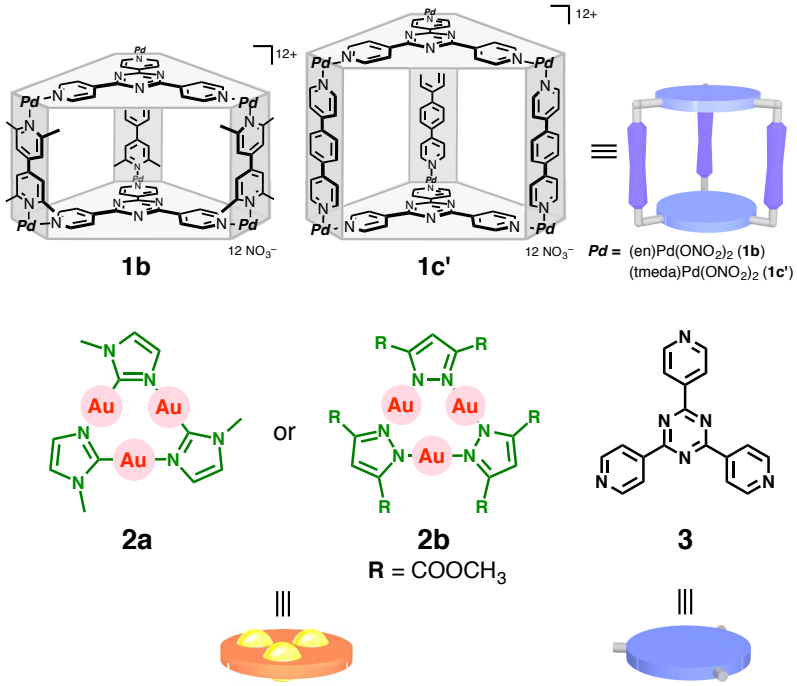

Figure 2. Box-shaped coordination cage 1, accumulated trinuclear $Au(I)_3$ complexes 2, and planar panel 3. Adapted with permission from *Angew. Chem. Int. Ed.* **2012**, *51*, 12199–12201. Copyright (2012) John Wiley and Sons.

3.2 Double-Decker Au(I)–Ag(I) Cluster 1b•(2a•Ag^+•2a)

When $AgNO_3$ (1.70 mg, 0.010 mmol) was added to an aqueous solution of [3 × 2] Au(I) ion cluster **1b**•(**2a**)$_2$ (46.7 mg, 0.010 mmol),[26] the solution color changed from orange to pale yellow (Figure 3a). The absorption spectra clearly revealed that [3 × 2] Au(I) ion cluster **1b**•(**2a**)$_2$ took up one equivalent of Ag(I) ions. The CT band, which is formed via charge transfer from electron-rich guest **2a** (donor, D) to the electron deficient panels **3** (acceptor, A) of cage **1b**, showed a decrease in absorbance at 430 nm and an increase at 350 nm, together with the appearance of an isosbestic point at 380 nm (Figure 3b). Spectrophotomeric titration curve at 350 nm elucidated a 1:1 association and the association constant to be 1.5×10^6 M^{-1} (Figure 3c). In the ^{1}H NMR spectroscopy as well, the signals of guests **2a** within the cage shifted downfield ($\Delta\delta \sim$ 0.3 ppm) upon addition of Ag(I) ions with the cage retained D_{3h} symmetry (Figure 3d,e). These observations concluded that one Ag(I) ion was bound between the pair of Au(I)$_3$ complexes **2a** within cage **1b** to form Au_3–Ag–Au_3 double-decker ion cluster **1b**•(**2a**•Ag^+•**2a**). The binding of Ag(I) ions with [3 × 2] Au(I) cluster **1b**•(**2a**)$_2$ was specific: the binding of similar-sized alkali ions was not observed. Furthermore, the Ag(I) ion binding was irreversible: AgCl precipitation was not observed upon addition of NH_4Cl (10 equiv.). Also, the Au_3–Ag–Au_3 ion cluster is inert within the cage: photoinduced Ag(0) colloids did not form under UV light irradiation.

The alignment of the metal ions was clearly visualized by single crystal X-ray analysis (Figure 4). Pale yellow crystals suitable for X-ray analysis were obtained by slow evaporation of an aqueous solution of Au_3–Ag–Au_3 double-decker ion cluster **1b**•(**2a**•Ag^+•**2a**) for about two weeks. The result showed that one Ag(I) ion was bound between two molecules of guest Au(I)$_3$ complexes **2a** within cage **1b**. Each Au(I)$_3$ guest **2a** was disordered into two portions around the vertical axis of the cage, indicating the possible rotation of guest **2a**. The Au_3–Ag–Au_3 alignment is the same as a unit of aforementioned [Au_3–Ag–Au_3]$_n$ crystalline chain composed of a similar Au(I) trinuclear complex and Ag(I) ions (Figure 1).[13] The short contacts of Au and Ag atoms in the cluster ranged from 2.774 to 2.818 Å, which are close to those found in an infinite [Au_3–Ag–Au_3]$_n$ crystalline chain (2.731–2.922 Å). As these Au···Ag distances are shorter than the sum of the van der Waals radii (3.4 Å),[27] this result indicates the existence of effective Au(I)–Ag(I) interactions.

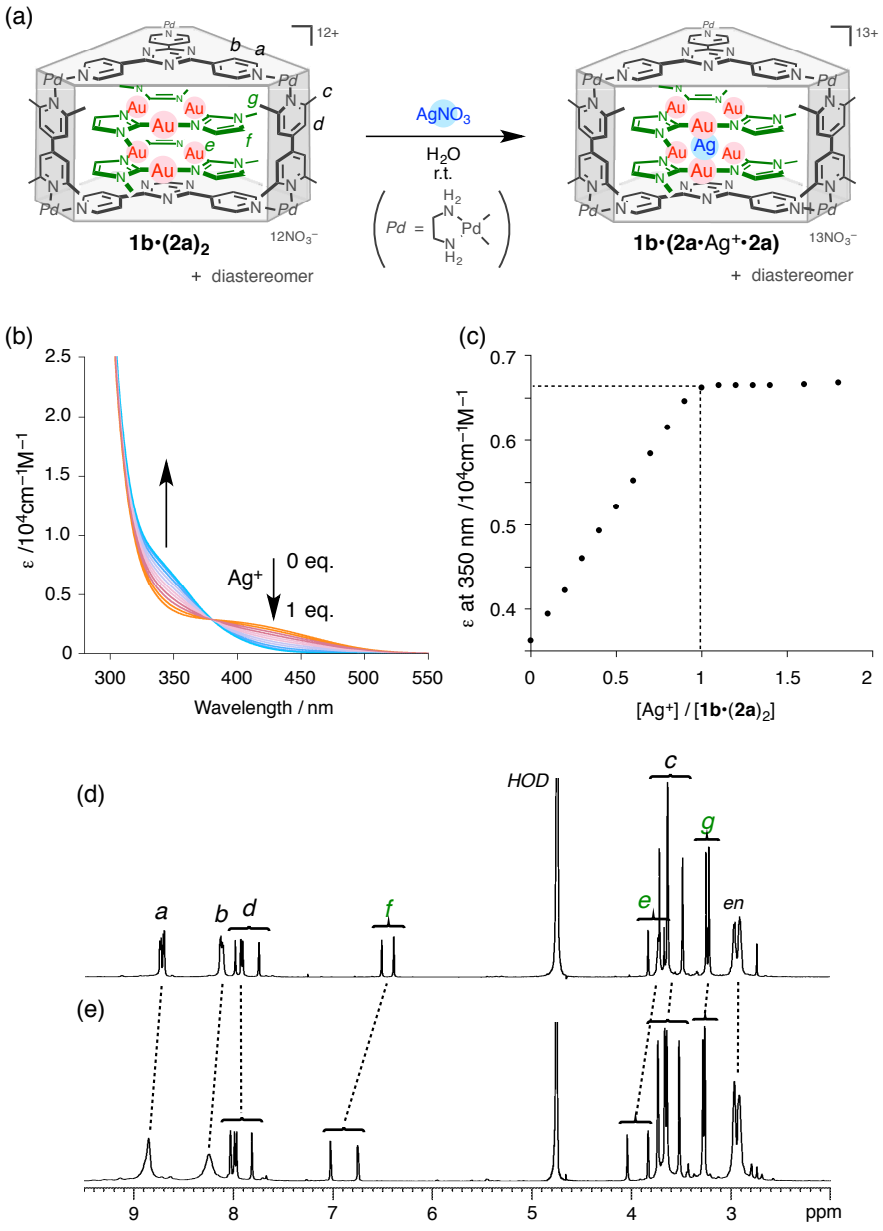

Figure 3. Au_3–Ag–Au_3 double-decker ion cluster 1b•(2a•Ag^+•2a). (a) Formation of Au_3–Ag–Au_3 double-decker ion cluster **1b**•(**2a**•Ag^+•**2a**) by insertion of Ag(I) ions into [3 × 2] Au(I) cluster **1b**•(**2a**)$_2$. (b) Change in the absorption spectra of [3 × 2] Au(I) cluster **1b**•(**2a**)$_2$ as the subsequent addition of $AgNO_3$. [**1b**•(**2a**)$_2$] = 0.10 mM in H_2O (3.2 mL, 1 cm cell). (c) Titration curve of the absorption spectra Indicates a 1:1 aggregation of cluster **1b**•(**2a**)$_2$ and $AgNO_3$ (at λ = 350 nm). (d,e) ^{1}H NMR spectrum (500 MHz, 300 K, D_2O) of (d) cluster **1b**•(**2a**)$_2$ and (e) **1b**•(**2a**•Ag^+•**2a**). Upon addition of Ag(I) ions, the signals of guest $Au(I)_3$ complex **2a** shifted downfield. The broaden signals ($H_{a,b}$) of cage **1b** indicate the bulkiness of guest moiety **2a**•Ag^+•**2a** prevents free rotation of pyridyl groups.

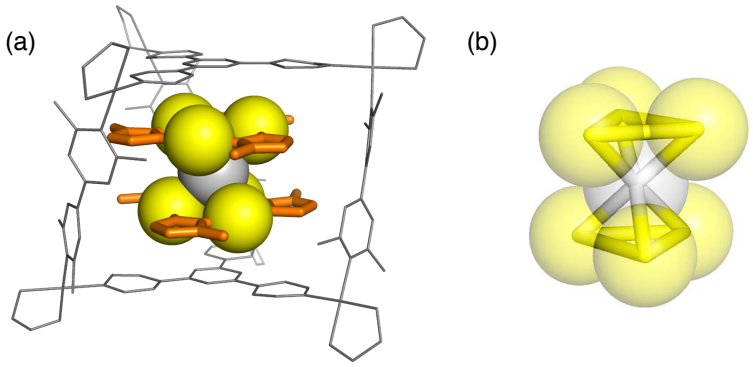

Figure 4. X-ray crystal structure of Au_3–Ag–Au_3 double-decker metal ion cluster 1b•(2a•Ag^+•2a). (a) The largest portion of the disordered guest molecule is shown and discussed in this study. The color codes are the same as those of Figure 1 (Box-shaped cage: black). All hydrogens are omitted for clarity. The guest $Au(I)_3$ complexes **2a** stack in a staggered mode with an Ag(I) ion binding. (b) Highlight of the Au_3–Ag–Au_3 array. The short contacts between Au ions less than 3.6 Å and Au–Ag ions less than 3.4 Å are shown in the solid lines.

3.3 Triple-Decker Au(I)–Ag(I) Cluster 1c'•(2a•Ag^+•2a•Ag^+•2a)

The synthesis of triple-decker Au(I)–Ag(I) cluster was not straightforward. To synthesize the desired cluster, I went through three types of synthetic routes (Figure 5). First of all, the same procedure to prepare double-decker cluster **1b**•(**2a**•Ag^+•**2a**) was applied, however [3 × 3] Au(I) cluster **1c**•(**2b**)$_3$[26] did not take up Ag(I) ions (path a, in Figure 5). This result indicates that the electric interaction between electron-rich trinuclear $Au(I)_3$ complexes and Ag(I) cations is one of the most important factor of the Au(I)–Ag(I) interaction,[28–30] and that electron-donor ability of pyrazolete-bridged $Au(I)_3$ complex **2b** used for [3 × 3] Au(I) cluster is not strong enough to bind Ag(I) ions. In consequence, the triple stack of electron-rich[31–33] imidazlate-bridged $Au(I)_3$ complexes **2a**[34] that is used for the component of [3 × 2] Au(I) cluster **1b**•(**2a**)$_2$, seems to be desirable for the precursor complex, but formation of Au(I) cluster **1c**•(**2a**)$_3$ failed owing to the electron repulsion between electron-rich $Au(I)_3$ complexes **2a**. Beside this, one-step accommodation of the all guest molecules (i.e., three $Au(I)_3$ **2a** and two Ag(I) ions) into empty cage **1c** (path b) is quite simple, but was not possible, because cage **1c** was not stable in the absence of guest molecules.

After consideration of various paths, I achieved to synthesize the desired

Au_3–Ag–Au_3–Ag–Au_3 hetero ion cluster **1c'•(2a•Ag^+•2a•Ag^+•2a)** by a guest exchange process (path c). As I previously mentioned in chapter 2, self-assembled complex **1c'•(2a•3•2a)** was obtained by chance during an attempt to prepare the [3 × 3] Au(I) cluster. Electron-rich $Au(I)_3$ complexes **2a** (donor, D) sandwiched electron-deficient panel ligand **3** (acceptor, A) and formed stable alternate D–A–D stack within the cage. Then, $AgNO_3$ (10.20 mg, 0.060 mmol) and additional $Au(I)_3$ complex **2a** (33.36 mg, 0.040 mmol) were combined in an aqueous solution (1.0 mL) of the precursor self-assembled complex **1c'•(2a•3•2a)** (53.8 mg, 0.010 mmol) (Figure 6a). The suspended mixture was stirred at 40 ºC for 12 h. After filtration of the resulting pale yellow solution, the ^{1}H NMR spectroscopy determined the quantitative exchange of guest moieties and formation of an Au_3–Ag–Au_3–Ag–Au_3 triple-decker ion cluster **1c'•(2a•Ag^+•2a•Ag^+•2a)**.

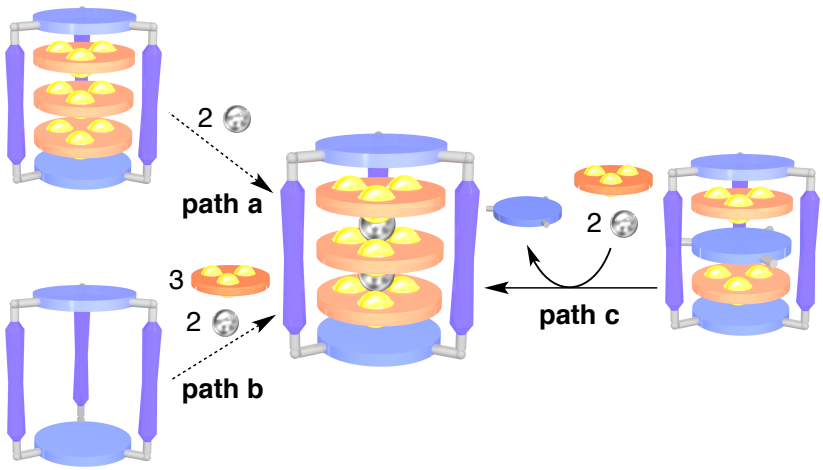

Figure 5. Schematic representation of three paths for the preparation of the Au–Ag triple-decker ion cluster within the self-assembled coordination cage. Adapted with permission from *Angew. Chem. Int. Ed.* **2012**, *51*, 12199–12201. Copyright (2012) John Wiley and Sons.

In the ^{1}H NMR spectrum, seven sets of signals for $H_{a–c}$ of guest **2a** were observed in a 2:2:2:2:2:1:1 integral ratio (Figure 6b). This result indicates that C_{3h} symmetrical guest **2a** can orient either clockwise (+) or counterclockwise (–), and forms a triple-stack with three possible stacking modes: (+, +, +), (+, +, –), and (+, –, +) within cage **1c'** (Figure 6c). In case of diastereomer (+, +, +) and (+, –, +), two sets of guest signals appear in a 2:1 ratio, whereas diastereomer (+, +, –) shows three signals in

a 1:1:1 ratio. In consequence, totally seven signals should be observed. Moreover, the ratio of the seven signals indicates that the three diastereomers exist in a 1:1:2 ratio, that is, in a statistical distribution. Because triple stacks of electron-rich $Au(I)_3$ complex **2a** was not available until the addition of Ag(I) ions into the system, this result shows the formation of an Au_3–Ag–Au_3–Ag–Au_3 triple-decker ion cluster **1c'•(2a•Ag^+•2a•Ag^+•2a)**. In the diffusion-ordered NMR spectroscopy (DOSY) spectrum, all signals derived from three diasteromers of the Au_3–Ag–Au_3–Ag–Au_3 complex showed a same diffusion constant ($D = 1.4 \times 10^{-10}$ m^2s^{-1}).

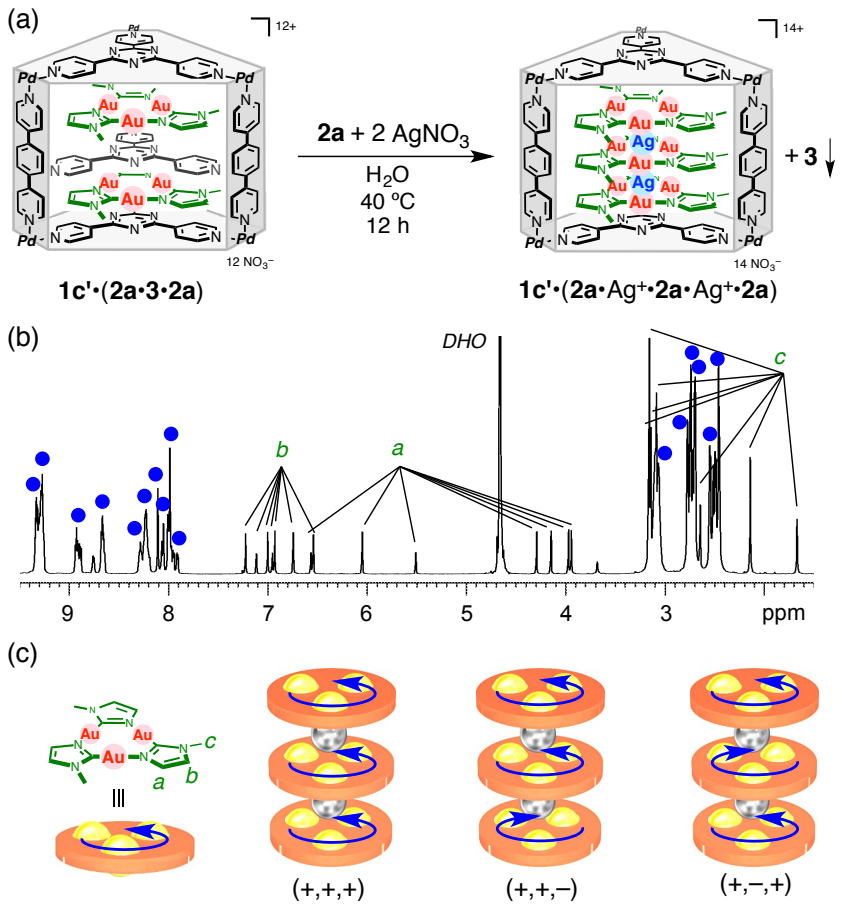

Figure 6. Au_3–Ag–Au_3–Ag–Au_3 triple-decker ion cluster 1c'•(2a•Ag^+•2a•Ag^+•2a). (a) Formation of Au_3–Ag–Au_3–Ag–Au_3 triple-decker ion cluster **1c'•(2a•Ag^+•2a•Ag^+•2a)** by guest exchange from self-assembled complex **1c'•(2a•3•2a)**. (b) The ^1H NMR spectrum of triple-decker cluster **1c'•(2a•Ag^+•2a•Ag^+•2a)** (500 MHz, 310 K, D_2O). Blue circles indicate the signals of cage **1c'**. (c) Cartoon representations of three stacking modes of the triple stacked guests. Adapted with permission from *Angew. Chem. Int. Ed.* **2012**, *51*, 12199–12201. Copyright (2012) John Wiley and Sons.

The structure of the triple-decker Au(I)–Ag(I) cluster was also determined by single-crystal X-ray analysis (Figure 7). Three $Au(I)_3$ complex **2a** and two Ag(I) ions alternately stack in cage **1c'** and the stacking motif of $Au(I)_3$ complexes **2a** is similar to that of double-decker cluster **1b•(2a•Ag^+•2a)**, namely a staggered mode. Au(I)–Ag(I) interactions are visible, as Au···Ag short contacts range from 2.694 to 2.823 Å, which are close to those observed in double-decker cluster **1b•(2a•Ag^+•2a)** and the crystalline chain.

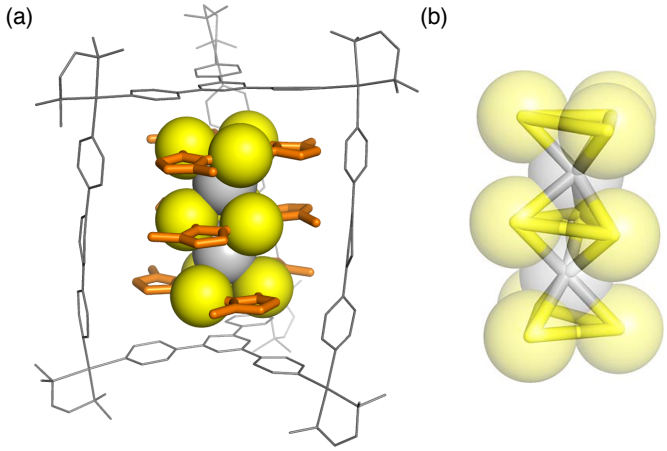

Figure 7. X-ray crystal structure of Au_3–Ag–Au_3–Ag–Au_3 triple-decker ion cluster 1c'•(2a•Ag^+•2a•Ag^+•2a). (a) In this figure, the largest portion of disordered molecule is shown (the color codes are the same as those of Figures 1,4). The guest $Au(I)_3$ complexes **2a** stack in a staggered orientation through Ag(I) ions. (b) Highlight of the Au_3–Ag–Au_3–Ag–Au_3 array.

3.4 Absorption Spectra

The effect of the Ag(I) ion insertion to the stacking aromatics was clearly visible in UV-vis absorption spectra (Figure 8). The strong charge transfer (CT) band from electron-rich guest **2a** to electron-deficient panel of the cage, was observed for the [3 × 2] Au(I) cluster **1b•$(2a)_2$** at around 415 nm (ε = 3000 $M^{-1}cm^{-1}$) (Figure 8a). In contrast, only a weak CT band (shoulder) was observed for Au(I)–Ag(I) double-decker cluster **1b•(2a•Ag^+•2a)** and triple-decker cluster **1c'•(2a•Ag^+•2a•Ag^+•2a)** at 355 nm (Figure 8b,c) because the electron density of guest **2a** decreased. Additionally, as the HOMO levels of Au–Ag ion sandwich clusters **2a•Ag^+•2a**, and **2a•Ag^+•2a•Ag^+•2a** are lower than that of [3 × 2] Au(I) homo cluster $(2a)_2$, these CT bands showed blue shift.

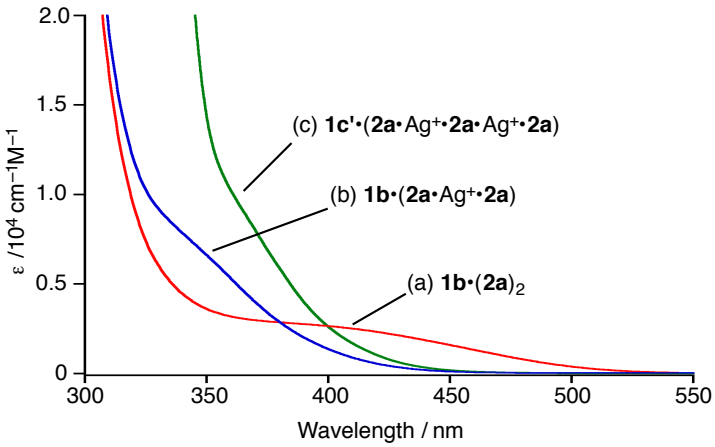

Figure 8. UV-visible sptctra (RT, 1.0 mM) of the ion clusters. (a) [3 × 2] Au(I) cluster **1b**•(**2a**)$_2$, (b) Au_3–Ag–Au_3 ion cluster **1b**•(**2a**•Ag^+•**2a**), and (c) Au_3–Ag–Au_3–Ag–Au_3 ion cluster **1c'**•(**2a**•Ag^+•**2a**•Ag^+•**2a**). Adapted with permission from *Angew. Chem. Int. Ed.* **2012**, *51*, 12199–12201. Copyright (2012) John Wiley and Sons.

3.5 Conclusion

In this chapter, I successfully synthesized Au(I)–Ag(I) hetero ion clusters by alternate stacks of $Au(I)_3$ complexes and Ag(I) ions within the self-assembled coordination cages. Particularly, a discrete Au_3–Ag–Au_3–Ag–Au_3 alignment was only available with the help of the cage. Each Ag(I) ion in the clusters was surrounded by six Au(I) ions and supported through metal-metal attractive interactions. This result demonstrates that the box-shaped cages not only arrange coordination sites of organic ligands as shown in chapter 2, but also provide the place to allocate metal ions through metal-metal interactions. Because the cage height can be precisely adjusted, the family of cage **1** are potential platforms for the synthesis of large Au(I)–Ag(I) multi-decker clusters. Moreover, this method will be applicable to obtain other metal clusters simply by using the appropriate template complexes and metal ions.

3.6 References

[1] D. Gatteschi, A. Caneschi, L. Pardi, R. Sessoli, *Science*, **1994**, *265*, 1054–1058.

[2] G. Schmid, M. Bäumle, M. Geerkens, I. Heim, C. Osemann, T. Sawitowski, *Chem. Soc. Rev.* **1999**, *28*, 179–185.

[3] J. Zheng, C. Zhang, R. M. Dickson, *Phys. Rev. Lett*. **2004**, *93*, 077402.

[4] H. Tsunoyama, H. Sakurai, Y. Negishi, T. Tsukuda, *J. Am. Chem. Soc.* **2005**, *127*, 9374–9375.

[5] K. Mashima, H. Nakano, A. Nakamura, *J. Am. Chem. Soc.* **1993**, *115*, 11632–11633.

[6] S.-M. Peng, C.-C. Wang, Y.-L. Jang, Y.-H. Chen, F.-Y. Li, C.-Y. Mou, M.-K. Leung, *J. Magn. Magn. Mater.* **2000**, *209*, 80–83.

[7] M. Ruben, J. Rojo, F. J. Romero-Salguero, L. H. Uppadine, J.-M. Lehn, *Angew. Chem. Int. Ed.* **2004**, *43*, 3644–3662.

[8] T. Murahashi, M. Fujimoto, M. Oka, Y. Hashimoto, T. Uemura, Y. Tatsumi, Y. Nakao, A. Ikeda, S. Sakaki, H. Kurosawa, *Science*, **2006**, *313*, 1104–1107.

[9] G. H. Clever, M. Shionoya, *Coord. Chem. Rev.* **2010**, *254*, 2391–2402.

[10] A. C. Jahnke, K. Pröpper, C. Bronner, J. Teichgräber, S. Dechert, M. John, O. S. Wenger, F. Meyer, *J. Am. Chem. Soc.* **2012**, *134*, 2938–2941.

[11] M. J. Katz, K. Sakai, D. B. Leznoff, *Chem. Soc. Rev.* **2008**, *37*, 1884–1895.

[12] S. Coco, P. Espinet in *Gold Chemistry: Applications and Future Directions in the Life Sciences* (Ed: F. Mohr), Wiley-VCH, Weinheim, **2008**, pp. 357–396.

[13] a) A. Burini, J. P. Fackler, Jr., R. Galassi, B. R. Pietroni, R. J. Staples, *Chem. Commun.* **1998**, 95–96; b) A. Burini, R. Bravi, J. P. Fackler, Jr., R. Galassi, T. A. Grant, M. A. Omary, B. R. Pietroni, R. J. Staples, *Inorg. Chem.* **2000**, *39*, 3158–3165.

[14] B. K. Teo, K. Keating, *J. Am. Chem. Soc.* **1984**, *106*, 2224–2226.

[15] O. Crespo, M. C. Gimeno, P. G. Jones, A. Laguna, M. D. Villacampa, *Angew. Chem. Int. Ed. Engl.* **1997**, *36*, 993–995.

[16] a) J. Vicente, M.-T. Chicote, M.-C. Lagunas, P. G. Jones, *J. Chem. Soc. Chem. Commun.* **1991**, 1730–1731; b) J. Vicente, M.-T. Chicote, M.-C. Lagunas, *Inorg. Chem.* **1993**, *32*, 3748–3754.

[17] V. J. Catalano, A. L. Moore, *Inorg. Chem.* **2005**, *44*, 6558–6566.

[18] a) A. C. Jahnke, K. Pröpper, C. Bronner, J. Teichgräber, S. Dechert, M. John, O. S. Wenger, F. Meyer, *J. Am. Chem. Soc.* **2012**, *134*, 2938-2941; b) M. Veronelli, N. Kindermann, S. Dechert, S. Meyer, F. Meyer, *Inorg. Chem.* **2014**, *53*, 2333–2341.

[19] a) A. A. Mohamed, A. Burini, J. P. Fackler, Jr. *J. Am. Chem. Soc.* **2005**, *127*,

5012–5013; b) A. A. Mohamed, R. Galassi, F. Papa, A. Burini, J. P. Fackler, Jr. *Inorg. Chem.* **2006**, *45*, 7770–7776.

[20] a) H. Schmidbaur, A. Schier, *Chem. Soc. Rev.* **2008**, *37*, 1931–1951; b) H. Schmidbaur, A. Schier, *Chem. Soc. Rev.* **2012**, *41*, 370–412.

[21] P. Pyykkö, *Chem. Rev.* **1997**, *97*, 597–636.

[22] C.-M. Che, S.-W. Lai, *Coord. Chem. Rev.* **2005**, *249*, 1296–1309.

[23] Formation of the liquid crystalline state with $Au(I)_3$ complexes and Ag(I) ions, see: a) A. Kishimura, T. Yamashita, T. Aida, *J. Am. Chem. Soc.* **2005**, *127*, 179–183; b) H. O. Lintang, K. Kinbara, T. Yamashita, T. Aida, *Chem. Asian J.* **2012**, *7*, 2068–2072.

[24] For recent synthesis of Au_3–Ag–Au_3 cluster, see: W.-X. Ni, Y.-M. Qiu, M. Li, J. Zheng, R. W.-Y. Sun, S.-Z. Zhan, S. W. Ng, D. Li, *J. Am. Chem. Soc.* **2014**, *136*, 9532–9535.

[25] a) A. Burini, A. A. Mohamed, J. P. Fackler Jr. *Comments Inorg. Chem.* **2003**, *24*, 253–280; b) H. E. Abdou, A. A. Mohamed, J. P. Fackler Jr. in *Gold chemistry: Applications and Future Directions in the Life Science* (Ed: F. Mohr) Wiley-VCH, Weinheim, **2008**, pp. 1–45.

[26] T. Osuga, T. Murase, K. Ono, Y. Yamauchi, M. Fujita, *J. Am. Chem. Soc.* **2010**, *132*, 15553–15555.

[27] A. Bondi, *J. Phys. Chem.* **1964**, *68*, 441–451.

[28] S. Sculfort, P. Braunstein, *Chem. Soc. Rev.* **2011**, *40*, 2741–2760.

[29] C. Silvestru, in *Modern Supermolecular Gold Chemistry: Gold-Metal Interactions and Applications* (Ed: A. Laguna), Wiley-VCH, Weinheim, **2008**, pp. 181–293.

[30] E. J. Fernández, C. Hardacre, A. Laguna, M. C. Lagunas, J. M. López-de-Luzuriaga, M. Monge, M. Montiel, M. E. Olmos, R. C. Puelles, E. Sánchez-Forcada, *Chem. Eur. J.* **2009**, *15*, 6222–6233.

[31] M. A. Omary, M. A. Rawashdeh-Omary, M. W. A. Gonser, O. Elbjeirami, T. Grimes, T. R. Cundari, H. V. K. Diyabalanage, C. S. P. Gamage, H. V. R. Dias, *Inorg. Chem.* **2005**, *44*, 8200–8210.

[32] L. E. Sansores, R. Salcedo, A. Martínez, N. Mireles, *THEOCHEM* **2006**, *763*, 7–11.

[33] S. M. Tekarli, T. R. Cundari, M. A. Omary, *J. Am. Chem. Soc.* **2008**, *130*, 1669–1675.

[34] F. Bonati, A. Burini, B. R. Pietroni, B. Bovio, *J. Organomet. Chem.* **1989**, *375*, 147–160.

3.7 Experimental Section

Materials and Instructions: Reagents and solvents were purchased from TCI Co., Ltd., WAKO Pure Chemical Industries Ltd., Sigma-Aldrich Co., and KANTO Chemical Co., Inc. Deuterated H_2O was used as supplied for the complexation reactions and NMR measurements. NMR spectra were recorded on Bruker DRX-500 (500 MHz) equipped with BBO gradient probe or Bruker AV-500 (500 MHz) with CP-TCI CryoProbe. TMS ($CDCl_3$ solution) in a capillary served as an external standard ($\delta = 0$ ppm). IR measurements were carried out using a DIGILAB FTS-7000 instrument. UV-visible spectral data were recorded on a SHIMADZU UV-3150. CSI-MS was measured on a four-sector (BE/BE) tandem mass spectrometer (JMS-700C, JEOL). Melting points were determined with a Yanaco MP-500P micro melting point apparatus. Elemental analyses were performed on a Yanaco MT-6. Diffraction measurements were made using a Bruker APEXII/CCD diffractometer equipped with a focusing mirror (MoKα radiation $\lambda = 0.71073$ Å). Trinuclear gold(I) complex **2a** was prepared according to the literature procedure.[1]

Reference

[1] F. Bonati, A. Burini, B. R. Pietroni, B. Bovio, *J. Organomet. Chem.* **1989**, *375*, 147–160.

Synthesis and Physical Data of Double-Decker Au(I)–Ag(I) Cluster 1b•(2a•Ag$^+$•2a)

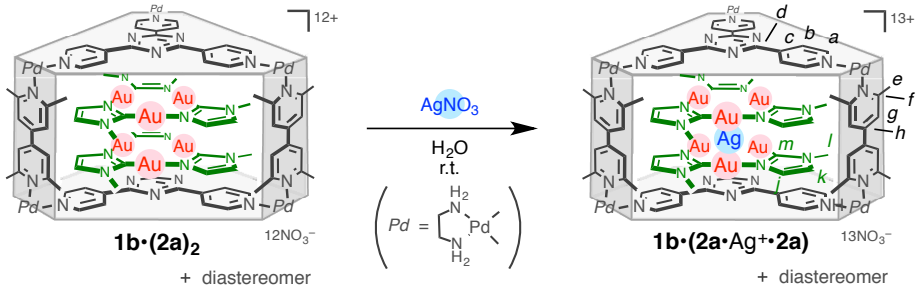

Scheme S1. Synthesis of Au(I)–Ag(I) cluster **1b**•(**2a**•Ag$^+$•**2a**).

$AgNO_3$ (1.70 mg, 10.0 mmol) was added to an aqueous solution (1.0 mL) of [3 × 2] Au(I) cluster **1b**•(**2a**)$_2$ (46.7 mg, 10.0 μmol). The solution color immediately changed from orange to pale yellow. NMR spectroscopy and UV-vis measurement of the resulting clear solution revealed that inclusion complex **1b**•(**2a**•Ag$^+$•**2a**) formed selectively. In the ^{1}H NMR spectrum, the signals of encapsulated guest molecules **2a** were shifted downfield (Δδ = ca. 0.3 ppm), and the CT band in the absorption spectrum was blue-shifted, indicating the insertion of Ag(I) ion between two molecules of guest **2a**. The solution was evaporated and dried by vacuum freeze-drying equipment to give inclusion complex **1b**•(**2a**•Ag$^+$•**2a**) (43.2 mg, 8.92 μmol, 89%) as a pale yellow solid. ^{1}H NMR (500 MHz, D_2O, 300 K) δ: 8.86 (br, 12H, **1b**, H^a), 8.26 (br, 12H, **1b**, H^b), 8.04 (s, 3H, **1b**, H^g), 8.00 (s, 3H, **1b**, H^g), 7.98 (s, 3H, **1b**, H^g), 7.83 (s, 3H, **1b**, H^g), 7.03 (s, 3H, **2a**, H^k), 6.75 (s, 3H, **2a**, H^k), 4.05 (s, 3H, **2a**, H^j), 3.84 (s, 3H, **2a**, H^j), 3.75 (s, 9H, **1b**, H^e), 3.68 (s, 9H, **1b**, H^w), 3.65 (s, 9H, **1b**, H^e), 3.53 (s, 9H, **1b**, H^e), 3.29 (s, 9H, **2a**, H^l), 3.28 (s, 9H, **2a**, H^l), 2.98 (br, 12H, **1b**, ethylenediamine-H), 2.92 (br, 12H, **1b**, ethylenediamine-H). ^{13}C NMR (125 MHz, D_2O, 300 K) δ: 169.4 (C, **1b**, C^d), 163.1 (C, **2a**, C^m), 162.7 (C, **2a**, C^m), 161.7 (C, **1b**, C^f), 161.2 (C, **1b**, C^f), 152.6 (CH, **1b**, C^a), 147.3 (C, **1b**, C^h), 146.8 (C, **1b**, C^h), 145.5 (C, **1b**, C^c), 125.4 (CH, **1b**, C^b), 123.5 (CH, **2a**, C^j), 123.4 (CH, **2a**, C^j), 122.6 (CH, **1b**, C^g), 122.2 (CH, **1b**, C^g), 122.0 (CH, **1b**, C^g), 121.9 (CH, **1b**, C^g), 121.4 (CH, **2a**, C^k), 121.3 (CH, **2a**, C^k), 47.6 (CH_2, **1b**, ethylenediamine-C), 46.5 (CH_2, **1b**, ethylenediamine-C), 34.9 (CH_3, **2a**, C^l), 34.7 (CH_3, **2a**, C^l), 25.9 (CH_3, **1b**, C^e), 25.6 (CH_3, **1b**, C^e). ^{1}H DOSY (D_2O, 300 K) (m^2/s): D = 1.5 × 10^{-10}. IR (KBr, cm^{-1}): 3422(br), 3179(br), 3098(br), 1684, 1616, 1520, 1384 (br), 1201, 1058, 805. m.p. = ~210 ºC (decomposed). E.A. Calcd. for $C_{114}H_{150}AgAu_6N_{55}$

$O_{39}Pd_6{\cdot}(H_2O)_{17}$: C, 26.59; H, 3.60; N, 14.96; Found: C, 26.75; H, 3.71; N, 14.81.

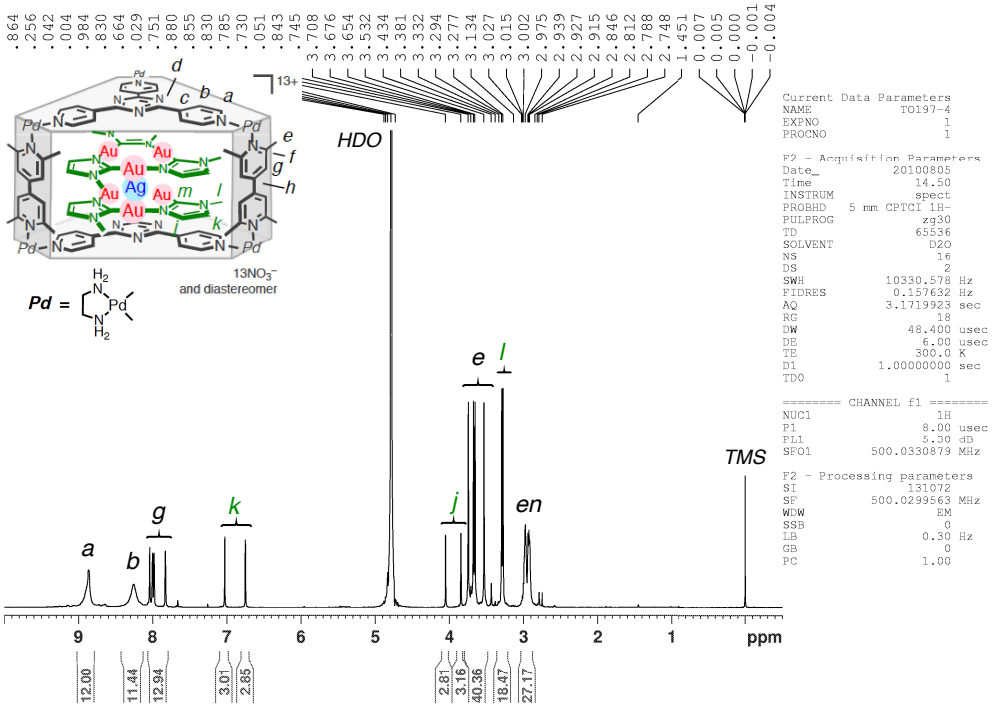

Figure S1. ^{1}H NMR (500 MHz, D_2O, 300 K) spectrum of **1b**•(**2a**•Ag^+•**2a**).

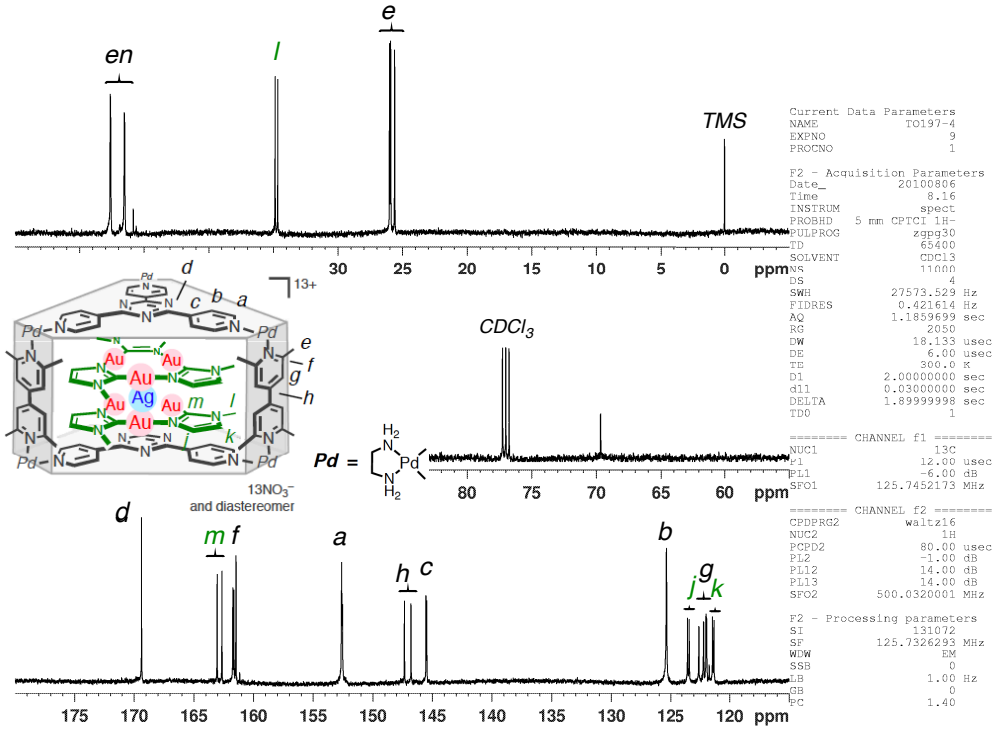

Figure S2. ^{13}C NMR (125 MHz, D_2O, 300 K) spectrum of **1b**•(**2a**•Ag^+•**2a**).

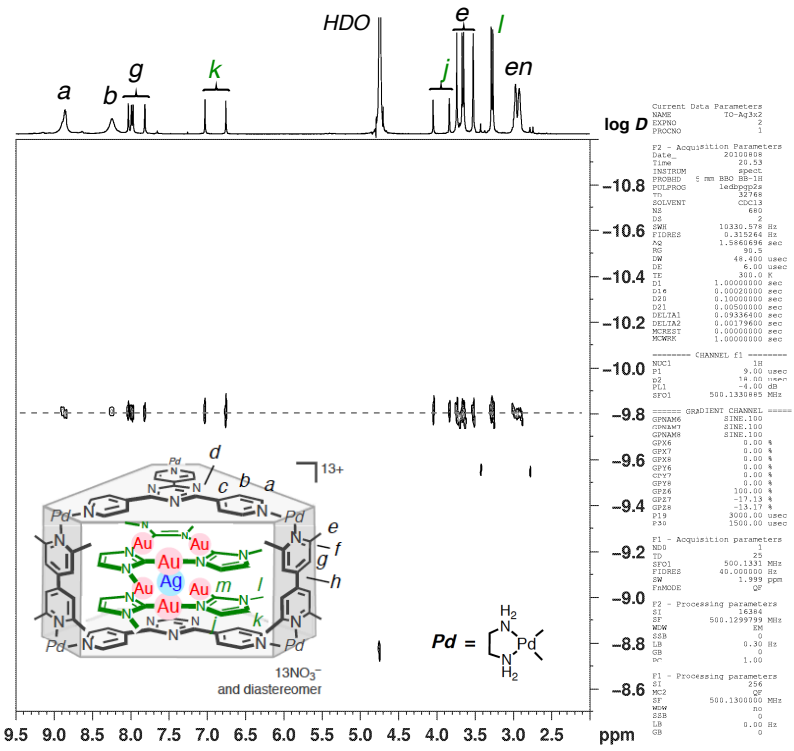

Figure S3. ^{1}H DOSY (500 MHz, D_2O, 300 K) spectrum of **1b**•(**2a**•Ag^{+}•**2a**).

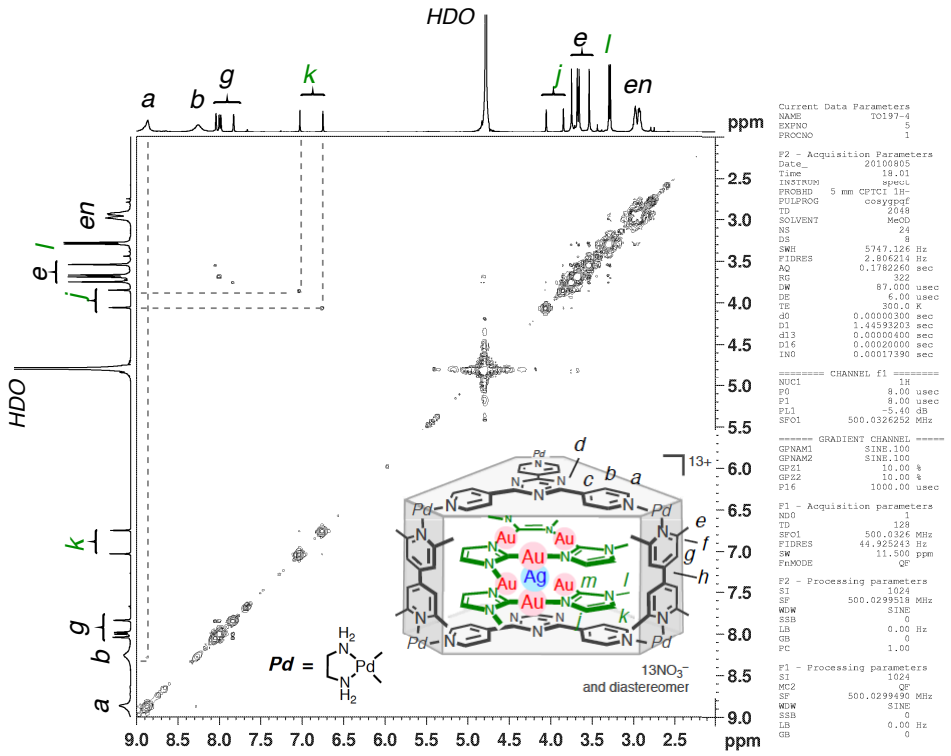

Figure S4. ^{1}H-^{1}H COSY (500 MHz, D_2O, 300 K) spectrum of **1b**•(**2a**•Ag^{+}•**2a**).

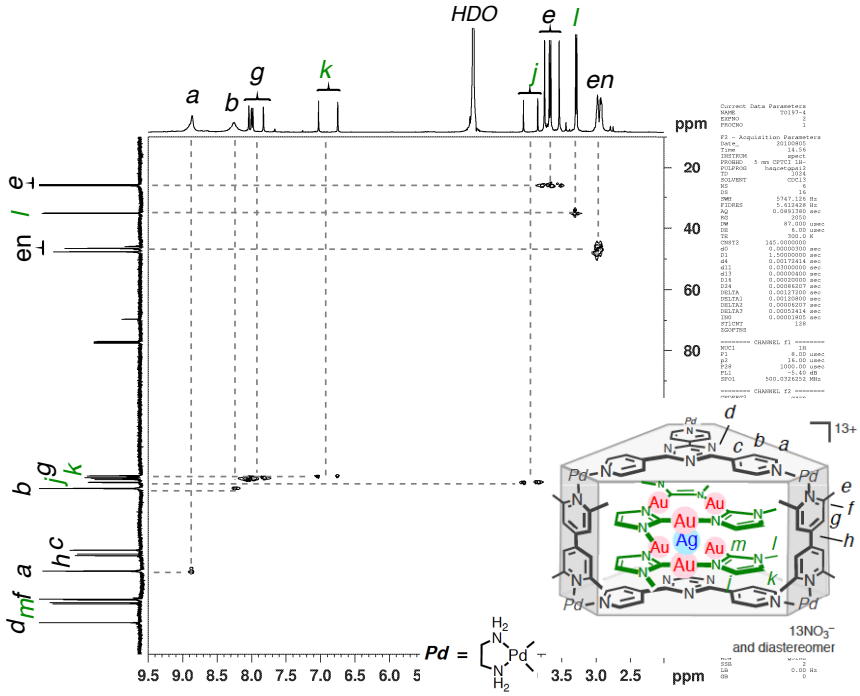

Figure S5. ^{1}H-^{13}C HSQC (500 MHz, D_2O, 300 K) spectrum of **1b**•(**2a**•Ag^{+}•**2a**).

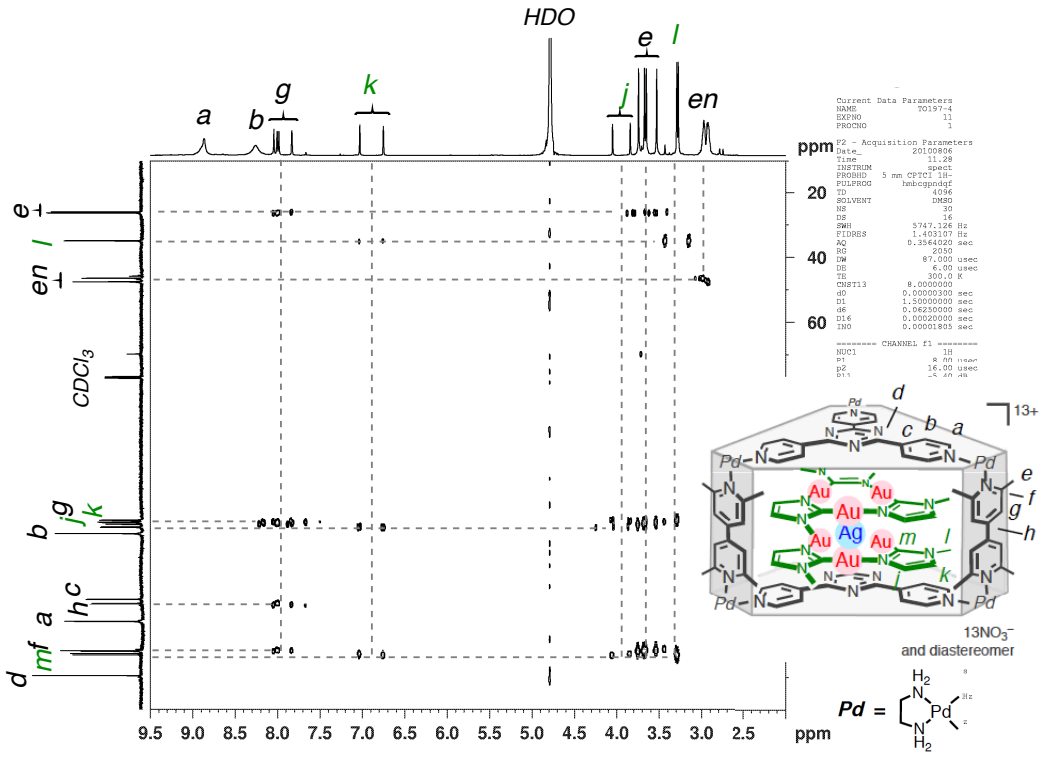

Figure S6. ^{1}H-^{13}C HMBC (500 MHz, D_2O, 300 K) spectrum of **1b**•(**2a**•Ag^{+}•**2a**).

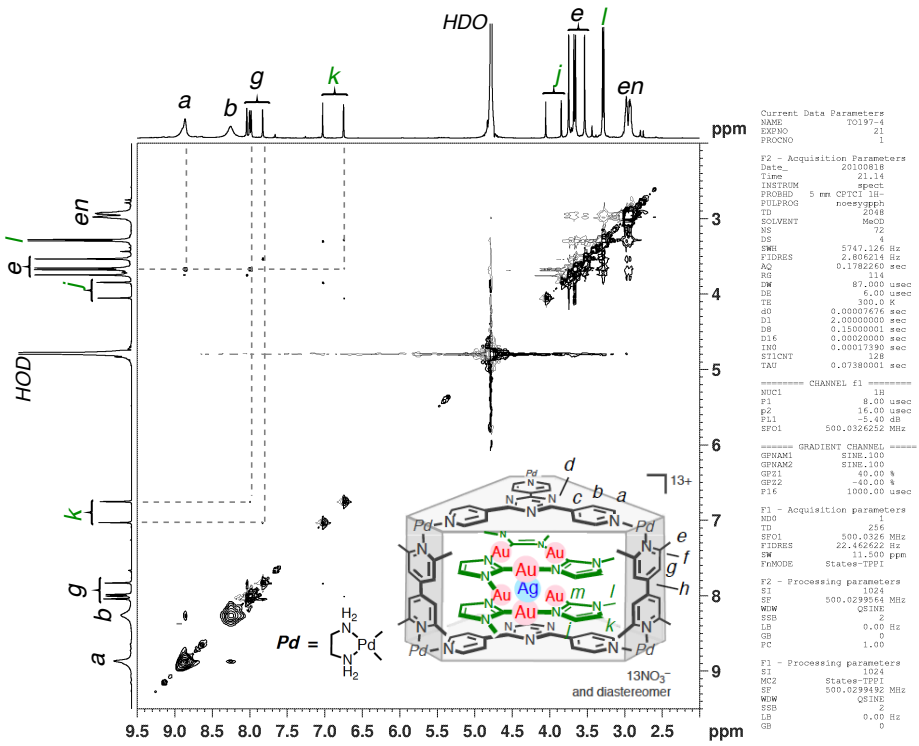

Figure S7. ^{1}H-^{1}H NOESY (500 MHz, D_2O, 300 K) spectrum of **1b**•(**2a**•Ag^{+}•**2a**).

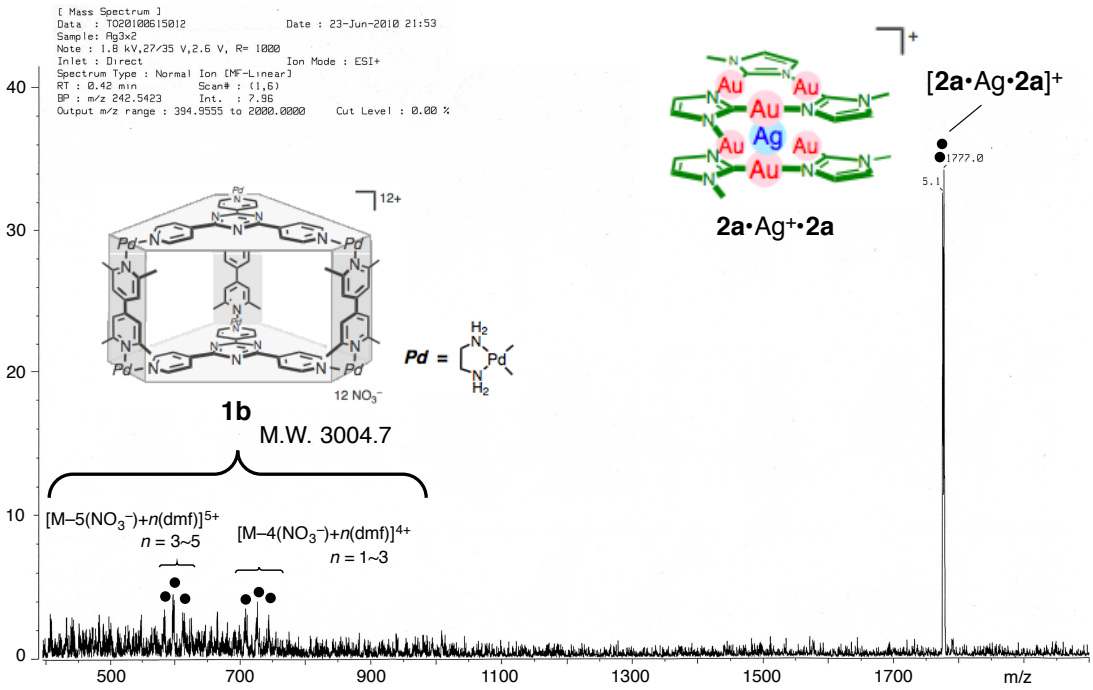

Figure S8. CSI-MS spectrum of **1b**•(**2a**•Ag^{+}•**2a**) (H_2O : CH_3CN : DMF = 1 : 1 : 0.1). Under this ionization condition, metal ion cluster **2a**•Ag^{+}•**2a** readily escaped from cage **1b** and was detected as a monovalent ion.

Table S1. Crystal data and structure refinement for **1b•(2a•Ag^+•2a)**.

Identification code	p321	
Empirical formula	C228 H300 Ag2 Au12 N104.64 O105.54 Pd12	
Formula weight	10051.53	
Temperature	90(2) K	
Wavelength	0.71073 Å	
Crystal system	Hexagonal	
Space group	*P*321	
Unit cell dimensions	a = 20.533(2) Å	α = 90°.
	b = 20.533(2) Å	β = 90°.
	c = 54.547(11) Å	γ = 120°.
Volume	19915(5) $Å^3$	
Z	2	
Density (calculated)	1.676 Mg/m^3	
Absorption coefficient	5.103 mm^{-1}	
F(000)	9678	
Crystal size	0.28 x 0.10 x 0.10 mm^3	
Theta range for data collection	1.37 to 24.12°.	
Index ranges	-23<=h<=23, -23<=k<=23, -61<=l<=62	
Reflections collected	169214	
Independent reflections	21042 [R(int) = 0.0533]	
Completeness to theta = 24.12°	99.4 %	
Absorption correction	Semi-empirical from equivalents	
Max. and min. transmission	0.6294 and 0.3291	
Refinement method	Full-matrix least-squares on F^2	
Data / restraints / parameters	21042 / 827 / 1626	
Goodness-of-fit on F^2	1.126	
Final R indices [I>2sigma(I)]	R_1 = 0.0873, wR_2 = 0.2245	
R indices (all data)	R_1 = 0.1098, wR_2 = 0.2414	
Absolute structure parameter	0.079(12)	
Largest diff. peak and hole	1.537 and -1.528 e.$Å^{-3}$	
CCDC reference number	866863	

(a)

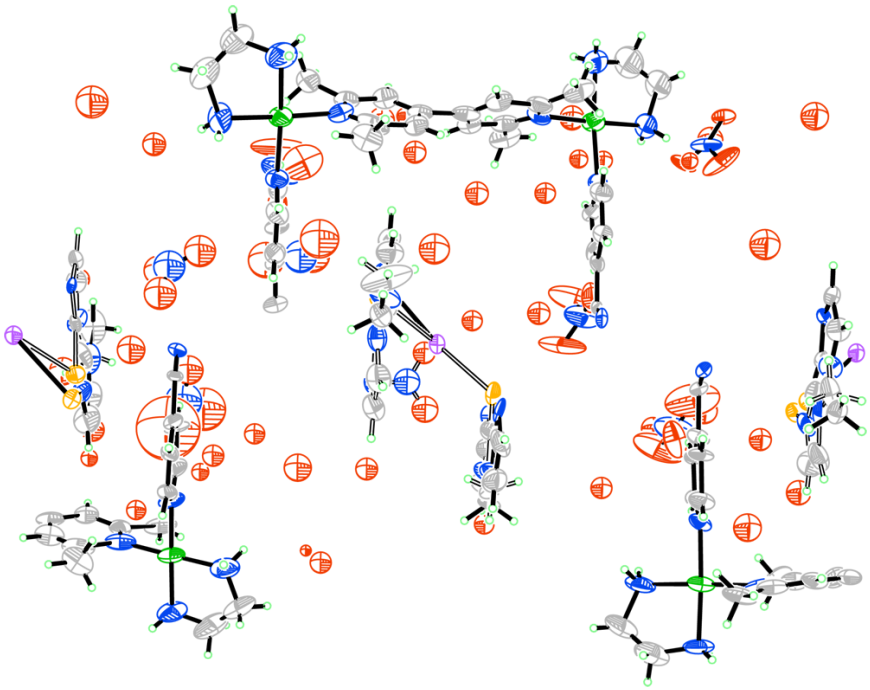

(b)

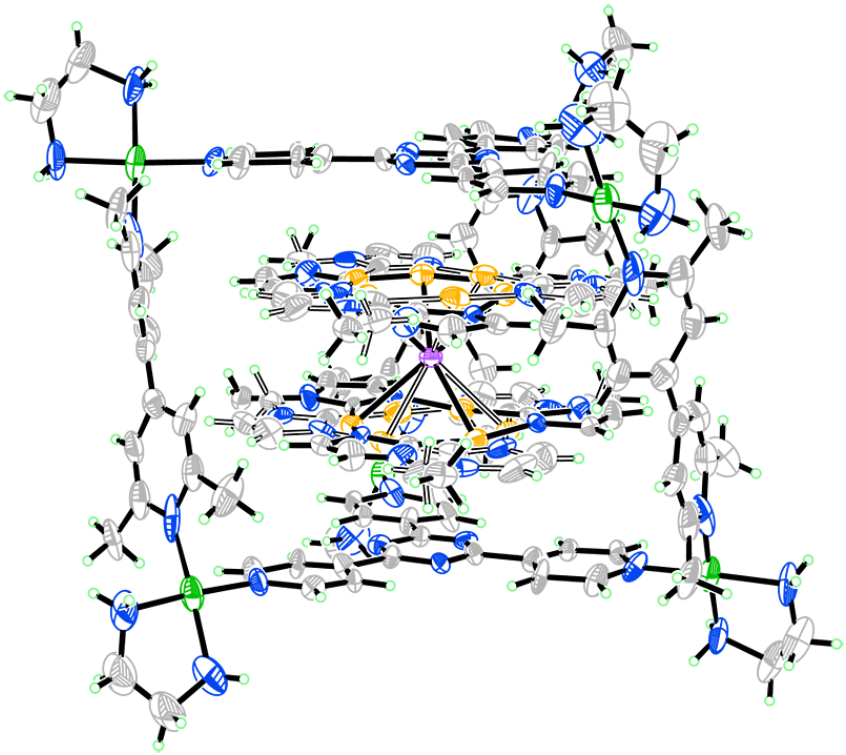

Figure S9. Thermal ellipsoid plots (30% probability level) of double-deckered cluster **1b•(2a•Ag^+•2a)**. (a) All independent atoms including water and nitrate ions and (b) one of the host-guest structures of **1b•(2a•Ag^+•2a)**.

Synthesis and Physical Data of Tripel-Decker Au(I)–Ag(I) Cluster 1c'•(2a•Ag⁺•2a•Ag⁺•2a)

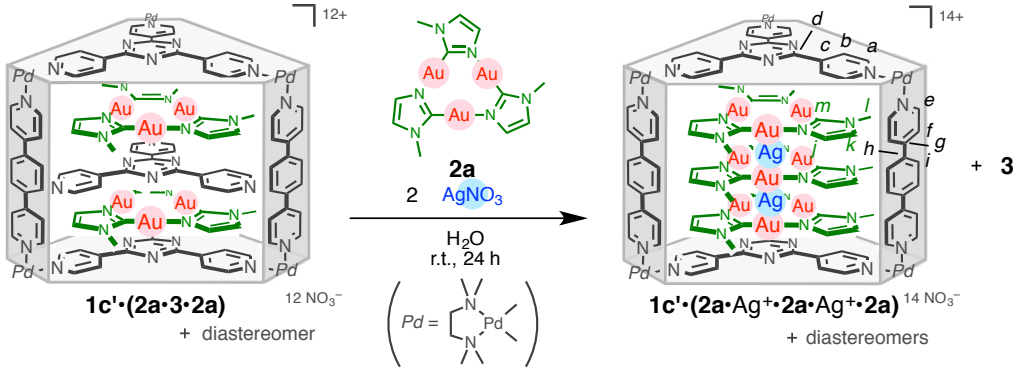

Scheme S2. Synthesis of Au(I)–Ag(I) cluster **1c'**•(**2a**•Ag⁺•**2a**•Ag⁺•**2a**).

Trinuclear Au(I) complex **2a** (8.34 mg, 10.0 μmol) and $AgNO_3$ (3.40 mg, 20.0 μmol) were added to an aqueous solution (1.0 mL) of the self assembled complex **1c'**•(**2a**•**3**•**2a**) (53.8 mg, 10.0 μmol). The suspended mixture was stirred at room temperature for 24 h to give a yellow solution and white precipitation. After filtration of the resulting solution, NMR spectroscopy revealed the selective formation of Au_3–Ag–Au_3–Ag–Au_3 ion cluster **1c'**•(**2a**•Ag^+•**2a**•Ag^+•**2a**). Seven sets of signals were observed for cage **1c'** and guest **2a**, indicating three stacking modes of the C_{3h} symmetrical guest **2a** within cages **1c'**. Although these three diastereomers were not distinguishable in NMR spectroscopy, the integral ratio revealed that three diastereomers exists in a 1:1:2 ratio; namely, they were statistically distributed isomers. Under cold-spray ionization mass spectroscopy (CSI-MS) conditions, metal ion cluster **1c'**•(**2a**•Ag^+•**2a**•Ag^+•**2a**) readily decomposed and only a **2a**•Ag^+•**2a** monovalent ion was detected. ^{1}H NMR (500 MHz, D_2O, 310 K) δ: 9.35–9.27 (m, 17.9H, **1c'**, H^a, H^e), 8.94–8.88 (m, 5.9H, **1c'**, H^a), 8.68–8.65 (m, 5.8H, **1c'**, H^b), 8.28–8.19 (br, 12.0H, **1c'**, H^f), 8.11(s, 3.9H, **1c'**, H^i), 8.07 (s, 1.3H, **1c'**, H^i), 8.05 (s, 2.0H, **1c'**, H^i), 8.01–7.98 (br, 8.5H, **1c'**, H^b, H^i), 7.95 (d, J = 6.5 Hz, 1.7H, **1c'**, H^b), 7.91 (d, J = 6.5 Hz, 1.5H, **1c'**, H^b), 7.22 (br, 1.4H, **2a**, H^k), 7.12 (br, 0.7H, **2a**, H^k), 7.00 (br, 1.4H, **2a**, H^k), 6.96 (br, 0.7H, **2a**, H^k), 6.93 (br, 1.4H, **2a**, H^k), 6.75 (br, 1.4H, **2a**, H^k), 6.57 (br, 0.7H, **2a**, H^j), 6.54 (br, 1.4H, **2a**, H^k), 6.05 (br, 1.4H, **2a**, H^j), 5.51 (br, 0.7H, **2a**, H^j), 4.29 (br, 1.4H, **2a**, H^j), 4.15 (br, 1.4H, **2a**, H^j), 3.97 (br, 1.4H, **2a**, H^j), 3.94 (br, 1.4H, **2a**, H^j), 3.16–3.07 (m, 41.7H, **1c'**, H^l, **2a**, H^n), 2.77–2.68 (m, 36.8H, **1c'**, H^o), 2.65 (s, 3.1H, **2a**, H^l), 2.55–2.46 (m, 36.4H, **1c'** , H^o), 2.14 (s, 4.3H, **2a**, H^l), 1.67 (s, 2.1H, **2a**, H^l). ^{13}C NMR (125 MHz,

D_2O, 310 K) δ: 169.6 (C, **1c'**, C^d), 169.5 (C, **1c'**, C^d), 162.6 (C, **2a**, C^m), 162.4 (C, **2a**, C^m), 162.0 (C, **2a**, C^m), 161.9 (C, **2a**, C^m), 160.4 (C, **2a**, C^m), 159.3 (C, **2a**, C^m), 158.6 (C, **2a**, C^m), 152.1 (CH, **1c'**, C^a), 152.0 (CH, **1c'**, C^a), 151.9 (CH, **1c'**, C^a), 151.8 (CH, **1c'**, C^e), 151.7 (CH, **1c'**, C^e), 151.2 (C, **1c'**, C^g), 151.1 (C, **1c'**, C^g), 145.8 (CH, **1c'**, C^c), 145.7 (CH, **1c'**, C^c), 145.7 (CH, **1c'**, C^c), 145.6 (CH, **1c'**, C^c) 137.2 (C, **1c'**, C^h), 137.1 (C, **1c'**, C^h), 136.9 (C, **1c'**, C^h), 128.8 (CH, **1c'**, C^i), 128.7 (CH, **1c'**, C^i), 128.6 (CH, **1c'**, C^i), 126.3 (CH, **1c'**, C^b), 126.2 (CH, **1c'**, C^b), 126.1 (CH, **2a**, C^j), 125.9 (CH, **2a**, C^j), 125.7 (CH, **2a**, C^j), 125.6 (CH, **1c'**, C^f), 125.4 (CH, **1c'**, C^f), 125.3 (CH, **1c'**, C^f), 125.2 (CH, **1c'**, C^f), 125.0 (CH, **1c'**, C^b), 125.0 (CH, **1c'**, C^b), 124.8 (CH, **1c'**, C^b), 124.7 (CH, **1c'**, C^b), 123.6 (CH, **2a**), 123.5 (CH, **2a**, C^k), 123.4 (CH, **2a**, C^k), 123.3 (CH, **2a**, C^j), 122.9 (CH, **2a**, C^j), 122.8 (CH, **2a**, C^j), 122.6 (CH, **2a**, C^k), 122.4 (CH, **2a**, C^k), 122.4 (CH, **2a**, C^k), 122.0 (CH, **2a**, C^k), 62.8 (CH_2, **1c'**, C^n), 62.8 (CH_2, **1c'**, C^n), 50.6 (CH_3, **1c'**, C^o), 50.5 (CH_3, **1c'**, C^o), 50.4 (CH_3, **1c'**, C^o), 50.4 (CH_3, **1c'**, C^o), 50.3 (CH_3, **1c'**, C^o), 50.2 (CH_3, **1c'**, C^o), 50.1 (CH_3, **1c'**, C^o), 50.1 (CH_3, **1c'**, C^o), 35.4 (CH_3, **2a**, C^l), 35.4 (CH_3, **2a**, C^l), 35.1 (CH_3, **2a**, C^l), 35.0 (CH_3, **2a**, C^l), 34.0 (CH_3, **2a**, C^l), 33.6 (CH_3, **2a**, C^l), 33.5 (CH_3, **2a**, C^l). ^{1}H DOSY (D_2O, 300 K) (m^2/s): $D = 1.4 \times 10^{-10}$. IR (KBr, cm^{-1}): 3439(br), 3098, 2932, 1614, 1574, 1522, 1470, 1438, 1352 (br), 1235, 1156, 1076, 1060, 1042, 1008, 955, 873, 810, 732, 674. m.p. = ~210 ºC (decomposed). E.A. Calcd. for $C_{156}H_{201}Ag_2Au_9N_{62}O_{42}Pd_6 \cdot (H_2O)_{21}$: C, 28.29; H, 3.70; N, 13.11; Found: C, 28.16; H, 3.58; N, 13.12.

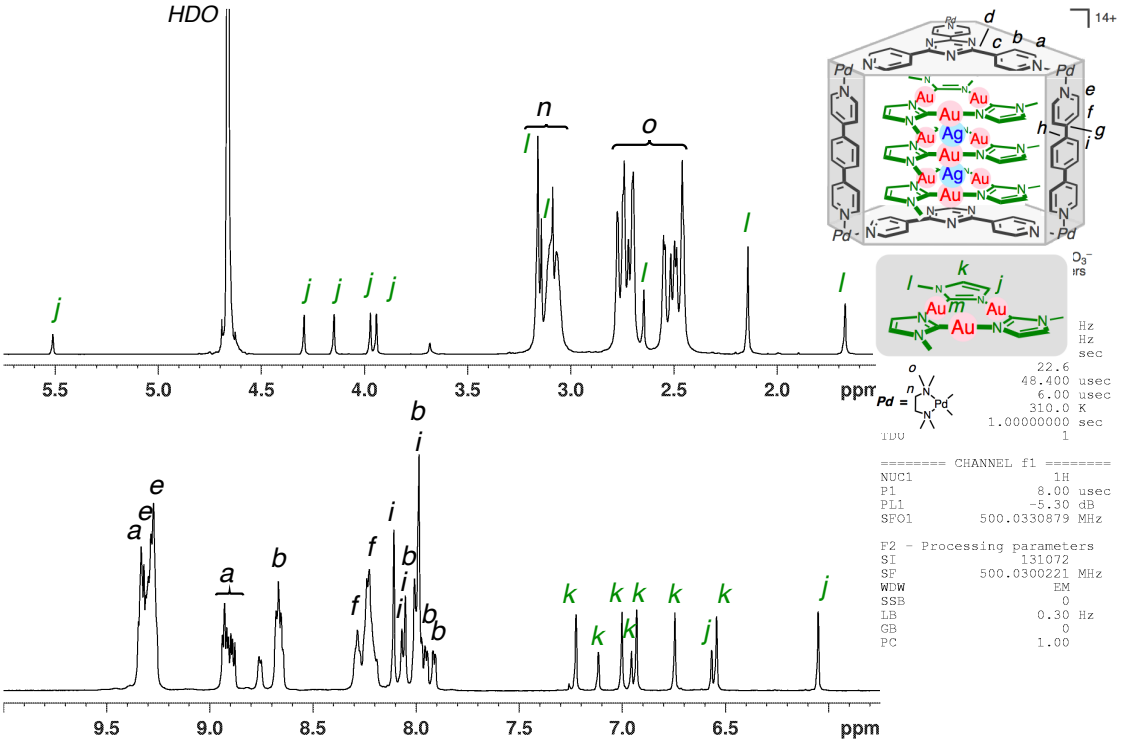

Figure S10. ^{1}H NMR (500 MHz, D_2O, 310 K) spectrum of **1c'**•(**2a**•Ag^+•**2a**•Ag^+•**2a**).

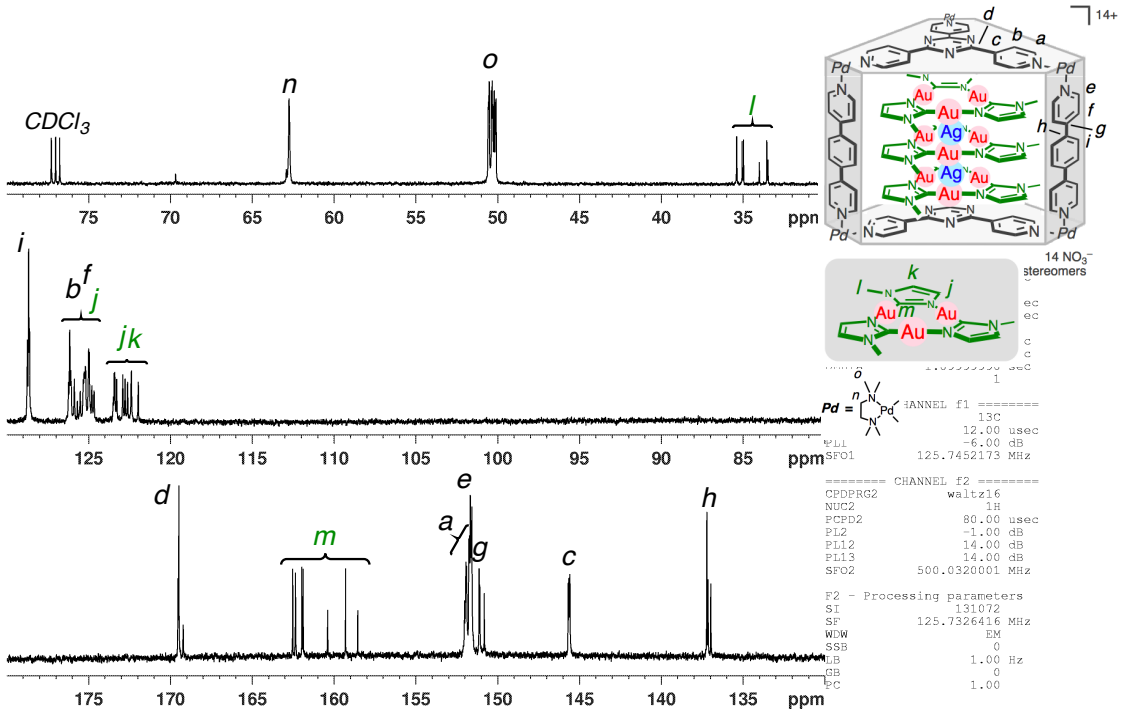

Figure S11. ^{13}C NMR (125 MHz, D_2O, 310 K) spectrum of **1c'**•(**2a**•Ag^+•**2a**•Ag^+•**2a**).

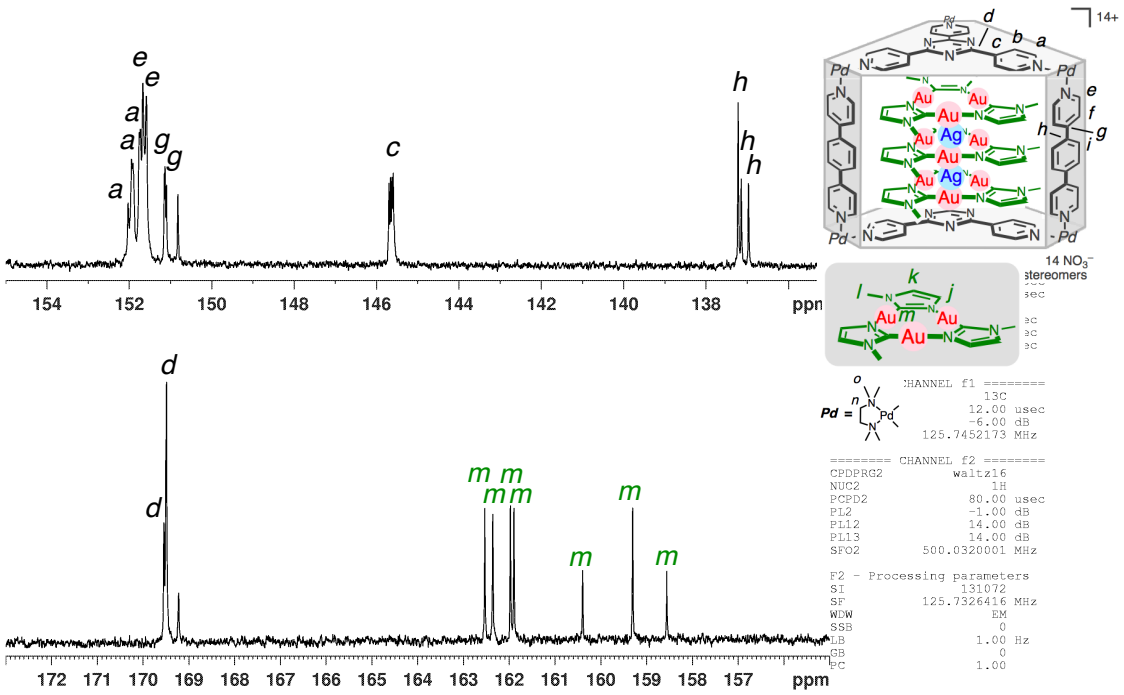

Figure S12. Enlarged ^{13}C NMR (125 MHz, D_2O, 310 K) spectrum of **1c'**•(**2a**•Ag^+•**2a**•Ag^+•**2a**).

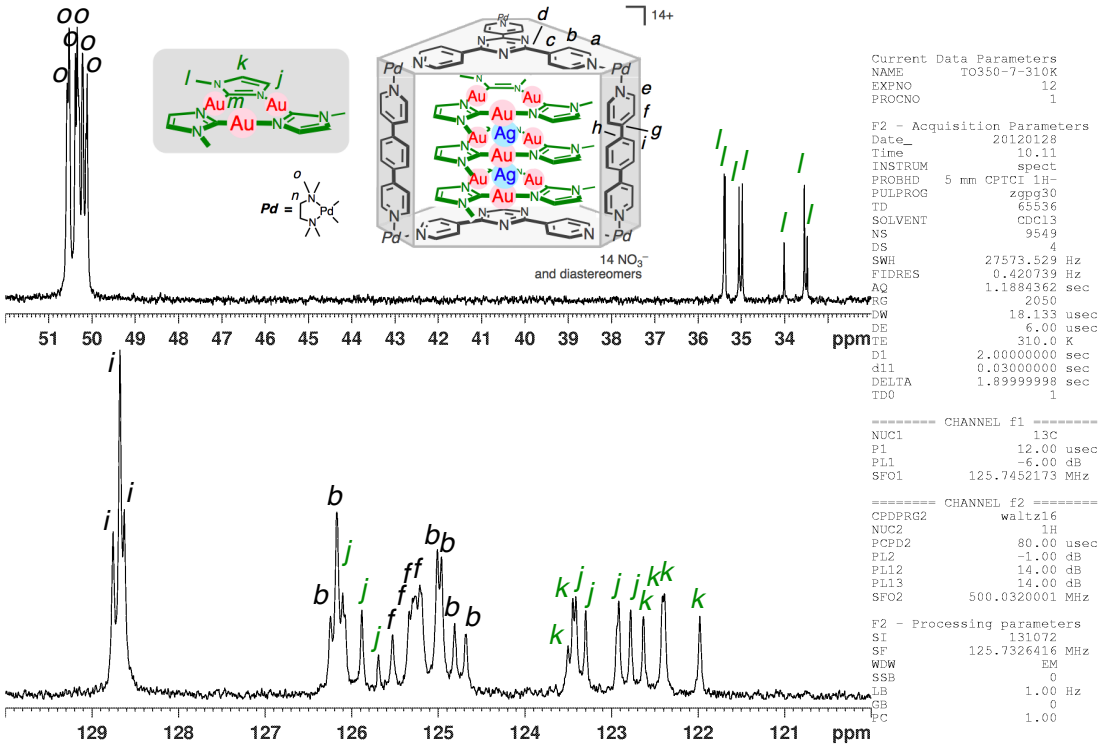

Figure S13. Enlarged ^{13}C NMR (125 MHz, D_2O, 310 K) spectrum of **1c'**•(**2a**•Ag^+•**2a**•Ag^+•**2a**).

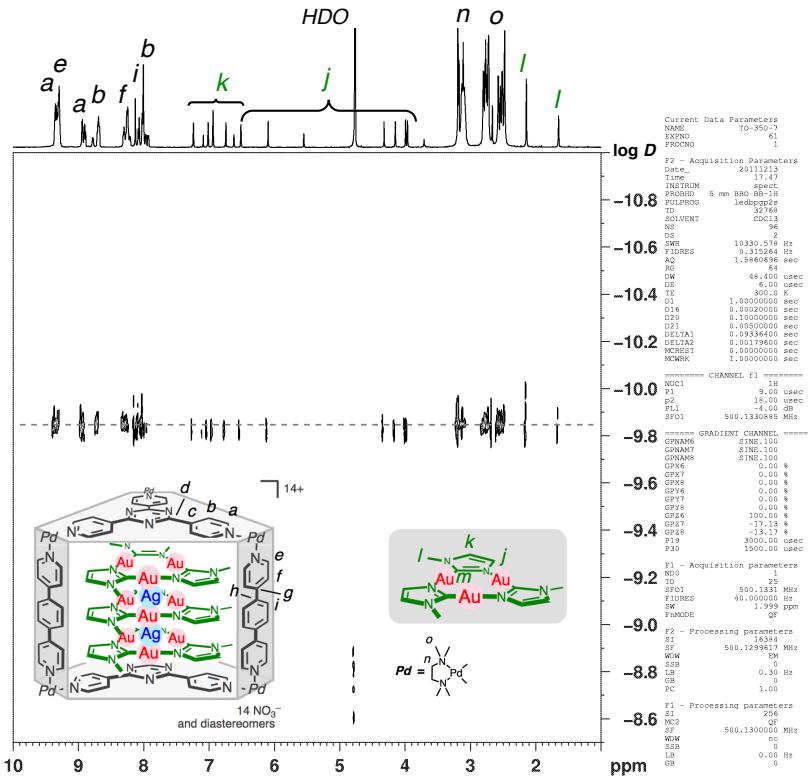

Figure S14. ^{1}H DOSY (500 MHz, D_2O, 300 K) spectrum of **1c'**•(**2a**•Ag^+•**2a**•Ag^+•**2a**).

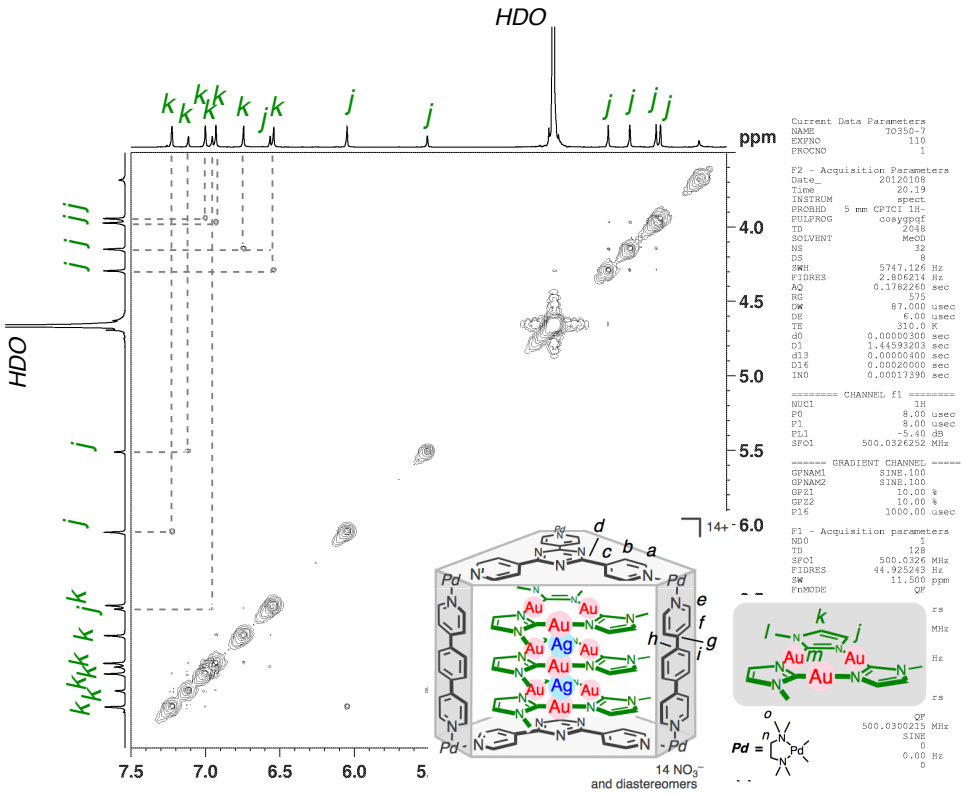

Figure S15. ^{1}H-^{1}H COSY (500 MHz, D_2O, 310 K) spectrum of **1c'**•(**2a**•Ag^+•**2a**•Ag^+•**2a**).

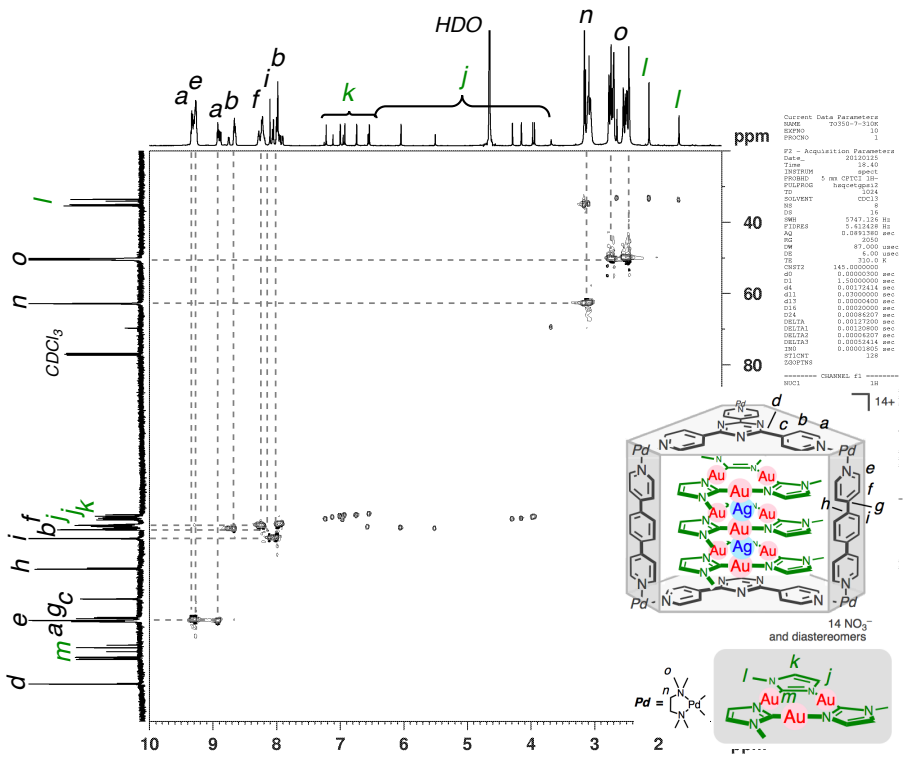

Figure S16. ^{1}H-^{13}C HSQC (500 MHz, D_2O, 310 K) spectrum of **1c'**•(**2a**•Ag^+•**2a**•Ag^+•**2a**).

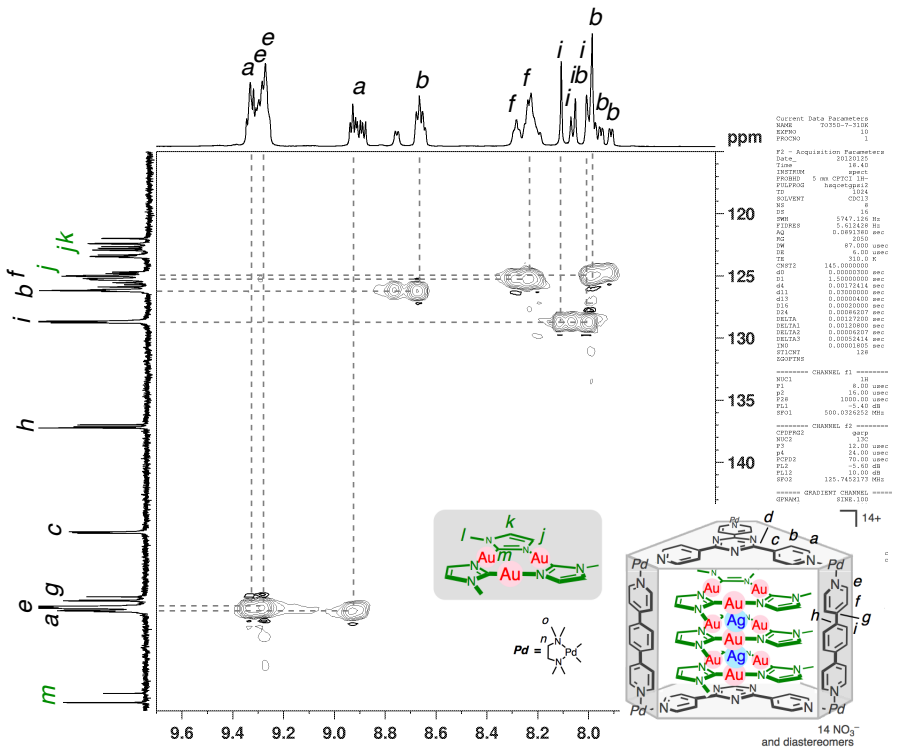

Figure S17. Enlarged ^{1}H-^{13}C HSQC (500 MHz, D_2O, 310 K) spectrum of **1c'**•(**2a**•Ag^+•**2a**•Ag^+•**2a**).

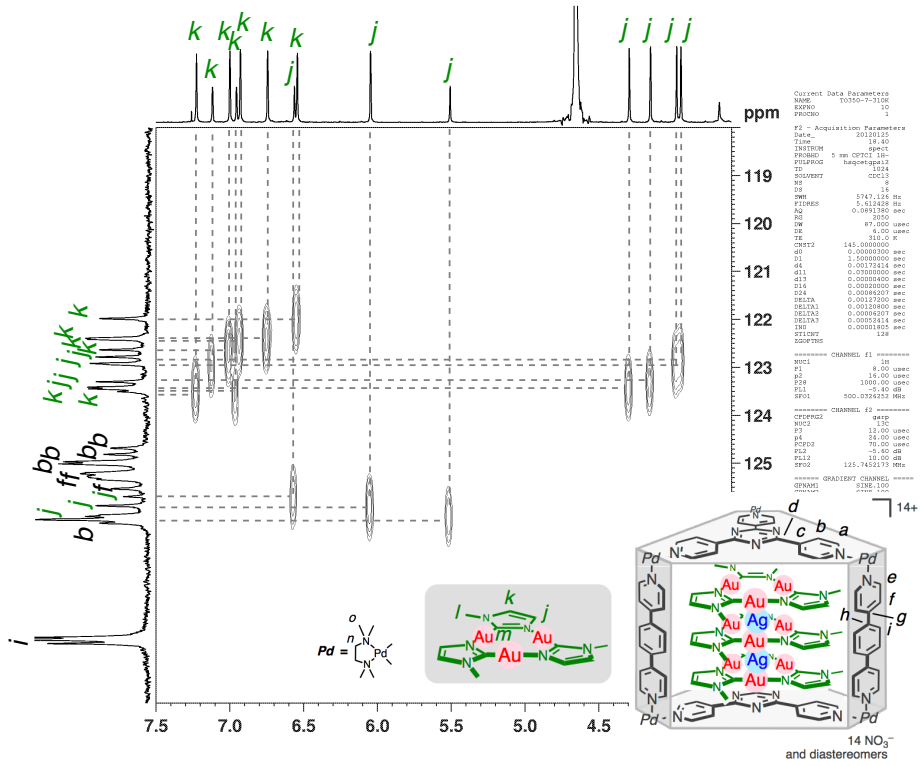

Figure S18. Enlarged ^{1}H-^{13}C HSQC (500 MHz, D_2O, 310 K) spectrum of **1c'**•(**2a**•Ag^{+}•**2a**•Ag^{+}•**2a**).

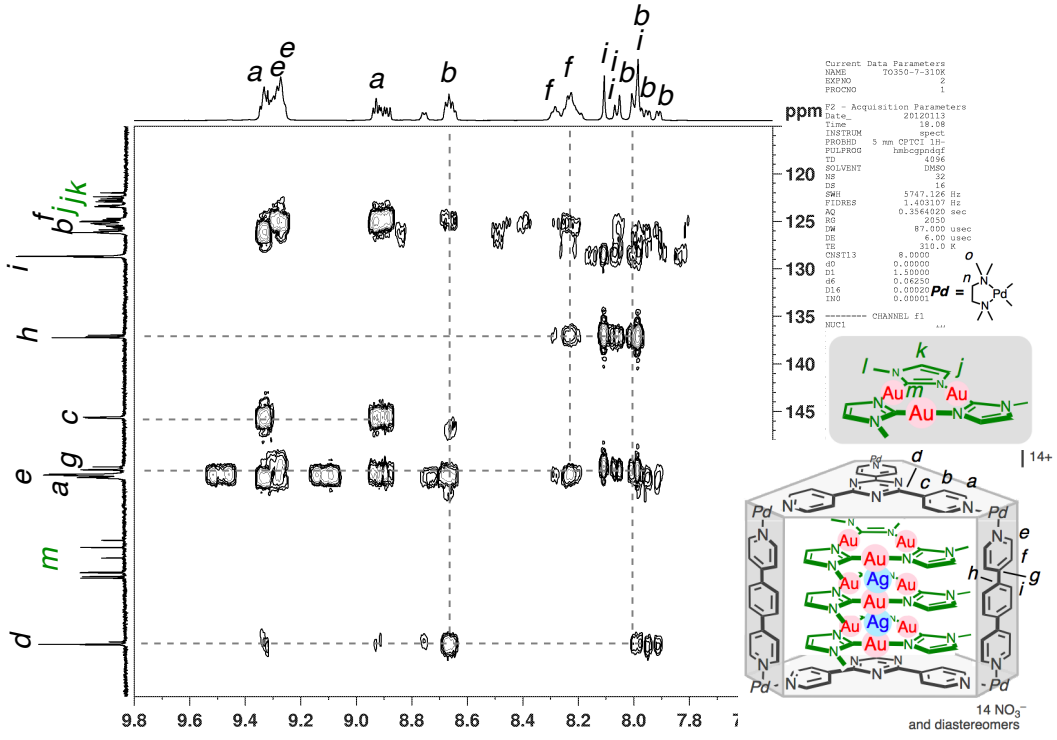

Figure S19. Enlarged ^{1}H-^{13}C HMBC (500 MHz, D_2O, 310 K) spectrum of **1c'**•(**2a**•Ag^{+}•**2a**•Ag^{+}•**2a**).

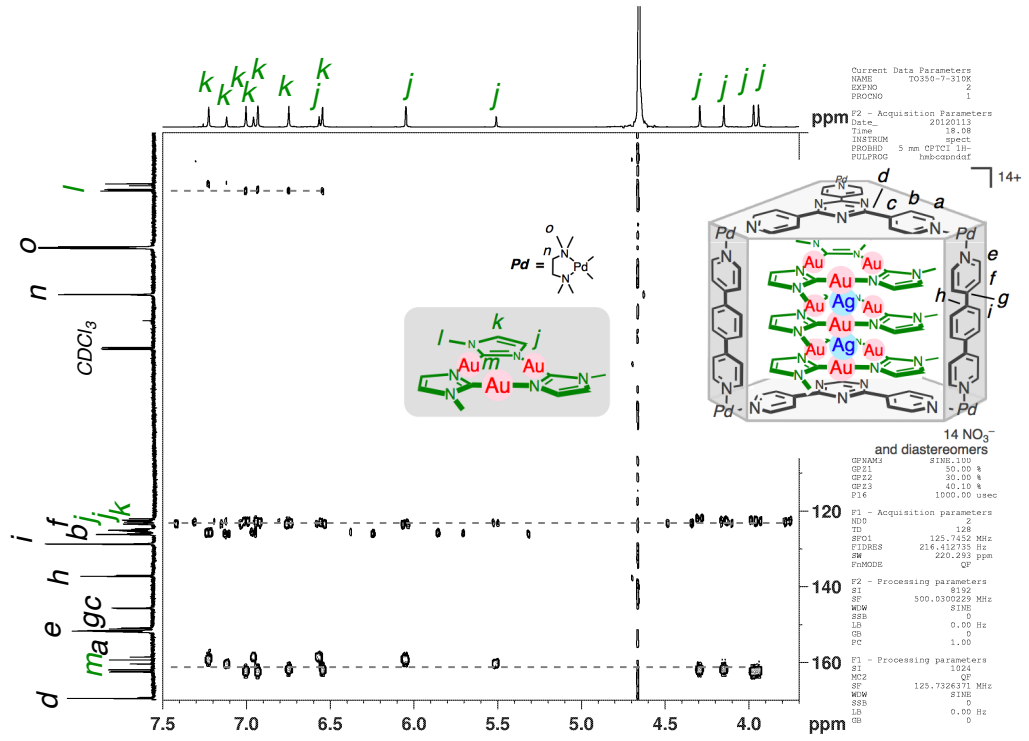

Figure S20 Enlarged ^{1}H-^{13}C HMBC (500 MHz, D_2O, 310 K) spectrum of **1c'**•(**2a**•Ag^{+}•**2a**•Ag^{+}•**2a**).

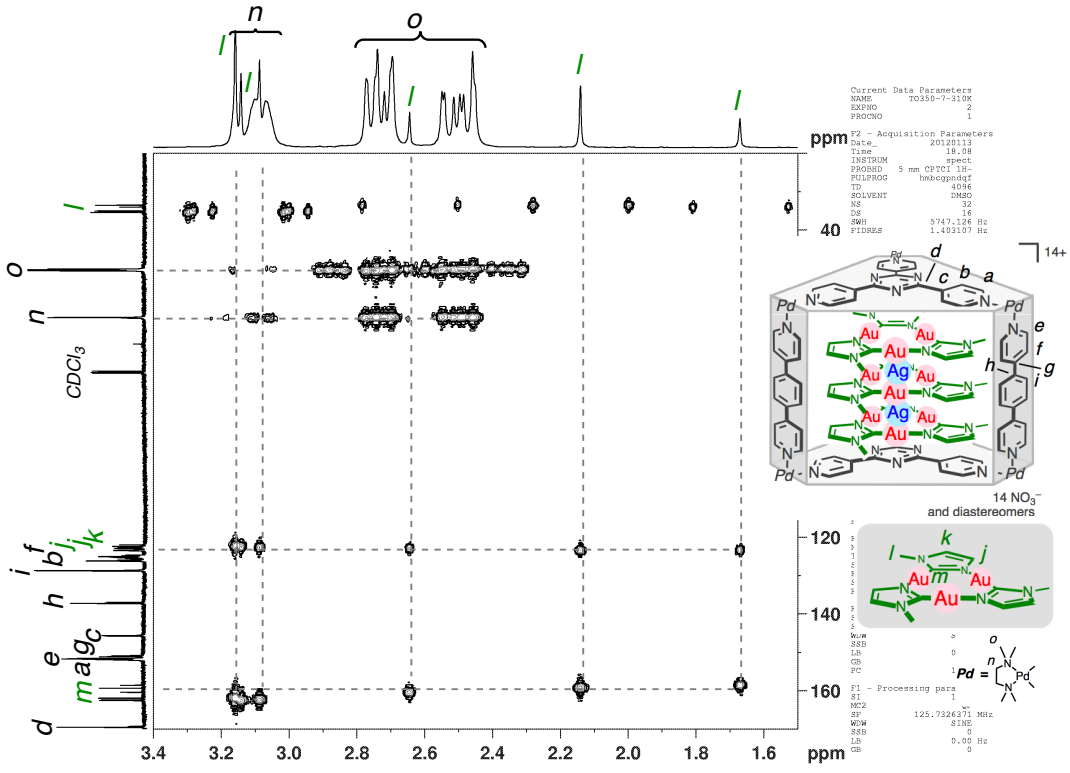

Figure S21. Enlarged ^{1}H-^{13}C HMBC (500 MHz, D_2O, 310 K) spectrum of **1c'**•(**2a**•Ag^{+}•**2a**•Ag^{+}•**2a**).

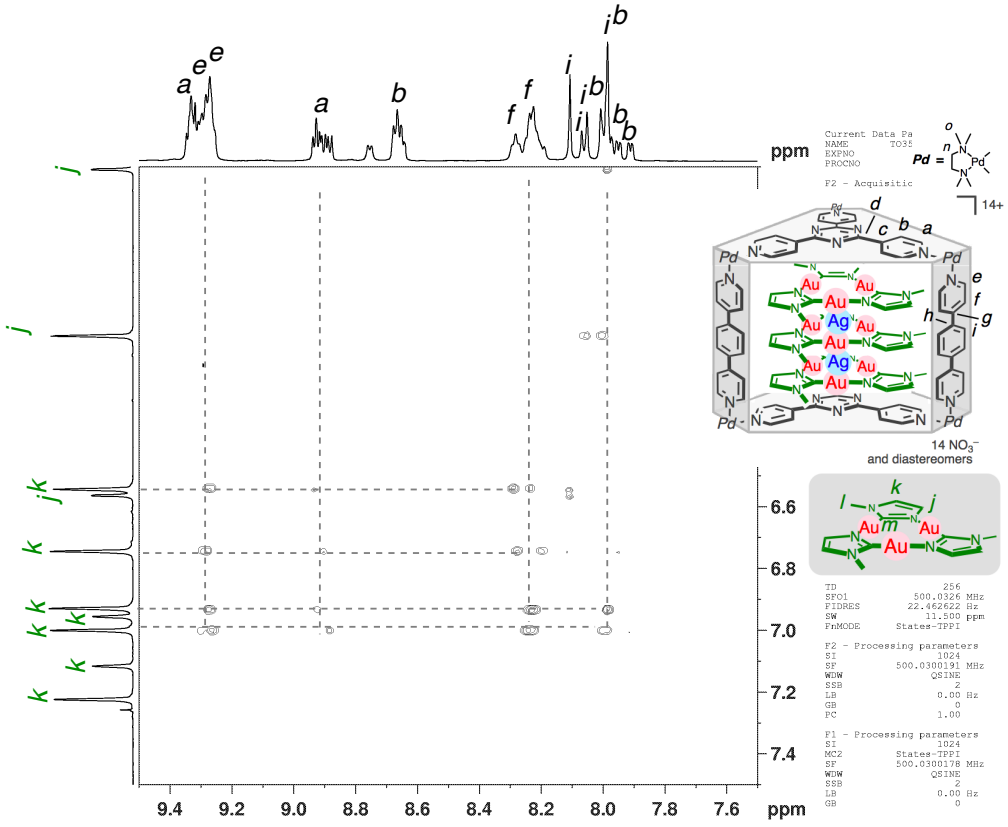

Figure S22. Enlarged ^{1}H-^{1}H NOESY (500 MHz, D_2O, 310 K) spectrum of **1c'**•(**2a**•Ag^{+}•**2a**•Ag^{+}•**2a**).

Table S2. Crystal data and structure refinement for **1c'•(2a•Ag^+•2a•Ag^+•2a)**.

Identification code	p-1-sr	
Empirical formula	C153.85 H198.32 Ag2 Au8.47 N46.93 Pd6	
Formula weight	5226.52	
Temperature	90(2) K	
Wavelength	0.71073 Å	
Crystal system	Triclinic	
Space group	*P*-1	
Unit cell dimensions	a = 19.4231(18) Å	α = 72.8860(10)°.
	b = 26.329(2) Å	β = 77.3130(10)°.
	c = 26.344(2) Å	γ = 77.2690(10)°.
Volume	12385(2) $Å^3$	
Z	2	
Density (calculated)	1.402 Mg/m^3	
Absorption coefficient	5.611 mm^{-1}	
F(000)	4977	
Crystal size	0.07 x 0.06 x 0.06 mm^3	
Theta range for data collection	0.82 to 26.24°.	
Index ranges	-24<=h<=24, -32<=k<=32, -32<=l<=32	
Reflections collected	130323	
Independent reflections	49353 [R(int) = 0.0418]	
Completeness to theta = 26.24°	98.8 %	
Absorption correction	Semi-empirical from equivalents	
Max. and min. transmission	0.7478 and 0.7118	
Refinement method	Full-matrix least-squares on F^2	
Data / restraints / parameters	49353 / 500 / 1813	
Goodness-of-fit on F^2	1.124	
Final R indices [I>2sigma(I)]	R_1 = 0.0818, wR_2 = 0.2373	
R indices (all data)	R_1 = 0.1066, wR_2 = 0.2587	
Largest diff. peak and hole	10.154 and -1.459 e.$Å^{-3}$	
CCDC reference number	894585	

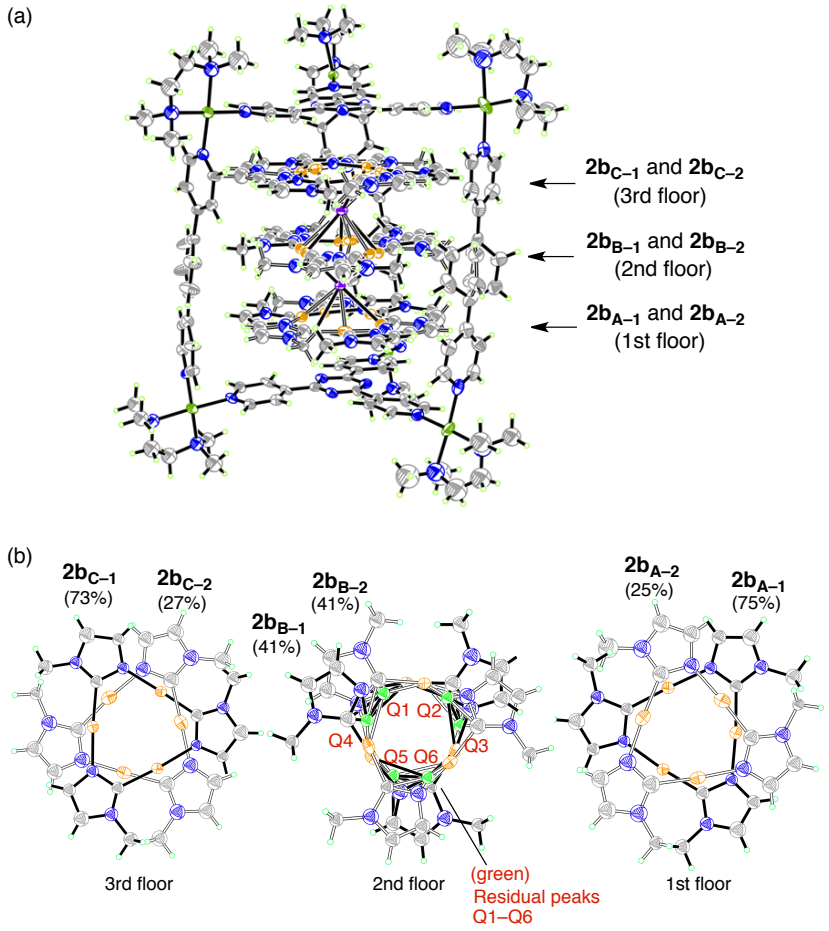

Figure S23. ORTEP drawing (30% probability ellipsoids) of **1c'•(2a•Ag$^+$•2a•Ag$^+$•2a).** (a) Crystal structure of **1c'•(2a•Ag$^+$•2a•Ag$^+$•2a)** and (b) top view of each layers.

There are three trinucular Au complexes **2a$_A$**, **2a$_B$**, and **2a$_C$** and two Ag ions within the cage molecule. The occupancy factors of guests **2a$_A$**, **2a$_B$**, and **2a$_C$** were converted to [75% (**2a$_{A-1}$**) and 25% (**2a$_{A-2}$**)], [41% (**2a$_{B-1}$**) and 41% (**2a$_{B-2}$**)], and [73% (**2a$_{C-1}$**) and 27% (**2a$_{C-2}$**)], respectively. Six large residual electron densities (10.15–7.76 eÅ^{-3}), which can be modeled as disordered Au atoms around **2a$_{B-1}$** and **2a$_{B-2}$** in a concentric fashion, were left unassigned because the occupancy factors were too small to model their bridging ligands (Figure S23b). Several restraints were applied to guest Au complexes on the basis of chemical symmetry. The thermal temperature factors of guest molecules without Au and tetramethylethylenediamine were isotropically refined. Most of the disordered counter anion and water molecules located outside the cage molecule could not be modeled, and the SQUEEZE procedure of PLATON was used in the refinement.

Chapter 4

Modular Assembly of Gold-Silver Ion Clusters with a Tray-Shaped Au_3 Scaffold

Abstract

Discrete stacks of planar $Au(I)_3$ complexes were achieved on a $Au(I)_3$ tray-shaped molecule in solution. The peripheral pyridyl groups in the tray were connected with each other via Pd(II) coordination, which provided a shallow concave scaffold for guest $Au(I)_3$ complexes. The stack number of $Au(I)_3$ complexes was specifically determined by solvent conditions. In a H_2O/CH_3CN (7:3) mixed solvent, the tray and the guest formed a 1:1 Au_3–Au_3 double stack. In water, two trays sandwiched one guest to enable a discrete 2:1 Au_3–Au_3–Au_3 triple stack. Moreover, introduction of Ag(I) ions into the system gave a 2:2 Au_3–Au_3–Ag–Au_3–Au_3 quadruple $Au(I)_3$ stack as a consequence of attractive interactions between the guest $Au(I)_3$ complexes and the Ag(I) ion.

4.1 Introduction

Stacking structures of planar aromatic compounds are widely seen in solution as well as in the crystalline and the liquid crystalline states.[1–3] Despite the fact that chemical and physical properties of the aggregates highly depend on the number of the stacking components,[4–6] precise modulation of the discrete stacking is not an easy matter, especially in solution,[7] and sophisticated and elaborated molecular designs are always demanded.[4–7]

In chapter 2, I have synthesized the finite stacks of trinuclear $Au(I)_3$ complexes bridged by aromatic ligands[8,9] to construct Au(I) ion clusters in a [3 × *n*] fashion (*n*: the number of the stacking $Au(I)_3$ complexes) (Figure 1).[10,11] In order to accumulate $Au(I)_3$ complexes and control their arrays, box-shaped confined cavities of self-assembled coordination cages were employed. The lateral rigid pillars determined the cage height, so that the number of the stacking $Au(I)_3$ complexes was precisely regulated (*n* = 1–3).

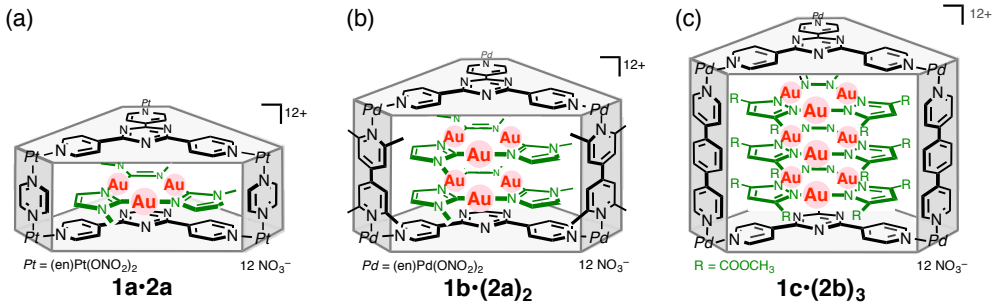

Figure 1. [3 × *n*] Au(I) clusters (*n* = 1–3) within box-shaped cages. (a) [3 × 1] Au(I) cluster **1a•2a**, [3 × 2] Au(I) cluster **1b•(2a)**$_2$, and [3 × 3] Au(I) cluster **1c•(2b)**$_3$. Self-assembled coordination cages **1** accommodated planar trinuclear $Au(I)_3$ complexes **2**. The number of stacking $Au(I)_3$ complexes **2** was precisely controlled by the height of coordination cages **1**.

Although the concept is quite simple, this system remains a matter of consideration in terms of an efficient accumulation of lots of Au(I) ions in the following reasons. First, box-shaped cages with different heights need to be prepared separately depending on the desired stacking number of the guest molecules. This implies that it is not possible to transform the formation of the ion clusters once they are synthesized. (Insertion of one equiv. of Ag(I) ions into the remaining site between two molecules of the guest $Au(I)_3$ complexes is an exceptional example, see chapter 3.) Next, two

organic panels at the top and the bottom of the cage, are not included in the components of the ion clusters, hence formation of metal ion clusters with metal-containing panel ligands is more preferable for large ion clusters.

Let us return to several early examples of self-assembled coordination architectures.[12] One of the attractive host for the recognition of a variety of guest molecules is a bowl-shaped molecule (Figure 2a).[13] The volume of the interior space can be tailored to the size and the number of guest molecules. Interestingly, both of 1:1 and 2:1 bowl/guest assembly manners are possible and these two manners are in equilibrium in solution.[13d] This system was responsive to the solvent conditions because hydrophobic effect is one of the most important driving force for the guest recognition. Meanwhile, some examples of π-conjugated receptors indicate that introduction of rigid planes at the bottom of the host is efficient for sandwiching planar guest molecules (Figure 2b).[14,15]

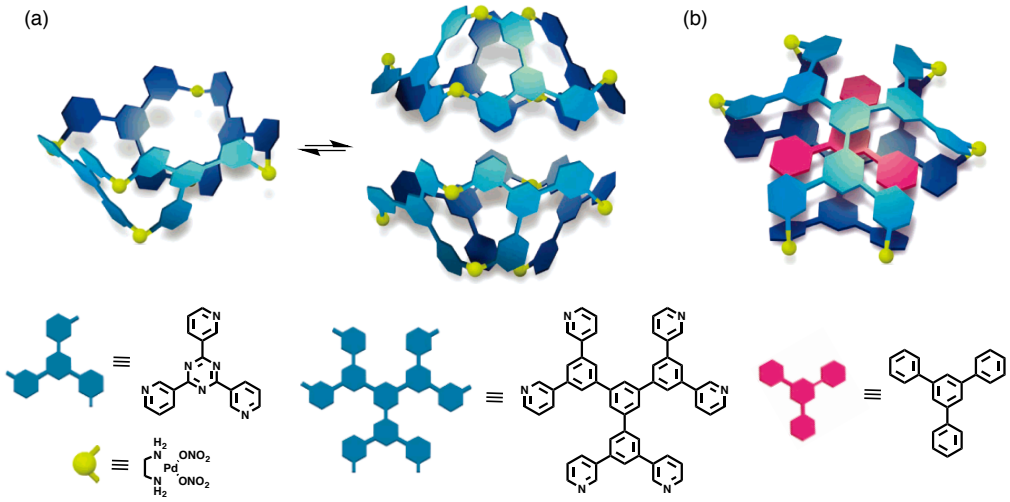

Figure 2. Early examples of self-assembled host molecules (a) A square-pyramidal bowl-shaped host complex assembled from triangular tridentated ligand and *cis*-protected (en)Pd(ONO_2)$_2$. In an aqueous media, two host molecules formed a dimeric capsule. (b) An aromatic sandwich compound assembled from π-conjugated hexadentated ligand and the same Pd hinges in the presence of a planar template (triphenylbenzene). Adapted with permission from *Acc. Chem. Res.* **2005**, *38*, 371–380. Copyright (2005) American Chemical Society.

Keep these in mind, here I design to synthesize tray-shaped Au(I)$_3$ complexes **4** and show that trays **4** act as molecular scaffolds for construction of Au(I)$_3$ stacks in

solution (Figure 3). The shallow concave cavity formed with peripheral pyridyl groups was suitable for accommodation of planar trinuclear $Au(I)_3$ complex **2a**. Moreover, the number of the stacking $Au(I)_3$ planes (n) was systematically controlled (n = 2–4) by the solvent conditions and addition of Ag(I) ions.

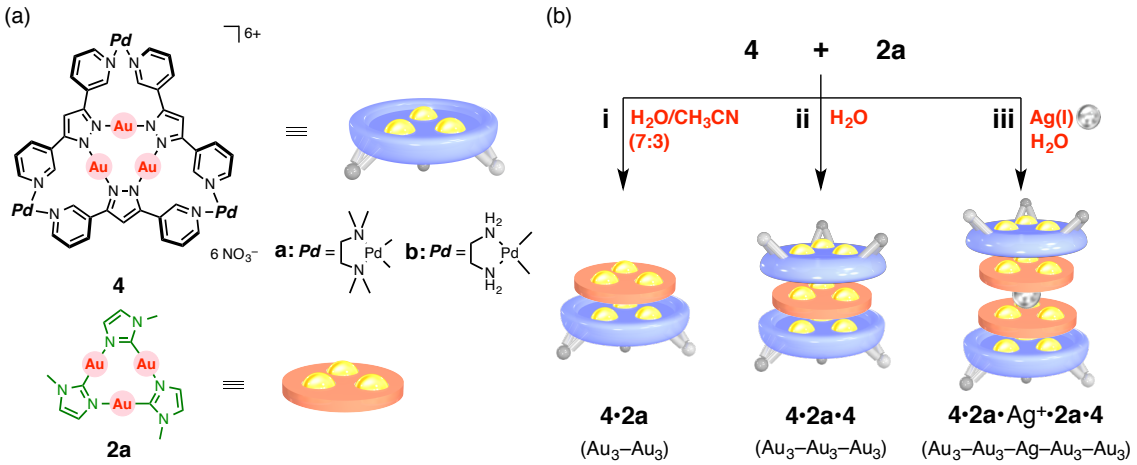

Figure 3. Controllable discrete stacks of $Au(I)_3$ complexes with tray-shaped hosts. (a) Cartoon illustration of tray-shaped $Au(I)_3$ complexes **4a** and **4b**, and planar $Au(I)_3$ guest **2a**. Trays **4a** and **4b** work as molecular scaffolds for the formation of $Au(I)_3$ stacks. (b) Schematic representation of a variety of $Au(I)_3$ stacks. In a H_2O/CH_3CN (7:3) mixed solvent, the tray and the guest formed a 1:1 double stack (i). In water, two trays sandwiched one guest to enable a 2:1 triple stack (ii). Addition of Ag(I) ions effected a 2:2 quadruple stack (iii).

4.2 Design of a Tray-Shaped Au_3 Complex

In order to effectively enlarge the number of accumulated metal ions, I synthesized a tray-shaped host molecule bearing trinuclear Au(I) complex at the bottom in the following procedure. Tricyclic $Au(I)_3$ metal-containing ligand **5** substituted with pyridyl groups was obtained by treating $ClAuS(CH_3)_2$ with tetradentate ligand 3,5-di(3-pyridyl)pyrazole under basic conditions (Scheme S1 in the Experimental Section). Only the pyrazolate moiety underwent Au(I) coordination, and then formed planar $Au(I)_3$ metal-containing ligand because of a linear coordination geometry of Au(I) and the stability caused by a metal-aromaticity of the product. The clipping of the adjacent pyridyl groups at the periphery of $Au(I)_3$ complex **5** proceeded quantitatively and formed tray-shaped $Au(I)_3Pd(II)_3$ complex **4a** when $Au(I)_3$

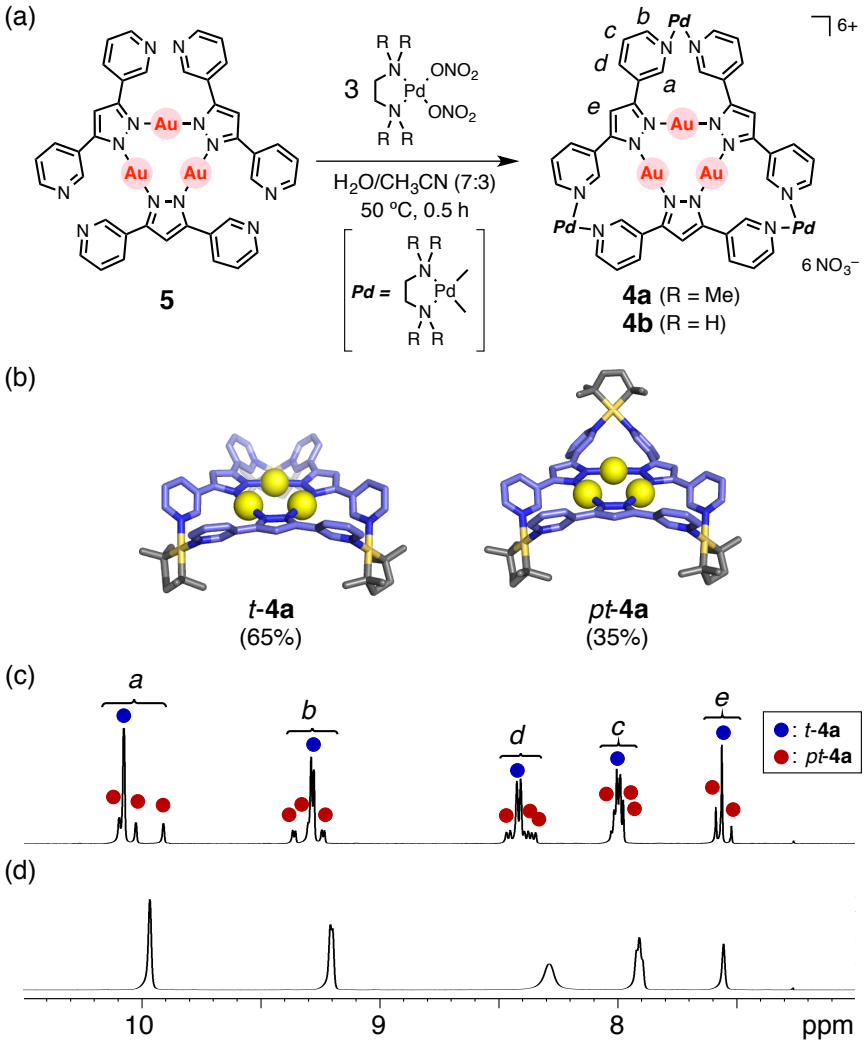

Figure 4. Synthesis of tray-shaped Au(I)$_3$ complex 4. (a) Trays **4a** and **4b** quantitatively assembled from Au(I)$_3$ metalloligand **5** and three equivalents of Pd hinges in H_2O/CH_3CN (7:3). (b) Molecular models of two isomers of Au(I)$_3$ complexes **4a**, tray form *t*-**4a** and partial-tray form *pt*-**4a**, optimized with force-field calculations (C: blue-gray, N: blue, Au: yellow, Pd: light-orange, tmeda:gray) All hydrogens are omitted for clarity. (c,d) ^{1}H NMR spectra of Au(I)$_3$ complexes **4** [500 MHz, 300 K, D_2O/CD_3CN (7:3), aromatic region]. (c) The two types of sharp signals of Au(I)$_3$ complex **4a** indicate the existence of two diastereomers, tray *t*-**4a** (65%, blue circle) and partial-tray *pt*-**4a** (35%, red circle). (d) One set of broad signals of Au(I)$_3$ complex **4b** shows the exchange between tray *t*-**4b** and partial-tray *pt*-**4b** in the NMR timescale.

metal-containing ligand **5** (6.3 mg, 0.005 mmol) was suspended in an H_2O/CH_3CN (7:3; 1.0 mL) mixed solution of [(tmeda)Pd$(ONO_2)_2$] (tmeda = tetramethylethylenediamine) (5.2 mg, 0.015 mmol, three equivalents) at 50 ºC for 30 min (Figure 4a). Cold spray

ionization MS (CSI-MS) analysis of the resulting clear pale-yellow solution suggested the coordination of three equivalents of Pd hinges to $Au(I)_3$ metal-containing ligand with a molecular weight of 2294.5 Da (Figure S9). ^{1}H NMR spectroscopy indicated the existence of two isomers, tray *t*-**4a** and partial-tray *pt*-**4a**, in a 2:1 ratio (Figure 4b, c). In the aromatic region, the five large signals are attributed to the $H_{a–e}$ protons of tray *t*-**4a**, where all the three Pd hinges are on the same side of the Au_3 plane. In addition, three sets of signals appeared in a 1:1:1 ratio around each $H_{a–d}$ signal and two in a 2:1 ratio around the H_e signal, corresponded to the symmetry of partial-tray *pt*-**4a** with one inverted Pd corner. A exchange between two diastereomers was not found in the NMR timescale in temperature range of 290–340 K, presumably owing to the bulkiness of the (tmeda)Pd hinges regardless of the lability of the Pd–N bonds. When less bulky $(en)Pd(ONO_2)_2$ (en = ethylenediamine) was used instead of $(tmeda)Pd(ONO_2)_2$, ^{1}H NMR spectrum of the solution only showed five broad signals (Figure 4d), suggesting the fluxional exchange between tray *t*-**4b** and partial-tray *pt*-**4b**.

Single crystals of tray **4b** were obtained by co-crystallization with a planar aromatic molecule (**6**; triphenylene). X-ray analysis revealed a structure of 1:1 aggregation complex (*t*-**4b**)•**6** (Figure 5). Peripheral pyridyl groups in the tray provided a shallow concave cavity with an Au_3 complex at the bottom, in which the

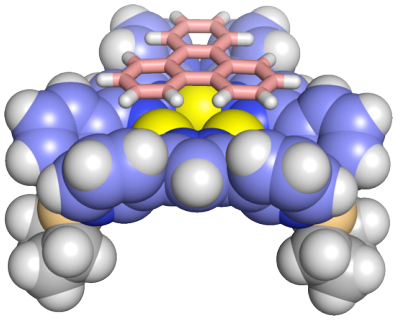

Figure 5. X-ray crystallographic analysis of 1:1 association complex (*t*-4b)•6 (6: triphenylene). A 1:1 stack of tray *t*-**4b** and planar aromatic **6** was clearly observed in the crystalline state (the color code of tray *t*-**4b** is the same as that of Figure 4b, triphenylene; light pink, H; white). All the counterions (NO_3^-) and solvents are omitted for clarity. The peripheral pyridyl gropus in the tray provided a shallow concave cavity for the guest. The Au···aromatic distances ranged from 3.31 to 3.40 Å. A couple of examples of Au···π interactions are reported previously.[19,20] Adapted with permission from *Angew. Chem. Int. Ed.* **2014**, *53*, 11186–11189. Copyright (2014) John Wiley and Sons.

planar guest **6** was recognized. The stable formation of a 1:1 stack with electron-rich (donor, D) aromatics such as triphenylene indicates the electron-poor (acceptor, A) nature[16–18] of tray-shaped Au_3 complex *t*-**4** and electrostatic interaction is one of the important driving force for the assembly.

4.3 Construction of Gold-Silver Ion Clusters

This result was applied to the construction of an Au_3–Au_3 double stack with electron-rich (D) $Au(I)_3$ complex.[8,16–18] Imidazolate-bridged $Au(I)_3$ complex **2a** (8.3 mg, 0.010 mmol) was suspended in an H_2O/CH_3CN (7:3) solution of a equilibrium mixture of Au_3 tray *t*-**4a** and partial-tray *pt*-**4a** (5.0 mM, 1.0 mL) at 50 ºC for 30 min (Figure 6a). After filtration of the residual excess guests, ^{1}H NMR spectroscopy

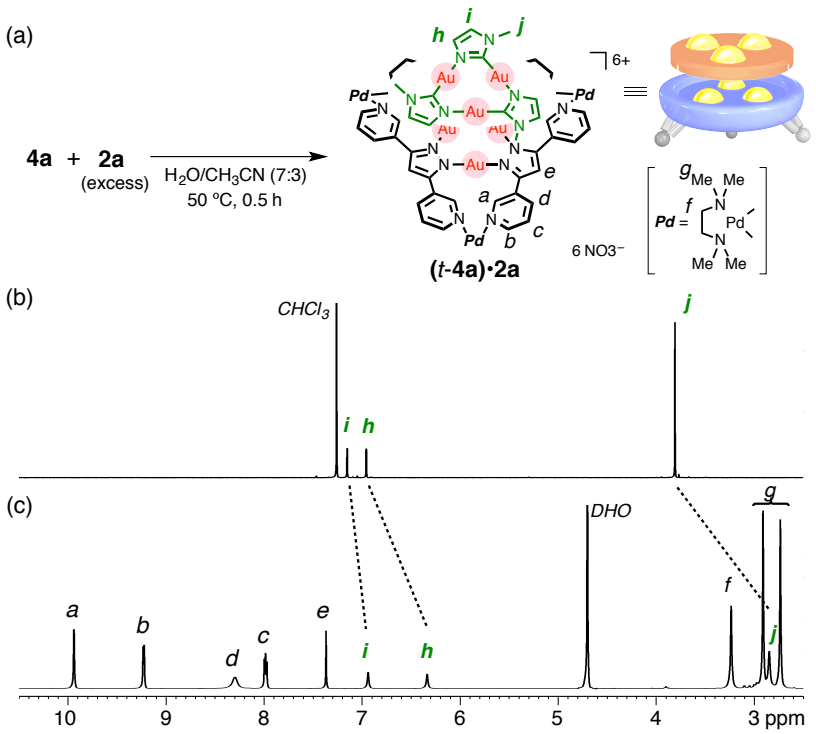

Figure 6. Formation of a 1:1 Au_3–Au_3 double stack. (a) Synthesis of an $Au(I)_3$ double stack (*t*-**4a**)•**2a**. (b,c) ^{1}H NMR spectra (500 MHz, 300K) of (b) $Au(I)_3$ guest complex **2a** (in $CDCl_3$) and (c) 1:1 aggregation complex (*t*-**4a**)•**2a** [in D_2O/CD_3CN (7:3)]. Adapted with permission from *Angew. Chem. Int. Ed.* **2014**, *53*, 11186–11189. Copyright (2014) John Wiley and Sons.

revealed a formation of a 1:1 Au_3–Au stacking complex, (*t*-**4a**)•**2a**, in 93%. Signals of guest **2a** showed upfield shift (e.g., $\Delta\delta_{max} = -1.0$ ppm for H_j) as a result of shielding effect by the aromatic panels of *t*-**4a** (Figure 6b, c), as can be seen in the case of the encapsulation within box-shaped cages in chapter 2. The fact that NMR signals of partial-tray *pt*-**4a** was not observed evidenced that the fluxional exchange between two diastereomers of Au_3 tray **4a** and the equilibrium was totally converted to tray form in the presence of guest **2a**. A diffusion-ordered spectroscopy (DOSY) NMR showed the same diffusion coefficient ($D = 1.9 \times 10^{-10}$ m^2s^{-1}) for the signals of tray *t*-**4a** and guest **2a**, indicating tray *t*-**4a** tightly associated with guest **2a** in solution (Figure S19). In the same manner, $Au(I)_3$ tray **4b** formed a similar stable association complex (*t*-**4b**)•**2a**.

On the basis of these observations, the solvent dependency of the present system was considered. In water, the following ^{1}H NMR experiment revealed that tray-shaped Au_3 complex forms an Au_3–Au_3 self-assembled dimer (*t*-**4**)•(*t*-**4**) in a face-to-face manner with hydrophobic $Au(I)_3$ planes inside (Figure 7). In the ^{1}H NMR spectrum of tray **4b** containing (en)$Pd(ONO_2)_2$, one set of signals are observed in aromatic region for each proton $H_{a–d}$ (blue circles in Figure 7a). On the other hand, the spectrum of tray **4c**, which has (1*S*,2*S*)-1,2-cyclohexanediamines instead of ethylenediamines as Pd hinges, showed two sets of $H_{a–d}$ signals in a 1:1 ratio (red circles in Figure 7b), indicating the asymmetric environment of these protons. With this in mind, when aqueous solutions of tray **4b** (5.0 mM, 1 mL) and **4c** (5.0 mM, 1 mL) were mixed, ^{1}H NMR spectrum of the resulting solution revealed four sets of $H_{a–d}$ signals (green circles in Figure 7c) around each signal of tray **4b** and **4c** (blue and red circles). The symmetry of these signals indicated that tray molecules formed a self-stacked dimer (*t*-**4b**)•(*t*-**4c**) as well as dimers (*t*-**4b**)•(*t*-**4b**) and (*t*-**4b**)•(*t*-**4b**). At the same time, a fluxional exchange between two isomers *t*-**4** and *pt*-**4** was suppressed in an aqueous media. The ratio of these self-stacked dimers (*t*-**4b**)•(*t*-**4b**), (*t*-**4c**)•(*t*-**4c**), and (*t*-**4b**)•(*t*-**4c**) was 1:1:2, indicating a statistical distribution of the three dimers. Continuous stirring of the mixture for 1 day generated many new signals in ^{1}H NMR spectrum because the lability of the Pd–N bonds allowed the trays to open and then close after the exchange of the Pd hinges (Figure 7d). Unfortunately, the CSI-MS study only detected ion peaks derived from single component **4b** as a fragmentation spices (Figure S24).

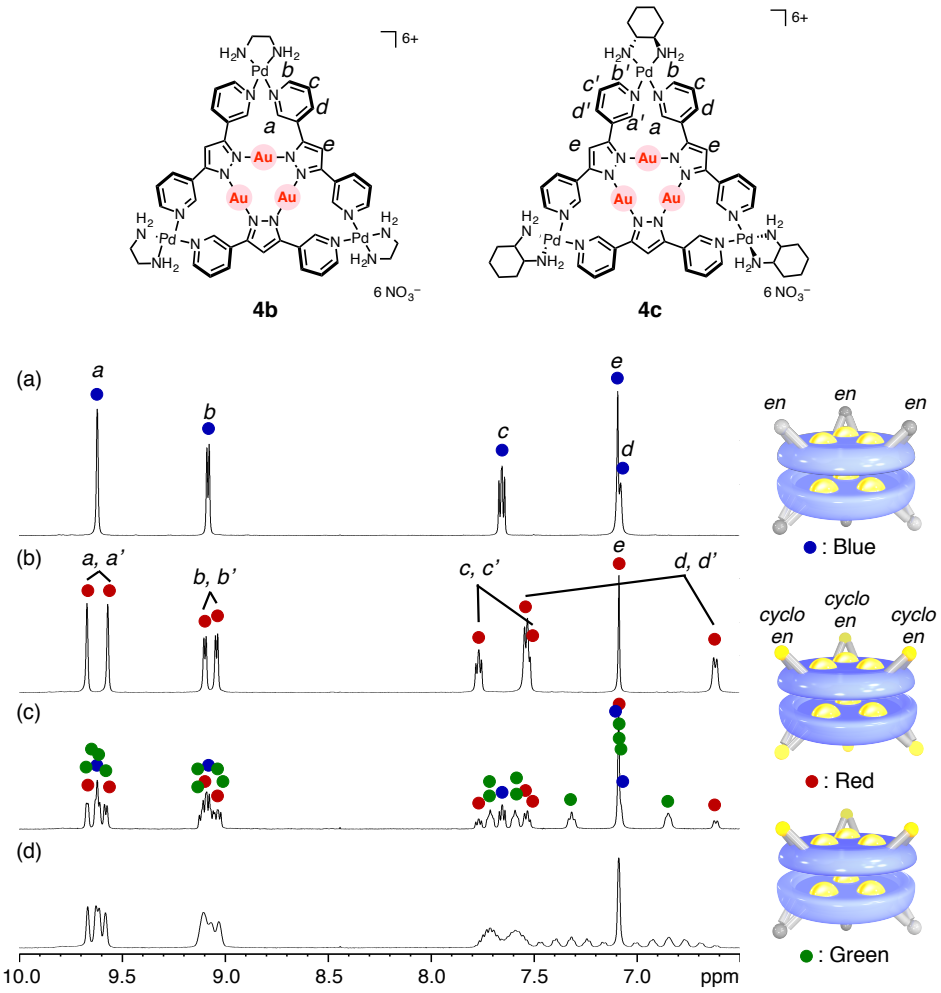

Figure 7. Formation of a 1:1 self-stack dimer in an aqueous solution. ^{1}H NMR spectra (500 MHz, 300 K, D_2O, aromatic region) of (a) tray **4b** and (b) tray **4c**, after mixing both solutions for (c) 5 min. and (d) 1 day.

When the foregoing guest recognition experiment was carried out in an aqueous solution, $Au(I)_3$ complex **2a** was sandwiched by two molecules of tray *t*-**4b** to give discrete Au_3–Au_3–Au_3 triple stack (*t*-**4b**)•**2a**•(*t*-**4b**) quantitatively as confirmed by NMR spectroscopy (Scheme **i** in Figure 8a). Note that tray **4b** was used because of its high solubility in water. In the ^{1}H NMR spectrum, signals of tray *t*-**4b** and guest **2a** were observed in a 2:1 integral ratio and notably, those of tray *t*-**4b** were observed in a 1:1 ratio (Figure 8b). This result suggests that the entire aggregate has a C_{3h} sandwiched structure without inversion or exchange of C_{3h} symmetrical guest **2a**. Then, the tray protons are in diastereomeric environments. Even when an excess amount of guest $Au(I)_3$ complex **2a** was employed to the system, the tray–guest ratio was saturated at a

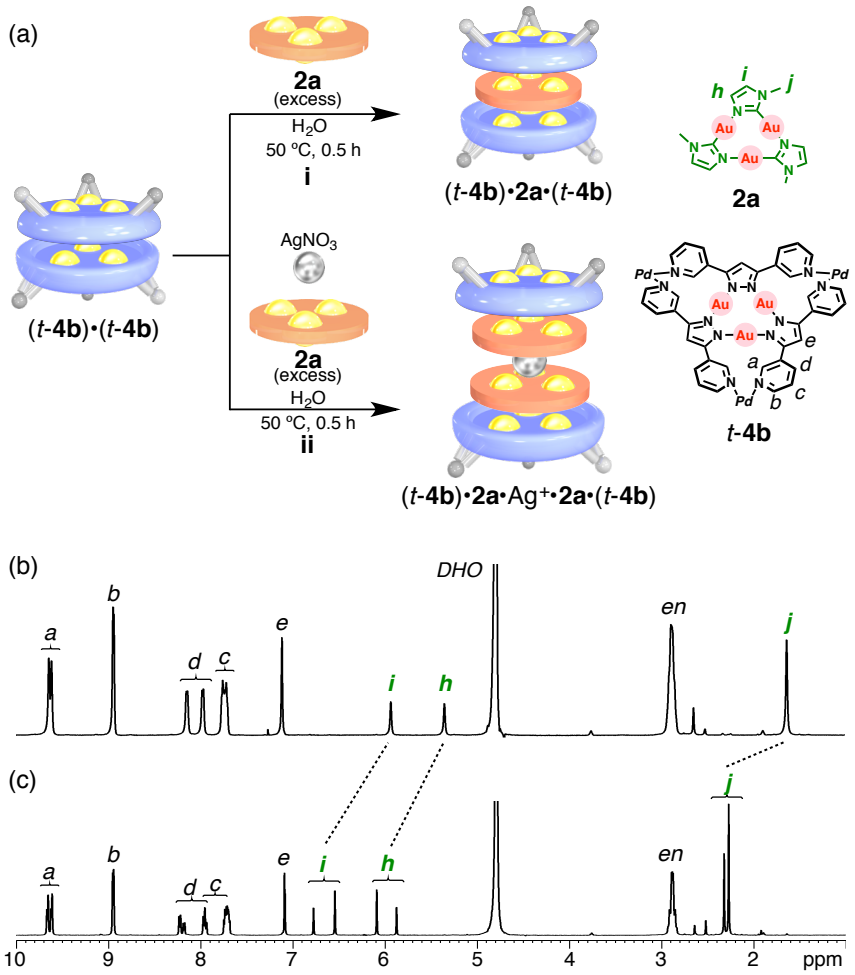

Figure 8. Formation of Au_3–Au_3–Au_3 triple and Au_3–Au_3–Ag–Au_3–Au_3 quadruple stacks. (a) Cartoon illustration of the synthesis of triple and quadruple $Au(I)_3$ stacks (*t*-**4b**)•**2a**•(*t*-**4b**) and (*t*-**4b**)•**2a**•Ag^+•**2a**•(*t*-**4b**) from the self-stacked dimer of $Au(I)_3$ trays (*t*-**4b**)•(*t*-**4b**). (b,c) ^1H NMR spectra (500 MHz, 300 K, D_2O) of each $Au(I)_3$ multiple stacks (b) 2:1 aggregation complex (*t*-**4b**)•**2a**•(*t*-**4b**), and (c) 2:2 complex (*t*-**4b**)•**2a**•Ag^+•**2a**•(*t*-**4b**). Adapted with permission from *Angew. Chem. Int. Ed.* **2014**, *53*, 11186–11189. Copyright (2014) John Wiley and Sons.

2:1 ratio. Furthermore, this 2:1 composition was supported by CSI-MS experiment (Figure S32). The fact that the solvent conditions controlled the association ratio means that the hydrophobic effect is one of the main driving forces in this tray–guest recognition system. Indeed, the following addition of CH_3CN into the aqueous solution of Au_3–Au_3–Au_3 triple stack (*t*-**4b**)•**2a**•(*t*-**4b**) disassembled the structure to regenerate Au_3–Au_3 double stack (*t*-**4b**)•**2a**.

To further achieve a higher-level stack of $Au(I)_3$ complexes, I focused on an interaction[21–23] between trinuclear $Au(I)_3$ complexes and Ag(I) ions that was used in chapter 3,[11] in addition to the hydrophobic effects. When an excess amount of guest **2a** and $AgNO_3$ (1 equiv.) was mixed in an aqueous solution of self-stacked dimer of tray (*t*-**4b**)•(*t*-**4b**), Au_3–Au_3–Ag–Au_3–Au_3 association complex (*t*-**4b**)•**2a**•Ag^+•**2a**•(*t*-**4b**) was obtained quantitatively (Scheme **ii** in Figure 8a). In the ^1H NMR spectrum, two sets of signals were observed for C_{3h} symmetrical guest **2a** and the integration ratio of guest **2a** to tray *t*-**4b** was the same (Figure 8c). This observation suggests that two guests **2a** tightly stacked with either the same or opposite orientations (for two stacking modes of C_{3h} symmetrical guest **2a**, see preceding chapters) and that two tray molecules *t*-**4b** sandwiched the guest dimer (**2a**)$_2$ to form a 2:2 tray–guest association complex. Indeed, diastereotopic protons of tray *t*-**4b** (originally C_{3v} symmetry) showed not less than four sets of signals. Since only 1 equivalent of Ag(I) ions is required for the construction of the quadruple $Au(I)_3$ stack, one Ag(I) ions is selectively sandwiched with electron-rich guest $Au(I)_3$ complexes **2a**, not with guest **2a** and electron-poor tray *t*-**4b** to form Au_3–Au_3–Ag–Au_3–Au_3 association complex (*t*-**4b**)•**2a**•Ag^+•**2a**•(*t*-**4b**). The results that the signals of guest **1a** shifted downfield compared to those in Au_3–Au_3–Au_3 triple stack (*t*-**4b**)•**2a**•(*t*-**4b**), also suggests the position of the Ag(I) ion. It should be noted that electron rich $Au(I)_3$ complexes **2a** sandwich a Ag(I) ion through Au(I)–Ag(I) interactions to from Au–Ag hetero ion clusters in the preceding chapter. The stack composition was stable even in H_2O/CH_3CN (7:3) mixed solvent, in which triple stack (*t*-**4b**)•**2a**•(*t*-**4b**) was not maintained.

The alignment of Au(I) and Ag(I) ions in the cluster was clearly determined by X-ray crystallographic analysis (Figure 9). Single crystals suitable for X-ray analysis were obtained by slow diffusion of THF vapor into an H_2O/CH_3CN (7:3) solution of the association complex (*t*-**4b**)•**2a**•Ag^+•**2a**•(*t*-**4b**) for 1 week. Guest $Au(I)_3$ complex **2a** was efficiently fixed in the shallow concave platform of tray *t*-**4a**, forming a columnar Au_3 quadruple stack. When we focus on the metal ion array, the hourglass-style metal ion cluster is composed of two vertical $Au(I)_6$ prismatic units and a single Ag(I) ion connecting them. The overall metal ion column largely twisted with each other around the vertical axis passing through the central Ag(I) atom. In addition, tray–guest stack in the both Au_3–Au_3 units slightly twisted in consequence of the steric demands of the methyl groups of guest **2a**. The Au···Ag distances [3.290(3)–3.372(3) Å] and the

intermolecular Au···Au contacts between tray *t*-**4a** and guest **2a** [2.745(3)–2.863(3) Å] were shorter than the sum of the van der Waals radii (~ 3.4 and 3.6 Å, respectively),[24] suggesting the attractive interactions between Au(I)–Ag(I)[25–29] and Au(I)–Au(I)[30–32] ions. The Au(I)–Ag(I) interaction is of particular interest because the Ag(I) ions efficiently worked as a glue connecting two Au_3–Au_3 stacks (*t*-**4a**)•**2a** in a face-to-face fashion.

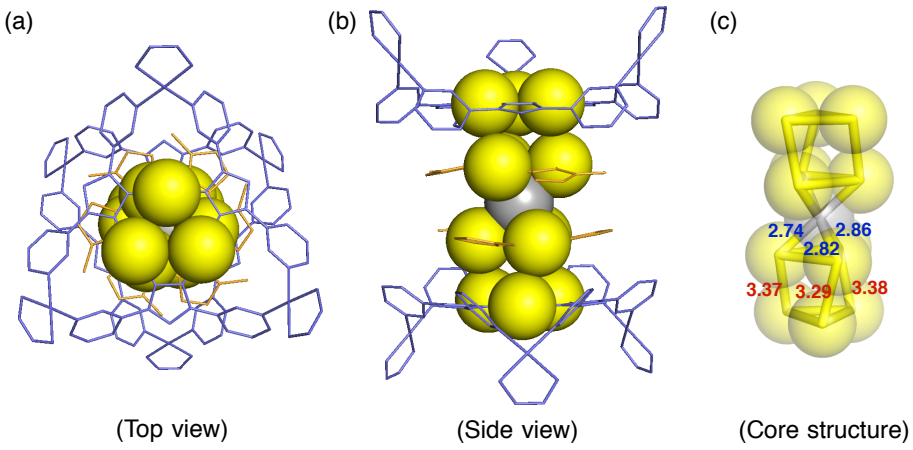

Figure 9. X-ray crystal structure of Au_3–Au_3–Ag–Au_3–Au_3 quadruple stack (*t*-4a)·2a·Ag^+·2a·(*t*-4a). (a,b) Two molecules of tray *t*-**4a** (blue) sandwiched the dimer of guest **2a** (orange) and a Ag(I) ion (gray) located at the center (Au: yellow). All the counterions (NO_3^-) and solvents are omitted for clarity. A disordered model was applied to the guest $Au(I)_3$ complexes **2a** and the molecular geometry of the largest portion of disordered molecules is discussed in this study. (c) Highlight of the Au(I)–Ag(I) core structure. The distances between Au···Ag and Au···Au are given in Å. The Au···Ag distances are closed to those observed in an infinite $(Au_3–Ag–Au_3)_n$ crystalline chain (2.731–2.922 Å), see ref. 21. Au(I)–Ag(I) and Au(I)–Au(I) interactions are effectively worked to form the $Au(I)_3$ quadruple stack.

4.4 Absorption and Emission Spectra

UV-vis absorption spectra of self-stacked tray (*t*-**4b**)•(*t*-**4b**) and Au(I) ion cluster (*t*-**4b**)•**2a**•(*t*-**4b**), and Au(I)–Ag(I) ion cluster (*t*-**4b**)•**2a**•Ag^+•**2a**•(*t*-**4b**) were measured in H_2O at room temperature (Figure 10). Compared to the spectrum of self-stacked dimer (*t*-**4b**)•(*t*-**4b**), guest sandwiching complex (*t*-**4b**)•**2a**•(*t*-**4b**) showed strong absorption at around 330 nm. Because dilute solution of Au_3 complex **1a** (in $CHCl_3$)

is colorless, the red shift of the absorption indicates tight stacking of guest **2a** and trays *t*-**4b**, and probably due to Au(I)–Au(I) interaction[30–32] between their Au(I) ions. Moreover, new absorption peak at 365 nm (ε = 2000 $M^{-1}cm^{-1}$) which is appeared in the spectrum of Au(I)–Ag(I) cluster (*t*-**4b**)•**2a**•Ag^+•**2a**•(*t*-**4b**) was derived from Au(I)–Ag(I) interactions[25–29] between guest **2a** and central Ag(I) ion.

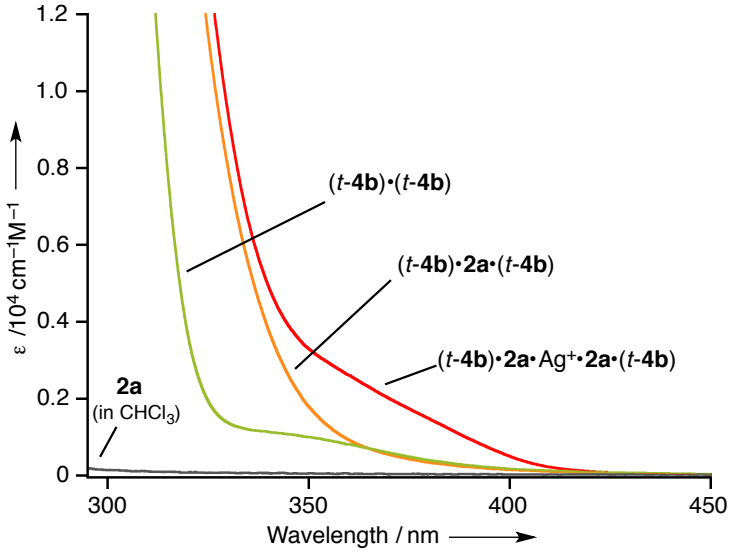

Figure 10. Absorption spectra of Au(I), Au(I)–Ag(I) ion clusters (RT, 1.0 mM, H_2O). UV/vis spectra (RT, 1.0 mM) of guest **2a** (in $CHCl_3$, gray line), Au_3–Au_3 self-stacked dimer (*t*-**4b**)•(*t*-**4b**) (in H_2O, green line), Au_3–Au_3–Au_3 triple stack (*t*-**4b**)•**2a**•(*t*-**4b**) (in H_2O, orange line), and quadruple Au_3 stack (*t*-**4b**)•**2a**•Ag^+•**2a**•(*t*-**4b**) (in H_2O, red line).

Among the aforementioned Au(I), Au(I)–Ag(I) clusters, only an aqueous solution of Au_3–Au_3–Ag–Au_3–Au_3 ion cluster (*t*-**4b**)•**2a**•Ag^+•**2a**•(*t*-**4b**) showed an emission. Figure 11 shows the emission and excitation spectra of the Au(I)–Ag(I) cluster at room temperature. An emission peak was observed at 528 nm under excitation at 333 nm. The excitation spectrum acquired at λ_{em} = 528 nm showed main peak at 333 nm and weak peak (shoulder) was observed at around 365 nm. These two peaks are consistent with two absorptions generated when guest **2a** was sandwiched between self-stacked tray (*t*-**4b**)•(*t*-**4b**), and Ag(I) ion was introduced in the system (Figure 11). A similar luminescence is observed for $[Au_3–Ag–Au_3]_n$ infinite crystalline chain[21] ,for which the green luminescence with λ_{max} ~ 535 nm at 293 K and also for recently reported discrete [Au_3–Ag–Au_3] cluster.[23] Thus, this emission seems

to be derived from interactions between Au(I) and Ag(I) ions. [25–29]

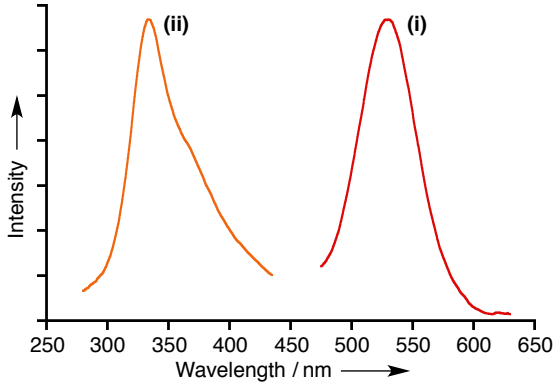

Figure 11. Emission and excitation spectra (RT, 0.10 mM) of Au_3–Au_3–Ag–Au_3–Au_3 stack (*t*-4b)·2a·Ag^+·2a·(*t*-4b) in H_2O. The emission spectrum (i) was measured at λ_{ex} = 333 nm and the excitation spectrum (ii) was acquired at λ_{em} = 528 nm.

4.5 Conclusion

In this chapter, I have shown that tray-shaped $Au(I)_3$ molecule **4** worked as a molecular scaffold to achieve discrete stacks of $Au(I)_3$ complexes with the guest Au_3 complexes **2a** in solution. The shallow concave cavity of the tray molecule **4** was formed by the Pd(II) clipping of peripheral pyridyl groups of $Au(I)_3$ complex **5**. Although the tray **4** showed fluxional exchange between tray form *t*-**4** and partial-tray form *pt*-**4** depending on the position of Pd(II) hinges, this dynamic exchange was converged to tray form *t*-**4** when tray molecule recognized planar guest molecules. The number of stacking $Au(I)_3$ planes was systematically controlled depending on the solvent conditions and addition of Ag(I) ions to form Au_3–Au_3, Au_3–Au_3–Au_3, and Au_3–Au_3–Ag–Au_3–Au_3 ion clusters (Figure 12). This chapter demonstrated that conventional confined cavities are not always necessary for construction of discrete molecular stacks, which are shown in the previous chapters. The present shallow concave platform will make it possible to achieve a variety of dynamic molecular stacks at will in solution.

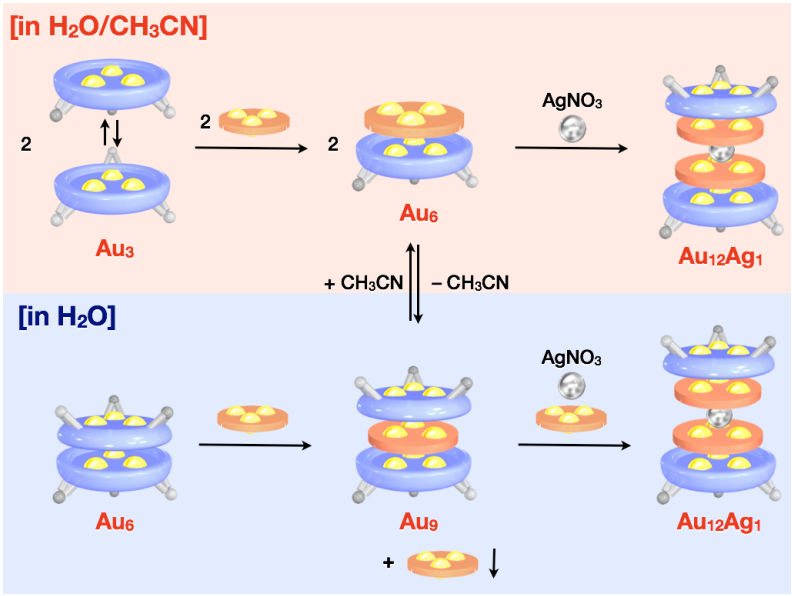

Figure 12. Survey of metal ion clusters constructed with tray shaped hosts and planar guests. In this chapter, a variety of Au(I) and Au(I)–Ag(I) clusters are constructed with a tray shaped $Au(I)_3$ complex. The assembled structure was systematically controlled depending on the solvent conditions and the addition of Ag(I) ions in this system.

4.6 References

[1] C. A. Hunter, J. K. M. Sanders, *J. Am. Chem. Soc.* **1990**, *112*, 5525–5534.

[2] C. A. Hunter, K. R. Lawson, J. Perkins, C. J. Urch, *J. Chem. Soc., Perkin Trans.* **2001**, *2*, 651–669.

[3] F. J. M. Hoeben, P. Jonkheijm, E. W. Meijer, A. P. H. J. Schenning, *Chem. Rev.* **2005**, *105*, 1491–1546.

[4] R. X.-F. Ren, N. C. Chaudhuri, P. L. Paris, S. Rumney IV, E. T. Kool, *J. Am. Chem. Soc.* **1996**, *118*, 7671–7678.

[5] T. Nakano, K. Takewaki, T. Yade, Y. Okamoto, *J. Am. Chem. Soc.* **2001**, *123*, 9182–9183.

[6] S. Yagi, I. Yonekura, M. Awakura, M. Ezoe, T. Takagishi, *Chem. Commun.* **2001**, 557–558.

[7] J. K. Klosterman, Y. Yamauchi, M. Fujita, *Chem. Soc. Rev.* **2009**, *38*, 1714–1725.

[8] F. Bonati, A. Burini, B. R. Pietroni, B. Bovio, *J. Organomet. Chem.* **1989**, *375*,

147–160.

[9] For reviews of $Au(I)_3$ complexes, see: a) A. Burini, A. A. Mohamed, J. P. Fackler Jr. *Comments Inorg. Chem.* **2003**, *24*, 253–280; b) H. E. Abdou, A. A. Mohamed, J. P. Fackler Jr. in *Gold chemistry: Applications and Future Directions in the Life Science* (Ed: F. Mohr) Wiley-VCH, Weinheim, **2008**, pp. 1–45.

[10] a) T. Osuga, T. Murase, K. Ono, Y. Yamauchi, M. Fujita, *J. Am. Chem. Soc.* **2010**, *132*, 15553–15555; b) M. Kiguchi, J. Inatomi, Y. Takahashi, R. Tanaka, T. Osuga, T. Murase, M. Fujita, T. Tada, S. Watanabe, *Angew. Chem. Int. Ed.* **2013**, *52*, 6202–6205.

[11] T. Osuga, T. Murase, M. Fujita, *Angew. Chem. Int. Ed.* **2012**, *51*, 12199–12201.

[12] a) M. Fujita, K. Umemoto, M. Yoshizawa, N. Fujita, T. Kusukawa, K. Biradha, *Chem. Commun.* **2001**, 509–518; b) M. Fujita, M. Tominaga, A. Hori, B. Therrien, *Acc. Chem. Res.* **2005**, *38*, 371–380.

[13] a) M. Fujita, S.-Y. Yu, T. Kusukawa, H. Funaki, K. Ogura, K. Yamaguchi, *Angew. Chem. Int. Ed.* **1998**, *37*, 2082–2085; b) S.-Y. Yu, T. Kusukawa, K. Biradha, M. Fujita, *J. Am. Chem. Soc.* **2000**, *122*, 2665–2666; c) S. Tashiro, M. Tominaga, Y. Yamaguchi, K. Kato, M. Fujita, *Angew. Chem. Int. Ed.* **2006**, *45*, 241–244; d) S. Tashiro, M. Tominaga, Y. Yamaguchi, K. Kato, M. Fujita, *Chem. Eur. J.* **2006**, *12*, 3211–3217.

[14] a) M. Fujita , S. Nagao, K. Ogura, *J. Am. Chem. Soc.* **1995**, *117*, 1649–1650; b) S. Hiraoka, M. Fujita, *J. Am. Chem. Soc.* **1999**, *121*, 10239–10240.

[15] K. Kumazawa, Y. Yamanoi, M. Yoshizawa, T. Kusukawa, M. Fujita, *Angew. Chem. Int. Ed.* **2004**, *43*, 5936–5940.

[16] M. A. Omary, M. A. Rawashdeh-Omary, M. W. A. Gonser, O. Elbjeirami, T. Grimes, T. R. Cundari, H. V. K. Diyabalanage, C. S. P. Gamage, H. V. R. Dias, *Inorg. Chem.* **2005**, *44*, 8200–8210.

[17] L. E. Sansores, R. Salcedo, A. Martínes, N. Mireles, *THEOCHEM,* **2006**, *763*, 7-11.

[18] S. M. Tekarli, T. R. Cundari, M. A. Omary, *J. Am. Chem. Soc.* **2008**, *130*, 1669–1675.

[19] a) F.-B. Xu, Q.-S. Li, L.-Z. Wu, X.-B. Leng, Z.-C. Li, X.-S. Zeng, Y. L. Chow, Z.-Z. Zhang, *Organometallics*, **2003**, *22*, 633–640; b) Q.-S. Li, C.-Q. Wan, R.-Y.

Zou, F.-B. Xu, H.-B. Song, X.-J. Wan, Z.-Z. Zhang, *Inorg. Chem.* **2006**, *45*, 1888–1890.

[20] J. D. Crowley, I. M. Steele, B. Bosnich, *Inorg. Chem.* **2005**, *44*, 2989–2991.

[21] a) A. Burini, J. P. Fackler, Jr., R. Galassi, B. R. Pietroni, R. J. Staples, *Chem. Commun.* **1998**, 95–96; b) A. Burini, R. Bravi, J. P. Fackler, Jr., R. Galassi, T. A. Grant, M. A. Omary, B. R. Pietroni, R. J. Staples, *Inorg. Chem.* **2000**, *39*, 3158–3165.

[22] a) A. Kishimura, T. Yamashita, T. Aida, *J. Am. Chem. Soc.* **2005**, *127*, 179–183; b) H. O. Lintang, K. Kinbara, T. Yamashita, T. Aida, *Chem. Asian J.* **2012**, *7*, 2068–2072.

[23] W.-X. Ni, Y.-M. Qiu, M. Li, J. Zheng, R. W.-Y. Sun, S.-Z. Zhan, S. W. Ng, D. Li, *J. Am. Chem. Soc.* **2014**, *136*, 9532–9535.

[24] A. Bondi, *J. Phys. Chem.* **1964**, *68*, 441–451.

[25] E. J. Fernández, C. Hardacre, A. Laguna, M. C. Lagunas, J. M., López-de-Luzuriaga, M. Monge, M. Montiel, M. E. Olmos, R. C. Puelles, E. Sánchez-Forcada, *Chem. Eur. J.* **2009**, *15*, 6222–6233.

[26] S. Sculfort, P. Braunstein, *Chem. Soc. Rev.* **2011**, *40*, 2741–2760.

[27] a) J. Vicente, M.-T. Chicote, M.-C. Lagunas, P. G. Jones, *J. Chem. Soc. Chem. Commun.* **1991**, 1730–1731; b) J. Vicente, M.-T. Chicote, M.-C. Lagunas, *Inorg. Chem.* **1993**, *32*, 3748–3754.

[28] a) A. A. Mohamed, A. Burini, J. P. Fackler, Jr. *J. Am. Chem. Soc.* **2005**, *127*, 5012–5013; b) A. A. Mohamed, R. Galassi, F. Papa, A. Burini, J. P. Fackler, Jr. *Inorg. Chem.* **2006**, *45*, 7770–7776.

[29] a) A. C. Jahnke, K. Pröpper, C. Bronner, J. Teichgräber, S. Dechert, M. John, O. S. Wenger, F. Meyer, *J. Am. Chem. Soc.* **2012**, *134*, 2938-2941; b) M. Veronelli, N. Kindermann, S. Dechert, S. Meyer, F. Meyer, *Inorg. Chem.* **2014**, *53*, 2333–2341.

[30] P. Pyykkö, *Chem. Rev.* **1997**, *97*, 597–636.

[31] C.-M. Che, S.-W. Lai, *Coord. Chem. Rev.* **2005**, *249*, 1296–1309.

[32] a) H. Schmidbaur, A. Schier, *Chem. Soc. Rev.* **2008**, *37*, 1931–1951; b) H. Schmidbaur, A. Schier, *Chem. Soc. Rev.* **2012**, *41*, 370–412.

4.7 Experimental Section

Materials and Instructions: Reagents and solvents were purchased from TCI Co., Ltd., WAKO Pure Chemical Industries Ltd., Sigma-Aldrich Co., and KANTO Chemical Co., Inc. Deuterated H_2O and CH_3CN were used as supplied for the complexation reactions and NMR measurements. NMR spectra were recorded on Bruker DRX-500 (500 MHz) equipped with BBO gradient probe or Bruker AV-500 (500 MHz) with CP-TCI CryoProbe. TMS ($CDCl_3$ solution) in a capillary served as an external standard (δ = 0 ppm). IR measurements were carried out using a JASCO FT/IR-6700 instrument. UV-visible spectral data were recorded on a SHIMADZU UV-3150. CSI-MS data were measured on a four-sector (BE/BE) tandem mass spectrometer (JMS-700C, JEOL). Melting points and elemental analyses were determined with a Yanaco MP-500P micro melting point apparatus and Yanaco MT-6, respectively. Imidazolate-bridged trinuclear Au(I) complex **2a**[1] and 3,5-di(3-pyridyl)pyrazole[2] were prepared according to the literature procedures.

Single crystal X-ray structure analysis: X-ray diffraction experiments of single crystals were performed using Bruker APEXII/CCD diffractometer equipped with a focusing mirror (MoKα radiation, λ = 0.71073 Å). The sample crystal was cooled to 90 K by cold nitrogen stream. Both of the structures in this report were solved by direct methods (*SHELXS-97*)[3] and refined using the full matrix least-squares method (*SHELXL-2013*).[3]

In 1:1 association complex (*t*-**4b**)•**6**, all non-hydrogen atoms were refined anisotropically. All hydrogen atoms were refined isotropically using $U_{iso} = 1.5U_{eq}$ (for the solvated acetonitrile) or $1.2U_{eq}$ (for others) of the connected carbon atom. Many low residual electron densities, which are considered as disordered water molecules, are flattened by the program SQUEEZE in PLATON.[4] We considered that this void was filled by disordered water molecules as follows. The volume of the void that made the flattening of electron densities was 2752 $Å^3$, which corresponds to ~70 water molecules (the volume of a water molecule is ca. 40 $Å^3$). The counted electrons in this void was 1384 e^-, which agrees with ~70 water molecules. The validation response form (vrf) about this void and the results of SQUEEZE are described in CIF.

In Au_3–Au_3–Ag–Au_3–Au_3 ion cluster (*t*-**4b**)•**2a**•Ag^+•**2a**•(*t*-**4b**), all the non-

hydrogen atoms in tray *t*-**4b**, the Au atoms in guest **2a**, and the central Ag atom were refined anisotropically. The bridging ligands in guest **2a** were refined isotropically because guest **2a** was disordered in the crystal and their electron densities were unclear in comparison to tray *t*-**4b**. All hydrogen atoms were refined isotropically using U_{iso} = 1.5U_{eq} (for the methyl groups) or 1.2U_{eq} (for others) of the connected carbon atom. Refinement of the ligand in guest **2a** without any geometrical constraint or restraint in *SHELXL-2013* led chemically inadequate distortion. Therefore, the geometry of similar compound reported by neutron crystal structure analysis[5] was applied to the ligands as a rigid body. In addition, atomic displacement parameters and positions of ligands were restrained using the commands SIMU and SADI in *SHELXL-2013*. All the water molecules and counter anions (NO_3^-) could not be refined anisotropically, thus refined isotropically. The hydrogen atoms in water molecules were omitted in refinement because their positions were not identified in the present analysis. The termination effect of a Fourier synthesis was appeared as some large residual electron densities (Au, Ag). Because dynamic motions of guest **2a** and solvated waters significantly decrease the diffraction intensity at a high-angle region, high-angle data was not able to obtain during the diffraction data collection even at 90 K. Note that the hourglass structure consisting of the Au_3–Au_3–Ag–Au_3–Au_3 ion array in this crystal is considered to be reliable because position and anisotropic displacement parameters of those atoms were properly refined without any constraint or restraint. The validation response forms (vrf) about the residual densities are described in CIF.

References

[1] F. Bonati, A. Burini, B. R. Pietroni, B. Bovio, *J. Organomet. Chem.* **1989**, *375*, 147–160.

[2] S.-Z. Zhan, R. Peng, S.-H. Lin, S. W. Ng, D. Li, *CrystEngComm.* **2010**, *12*, 1385–1387.

[3] G. M. Sheldrick, *Acta Crystallogr. Sect. A*. **2008**, *64*, 112–122.

[4] A. L. Spek, *Acta Crystallogr. Sect. D*. **2009**, *65*, 148–155.

[5] R. K. McMullan, J. Epstein, J. R. Ruble, B. M. Craven, *Acta Crystallogr. Sect. B*. **1979**, *35*, 688–691.

Table S1. Crystal data and structure refinement for 1:1 complex (*t*-**4b**)•**6**.

Identification code	pnma-sr	
Empirical formula	C65 H66 Au3 N21 O6 Pd3	
Formula weight	2147.48	
Temperature	90(2) K	
Wavelength	0.71073 Å	
Crystal system	Orthorhombic	
Space group	*P n m a*	
Unit cell dimensions	a = 14.1734(15) Å	α = 90°
	b = 19.427(2) Å	β = 90°
	c = 32.499(3) Å	γ = 90°
Volume	8948.6(16) $Å^3$	
Z	4	
Density (calculated)	1.594 Mg/m^3	
Absorption coefficient	5.542 mm^{-1}	
F(000)	4104	
Crystal size	0.090 x 0.030 x 0.030 mm^3	
Theta range for data collection	1.886 to 24.998°.	
Index ranges	-16<=h<=16, -23<=k<=23, -38<=l<=38	
Reflections collected	84007	
Independent reflections	8128 [R(int) = 0.0411]	
Completeness to theta = 25.242°	97.4 %	
Absorption correction	Semi-empirical from equivalents	
Max. and min. transmission	0.8514 and 0.6354	
Refinement method	Full-matrix least-squares on F^2	
Data / restraints / parameters	8128 / 57 / 451	
Goodness-of-fit on F^2	1.170	
Final R indices [I>2sigma(I)]	R_1 = 0.0420, wR_2 = 0.0887	
R indices (all data)	R_1 = 0.0472, wR_2 = 0.0902	
Extinction coefficient	n/a	
Largest diff. peak and hole	2.000 and -2.136 $e.Å^{-3}$	
CCDC reference number	996176	

Table S2. Crystal data and structure refinement for (*t*-**4b**)•**2a**•Ag^+•**2a**•(*t*-**4b**).

Identification code	c2m	
Empirical formula	C114 H132 Ag Au12 N57.20 O56.35 Pd6	
Formula weight	6315.03	
Temperature	90(2) K	
Wavelength	0.71073 Å	
Crystal system	Monoclinic	
Space group	*C* 2/*m*	
Unit cell dimensions	a = 37.169(14) Å	α = 90°
	b = 18.900(7) Å	β = 111.246(4)°
	c = 14.433(6) Å	γ = 90°
Volume	9450(6) $Å^3$	
Z	2	
Density (calculated)	2.219 Mg/m^3	
Absorption coefficient	10.016 mm^{-1}	
F(000)	5876	
Crystal size	0.120 x 0.060 x 0.060 mm^3	
Theta range for data collection	1.227 to 24.804°.	
Index ranges	-43<=h<=43, -22<=k<=22, -17<=l<=17	
Reflections collected	41978	
Independent reflections	8340 [R(int) = 0.1321]	
Completeness to theta = 25.242°	94.3 %	
Absorption correction	Semi-empirical from equivalents	
Max. and min. transmission	0.5848 and 0.3794	
Refinement method	Full-matrix least-squares on F^2	
Data / restraints / parameters	8340 / 110 / 479	
Goodness-of-fit on F^2	1.105	
Final R indices [I>2sigma(I)]	R_1 = 0.0941, wR_2 = 0.1950	
R indices (all data)	R_1 = 0.1455, wR_2 = 0.2290	
Extinction coefficient	n/a	
Largest diff. peak and hole	4.782 and -3.576 $e.Å^{-3}$	
CCDC reference number	996175	

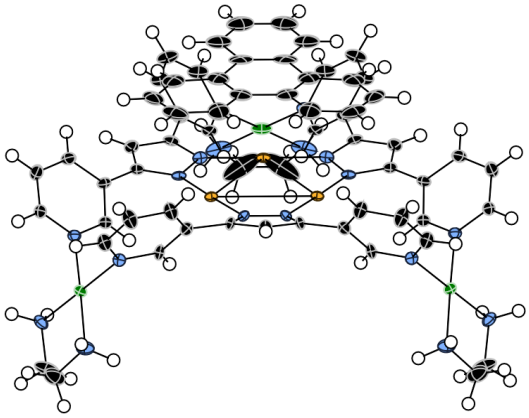

Figure S1. ORTEP diagram (30% probability ellipsoids) of (*t*-**4b**)•**6**.

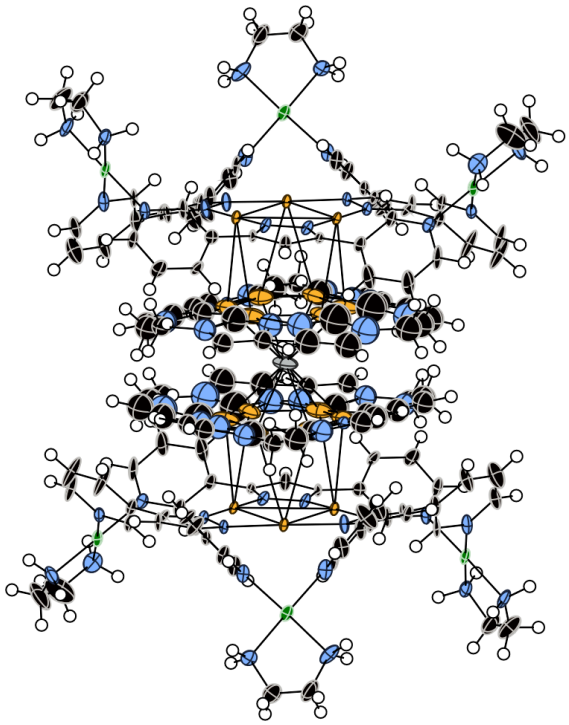

Figure S2. ORTEP diagram (30% probability ellipsoids) of (*t*-**4b**)•**2a**•Ag^{+}•**2a**•(*t*-**4b**).

Preparation and physical data of Au_3 metal-containing ligand 5

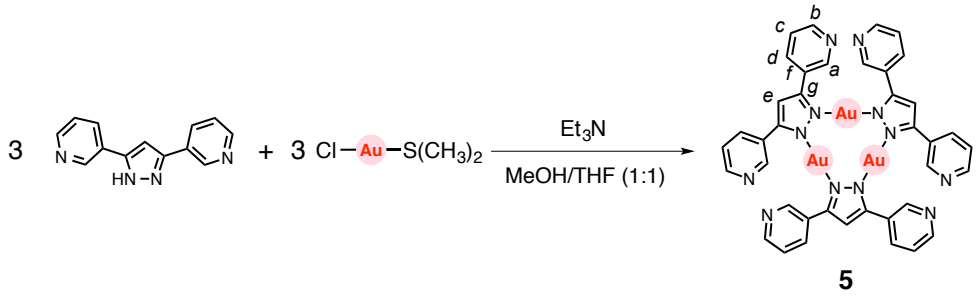

Scheme S1. Synthesis of Au_3 complex **5**.

3,5-Di(3-pyridyl)pyrazole (1.11 g, 5.00 mmol) and chloro(dimethylsulfide)gold(I) (1.16 g, 3.94 mmol) were combined in a MeOH/THF (1:1) mixed solvent (200 mL). Once Et_3N (~ 1 mL) was slowly added in this mixture, the suspension became a clear solution. After a continuous stirring, Au_3 metal-containing ligand **5** formed as a white precipitation. The solid was collected by filtration and washed with a MeOH/THF (1:1) mixed solvent (1.23 g, 0.980 mmol, 75% yield): ^{1}H NMR (500 MHz, $CDCl_3$, 300 K) δ: 8.88 (s, 6H, H^a), 8.58 (d, J = 3.5 Hz, 6H, H^b), 8.00 (d, J = 8.0 Hz 6H, H^d), 6.99 (dd, J = 3.5, 8.0 Hz, 6H, H^c), 6.98 (s, 3H, H^e). ^{13}C NMR (125 MHz, $CDCl_3$, 300 K) δ: 150.7 (C, C^g), 149.7 (CH, C^b), 148.5 (CH, C^a), 134.2 (CH, C^d), 127.6 (C, C^f), 123.3 (CH, C^c), 105.1 (CH, C^e). CSI-MS ($CHCl_3$): m/z Calcd for $[M+H]^+$: 1255.15; Found 1255.33. E.A. Calcd. for $C_{39}H_{27}Au_3N_{12}$: C, 37.34; H, 2.17; N, 13.40; Found: C, 37.41; H, 2.32; N, 13.12. IR (ATR, cm^{-1}): 1571, 1469, 1412, 1313, 1196, 1177, 1138, 1119, 1025, 1002, 810, 795, 783, 703, 691, 621, 472, 441, 426, 408. m.p. ~240 ºC (decomposed).

Preparation and physical data of tray-shaped Au_3 complex 4a in H_2O/CH_3CN (7:3)

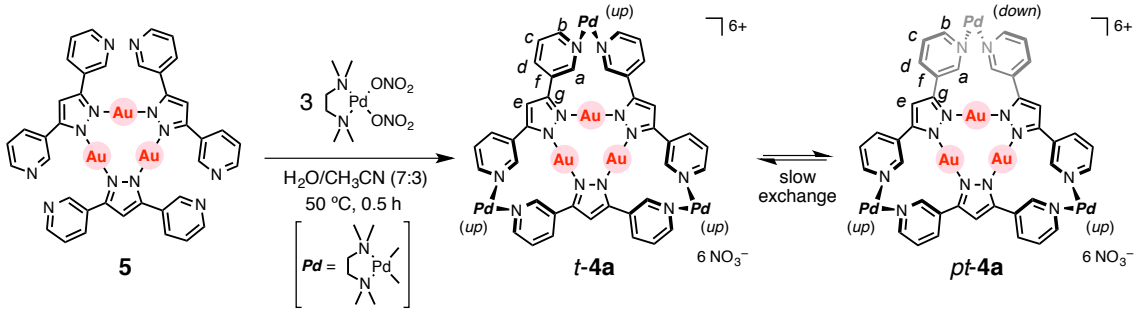

Scheme S2. Synthesis of tray-shaped Au_3 complex **4a**.

Trinuclear Au_3 metal-containing ligand **5** (6.3 mg, 5.0 μmol) and (tmeda)Pd(ONO_2)$_2$ (5.2 mg, 15.0 μmol) were suspeneded in H_2O/CH_3CN (7:3, 1.0 mL) at 50 ºC for 30 min. The ^{1}H NMR spectrum of the resulting clear solution revealed the quantitative formation of tray-shaped Au_3 complex **4a**. The spectrum indicated the existence of two diastereomers, tray form *t*-**4a** and partial-tray form *pt*-**4a**, in a 65:35 ratio at 300 K (Figure S3). All the three Pd(II) hinges of tray *t*-**4a** are on the same $Au(I)_3$ plane, while on the other hand, one hinge of partial-tray *pt*-**4a** is located in the opposite side. A fluxional exchange between two isomers was not observed on the NMR time scale at a temperature range of 290–340 K. A quantitative formation of association complex (*t*-**4a**)•**2a** from the mixture of *t*-**4a** and *pt*-**4a** suggested the existence of a slow exchange between two isomers (Scheme S4). The solution was evaporated and dried by a vacuum freeze-drying equipment to isolate tray-shaped Au_3 complex **4a** as a white solid (11.5 mg, 97%).

Physical data: ^{1}H NMR [D_2O/CD_3CN (7:3), 500 MHz, 300 K] (tray form) δ: 10.03 (s, 6H, H^a), 9.23 (d, J = 5.0 Hz, 6H, H^b), 8.36 (dd, J = 5.0 Hz, J = 7.0 Hz, 6H, H^d), 7.94 (d, J = 7.0 Hz, 6H, H^c), 7.51 (s, 3H, H^e), 3.27 (br, 12H, H^h), 2.91 (s, 18H, H^i), 2.81 (s, 18H, H^i); (partial-tray form) δ: 10.05 (s, 2H, H^a), 9.97 (s, 2H, H^a), 9.87 (s, 2H, H^a), 9.31 (d, J = 5.0 Hz, 6H, H^b), 9.24 (d, J = 5.0 Hz, 6H, H^b), 9.18 (d, J = 5.0 Hz, 6H, H^b), 8.41 (dd, J = 5.0 Hz, J = 7.0 Hz, 6H, H^d), 8.33 (dd, J = 5.0 Hz, J = 7.0 Hz, 6H, H^d), 8.30 (dd, J = 5.0 Hz, J = 7.0 Hz, 6H, H^d), 7.97 (d, J = 7.0 Hz, 6H, H^c), 7.95 (d, J = 7.0 Hz, 6H, H^c), 7.92 (d, J = 7.0 Hz, 6H, H^c), 7.53 (s, 6H, H^e), 7.47 (s, 3H, H^e), 3.23 (br, 12H, H^h), 2.96–2.74 (m, 36H, H^i); ^{13}C NMR [D_2O/CD_3CN (7:3), 125 MHz, 300 K] (tray

form) δ: 152.0 (CH, C^b), 150.0 (C, C^g), 148.7 (CH, C^a), 141.5 (CH, C^d), 132.2 (C, C^f), 129.1 (CH, C^c), 110.1 (CH, C^e), 63.5 (CH_2, C^h), 51.3 (CH_3, C^i), 51.1 (CH_3, C^i); (partial-tray form) δ: 152.1 (CH, C^b), 152.1 (CH, C^b), 152.0 (CH, C^b), 149.8 (C, C^g), 149.8 (C, C^g), 149.6 (C, C^g), 149.0 (CH, C^a), 148.7 (CH, C^a), 148.2 (CH, C^a), 142.3 (CH, C^d), 142.0 (CH, C^d), 141.1 (CH, C^d), 132.4 (C, C^f), 132.3 (C, C^f), 132.2 (C, C^f), 129.1 (CH, C^c), 129.0 (CH, C^c), 129.0 (CH, C^c), 110.1 (CH, C^e), 63.5 (CH_2, C^h), 51.5–51.0 (CH_3, C^i). ^{1}H DOSY [D_2O/CD_3CN (7:3), 300 K] (m^2/s): $D = 2.09 \times 10^{-10}$ (log D = –9.68). CSI-MS (H_2O : CH_3CN : DMF = 7 : 3 : 1): m/z = 418.0 [**4a**–6·NO_3^-+8·DMF]$^{6+}$, 430.2 [**4a**–6·NO_3^-+9·DMF]$^{6+}$, 442.2 [**4a**–6·NO_3^-+10·DMF]$^{6+}$, 454.4 [**4a**–6·NO_3^-+11·DMF]$^{6+}$, 466.6 [**4a**–6·NO_3^-+12·DMF]$^{6+}$, 469.8 [**4a**–5·NO_3^-+5·DMF]$^{5+}$, 484.6 [**4a**–5·NO_3^-+6·DMF]$^{5+}$, 499.2 [**4a**–5·NO_3^-+7·DMF]$^{5+}$, 513.8 [**4a**–5·NO_3^-+8·DMF]$^{5+}$, 528.2 [**4a**–5·NO_3^-+9·DMF]$^{5+}$, 543.1 [**4a**–5·NO_3^-+10·DMF]$^{5+}$, 566.3 [**4a**–4·NO_3^-+3·DMF]$^{4+}$, 584.7 [**4a**–4·NO_3^-+4·DMF]$^{4+}$, 602.9 [**4a**–4·NO_3^-+5·DMF]$^{4+}$, 702.8 [**4a**–3·NO_3^-]$^{3+}$, 727.1 [**4a**–3·NO_3^-+1·DMF]$^{3+}$, 751.6 [**4a**–3·NO_3^-+2·DMF]$^{3+}$, 775.6 [**4a**–3·NO_3^-+3·DMF]$^{3+}$. IR (ATR, cm^{-1}): 3392 (br), 3216 (br), 3109 (br), 1614, 1471, 1327 (br), 1198, 1108, 809, 700, 661, 619, 576, 548, 533, 509, 495, 472, 461, 441, 422. m.p. ~210 ºC (decomposed).

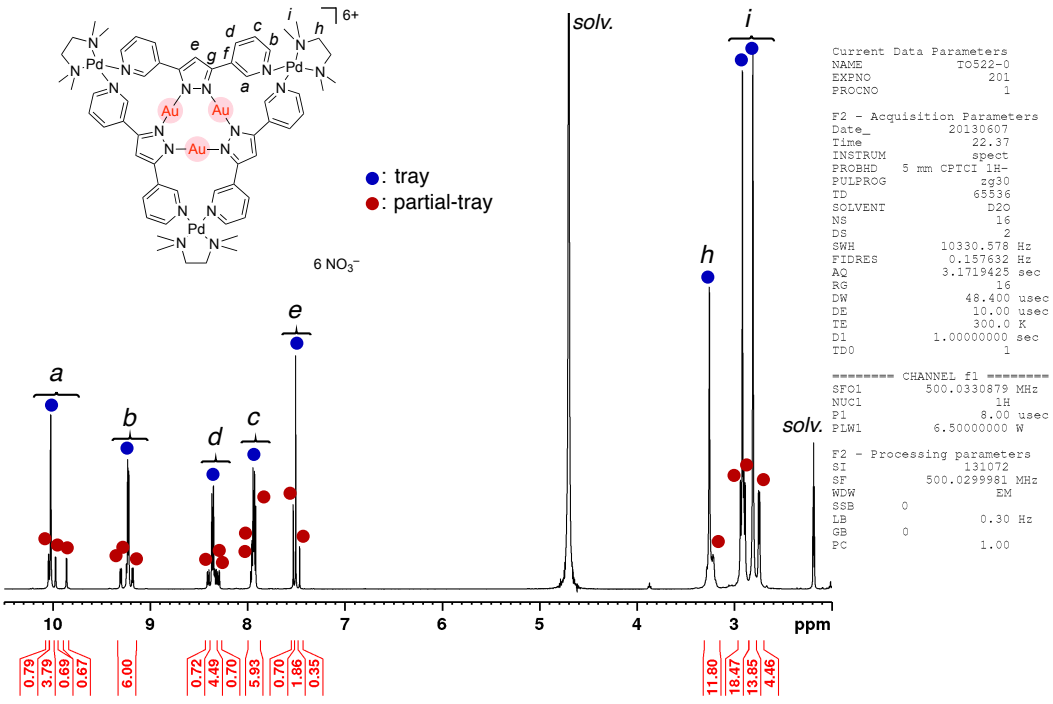

Figure S3. ^{1}H NMR [500 MHz, 300 K, D_2O/CD_3CN (7:3)] spectrum of **4a**.

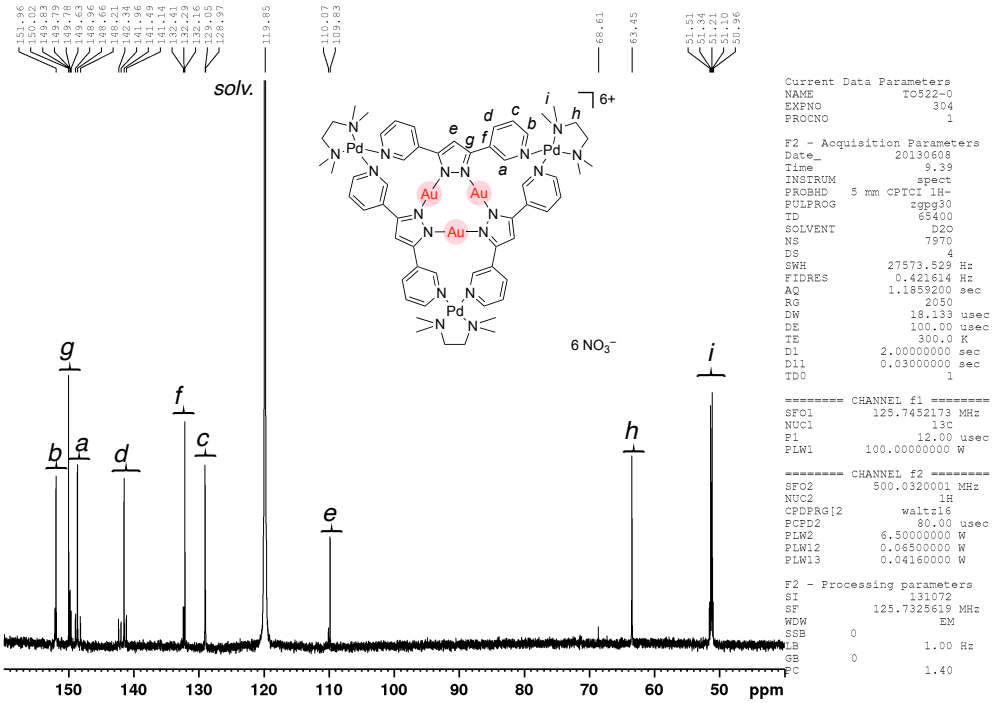

Figure S4. ^{13}C NMR [125 MHz, 300 K, D_2O/CD_3CN (7:3)] spectrum of **4a**.

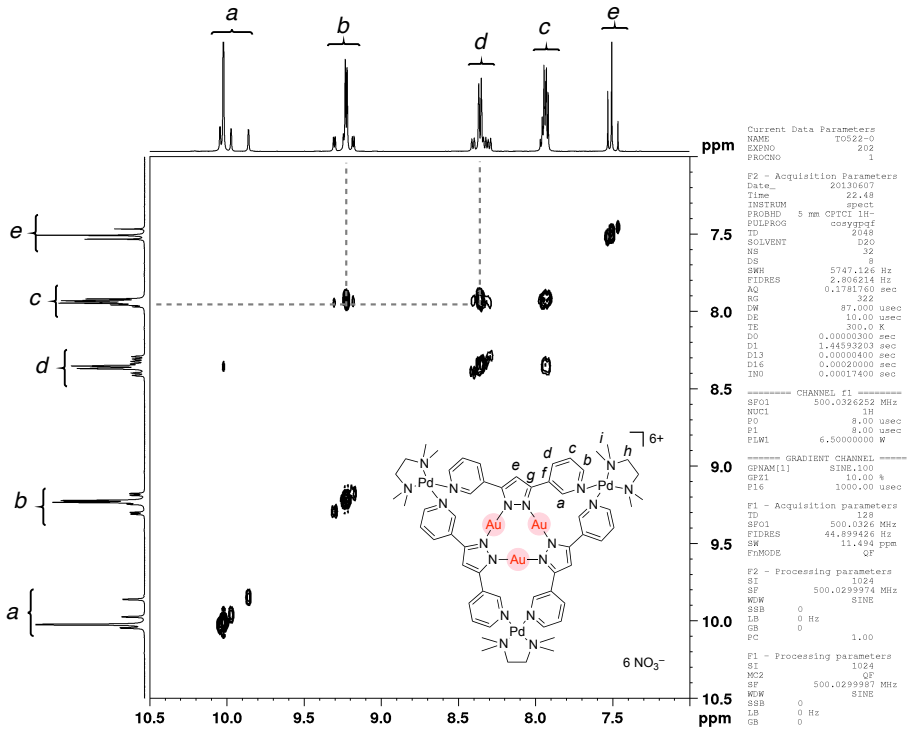

Figure S5. ^{1}H-^{1}H COSY [500 MHz, 300 K, D_2O/CD_3CN (7:3)] spectrum of **4a**.

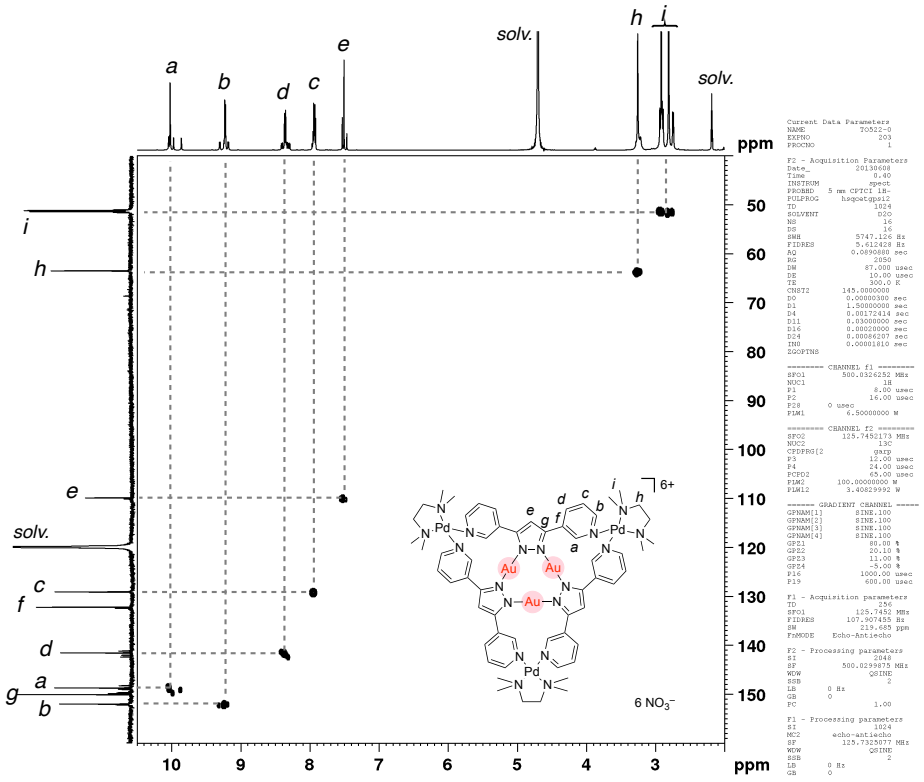

Figure S6. ^{1}H-^{13}C HSQC [500 MHz, 300 K, D_2O/CD_3CN (7:3)] spectrum of **4a**.

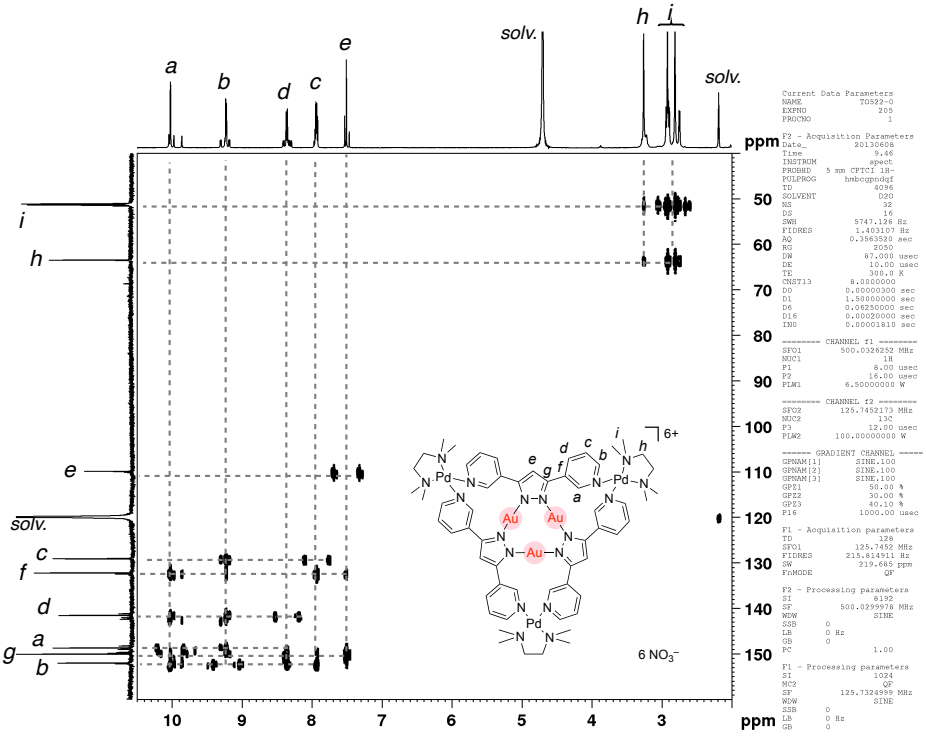

Figure S7. ^{1}H-^{13}C HMBC [500 MHz, 300 K, D_2O/CD_3CN (7:3)] spectrum of **4a**.

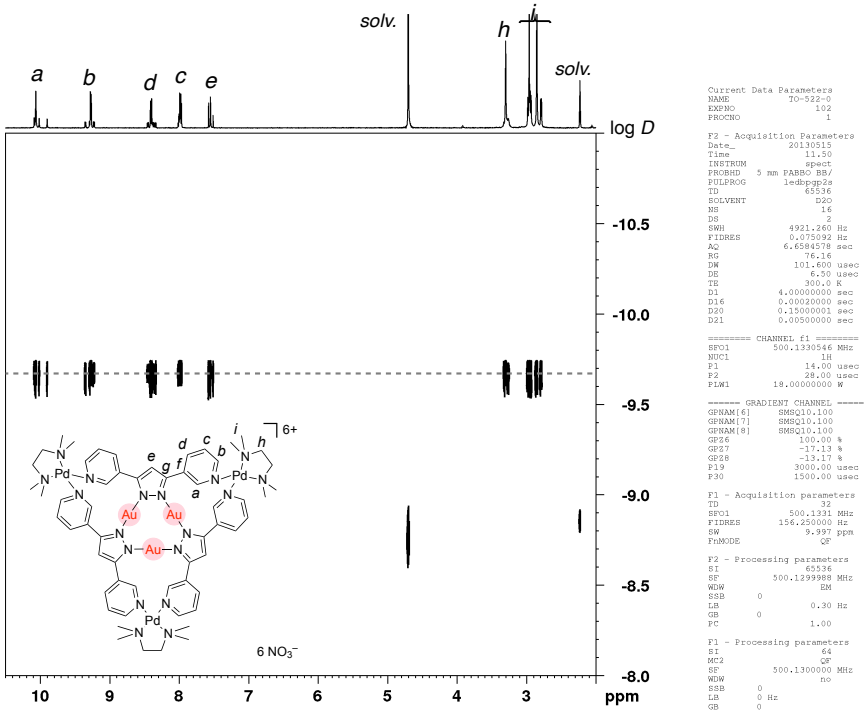

Figure S8. ^{1}H DOSY [500 MHz, 300 K, D_2O/CD_3CN (7:3)] spectrum of **4a**.

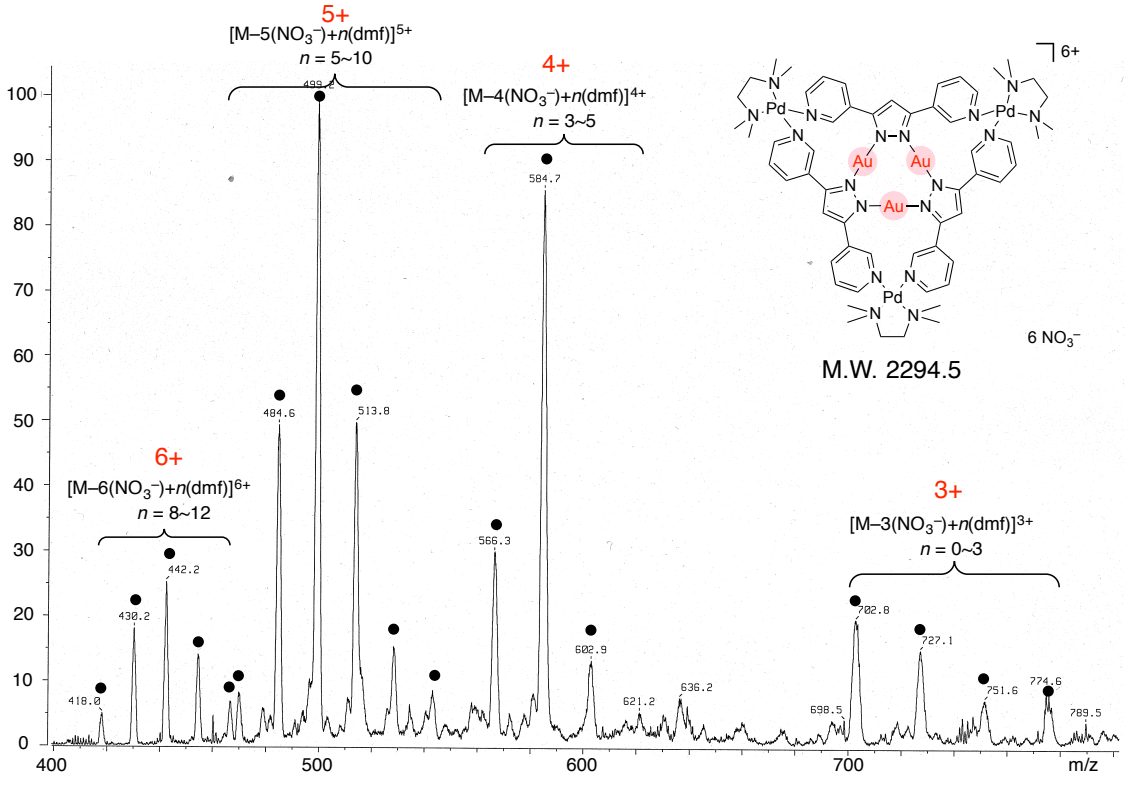

Figure S9. CSI-MS spectrum of **4a** [H_2O/CH_3CN/DMF (7:3:1)].

Preparation and physical data of tray-shaped Au_3 complex 4b in H_2O/CH_3CN (7:3)

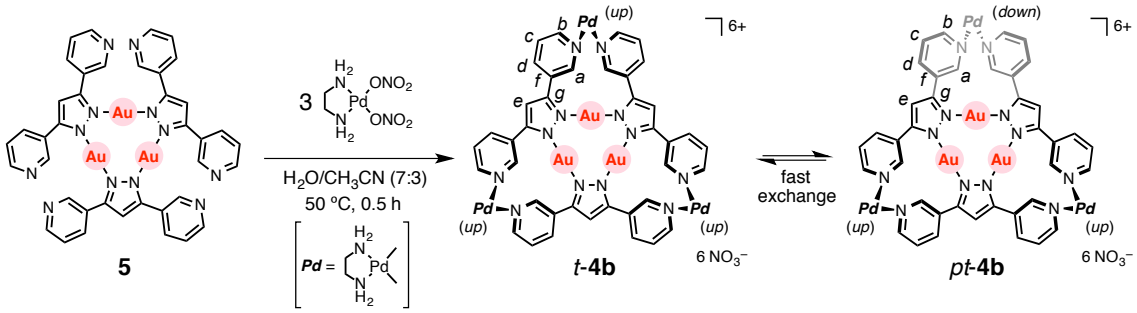

Scheme S3. Synthesis of tray-shaped Au_3 complex **4b**.

Trinuclear Au(I) metal-containing ligand **5** (6.3 mg, 5.0 μmol) and $(en)Pd(ONO_2)_2$ (4.4 mg, 15.0 μmol) were suspended in H_2O/CH_3CN (7:3, 1.0 mL) at 50 ºC for 30 min. The ^1H NMR spectrum of the resulting clear solution revealed the quantitative formation of tray-shaped $Au(I)_3$ complex **4b**. One set of broad signals of $Au(I)_3$ complex **4b** shows the relatively fast exchange between two diastereomers, tray form *t*-**4b** and partial-tray form *pt*-**4b** in NMR time scale compared to that of $Au(I)_3$ complex **4a** (Figure S10). The solution was evaporated and dried by a vacuum freeze-drying equipment to isolate tray-shaped Au_3 complex **4b** as a white solid (9.39 mg, 88%).

Physical data: ^1H NMR [D_2O/CD_3CN (7:3), 500 MHz, 300 K] δ: 9.97 (s, 6H, H^a), 9.20 (br, 6H, H^b), 8.29 (br, 6H, H^d), 7.91 (br, 6H, H^c), 7.55 (s, 3H, H^e), 3.08 (br, 12H, H^h); ^{13}C NMR [D_2O/CD_3CN (7:3), 125 MHz, 300 K] δ: 153.3 (CH, C^b), 150.6 (C, C^g), 149.2 (CH, C^a), 141.7 (CH, C^d), 132.0 (C, C^f), 128.7 (CH, C^c), 110.9 (CH, C^e), 48.0 (CH_2, C^h). ^1H DOSY [D_2O/CD_3CN (7:3), 300 K] (m^2/s): $D = 2.04 \times 10^{-10}$ (log D = –9.69). E.A. Calcd. for $C_{45}H_{51}Au_3N_{24}O_{18}Pd_3 \cdot (H_2O)_8$: C, 23.81; H, 2.97; N, 14.81; Found: C, 23.99; H, 3.08; N, 14.54. IR (ATR, cm^{-1}): 3431 (br), 3212 (br), 3119 (br), 1573, 1471, 1328 (br), 1198, 1107, 1061, 1041, 1024, 809, 769, 783, 701, 661, 621, 576, 549, 533, 515, 506, 496, 472, 450, 419. m.p. ~220 ºC (decomposed).

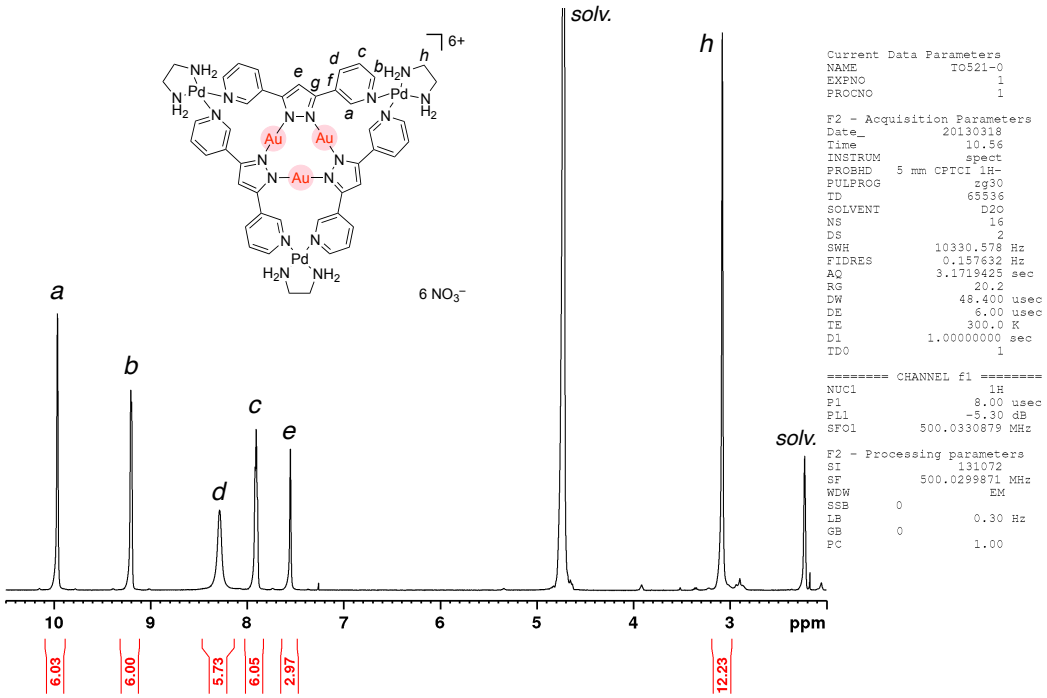

Figure S10. ^{1}H NMR [500 MHz, 300 K, D_2O/CD_3CN (7:3)] spectrum of **4b**.

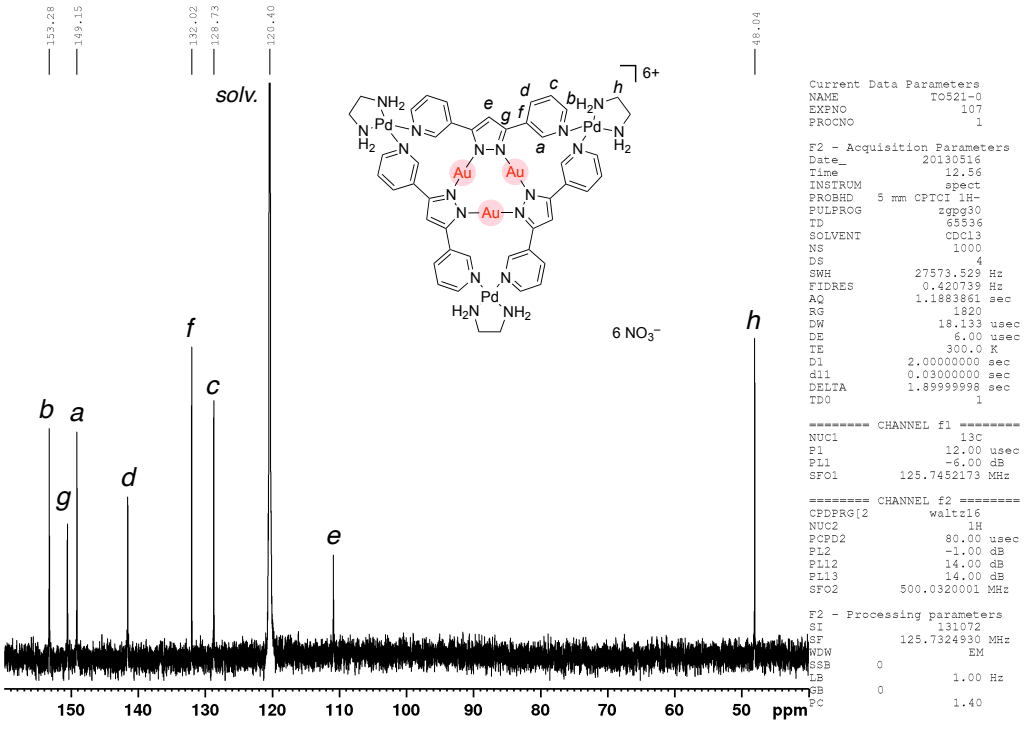

Figure S11. ^{13}C NMR [125 MHz, 300 K, D_2O/CD_3CN (7:3)] spectrum of **4b**.

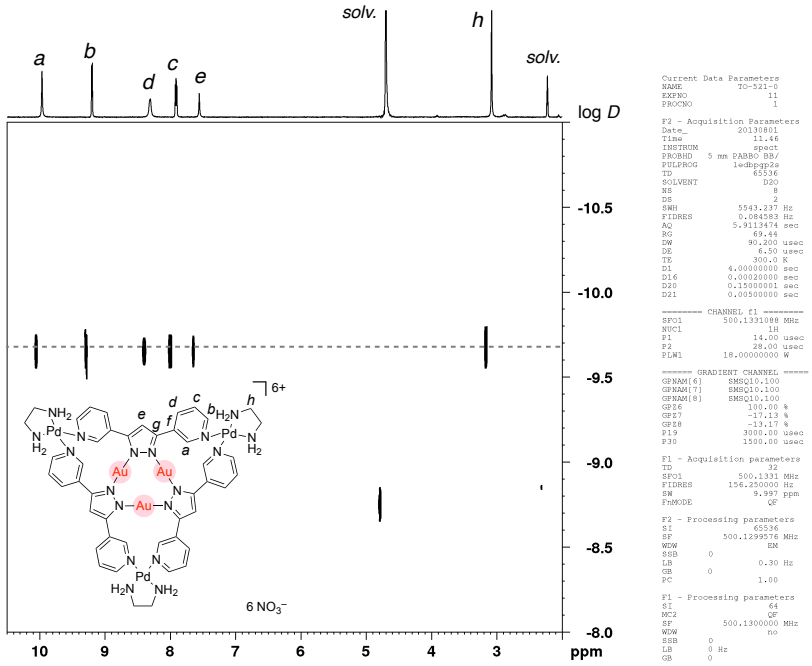

Figure S12. ^{1}H DOSY [500 MHz, 300 K, D_2O/CD_3CN (7:3)] spectrum of **4b**.

Formation of Au_3–Au_3 double stack (*t*-4a)•2a in H_2O/CH_3CN (7:3)

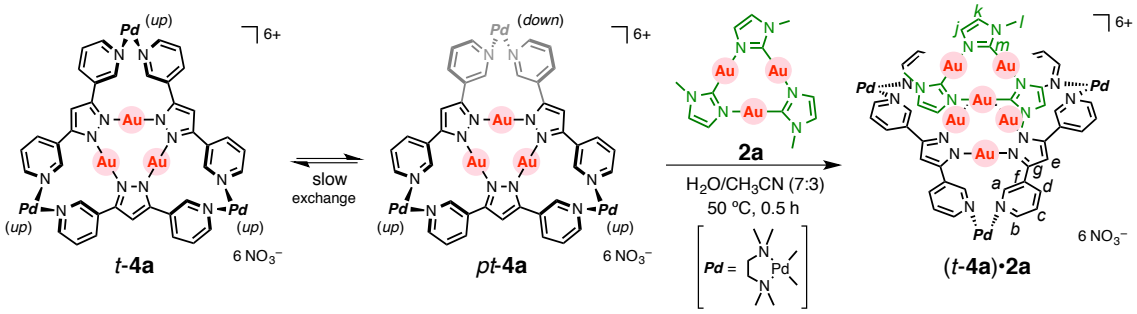

Scheme S4. Synthesis of Au_3–Au_3 double stack (*t*-**4a**)•**2a**.

Imidazolate-bridged Au_3 complex **2a** (8.3 mg, 10.0 μmol) was suspended in a H_2O/CH_3CN (7:3) solution of tray **4a** (a 65:35 equilibrium mixture of *t*-**4a** and *pt*-**4a**, 5.0 mM, 1.0 mL) at 50 ºC for 30 min. After removal of the residual excess guest by filtration, ^{1}H NMR spectroscopy of the pale yellow solution revealed the formation of $Au_{4a}u_3$ double stack (*t*-**4a**)•**2a** in 93% yield. Signals of *pt*-**4a** were not observed since the equilibration was totally pushed to Au_3–Au_3 double stack (*t*-**4a**)•**2a**.

Physical data: ^{1}H NMR [D_2O/CD_3CN (7:3), 500 MHz, 300 K] δ: 9.94 (s, 6H, *t*-**4a**, H^a), 9.24 (d, J = 5.5 Hz, 6H, *t*-**4a**, H^b), 8.30 (br, 6H, *t*-**4a**, H^d), 7.98 (t, J = 6.0 Hz, 6H, *t*-**4a**, H^c), 7.37 (s, 3H, *t*-**4a**, H^e), 6.95 (br, 2.8H, **2a**, H^k), 6.35 (br, 2.8H, **2a**, H^j), 3.24 (s, 12H, *t*-**4a**, H^h), 2.91 (s, 18H, *t*-**4a**, H^i), 2.86 (s, 8.4H, **2a**, H^l), 2.73 (s, 18H, *t*-**4a**, H^i). ^{13}C NMR [D_2O/CD_3CN (7:3), 125 MHz, 300 K] δ: 168.0 (C, **2a**, C^m), 151.7 (CH, *t*-**4a**, C^b), 149.2 (CH, *t*-**4a**, C^a), 148.5 (C, *t*-**4a**, C^g), 141.5 (CH, *t*-**4a**, C^d), 132.5 (C, *t*-**4a**, C^f), 128.8 (CH, *t*-**4a**, C^c), 128.1 (CH, **2a**, C^k), 121.1 (CH, **2a**, C^j), 110.3 (C, *t*-**4a**, C^e), 63.5 (CH_2, *t*-**4a**, C^h), 51.4 (CH_3, *t*-**4a**, C^i), 51.2 (CH_3, *t*-**4a**, C^i), 35.6 (CH_3, **2a**, C^l). ^{1}H DOSY [D_2O/CD_3CN (7:3), 300 K] (m^2/s): $D = 1.91 \times 10^{-10}$ (log D = –9.72). CSI-MS (H_2O : DMF = 10 : 1): m/z = 544.7 [**4a•2a**–6·NO_3^-+7·DMF]$^{6+}$, 557.0 [**4a•2a**–6·NO_3^-+8·DMF]$^{6+}$, 569.1 [**4a•2a**–6·NO_3^-+9·DMF]$^{6+}$, 581.2 [**4a•2a**–6·NO_3^-+10·DMF]$^{6+}$, 593.2 [**4a•2a**–5·NO_3^-+11·DMF]$^{5+}$, 622.0 [**4a•2a**–5·NO_3^-+4·DMF]$^{5+}$, 636.8 [**4a•2a**–5·NO_3^-+5·DMF]$^{5+}$, 651.4 [**4a•2a**–4·NO_3^-+6·DMF]$^{4+}$, 666.0 [**4a•2a**–4·NO_3^-+7·DMF]$^{4+}$, 680.6 [**4a•2a**–4·NO_3^-+8·DMF]$^{4+}$, 695.4 [**4a•2a**–4·NO_3^-+9·DMF]$^{4+}$, 710.0 [**4a•2a**–4·NO_3^-+10·DMF]$^{4+}$, 724.4 [**4a•2a**–4·NO_3^-+11·DMF]$^{4+}$, 738.7 [**4a•2a**–4·NO_3^-+12·DMF]$^{4+}$, 756.5 [**4a•2a**–4·NO_3^-+2·DMF]$^{4+}$, 774.7

[**4a•2a**–4·NO_3^-+3·DMF]$^{4+}$, 793.0 [**4a•2a**–4·NO_3^-+4·DMF]$^{4+}$, 811.2 [**4a•2a**–4·NO_3^-+5·DMF]$^{4+}$, 980.8 [**4a•2a**–3·NO_3^-]$^{3+}$, 1004.9 [**4a•2a**–3·NO_3^-+1·DMF]$^{3+}$, 1029.9 [**4a•2a**–3·NO_3^-+2·DMF]$^{3+}$, 1053.9 [**4a•2a**–3·NO_3^-+3·DMF]$^{3+}$. IR (ATR, cm^{-1}): 3430 (br), 3213 (br), 3110 (br), 2933, 1613 (br), 1471, 1320 (br), 1199, 1107, 1060, 1041, 1023, 1004, 809, 782, 698 (br), 660, 621, 604, 594, 575, 550, 533, 512, 503, 474, 438, 422, 402. m.p. ~220 ºC (decomposed).

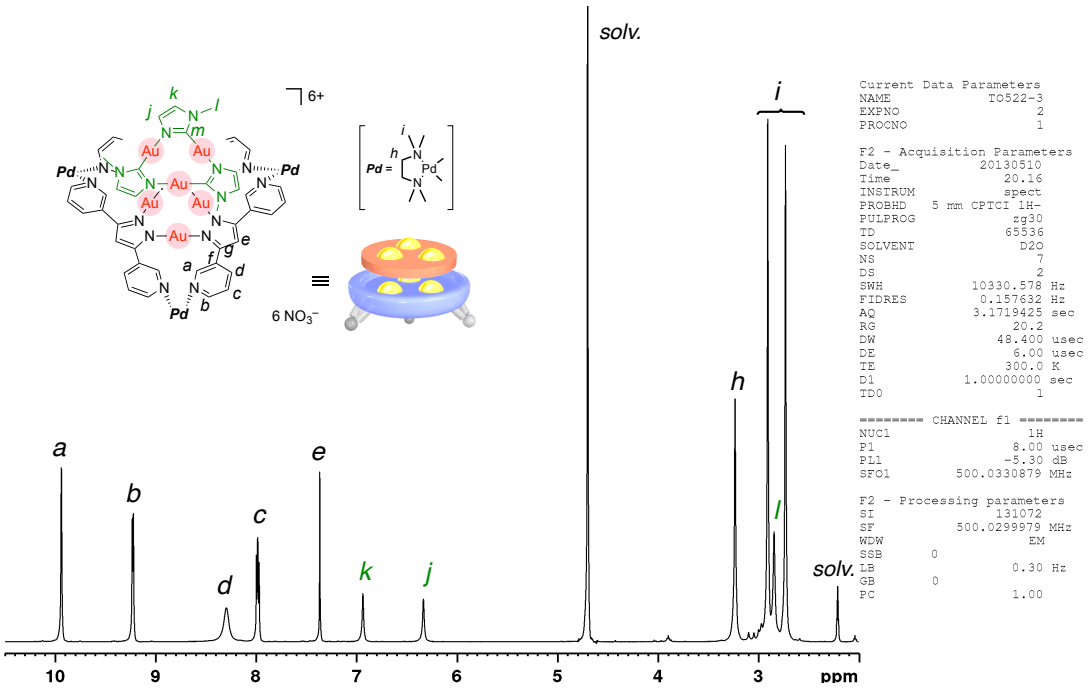

Figure S13. ^{1}H NMR [500 MHz, 300 K, D_2O/CD_3CN (7:3)] spectrum of (*t*-**4a**)•**2a**.

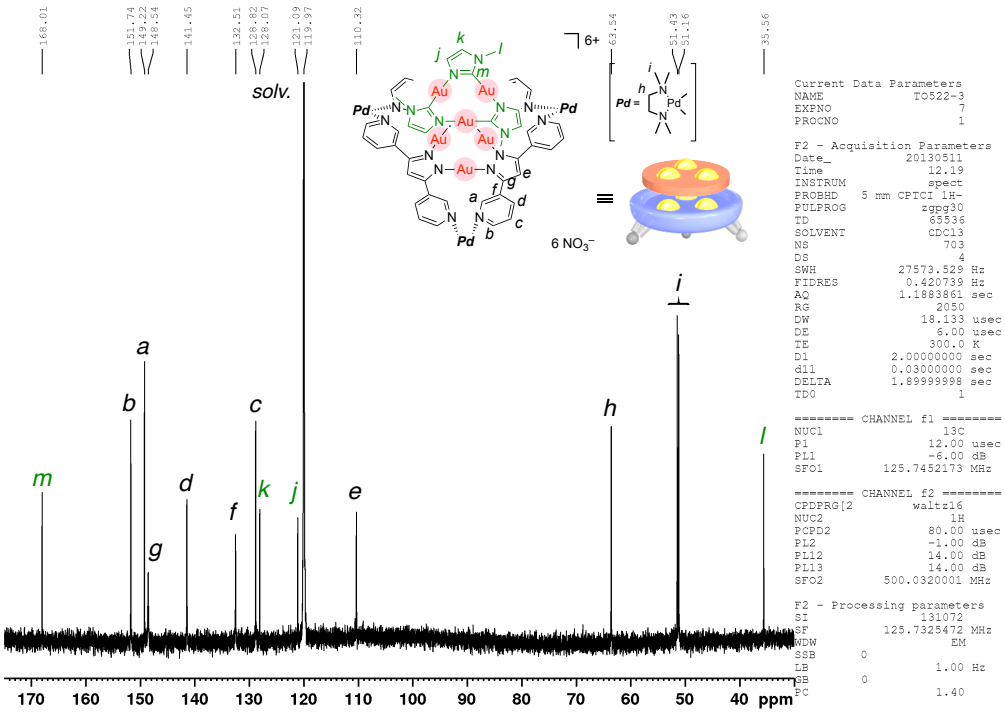

Figure S14. ^{13}C NMR [125 MHz, 300 K, D_2O/CD_3CN (7:3)] spectrum of (*t*-**4a**)•**2a**.

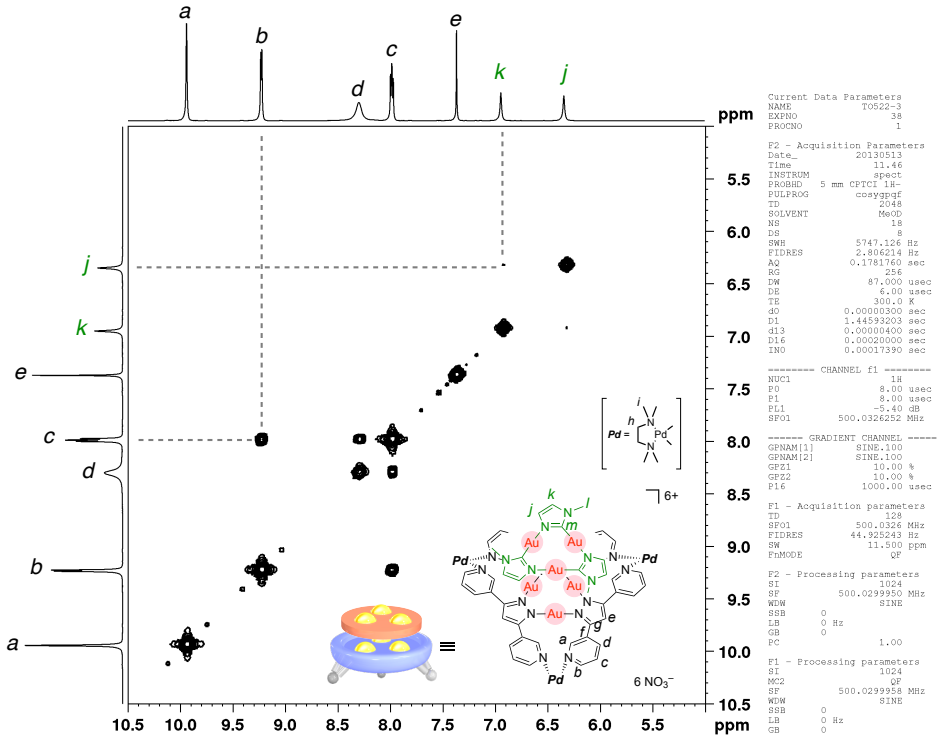

Figure S15. ^{1}H-^{1}H COSY [500 MHz, 300 K, D_2O/CD_3CN (7:3)] spectrum of (*t*-**4a**)•**2a**.

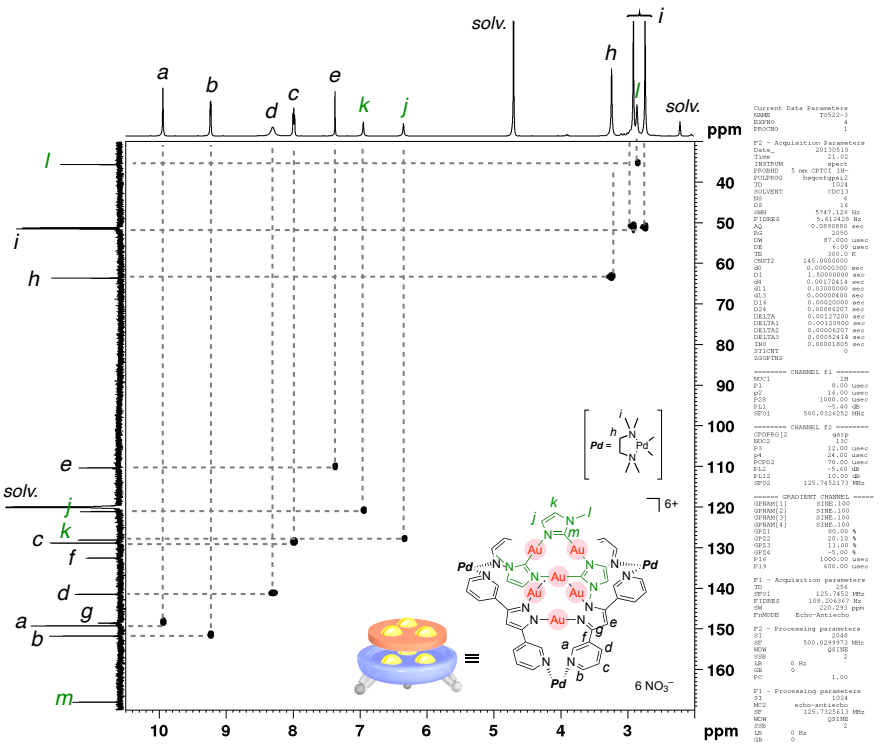

Figure S16. ^{1}H-^{13}C HSQC [500 MHz, 300 K, D_2O/CD_3CN (7:3)] spectrum of (*t*-**4a**)•**2a**.

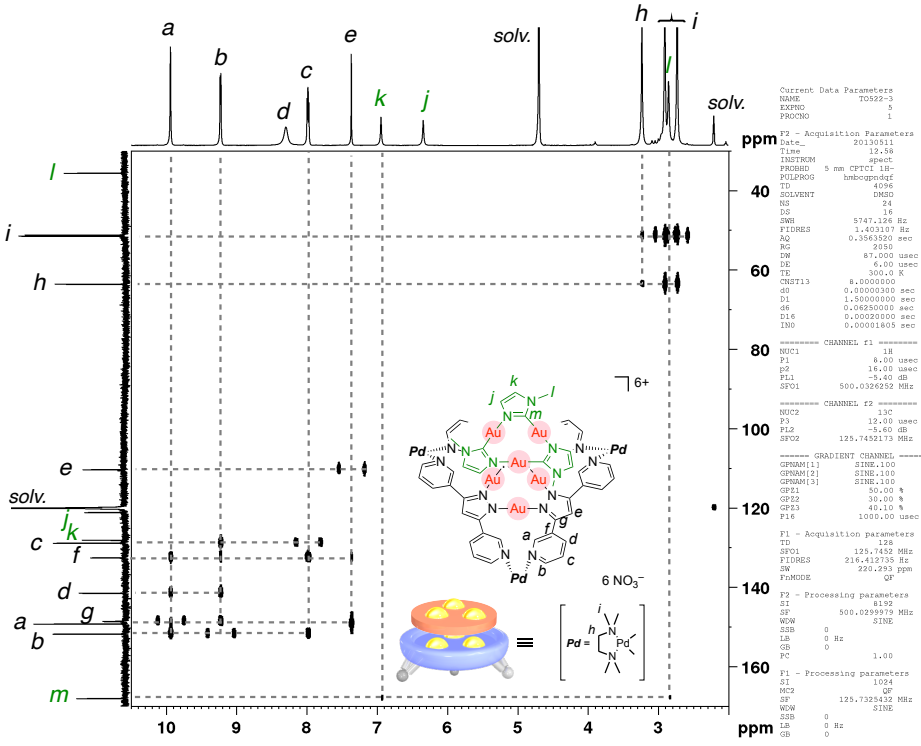

Figure S17. ^{1}H-^{13}C HMBC [500 MHz, 300 K, D_2O/CD_3CN (7:3)] spectrum of (*t*-**4a**)•**2a**.

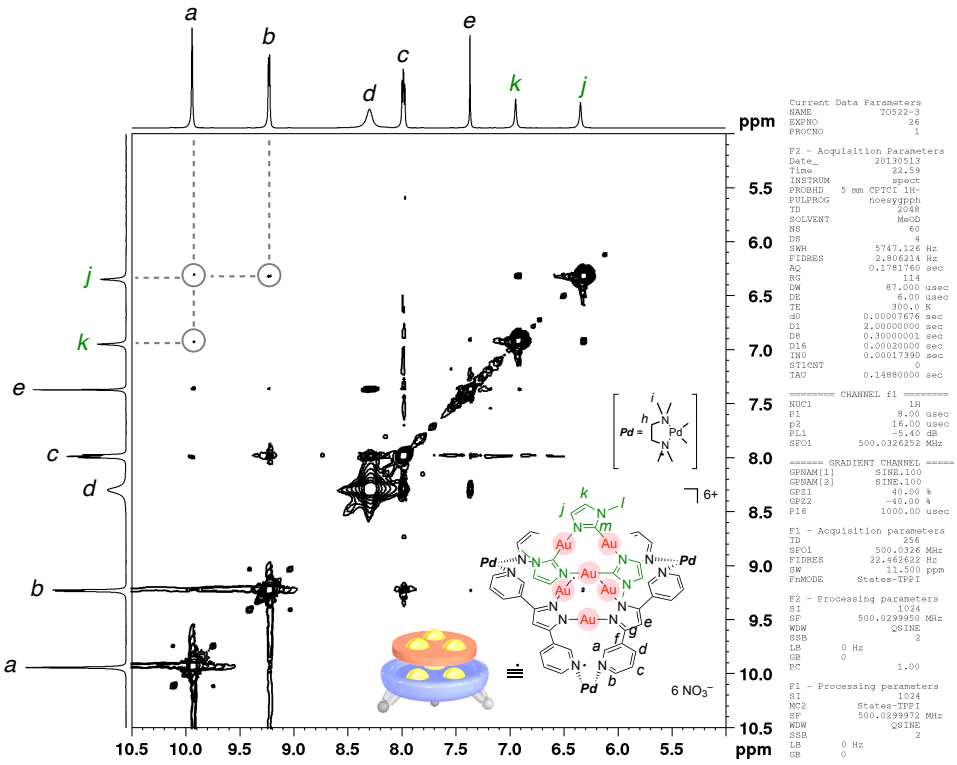

Figure S18. ^{1}H-^{1}H NOESY [500 MHz, 300 K, D_2O/CD_3CN (7:3)] spectrum of (*t*-**4a**)•**2a**.

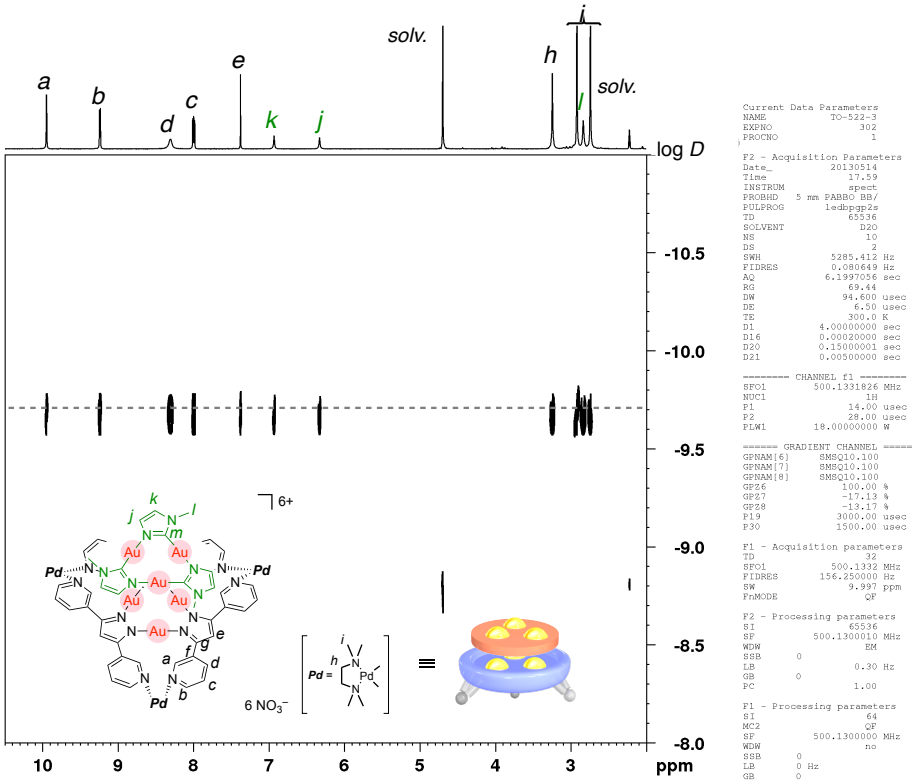

Figure S19. ^{1}H DOSY [500 MHz, 300 K, D_2O/CD_3CN (7:3)] spectrum of (*t*-**4a**)•**2a**.

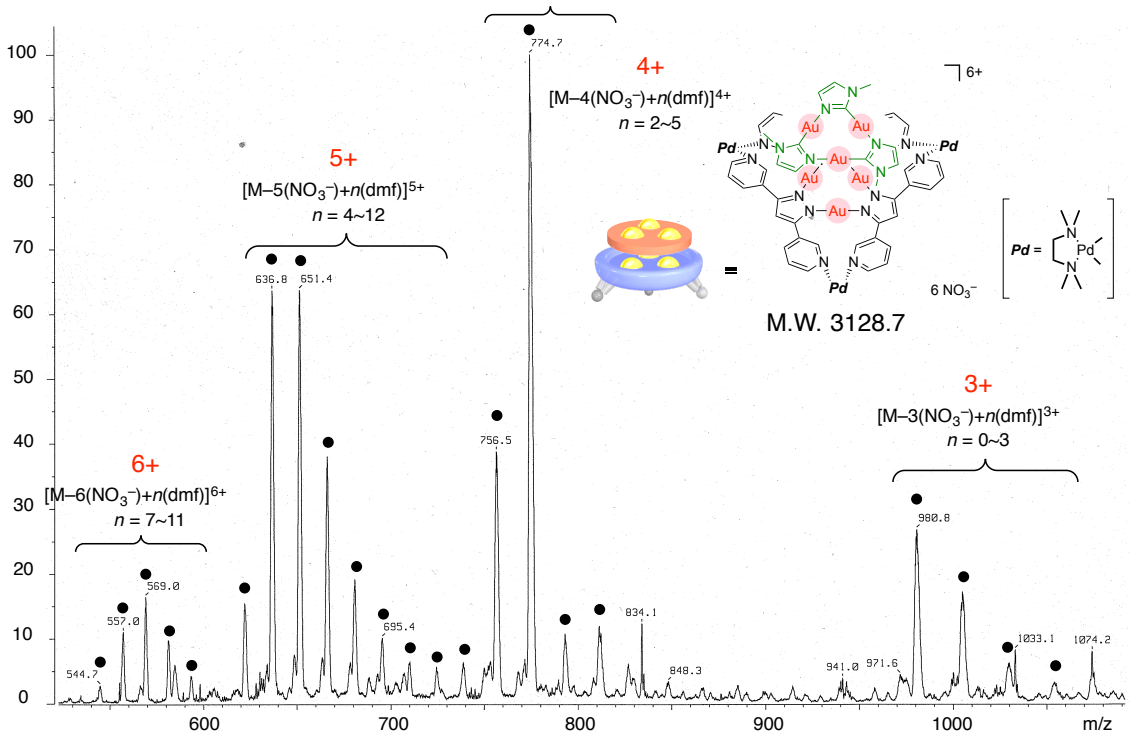

Figure S20. CSI-MS spectrum of (*t*-**4a**)•**2a** [H_2O/CH_3CN/DMF (7:3:1)].

Preparation and physical data of Au_3–Au_3 self-stacked dimer (*t*-4b)•(*t*-4b) in H_2O

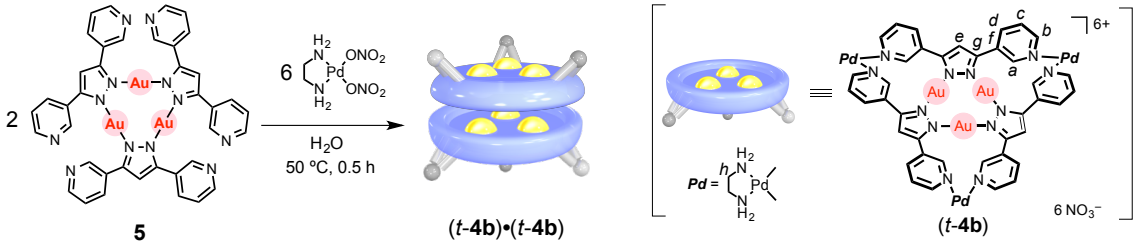

Scheme S5. Formation of Au_3–Au_3 self-stacked dimer (*t*-**4b**)•(*t*-**4b**) in H_2O.

Trinuclear Au(I) ligand **5** (6.3 mg, 5.0 μmol) and (en)Pd(ONO_2)$_2$ (4.4 mg, 15.0 μmol) were suspended in H_2O at 50 ºC for 30 min. In water, Pd(II) coordination to the adjacent pyridyl groups of ligand **5** also proceeded efficiently. The NMR study revealed that tray **4b** forms Au_3–Au_3 self-stacked dimer (*t*-**4b**)•(*t*-**4b**) in a face-to-face fashion with hydrophobic Au_3 plane inside (Figure 7). Unfortunately, CSI-MS spectrum of Au_3 complex **4b** in H_2O/DMF (10 : 1) showed ion peaks of the single composition of Pd_3**5** as DMF adducts. The solution was evaporated and dried by a vacuum freeze-drying equipment to give a recognition complex (*t*-**4b**)•(*t*-**4b**) (10.3 mg, 2.43 μmol, 97%) as a white solid.

Physical data of (*t*-**4b**)•(*t*-**4b**): ^{1}H NMR (D_2O, 500 MHz, 300 K) δ: 9.62 (s, 12H, H^a), 9.09 (d, J = 5.0 Hz, 12H, H^b), 7.66 (dd, J = 5.0 Hz, J = 7.0 Hz, 12H, H^c), 7.10 (s, 6H, H^e), 7.09 (d, J = 7.0 Hz, 12H, H^d), 2.88 (m, 24H, H^h). ^{13}C NMR (125 MHz, D_2O, 300 K) δ: 151.7 (CH, C^b), 148.3 (CH, C^a), 147.7 (C, C^g), 138.6 (CH, C^d), 130.7 (C, C^f), 127.5 (CH, C^c), 111.0 (CH, C^e), 46.7 (CH_2, C^h). ^{1}H DOSY [D_2O, 300 K] (m^2/s): D = 1.62 × 10^{-10} (log D = –9.79). CSI-MS (H_2O : DMF = 10 : 1): m/z = 414.1 [**4b**–6·NO_3^-+10·DMF]$^{6+}$, 426.3 [**4b**–6·NO_3^-+11·DMF]$^{6+}$, 438.6 [**4b**–6·NO_3^-+12·DMF]$^{6+}$, 450.1 [**4b**–6·NO_3^-+13·DMF]$^{6+}$, 480.0 [**4b**–5·NO_3^-+8·DMF]$^{5+}$, 494.8 [**4b**–5·NO_3^-+9·DMF]$^{5+}$, 509.2 [**4b**–5·NO_3^-+10·DMF]$^{5+}$, 560.7 [**4b**–4·NO_3^-+5·DMF]$^{4+}$, 578.9 [**4b**–4·NO_3^-+6·DMF]$^{4+}$, 597.4 [**4b**–4·NO_3^-+7·DMF]$^{4+}$, 615.4 [**4b**–4·NO_3^-+8·DMF]$^{4+}$, 634.2 [**4b**–4·NO_3^-+9·DMF]$^{4+}$, 670.6 [**4b**–3·NO_3^-+1·DMF]$^{3+}$, 695.3 [**4b**–3·NO_3^-+2·DMF]$^{3+}$, 719.5 [**4b**–3·NO_3^-+3·DMF]$^{3+}$, 743.3 [**4b**–3·NO_3^-+4·DMF]$^{3+}$, 768.8 [**4b**–3·NO_3^-+5·DMF]$^{3+}$. IR (ATR, cm^{-1}): 3391 (br), 3215 (br), 3113 (br), 2925, 1614 (br), 1471, 1325 (br), 1198, 1106, 1060, 1041, 1023, 1004, 809, 783, 698 (br), 661, 622, 576, 544, 529, 508, 497, 482, 472, 463, 450, 441, 420,

406. m.p. ~210 ºC (decomposed).

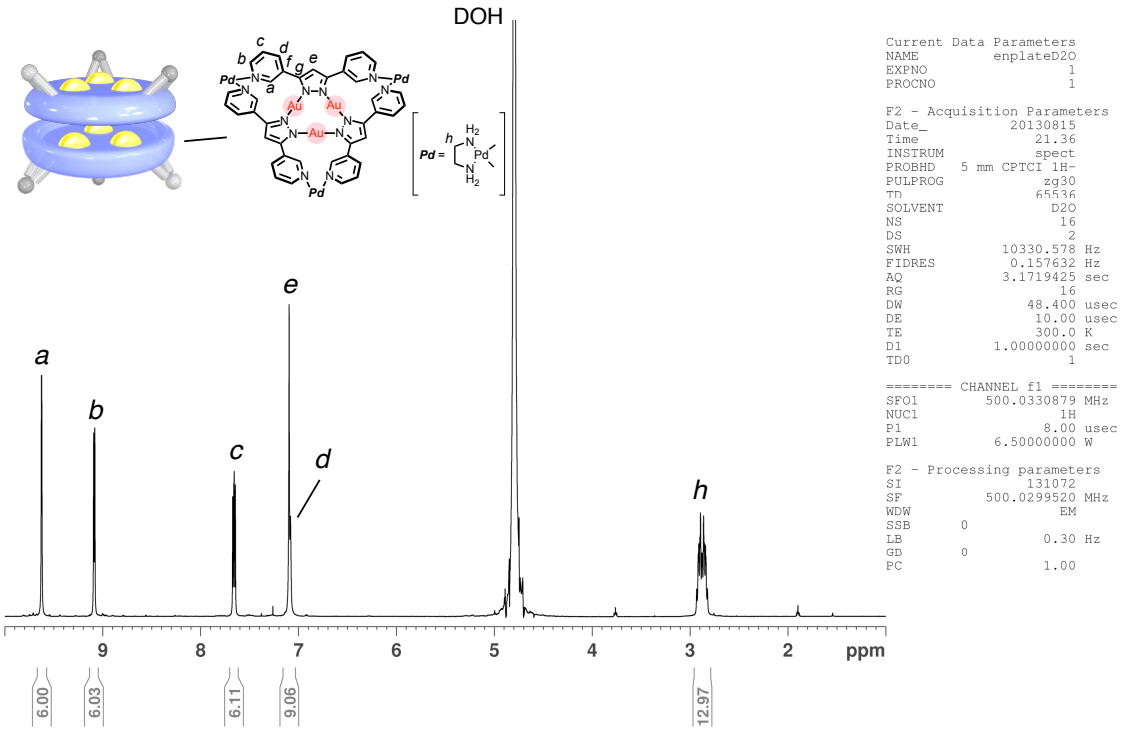

Figure S21. ^{1}H NMR (500 MHz, 300 K, D_2O) spectrum of (*t*-**4b**)•(*t*-**4b**).

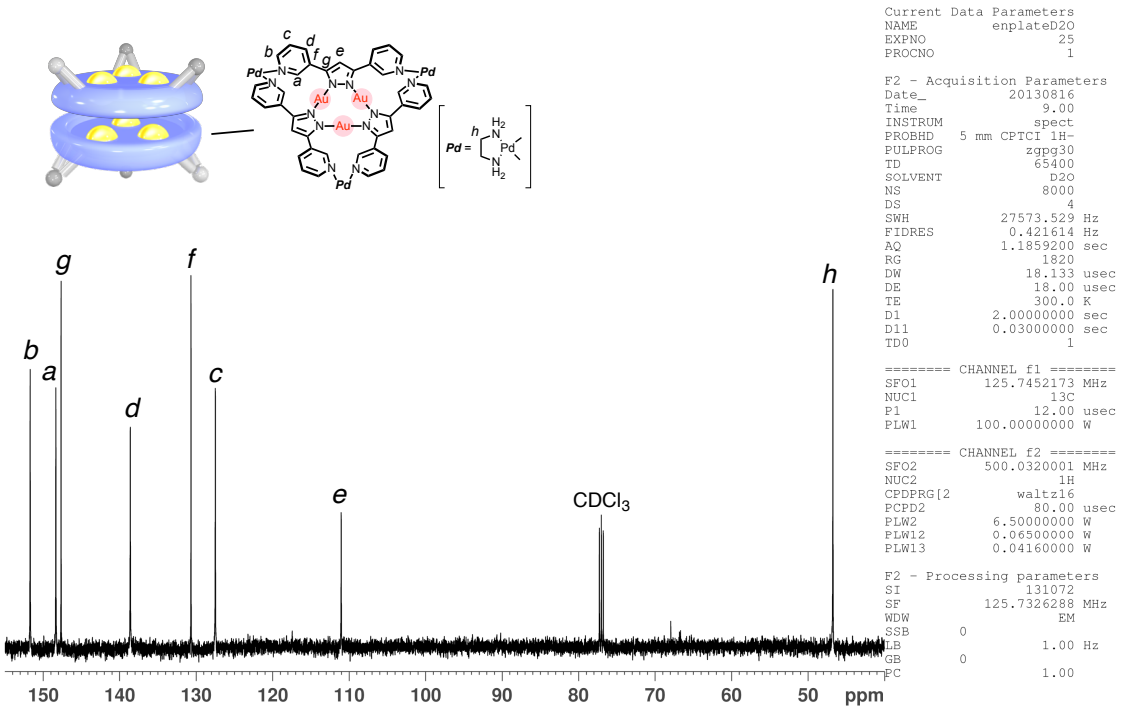

Figure S22. ^{13}C NMR (125 MHz, 300 K, D_2O) spectrum of (*t*-**4b**)•(*t*-**4b**).

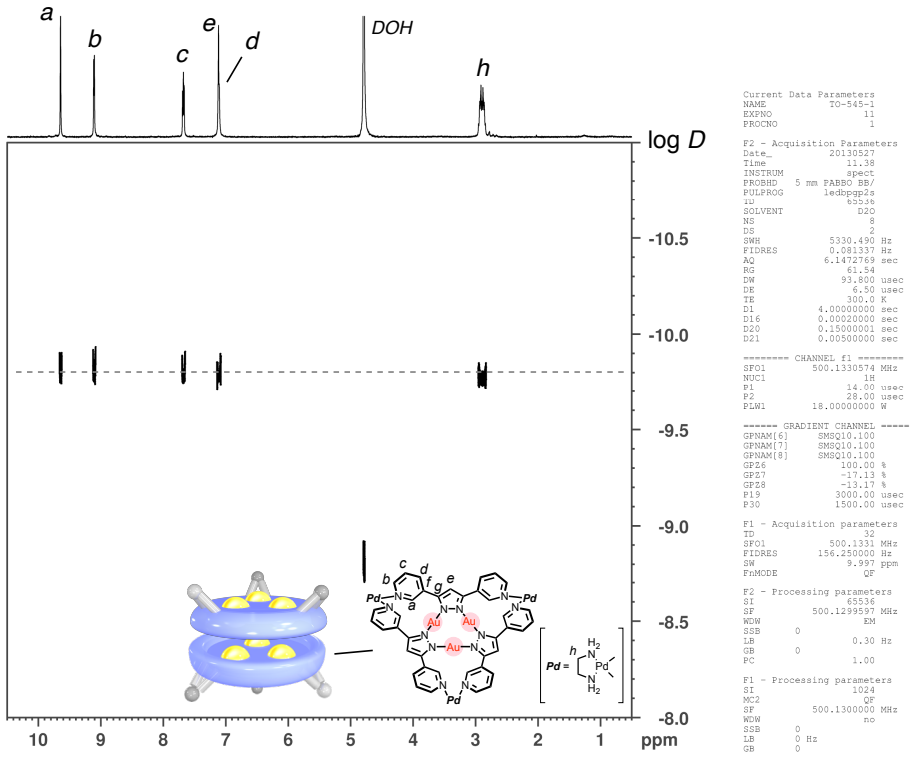

Figure S23. ^{1}H DOSY (500 MHz, 300 K, D_2O) spectrum of (*t*-**4b**)•(*t*-**4b**).

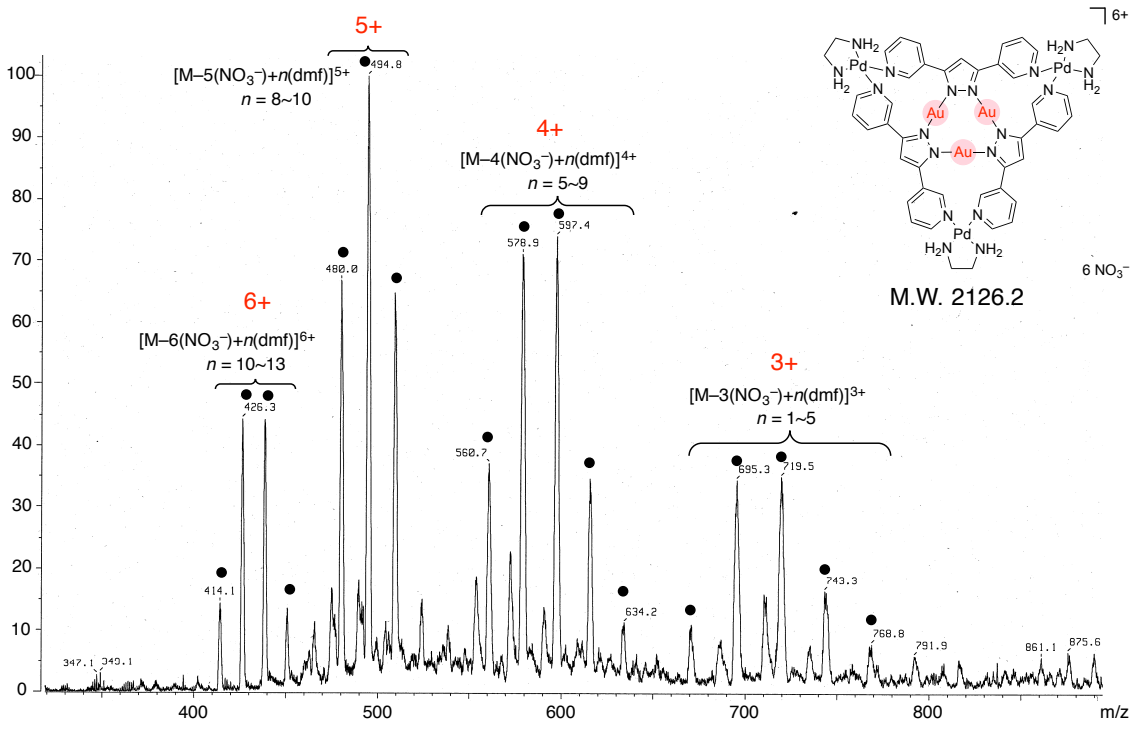

Figure S24. CSI-MS spectrum of **4b** [H_2O/DMF (10:1)].

Formation of Au_3–Au_3–Au_3 triple stack (*t*-4b)•2a•(*t*-4b) in H_2O

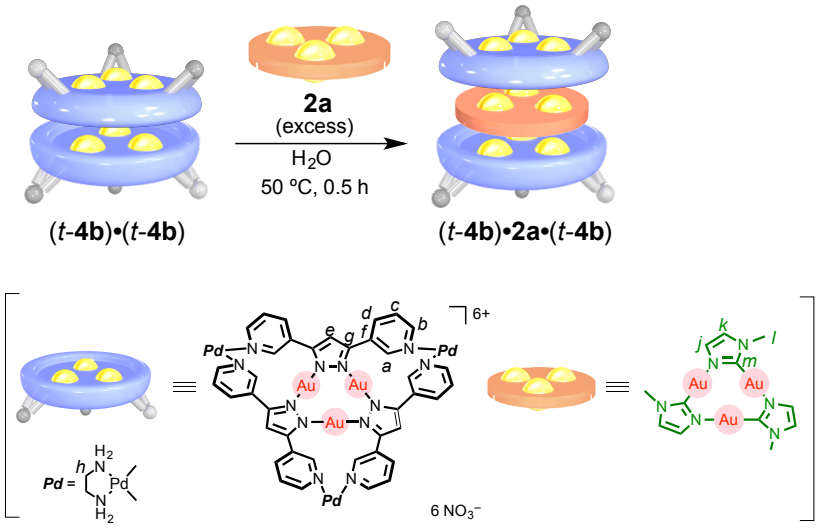

Scheme S6. Formation of Au_3–Au_3–Au_3 triple stack (*t*-**4b**)•**2a**•(*t*-**4b**) in H_2O.

Imidazolate-bridged Au_3 complex **2a** (4.2 mg, 5.0 μmol) was suspended in an aqueous solution of Au_3–Au_3 self-stacked (*t*-**4b**)•(*t*-**4b**) dimer (2.5 mM, 1.0 mL) at 50 ºC for 30 min. After removal of the residual excess guests by filtration, the NMR analysis of the pale yellow solution revealed quantitative formation of Au_3–Au_3–Au_3 triple stack (*t*-**4b**)•**2a**•(*t*-**4b**). The solution was evaporated and dried by a vacuum freeze-drying equipment to give a recognition complex (*t*-**4b**)•**2a**•(*t*-**4b**) (11.8 mg, 2.32 μmol, 93%) as a white solid.

Physical data: ^{1}H NMR (D_2O, 500 MHz, 300 K) δ: 9.64 (s, 6H, *t*-**4b**, H^a), 9.61 (s, 6H, *t*-**4b**, H^a), 8.94 (d, J = 10.0 Hz, 12H, *t*-**4b**, H^b), 8.15 (d, J = 10.0 Hz, 6H, *t*-**4b**, H^d), 7.97 (d, J = 10.0 Hz, 6H, *t*-**4b**, H^d), 7.78–7.68 (m, 12H, *t*-**4b**, H^c), 7.11 (s, 6H, *t*-**4b**, H^e), 5.93 (s, 3H, **2a**, H^j), 5.34 (s, H, **2a**, H^k), 2.93–2.82 (m, 24H, *t*-**4b**, H^h), 1.63 (s, 9H, **2a**, H^i). ^{13}C NMR (D_2O, 125 MHz, 300 K) δ: 166.7 (C, **2a**, C^m), 151.5 (CH, *t*-**4b**, C^b), 151.2 (CH, *t*-**4b**, C^b), 148.3 (C, *t*-**4b**, C^g), 148.1 (CH, *t*-**4b**, C^a), 147.9 (C, *t*-**4b**, C^g), 146.8 (CH, *t*-**4b**, C^a), 140.2 (CH, *t*-**4b**, C^d), 139.6 (CH, *t*-**4b**, C^d), 131.3 (C, *t*-**4b**, C^f), 130.6 (C, *t*-**4b**, C^f), 126.8 (CH, *t*-**4b**, C^c), 126.5 (CH, **2a**, C^k), 119.4 (CH, **2a**, C^j), 109.4 (CH, *t*-**4b**, C^e), 46.7 (CH_2, *t*-**4b**, C^h), 33.6 (CH_3, **2a**, C^l). DOSY-NMR (D_2O, 300 K) (m^2/s): $D = 1.51 \times 10^{-10}$ (log D = –9.82). CSI-MS (H_2O : DMF = 10 : 1): m/z = 969.5 [**4b•2a•4b**–5·NO_3^-+1·DMF]$^{5+}$, 984.5 [**4b•2a•4b**–5·NO_3^-+2·DMF]$^{5+}$, 1000.2

[**4b•2a•4b**–5·NO_3^-+3·DMF]$^{5+}$, 1013.5 [**4b•2a•4b**–5·NO_3^-+4·DMF]$^{5+}$, 1028.4 [**4b•2a•4b**–5·NO_3^-+5·DMF]$^{5+}$, 1042.9 [**4b•2a•4b**–5·NO_3^-+6·DMF]$^{5+}$, 1210.0 [**4b•2a•4b**–4·NO_3^-]$^{4+}$, 1227.3 [**4b•2a•4b**–4·NO_3^-+1·DMF]$^{4+}$, 1246.1 [**4b•2a•4b**–4·NO_3^-+2·DMF]$^{4+}$, 1632.9 [**4b•2a•4b**–3·NO_3^-]$^{3+}$. IR (ATR, cm^{-1}): 3391 (br), 2314 (br), 3111 (br), 2927, 1613 (br), 1471, 1319 (br), 1198, 1106, 1060, 1040, 1024, 809, 783, 692 (br), 660, 620, 605, 572, 545, 535, 495, 472, 456, 445, 419, 409. m.p. ~210 ºC (decomposed).

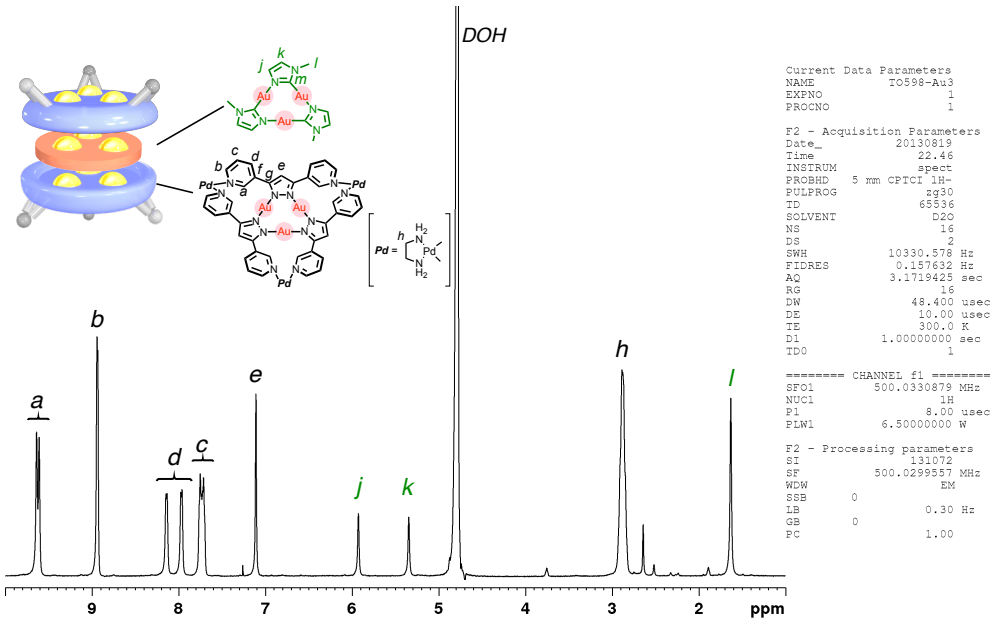

Figure S25. ^{1}H NMR (500 MHz, 300 K, D_2O) spectrum of (*t*-**4b**)•**2a**•(*t*-**4b**).

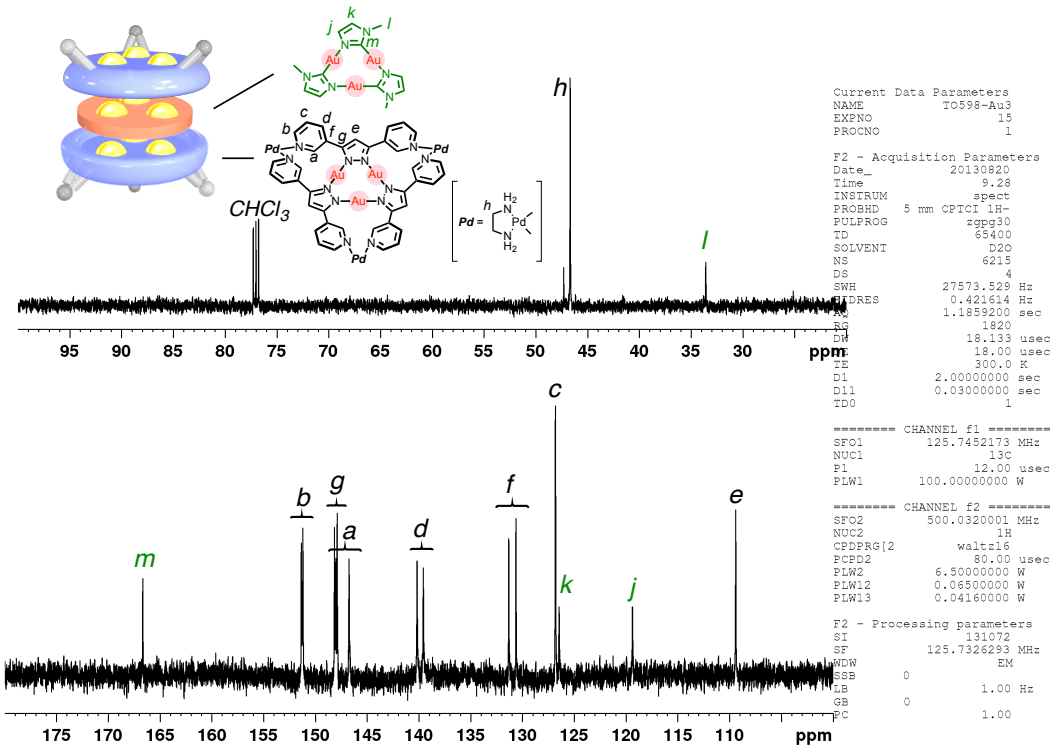

Figure S26. ^{13}C NMR (125 MHz, 300 K, D_2O) spectrum of (*t*-**4b**)•**2a**•(*t*-**4b**).

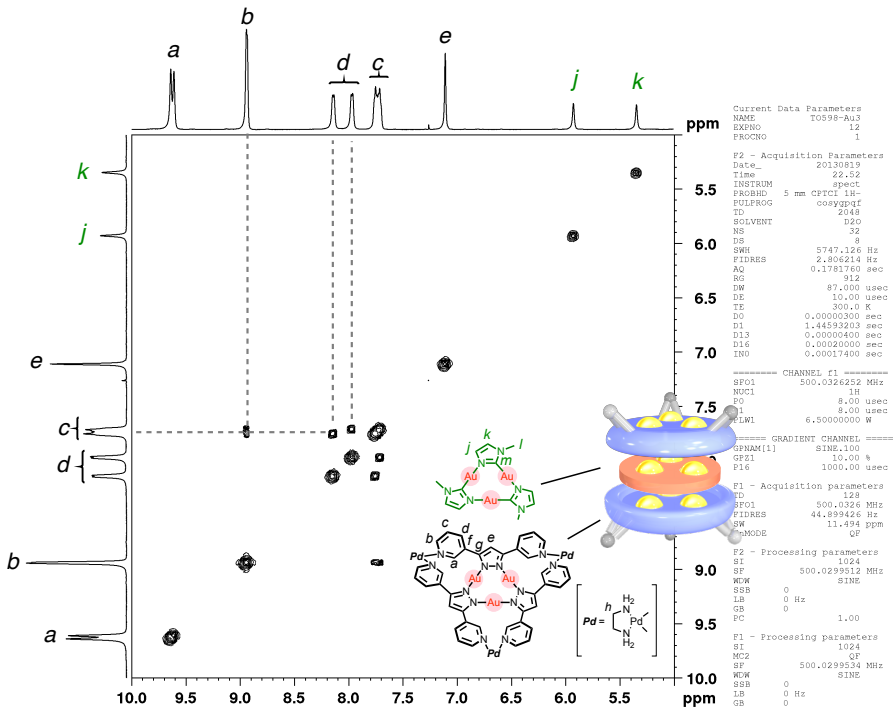

Figure S27. ^{1}H-^{1}H COSY (500 MHz, 300 K, D_2O) spectrum of (*t*-**4b**)•**2a**•(*t*-**4b**).

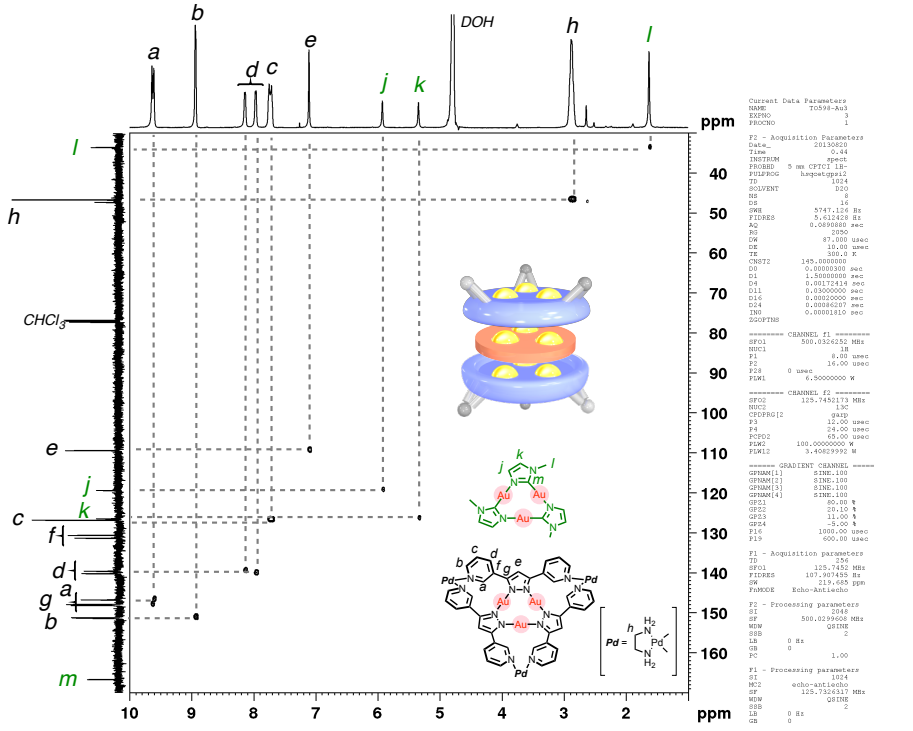

Figure S28. ^{1}H-^{13}C HSQC (500 MHz, 300 K, D_2O) spectrum of (*t*-**4b**)•**2a**•(*t*-**4b**).

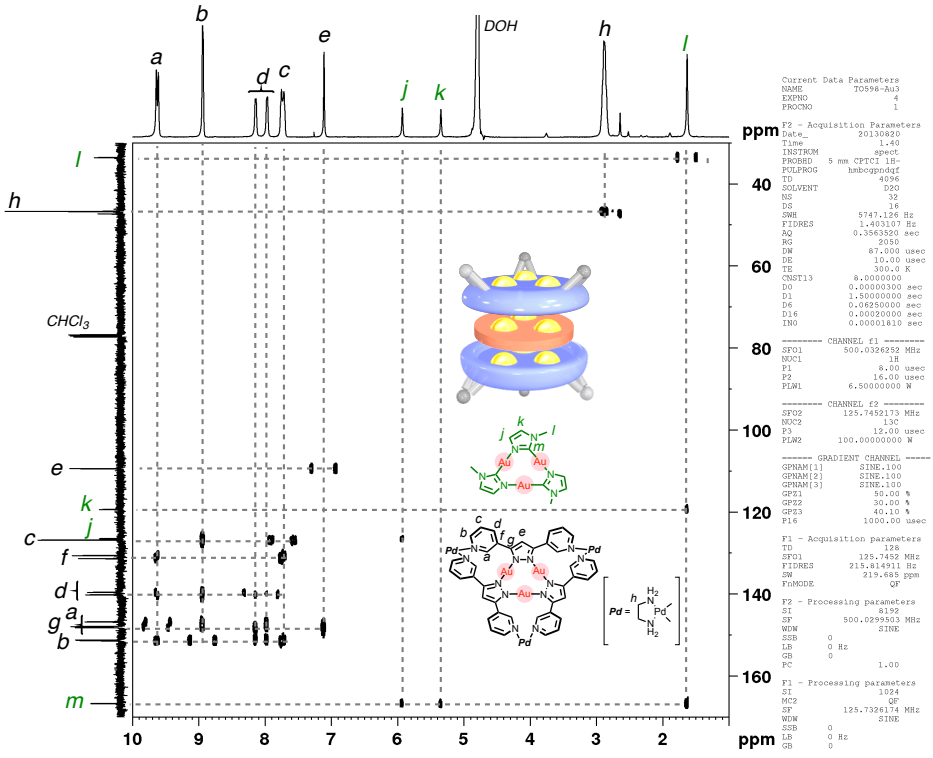

Figure S29. ^{1}H-^{13}C HMBC (500 MHz, 300 K, D_2O) spectrum of (*t*-**4b**)•**2a**•(*t*-**4b**).

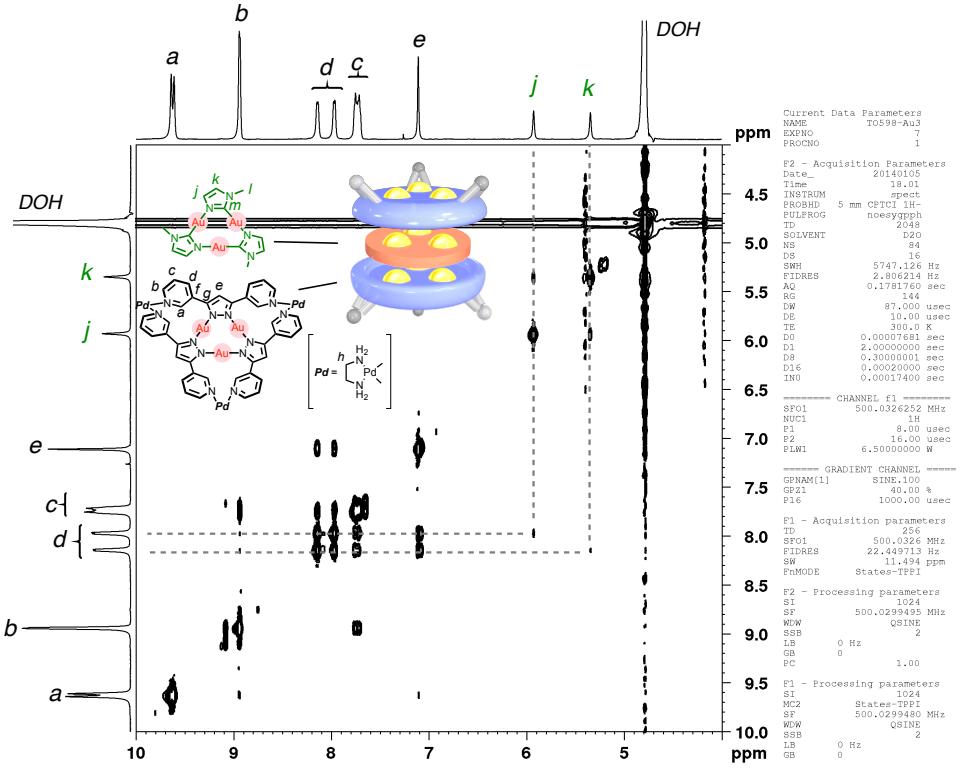

Figure S30. ^{1}H-^{1}H NOESY (500 MHz, 300 K, D_2O) spectrum of (*t*-**4b**)•**2a**•(*t*-**4b**).

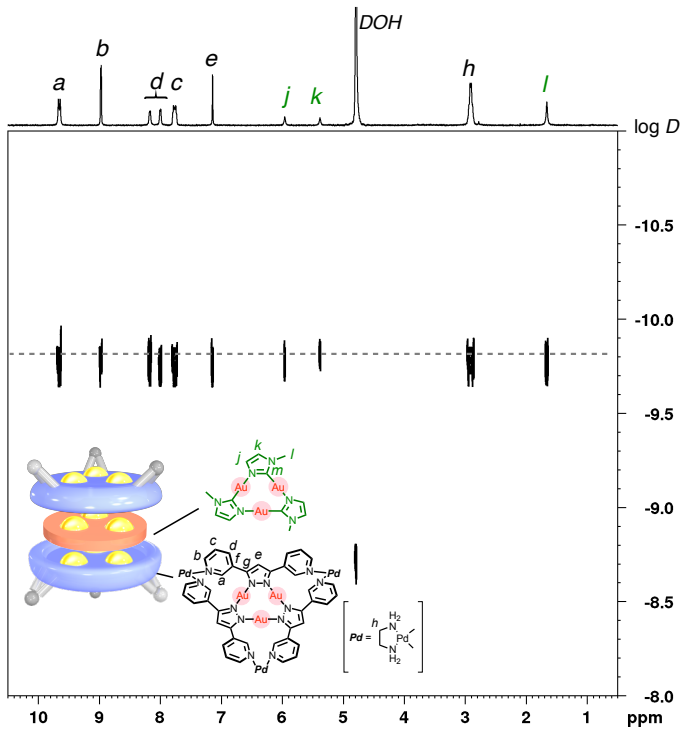

Figure S31. ^{1}H DOSY (500 MHz, 300 K, D_2O) spectrum of (*t*-**4b**)•**2a**•(*t*-**4b**).

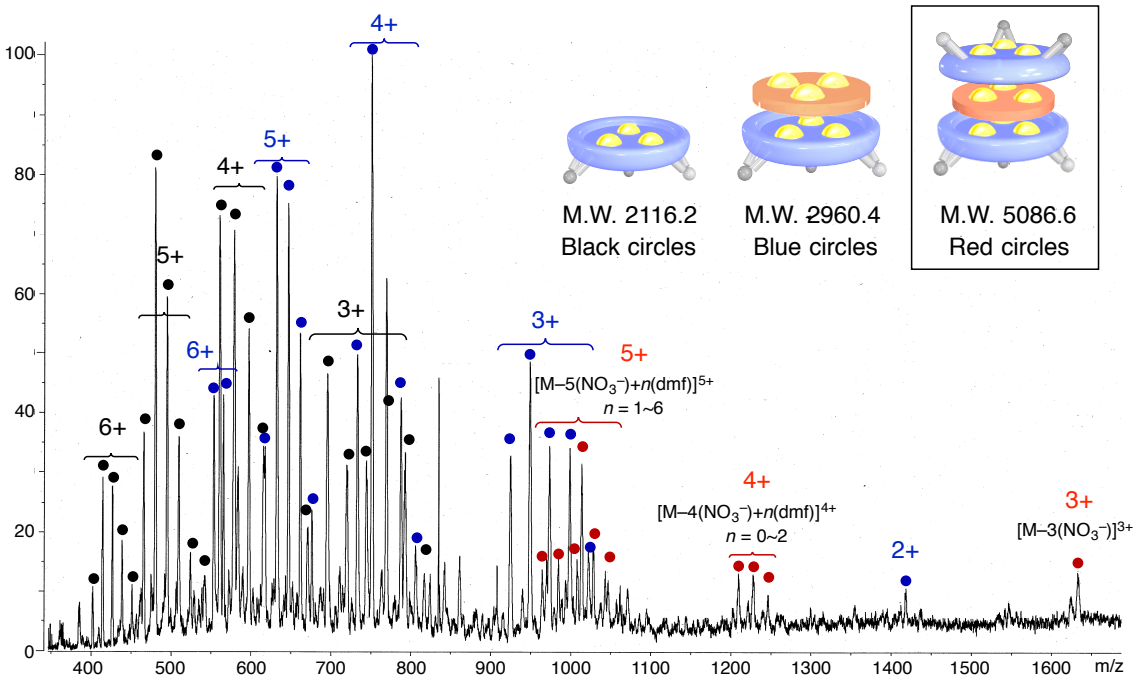

Figure S32. CSI-MS spectrum of (*t*-**4b**)•**2a**•(*t*-**4b**) [H_2O/DMF (10:1)].

Formation of quadruple Au_3 stack (*t*-4b)•2a•Ag^+•2a•(*t*-4b) in H_2O

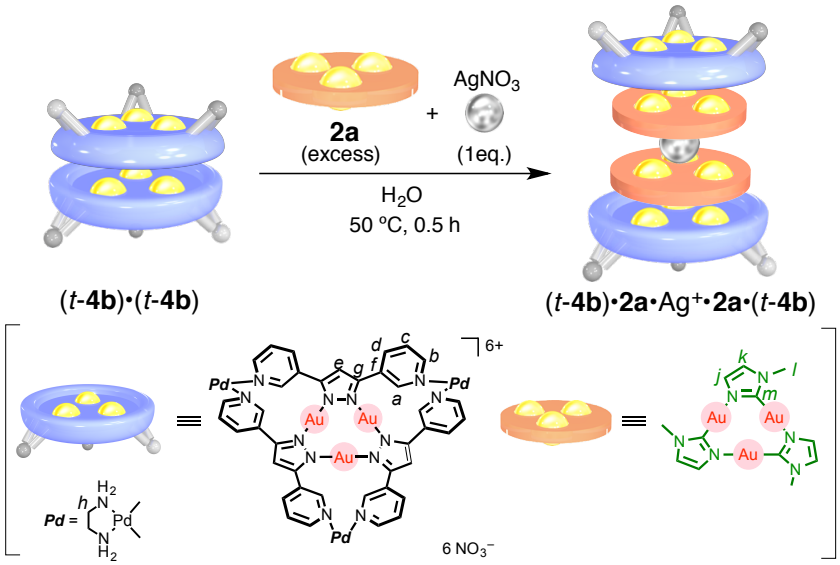

Scheme S7. Formation of quadruple Au_3 stack (*t*-**4b**)•**2a**•Ag^+•**2a**•(*t*-**4b**) in H_2O.

Imidazolate-bridged Au_3 complex **2a** (8.3 mg, 0.010 μmol) and $AgNO_3$ (0.85 mg, 0.050 μmol) were suspended in an aqueous solution of Au_3–Au_3 self-stacked (*t*-**4b**)•(*t*-**4b**) dimer (2.5 mM, 1.0 mL) at 50 ºC for 30 min. After removal of the residual excess guests by filtration, NMR analysis of the pale yellow solution revealed quantitative formation of Au_3–Au_3–Ag–Au_3–Au_3 ion cluster (*t*-**4b**)•**2a**•Ag^+•**2a**•(*t*-**4b**). The spectrum indicated the existence of two diastereomers, associated with the same and opposite stacking modes of guest **2a** (Figure S33). The solution was evaporated and dried by a vacuum freeze-drying equipment to give a recognition complex (*t*-**4b**)•**2a**•Ag^+•**2a**•(*t*-**4b**) (14.3 mg, 2.35 μmol, 94%) as a white solid.

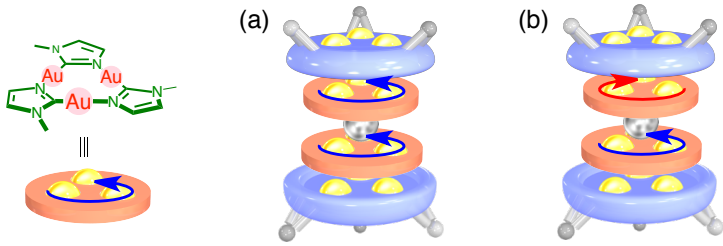

Figure S33. Schematic illustration of (a) the same and (b) opposite stacking modes of C_{3h} symmetrical guest **2a** in Au_3–Au_3–Ag–Au_3–Au_3 ion cluster (*t*-**4b**)•**2a**•Ag^+•**2a**•(*t*-**4b**).

Physical data: ^{1}H NMR (D_2O, 500 MHz, 300 K) (major diastereomer) δ: 9.66 (s, 6H, *t*-**4b**, H^a), 9.61 (s, 6H, *t*-**4b**, H^a), 8.95 (d, J = 5.0 Hz, 12H, *t*-**4b**, H^b), 8.23 (d, J =

8.0 Hz, 6H, *t*-**4b**, H^{d}), 7.96 (d, J = 8.0 Hz, 6H, *t*-**4b**, H^{d}), 7.75–7.68 (m, 12H, *t*-**4b**, H^{c}), 7.09 (s, 6H, *t*-**4b**, H^{e}), 6.54 (s, 6H, **2a**, H^{j}), 6.09 (s, 6H, **2a**, H^{k}), 2.94–2.82 (m, 24H, *t*-**4b**, H^{h}), 2.27 (s, 18H, **2a**, H^{i}); (minor diastereomer) δ: 9.67 (s, 6H, *t*-**4b**, H^{a}), 9.62 (s, 6H, *t*-**4b**, H^{a}), 8.95 (d, J = 5.0 Hz, 12H, *t*-**4b**, H^{b}), 8.18 (d, J = 8.0 Hz, 6H, *t*-**4b**, H^{d}), 7.95 (d, J = 8.0 Hz, 6H, *t*-**4b**, H^{d}), 7.75–7.68 (m, 12H, *t*-**4b**, H^{c}), 7.09 (s, 6H, *t*-**4b**, H^{e}), 6.78 (s, 6H, **2a**, H^{j}), 5.87 (s, 6H, **2a**, H^{k}), 2.94–2.82 (m, 24H, *t*-**4b**, H^{h}), 2.32 (s, 18H, **2a**, H^{l}). ^{13}C NMR (D_2O, 125 MHz, 300 K) (major diastereomer) δ: 162.3 (C, **2a**, C^{m}), 151.3 (CH, *t*-**4b**, C^{b}), 151.2 (CH, *t*-**4b**, C^{b}), 148.2 (C, *t*-**4b**, C^{g}), 148.2 (CH, *t*-**4b**, C^{a}), 147.9 (C, *t*-**4b**, C^{g}), 146.5 (CH, *t*-**4b**, C^{a}), 140.2 (CH, *t*-**4b**, C^{d}), 140.0 (CH, *t*-**4b**, C^{d}), 131.2 (C, *t*-**4b**, C^{f}), 130.2 (C, *t*-**4b**, C^{f}), 127.0 (CH, *t*-**4b**, C^{c}), 126.8 (CH, *t*-**4b**, C^{c}), 126.0 (CH, **2a**, C^{k}), 121.6 (CH, **2a**, C^{j}), 109.6 (CH, *t*-**4b**, C^{e}), 46.6 (CH_2, *t*-**4b**, C^{h}), 34.3 (CH_3, **2a**, C^{l}); (minor diastereomer) δ: 162.6 (C, **2a**, C^{m}), 151.3 (CH, *t*-**4b**, C^{b}), 151.2 (CH, *t*-**4b**, C^{b}), 148.3 (C, *t*-**4b**, C^{g}), 148.0 (CH, *t*-**4b**, C^{a}), 147.9 (C, *t*-**4b**, C^{g}), 146.6 (CH, *t*-**4b**, C^{a}), 140.2 (CH, *t*-**4b**, C^{d}), 139.8 (CH, *t*-**4b**, C^{d}), 131.2 (C, *t*-**4b**, C^{f}), 130.2 (C, *t*-**4b**, C^{f}), 127.0 (CH, *t*-**4b**, C^{c}), 126.8 (CH, *t*-**4b**, C^{c}), 126.4 (CH, **2a**, C^{k}), 121.2 (CH, **2a**, C^{j}), 109.6 (CH, *t*-**4b**, C^{e}), 46.6 (CH_2, *t*-**4b**, C^{h}), 34.2 (CH_3, **2a**, C^{l}). DOSY-NMR (D_2O, 300 K) (m^2/s): D = 1.48 × 10^{-10} (log D = –9.83). IR (ATR, cm^{-1}): 3410 (br), 3211 (br), 3110 (br), 2925, 1614 (br), 1471, 1319 (br), 1198, 1107, 1060, 1040, 1024, 1004, 808, 782, 750, 736, 722, 691 (br), 661, 619, 607, 594, 575, 565, 547, 535, 515, 509, 495, 483, 471, 453, 441, 419. m.p. ~210 ºC (decomposed).

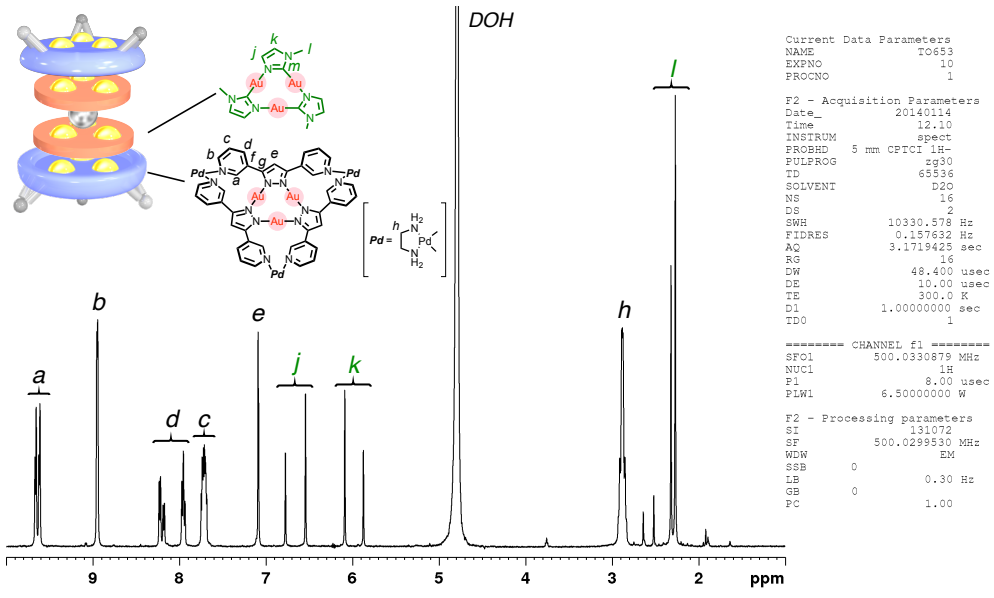

Figure S34. ^{1}H NMR (500 MHz, 300 K, D_2O) spectrum of (*t*-**4b**)•**2a**•Ag^{+}•**2a**•(*t*-**4b**).

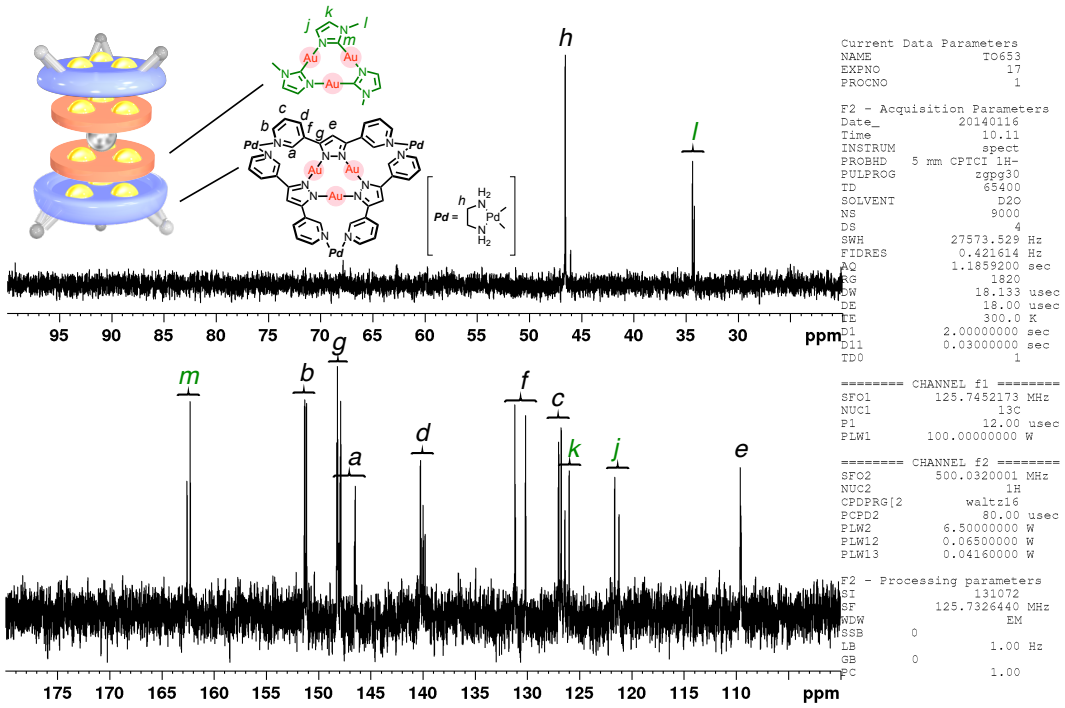

Figure S35. ^{13}C NMR (125 MHz, 300 K, D_2O) spectrum of (*t*-**4b**)•**2a**•Ag^+•**2a**•(*t*-**4b**).

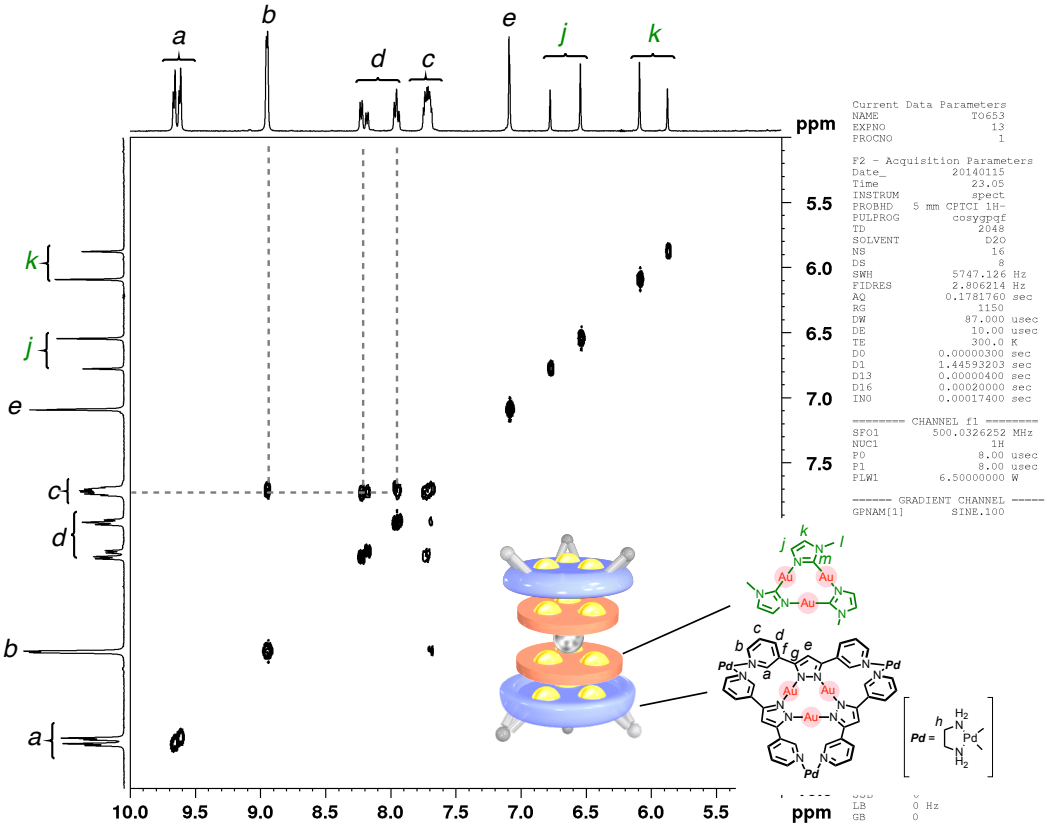

Figure S36. ^{1}H-^{1}H COSY (500 MHz, 300 K, D_2O) spectrum of (*t*-**4b**)•**2a**•Ag^+•**2a**•(*t*-**4b**).

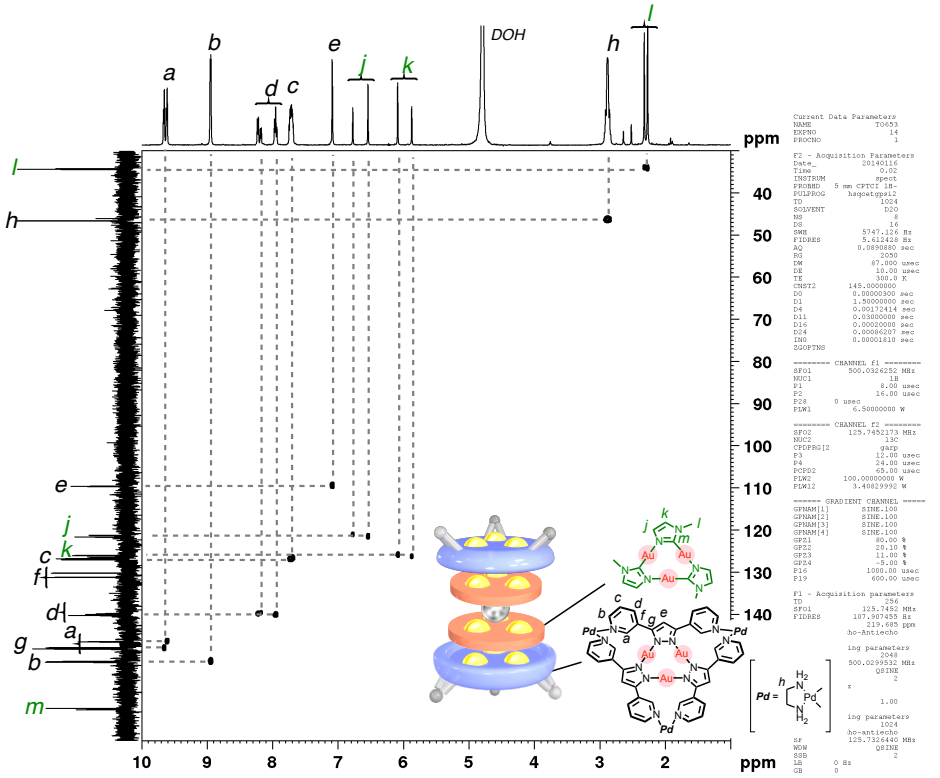

Figure S37. ^{1}H-^{13}C HSQC (500 MHz, 300 K, D_2O) spectrum of (*t*-**4b**)•**2a**•Ag^{+}•**2a**•(*t*-**4b**).

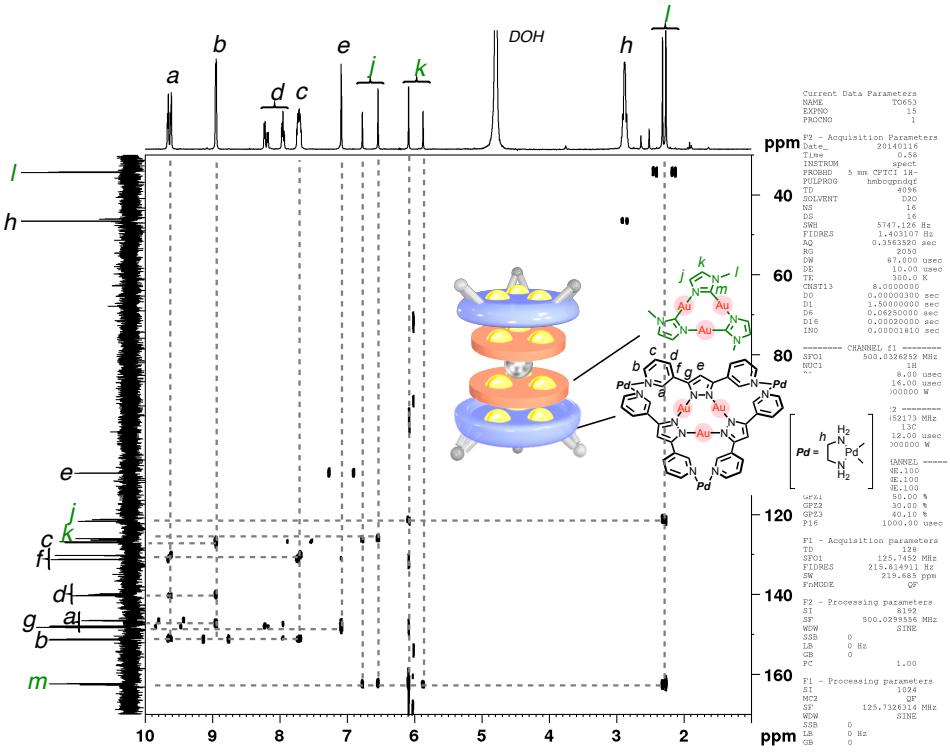

Figure S38. ^{1}H-^{13}C HMBC (500 MHz, 300 K, D_2O) spectrum of (*t*-**4b**)•**2a**•Ag^{+}•**2a**•(*t*-**4b**).

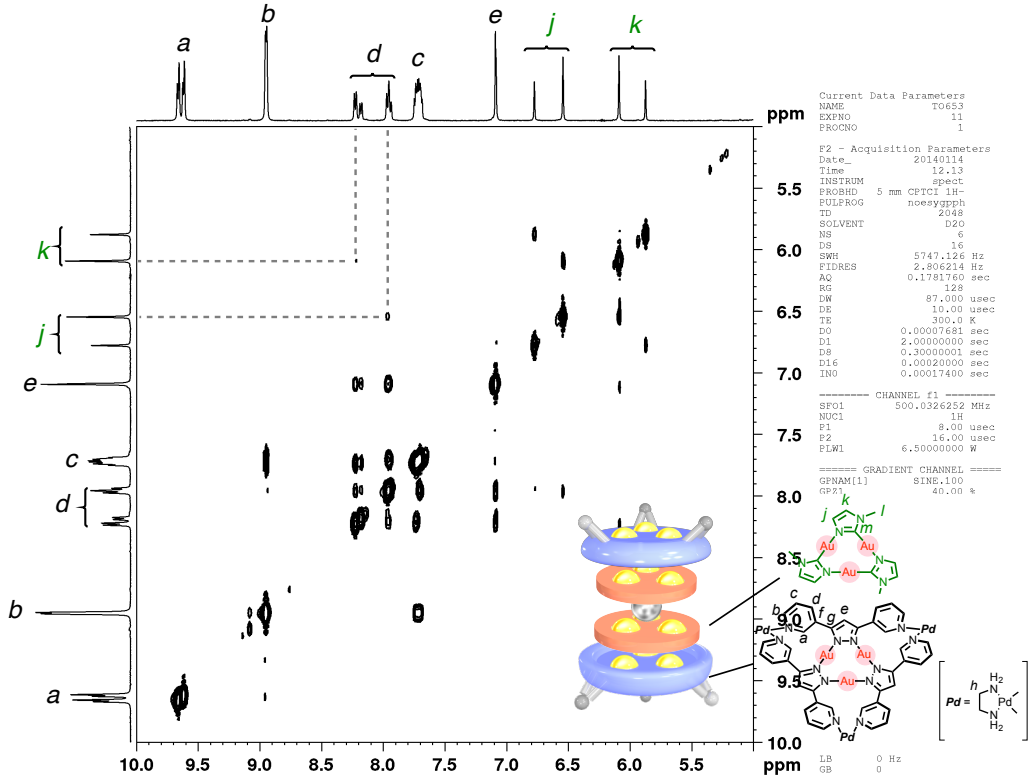

Figure S39. ^{1}H-^{1}H NOESY (500 MHz, 300 K, D_2O) spectrum of (*t*-**4b**)•**2a**•Ag^{+}•**2a**•(*t*-**4b**).

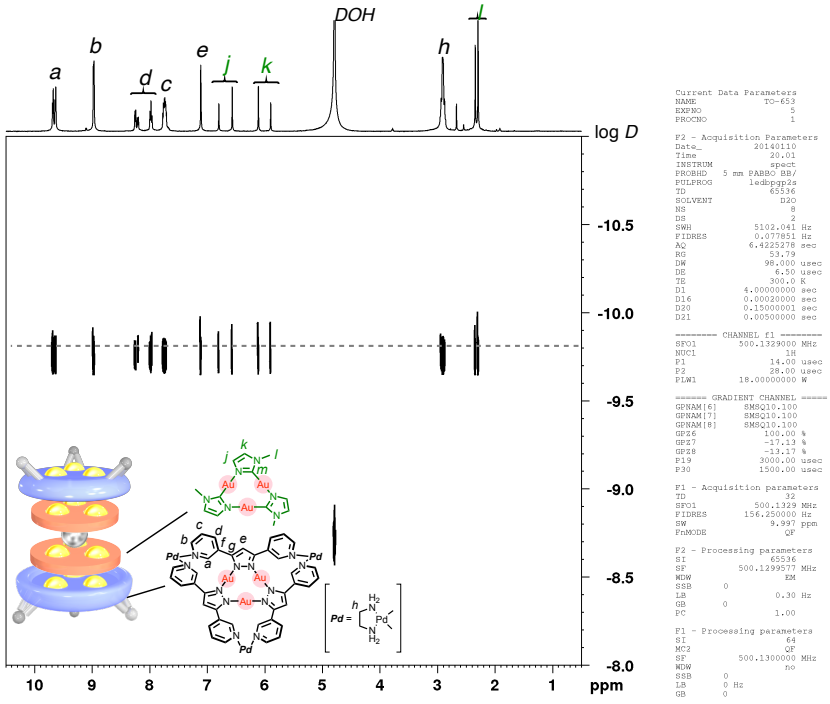

Figure S40. ^{1}H DOSY (500 MHz, 300 K, D_2O) spectrum of (*t*-**4b**)•**2a**•Ag^{+}•**2a**•(*t*-**4b**).

Chapter 5

Electron Transport through [3 × *n*] Gold Ion Clusters within Self-Assembled Coordination Cages

Abstract

Single-molecular electron conductance through [3 × *n*] Au(I) clusters (*n* = 1–3) was measured by using an STM break junction method. The box-shaped coordination cages of the Au(I) clusters formed molecular junctions between two Au electrodes. The observed conductance values were much higher than those of π-stacked aromatic molecules enclosed in the cages. No temperature dependency of the conductance indicated a tunneling mechanism for the electron transport. Moreover, the small attenuation factor toward the transport distance guaranteed a long range electron transfer of metal ion arrays.

5.1 Introduction

Electron transport through metal ion arrays has attracted increasing interest for application in nanometer scale electronics.[1–3] Because the electron transport ability highly depends on the length, conjugation, conformation, and substituents of the molecules,[4,5] a method that can precisely construct metal ion arrays is highly demanded to evaluate their electron properties.

Anderson and coworkers studied an electron transport through a series of oligo-porphyrin wires with one, two, and three Zn(II) units (Figure 1).[6–8] The single molecular conductance was measured with the scanning tunneling microscope break junction (STM-BJ) technique established by Tao's group in 2003.[9–12] The pyridyl groups in the both ends of the molecular wire were anchored to the two Au electrodes and formed molecular junctions. The conductance behavior showed a weak dependence of the length of the wire (Figure 2), namely this Zn(II) wire has a long range electron transport ability. The DFT calculations by Lambert suggested that this

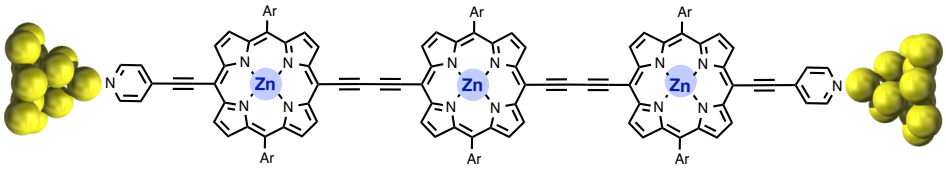

Figure 1. Illustration of a single molecule of oligo-porphyrin with three Zn(II) centers bounded between the two Au electrodes.

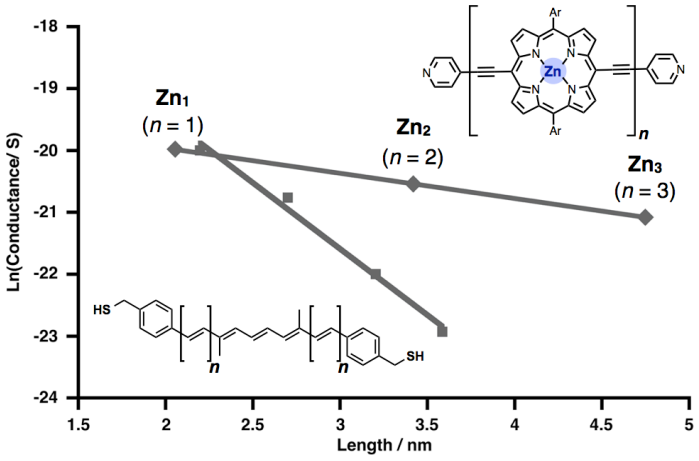

Figure 2. Distance dependence of conductance oligo-porphyrin Zn(II) wires. The conductance of a typical conjugated organic molecule is also shown for a comparison.[13]

conductance mechanism was consistent with phase-coherent tunneling model through the molecular junction.

Peng's group achieved to synthesize metal ion chains with direct meta-metal bonds or interactions (Figure 3). They measured single-molecule conductance of one dimensional multinuclear metal chains $[M_nL_4(NCS)_2]$ (M = Cr, Co, Ni; n = 3, 5, 7; L = oligo-α-pyridylamine) by using the same method.[14–16] In this case, metal-metal bonds or interactions formed an effective pathway of electron transport, while current is protected from leaking with insulating organic ligands surrounding the metal ion chains. The resistances of Cr_5, Co_5, and Ni_5 chains were determined to be 3.2 MΩ, 10.0 MΩ, and 24.0 MΩ, respectively. The discrepancy between three metal chains seems to lie in the order of electronic coupling of the d-orbitals between the adjacent metal atoms. In fact, extended Hückel MO calculations revealed that metal-metal bond orders for Cr, Co, and Ni strings are 1.5, 0.5, and 0, respectively.

Figure 3. Illustration of a one-dimensional Ni(II) array forming a molecular junction. Metal-metal bonds (Cr, Co) or interactions (NI) between adjacent metal ions formed electron transport pathways.

In this chapter, we measured the electron transport through metal ion clusters trapped between the Au electrodes (Figure 4). Among several kinds of metal ion clusters synthesized in the precious chapters 2–4, the most simple [3 × n] Au(I) ion clusters (n = 1–3)[17] were selected for the evaluation of electron properties because box-shaped coordination cages **1** precisely controlled the number and arrays of metal ions. Moreover, the trigonal prismatic arrays of Au(I) ions through multiple Au(I)–Au(I) interactions are expected to contribute to an efficient electron transport.

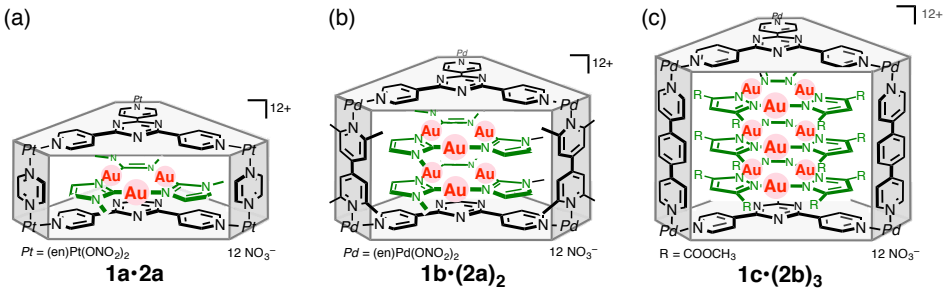

Figure 4. [3 × *n*] Au(I) clusters (*n* = 1–3) constructed within box-shaped cages. (a) [3 × 1] Au(I) cluster **1a•2a**, [3 × 2] Au(I) cluster **1b•(2a)**$_2$, and [3 × 3] Au(I) cluster **1c•(2b)**$_3$. Self-assembled coordination cages **1** accommodated planar trinuclear Au(I)$_3$ complexes **2**.

5.2 Box-shaped coordination cages

In 2011, electron transport through multiple stacks of aromatic molecules was successfully measured with the same columnar box-shaped cages **1**.[18,19] Cages **1** served as molecular containers for discrete stacks of pyrene-4,5-diones (**7**) (Figure 5).[20,21] The result shows that the discrete stacks exhibit high conductance with only moderate loss with increasing transport length. It should be noted that box-shaped cages **1** favorably form molecular junctions between two Au electrodes in a vertical direction without conventional anchoring groups, such as thiol, thiocyanate, and amine groups. In consequence, I expected that box-shaped cages **1** serve molecular containers for the measurement of single molecular conductance, and then I can prepare

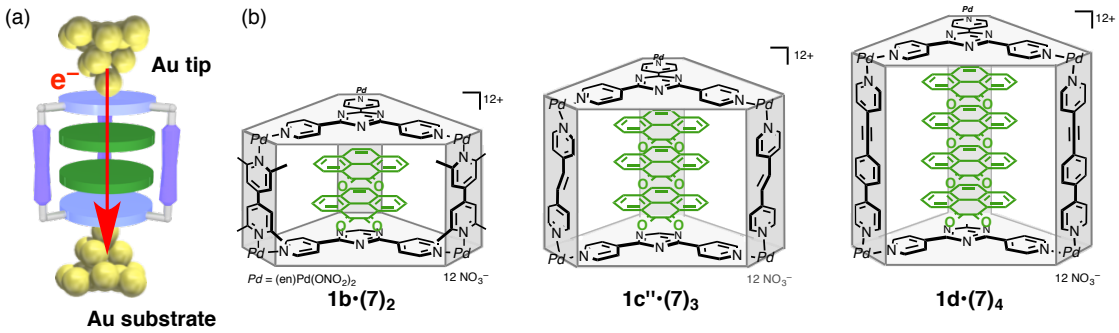

Figure 5. Electron transport through discrete π-stacks encapsulated with box-shaped cage 1. (a) Illustration of a molecular junction of discrete π-stacks within cage **1** between the Au nanogap. (b) Structure of π-stacked systems. Cages **1** accommodate two, three, and four molecules of pyrene-4,5-diones depending on the height.

a series of ultra small devices because the cages can accommodate a variety of planar molecules (Figure 6).[22]

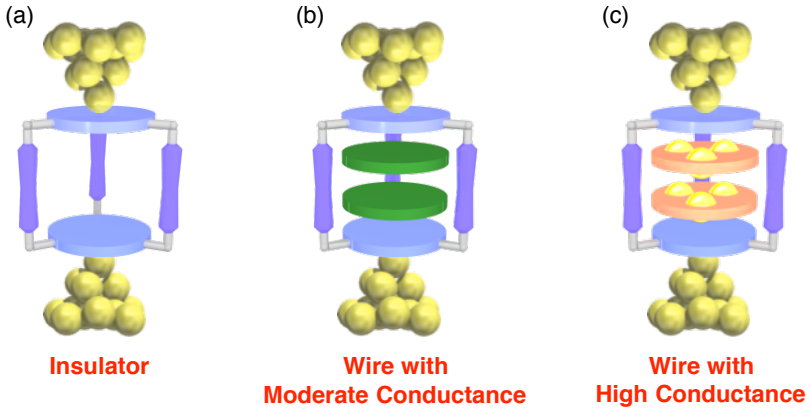

Figure 6. Family of molecular devices encapsulated within box-shaped cages 1. (a) The empty cage exhibits insulating character,[18] (b) the cage enclosing aromatic π-stack is considered to be a molecular wire (resistor) with moderate conductance, and (c) the cage with metal ions is expected to exhibit relatively high conductance.

5.3 Conductance measurements

Experimental procedures were reported in detail by Kiguchi and coworkers.[23] An Au tip was repeatedly moved into and out of contact with an Au substrate in an aqueous solution of [3 × *n*] Au(I) ion clusters (Figure 7). Upon repeating formation of

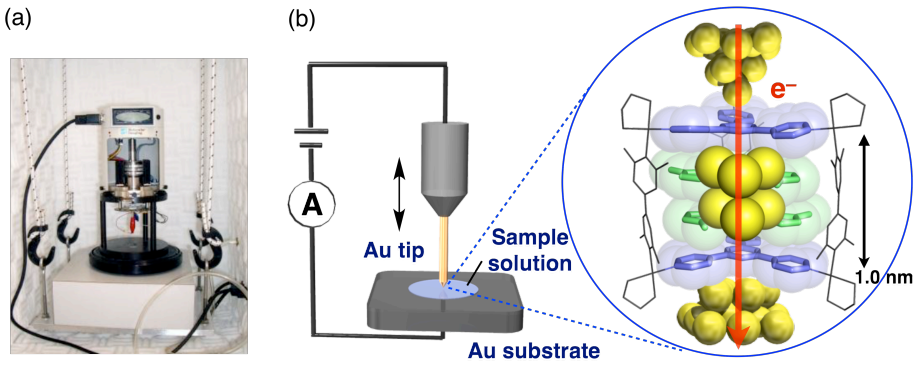

Figure 7. STM break junction technique. (a) A photograph of STM used for the single molecule conductance measurement. (b) Illustration of STM (left) and molecular junction of Au electrodes (Au tip and substrate) (right). Modeled structure of [3 × 2] Au(I) cluster $\mathbf{1b}\bullet(\mathbf{2a})_2$ is shown between the Au electrodes.

the tip-substrate nanogap, molecules are bound between two electrodes to from Au–molecule–Au molecular junctions.

Figure 8a shows conductance traces obtained from Au contacts in a solution of [3 × *n*] Au(I) ion clusters. When a blank water or aqueous solution of empty cage **1b** was measured, the conductance dropped sharply and no trail was observed (black lines). In contrast, when the measurement was performed with aqueous solution of [3 × *n*] Au(I) ion clusters (*n* = 1–3), several steps appeared during the drop of the measured conductance (red, green, and blue lines), which indicates the formation of molecular junctions. From the repeated measurement, each histogram constructed from 1000 conductance curves shows peaks at integer multiple of certain values (Figure 8b–d). In this way, the single-molecule conductance values of [3 × 1], [3 × 2], and [3 × 3] Au(I) clusters **1a•2a**, **1b•(2a)**$_2$, and **1c•(2b)**$_3$ were determined to be 7.0 ± 1.6 × 10^{-3} G_0 ($2e^2/h$), 5.7 ± 0.9 × 10^{-3} G_0, and 5.1 ± 1.4 × 10^{-3} G_0, respectively. The conductance value 1 G_0 ($G_0 = 2e^2/h$, where e is the charge of an electron, and h is Plank's contact), is the quantized value which is obtained when the size of a metallic contact is decreased to a single chain of Au atoms.[24,25] As expected, the conductance values of [3 × *n*] Au(I) clusters are much higher than those of π-stacks of aromatic molecules. No temperature dependency of [3 × 3] Au(I) clusters at temperature range of 5–50 ºC indicated that electron transport occurs by a tunneling mechanism rather than a hopping mechanism (Figure 9).

Based on the tunneling model, these conductance values were fitted with the exponential decay of conductance [Eq. (1)]

$$G = A_N \exp(-\beta L) \quad (1)$$

where G is the conductance value; A_N is the contact resistance determined by the nanowire-electrode electronic coupling; β is the exponential pre-factor that represents attenuation of conductance; L is the length of the nanowire. The attenuation factor (β) for the single [3 × *n*] Au(I) clusters (*n* = 1–3) was determined to be 0.05 $Å^{-1}$ from the slope of L versus InG plots (Figure 10). The small attenuation factor represents a large electronic coupling between Au(I) ions in a vertical direction and then, a long-range electron transport ability. The β value is smaller than that of the vacuum gap (β = 2.2 $Å^{-1}$), organic alkanes (β = 0.7 to 0.9 $Å^{-1}$),[13] π-stacks of pyrene-4,5-dione within the

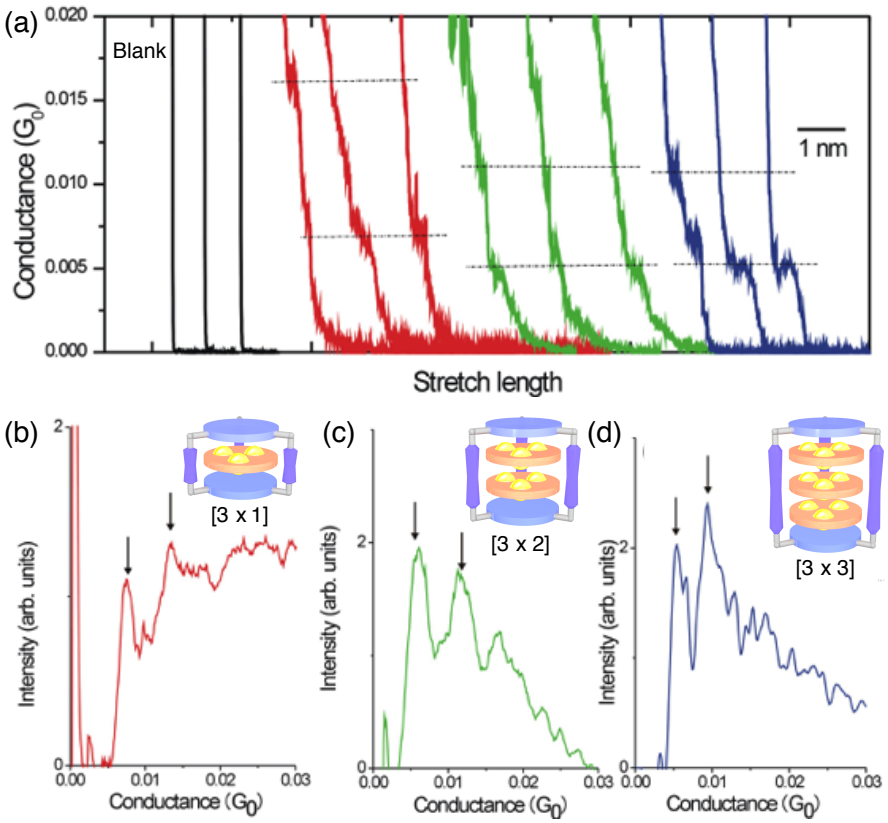

Figure 8. Conductance of [3 × *n*] Au(I) clusters (*n* = 1–3). (a) Typical conductance curves acquired by stretching the Au electrodes with blank water (standard), and aqueous solutions of [3 × 1], [3 × 2], and [3 × 3] Au(I) clusters (black, red, green, and blue lines, respectively). (b–d) Conductance histograms of (b) [3 × 1], (c) [3 × 2], and (d) [3 × 3] Au(I) clusters obtained from 1000 measurements. The tunneling background was subtracted. In the blank measurement, no such peaks were identified.

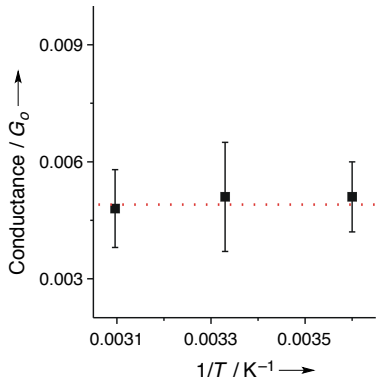

Figure 9. Conductance of [3 × 3] Au(I) ion cluster 1c·$(2b)_3$ as a function of temperature. No temperature dependency indicates the tunneling mechanism of electron transport.

same cage ($\beta = 0.1$ Å^{-1}),[18,19] and comparable to that of porphyrin Zn(II) wires ($\beta = 0.04$ Å^{-1}).[7] The A_N value for the [3 × n] Au(I) clusters was 1.1 × 10^{-2} G_0, which is larger than that of π-stacked system within the cage (A_N = 1.5 x 10^{-3} G_0) and porphyrin Zn(II) wires (A_N = 6 × 10^{-5} G_0). This result indicats that two panels at the top and the bottom the cage are well connected to Au electrodes.

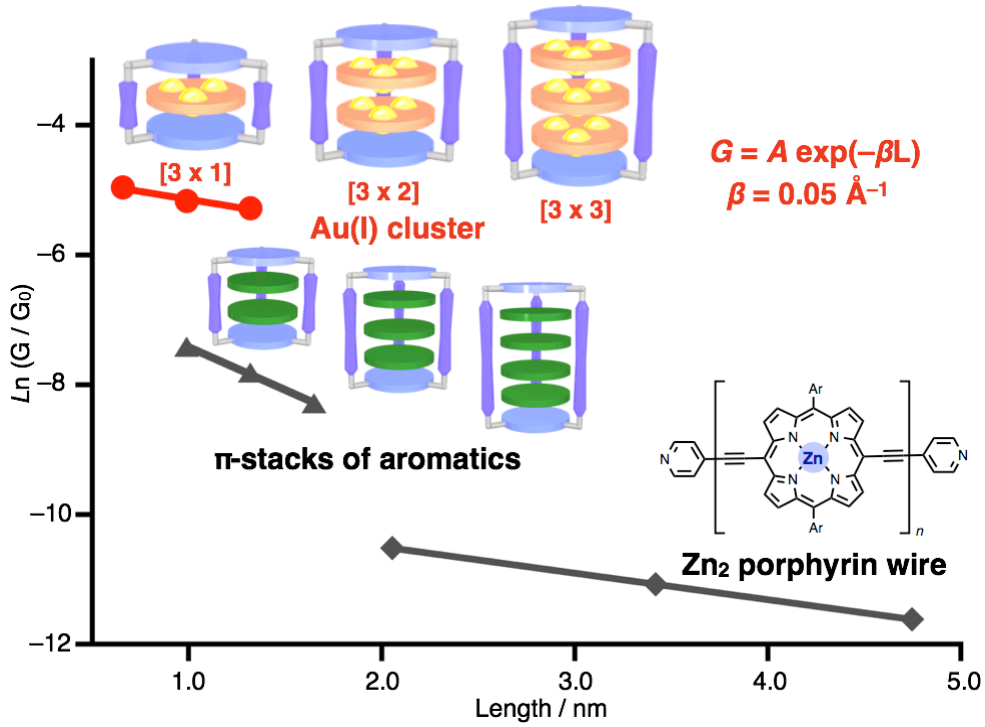

Figure 10. Distance dependence of the observed conductance *G* for [3 × *n*] (*n* = 1–3) Au(I) arrays (red circles) and π-stacks of pyrene-4,5-diones (black triangles). The conductance of Zn(II) porphyrin wire (black rhomboid) are also shown for a comparison.[9]

5.4 Conductance calculations

A transmission function and LDOS (local density of states) of [3 × 2] Au(I) cluster **1b**•(**2a**)$_2$ were calculated with a model stacking structure **3**•(**2a**)$_2$•**3** sandwiched with two Au electrodes (Figure 11). For modeling, Pd hinges and pillar ligands were removed from the original cage framework **1b**, and the geometry of the stacking structure (**2a**)$_2$ was optimized with Gaussian 09.[26] It should be noted that eclipsed stacking mode was the most stable stacking mode for the cofacial dimer of Au(I)$_3$ complexes (**2a**)$_2$ (Figure 11c) as in the case of [3 × 3] Au(I) cluster **1c'**•(**2b**)$_3$ (for the

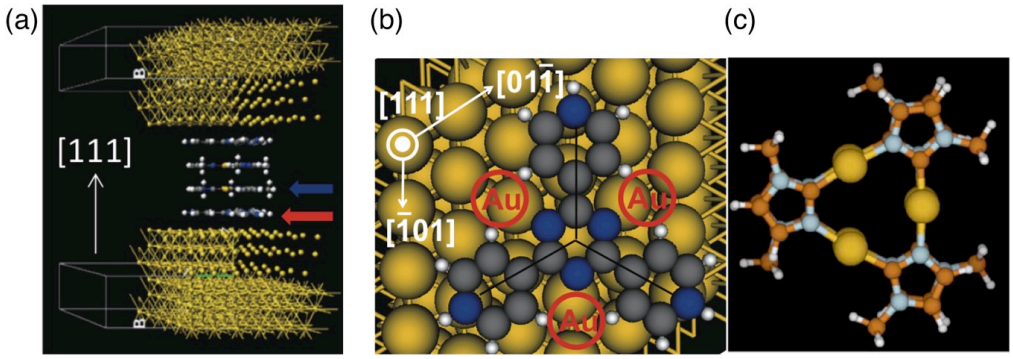

Figure 11. Computational model of [3 × 2] Au(I) cluster 1b•$(2a)_2$ sandwiched with two Au electrodes. (a) Side view of the stacking model sandwiched with two Au electrodes. Stacking model **3**•$(\mathbf{2a})_2$•**3** was adopted for the calculation. (b) Top view of panel ligand **3** and the bottom electrodes of the stacking model (Au: yellow, N: blue, C: gray, H: white). The three red circles with Au index indicate the position of three Au(I) ions in $Au(I)_3$ complex **2a** located above panel ligand **3**. (c) Top view of the optimized stacking model of [3 × 2] Au(I) cluster $(\mathbf{2a})_2$. Eclipsed mode was the most stable sacking mode for cofacial dimer of $Au(I)_3$ complexes $(\mathbf{2a})_2$. Adapted with permission from *Angew. Chem. Int. Ed.* **2013**, *52*, 6202–6205. Copyright (2013) John Wiley and Sons.

stacking mode of $Au(I)_3$ planes, see chapter 2).

Calculated transmission function from ab initio non-equilibrium Green's function calculation[27] with the density functional method in Atomistix Tool Kit (ATK)[28–30] showed high conductance region below Fermi level (Figure 12a). The calculated LDOS at 0.1 eV below the Fermi level clearly shows that the d-orbitals of trinuclear $Au(I)_3$ complexes **2a** (Figure 12b) and the π-orbitals of panel ligands **3** (Figure 12c) are well connected with the electrodes. In consequence, the main electron pathway is the three vertical chains composed of d orbitals of Au(I) ions. In contrast, the transmission above the Fermi level was relatively small. In fact, the electron pathway from the d-orbitals of the guest $Au(I)_3$ complex **2a** (Figure 12d) was not found although the π-orbitals of the ligands still serve the electron pathway (Figure 12e). The similar behavior of the transmission function was observed in [3 × 1] and [3 × 3] Au(I) ion clusters. Therefore, this high transmission region close to the Fermi level is essential to the high conductance in the molecular junctions.

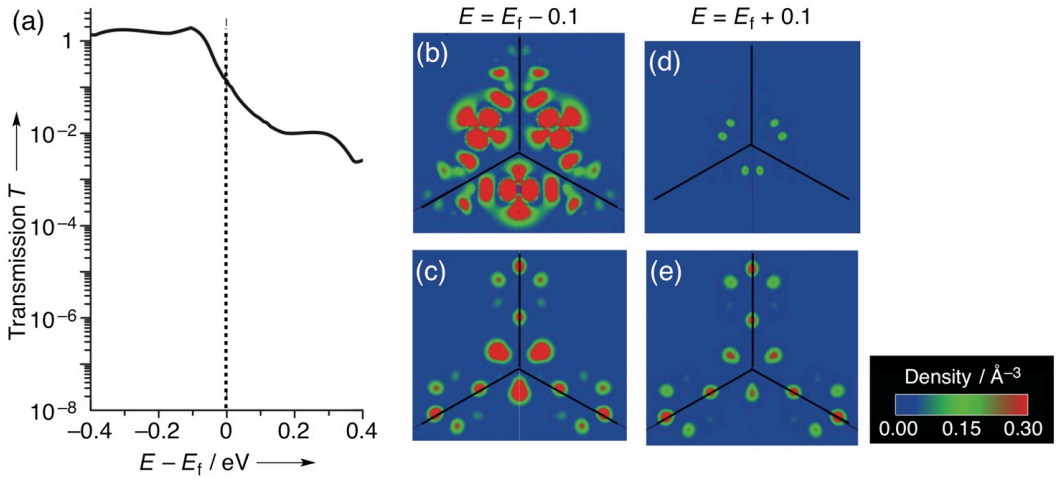

Figure 12. Calculated conductance of model Au_3–Au_3 cluster 3•2a•2a•3. (a) Calculated transmission function of model stacks **3•2a•2a•3** (**3**: panel ligands of cage **2a**). (b,c) The LDOS (local density of states) at 0.1 eV below the Fermi level on (b) $Au(I)_3$ complex **2a** plane and (c) panel ligand **3** plane. (d,e) The LDOS at 0.1 eV above the Fermi level on **2a** and **3** planes. Adapted with permission from *Angew. Chem. Int. Ed.* **2013**, *52*, 6202–6205. Copyright (2013) John Wiley and Sons.

5.5 Conclusion

In this chapter, we evaluated the electron transport through [3 × *n*] Au(I) clusters (*n* = 1–3) encapsulated within box-shaped coordination cages using the STM-BJ technique. The high conductance values (*G*) and the small attenuation factor (β) of the series of the Au(I) clusters represented a long-range electron transport ability of the Au(I) arrays. The wide range transmission function below the Fermi level and LDOS revealed that in the vertical direction, d-orbitals of trinuclear $Au(I)_3$ complexes and π-orbitals of the cage panels were well connected and formed three electron transport pathways.

5.6 References

[1] N. J. Tao, *Nature Nanotech.* **2006**, *1*, 173–181.

[2] F. Chen, J. Hihath, Z. Huang, X. Li, N. J. Tao, *Annu. Rev. Phys. Chem.* **2007**, *58*, 535–564.

[3] S. V. Aradhya, L. Venkataraman, *Nature Nanotech.* **2013**, *8*, 399–410.

[4] C. Joachim, J. K. Gimzewski, A. Aviram, *Nature*, **2000**, *408*, 541–548.

[5] J. He, F. Chen, P. A. Liddell, J. Andréasson, S. D. Straight, D. Gust, T. A. Moore, A. L. Moore, J. Li, O. F. Sankey, S. M. Linday, *Nanotechnology*, **2005**, *16*, 695–702.

[6] G. Sedghi, K. Sawada, L. J. Esdaile, M. Hoffmann, H. L. Anderson, D. Bethell, W. Haiss, S. J. Higgins, R. J. Nichols, *J. Am. Chem. Soc.* **2008**, *130*, 8582–8583.

[7] G. Sedghi, V. M. García-Suárez, L. J. Esdaile, H. L. Anderson, C. J. Lambert, S. Martín, D. Bethell, S. J. Higgins, M. Elliott, N. Bennett, J. E. Macdonald, R. J. Nichols, *Nature Nanotech.* **2011**, *6*, 517–523.

[8] G. Sedghi, L. J. Esdaile, H. L. Anderson, S. Martin, D. Bethell, S. J. Higgins, R. J. Nichols, *Adv. Mater.* **2012**, *24*, 653–657.

[9] B. Xu, N. J. Tao, *Science* **2003**, *301*, 1221–1223.

[10] X. Xiao, B. Xu, N. J. Tao, *Nano Lett.* **2004**, *4*, 267–271.

[11] X. Li, J. He, J. Hihath, B. Xu, S. M. Lindsay, N. Tao, *J. Am. Chem. Soc.* **2006**, *128*, 2135–2141.

[12] L. Venkataraman, J. E. Klare, I. W. Tam, C. Nuckolls, M. S. Hybertsen, M. L. Steigerwald, *Nano Lett.* **2006**, *6*, 458–462.

[13] J. He, F. Chen, J. Li, O. F. Sankey, Y. Terazono, C. Herrero, D. Gust, T. A. Moore, A. L. Moore, S. M. Lindsay, *J. Am. Chem. Soc.* **2005**, *127*, 1384–1385.

[14] S.-Y. Lin, I-W. P. Chen, C.-h. Chen, M.-H. Hsieh, C.-Y. Yeh, T.-W. Lin, Y.-H. Chen, S.-M. Peng, *J. Phys. Chem. B* **2004**, *108*, 959–964.

[15] I-W. P. Chen, M.-D. Fu, W.-H. Tseng, J.-Y. Yu, S.-H. Wu, C.-J. Ku, C.-h. Chen, S.-M. Peng, *Angew. Chem. Int. Ed.* **2006**, *45*, 5814–5818.

[16] T.-W. Tsai, Q.-R. Huang, S.-M. Peng, B.-Y. Jin, *J. Phys. Chem. C* **2010**, *114*, 3641–3644.

[17] T. Osuga, T. Murase, K. Ono, Y. Yamauchi, M. Fujita, *J. Am. Chem. Soc.* **2010**, *132*, 15553–15555.

[18] M. Kiguchi, T. Takahashi, Y. Takahashi, Y. Yamauchi, T. Murase, M. Fujita, T. Tada, S. Watanabe, *Angew. Chem. Int. Ed.* **2011**, *50*, 5708–5711.

[19] M. Kiguchi, S. Kaneko, *ChemPhysChem* **2012**, *13*, 1116–1126.

[20] Y. Yamauchi, M. Yoshizawa, M. Akita, M. Fujita, *Proc. Nat. Acad. Sci, U. S. A.* **2009**, *106*, 10435–10437.

[21] Y. Yamauchi, M. Yoshizawa, M. Akita, M. Fujita, *J. Am. Chem. Soc.* **2010**, *132*,

960–966.

[22] J. K. Klosterman, Y. Yamauchi, M. Fujita, *Chem. Soc. Rev.* **2009**, *38*, 1714–1725.

[23] M. Kiguchi, S. Kaneko, *Phys. Chem. Chem. Phys.* **2013**, *15*, 2253–2267.

[24] J. I. Pascual, J. Mendez, J. Gómez-Herrero, A. M. Baró, N. García, *Phys. Rev. Lett.* **1993**, *71*, 1852–1855.

[25] J. M. Krans, J. M. v. Ruitenbeek, V. V. Fisun, I. K. Yanson, L. J. d. Jongh, *Nature*, **1995**, *375*, 767–769.

[26] Gaussian 09, Revision C.01, M. J. Frisch, G. W. Trucks, H. B. Schlegel, G. E. Scuseria, M. A. Robb, J. R. Cheeseman, G. Scalmani, V. Barone, B. Mennucci, G. A. Petersson, H. Nakatsuji, M. Caricato, X. Li, H. P. Hratchian, A. F. Izmaylov, J. Bloino, G. Zheng, J. L. Sonnenberg, M. Hada, M. Ehara, K. Toyota, R. Fukuda, J. Hasegawa, M. Ishida, T. Nakajima, Y. Honda, O. Kitao, H. Nakai, T. Vreven, J. A. Montgomery, Jr., J. E. Peralta, F. Ogliaro, M. Bearpark, J. J. Heyd, E. Brothers, K. N. Kudin, V. N. Staroverov, T. Keith, R. Kobayashi, J. Normand, K. Raghavachari, A. Rendell, J. C. Burant, S. S. Iyengar, J. Tomasi, M. Cossi, N. Rega, J. M. Millam, M. Klene, J. E. Knox, J. B. Cross, V. Bakken, C. Adamo, J. Jaramillo, R. Gomperts, R. E. Stratmann, O. Yazyev, A. J. Austin, R. Cammi, C. Pomelli, J. W. Ochterski, R. L. Martin, K. Morokuma, V. G. Zakrzewski, G. A. Voth, P. Salvador, J. J. Dannenberg, S. Dapprich, A. D. Daniels, Ö. Farkas, J. B. Foresman, J. V. Ortiz, J. Cioslowski, D. J. Fox, Gaussian, Inc., Wallingford CT, 2010.

[27] S. Datta, *Electronic transport in mesoscopic systems*, Cambridge University Press, Cambridge**, 1995.**

[28] M. Brandbyge, J.-L. Mozos, P. Ordejón, J. Taylor, K. Stokbro, *Phys. Rev. B* **2002**, *65*, 165401 1–17.

[29] ATK Manual “ATK version 11.8.1”, QuantumWise A/S (http://www.quantumwise.com).

[30] J. P. Perdew, K. Burke, M. Ernzerhof, *Phys. Rev. Lett.* **1996**, *77*, 3865–3868.

Summary and Perspectives

In this thesis, the author focused on the precise synthesis of three-dimensional metal ion arrays by piling up multinuclear complexes with planar geometries. In chapter 2, Au(I) clusters were prepared in a [3 × *n*] (*n* = 1–3) fashion by encapsulation of trinuclear $Au(I)_3$ complexes within box-shaped cages. The shape and symmetry of the confined cavity precisely determined the number and array of Au(I) ions. X-ray crystallographic analysis of [3 × 3] Au(I) ion cluster revealed the trigonal prismatic array of Au(I) ions through attractive Au(I)–Au(I) interactions. In chapter 3, the Au(I) homo ion clusters were expanded to Au(I)–Ag(I) hetero ion clusters with Au(I)–Ag(I) metal-metal interactions. Interestingly, triple-decker Au(I)–Ag(I) cluster was only available with the cage. In chapter 4, a tray-shaped $Au(I)_3$ complex was prepared for a molecular scaffold to construct discrete stacks of planar complexes. The stacking number was precisely controlled by changing the assemble conditions without the help of the conventional cage. In chapter 5, single-molecular conductance measurement revealed that [3 × *n*] Au(I) clusters (*n* = 1–3) showed high conductivity and low attenuation factor. The trigonal prismatic alignment of Au(I) ions with intermolecular

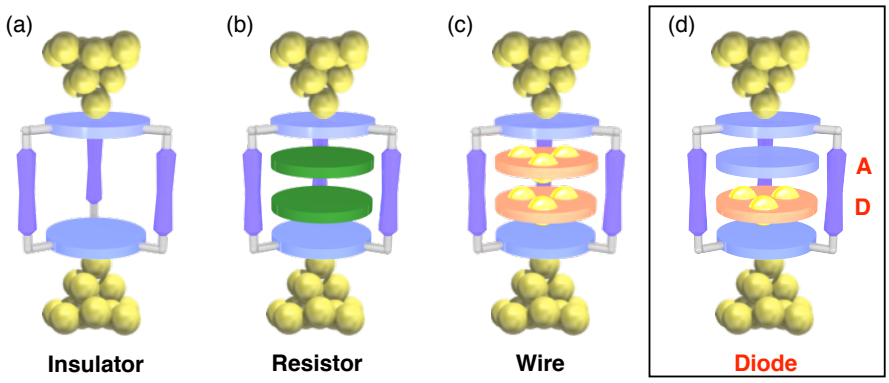

Figure 1. Family of molecular devices with the box-shaped cage. (a) Electron transport of the empty cage was not observed. (b) Discrete stacks of planar aromatics (pyrene-4,5-dione) showed a moderate conductance. (c) Large conductance and small attenuation factor were determined for [3 × *n*] Au(I) cluster in chapter 5. (d) A pairwise encapsulation of electrically donor (D) and acceptor (A) molecule will exhibit a rectification behavior of electron transport.

Au(I)–Au(I) interactions, and electron coupling between Au(I) clusters and also the cage panel contributed to the high efficiency for a long range electron transport.

The result in the last chapter suggested me that the self-assembled coordination cage is a suitable box-shaped container for the measuremet of single-molecular conductaice. This is because the cage has a small contact resistance (A_N) when it formed a molecular junction between the Au elctrodes. Moreover, potential candidates of guest molecules range a variety of planar molecules, from aromatic molecules to metal complexes with planar geometry. Consequently, I propose a new family of nanometer scale devices, a molecular diord (Figure 1).

A pairwise stacks of planar aromatic molecules was quantitatively achieved by using both electron-rich (donor, D) and poor (acceptor, A) guest molecules (*J. Am. Chem. Soc.* **2010**, *132*, 7864–7865). The different property of the two guests is important not only for selectively synthesize desired pairwise products but also for rectification behavior of the single molecule. A variety of molecular pair, for example, a pair of organic compound and metal complexes, and two different metal complex as well as a pair of two aromatic compounds will be posible (Figure 2). In consequence, the rectification behavior of the molecular diode can be tuned depending on a pair of the guest molecules.

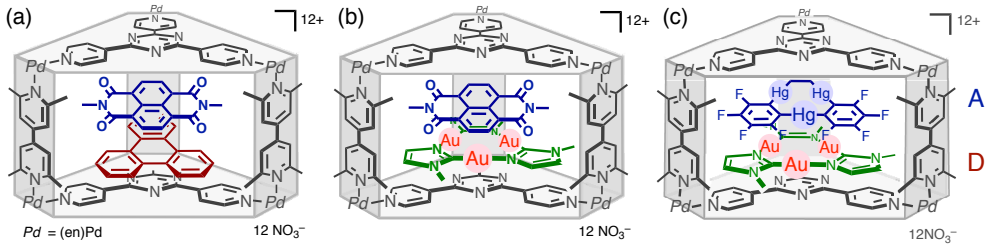

Figure 2. Pairwise accumulation of planar guests within a box-shaped cage. (a) The pair of aromatic molecules, triphenylene (D) and naphthalene diimide (A) was reported as mentioned above. (b) The pair of aromatics and metal complex. The author confirmed the quantitative formation of a pair of trinuclear $Au(I)_3$ complex (D) and naphthalene diimide (A). (c) The pair of different metal complexes would also be possible.

List of Publications

1. "[$m \times n$] Metal Ion Arrays Templated by Coordination Cages"
   Takafumi Osuga, Takashi Murase, Kosuke Ono, Yoshihiro Yamauchi,
   Makoto Fujita,
   Journal of the American Chemical Society **2010**, *132*, 15553–15555. [Chapter 2]

2. "Triple-Decker Au_3–Ag–Au_3–Ag–Au_3 Ion Cluster Enclosed in a Self-Assembled Cage"
   Takafumi Osuga, Takashi Murase, Makoto Fujita,
   Angewandte Chemie International Edition **2012**, *51*, 12199–12201. [Chapter 3]

3. "A Tray-Shaped, Pd^{II}-Clipped Au_3 Complex as a Scaffold for the Modular Assembly of [$3 \times n$] Au Ion Cluster"
   Takafumi Osuga, Takashi Murase, Manabu Hoshino, Makoto Fujita,
   Angewandte Chemie International Edition **2014**, *53*, 11186–11189. [Chapter 4]

4. "Highly Conductive [$3 \times n$] Gold-Ion Clusters Enclosed within Self-Assembled Cages"
   Manabu Kiguchi, Junichi Inatomi, Yuuta Takahashi, Ryota Tanaka, Takafumi Osuga, Takashi Murase, Makoto Fujita, Tomofumi Tada, Satoshi Watanabe,
   Angewandte Chemie International Edition **2013**, *52*, 6202–6205. [Chapter 5]

5. "Versatile Electron-Transport Properties of Single-Molecule Aromatic Stacks Inserted into a Self-Assembled Cage"
   Shintaro Fujii, Yuki Komoto, Manabu Kiguchi, Takafumi Osuga,
   Takashi Murase, Makoto Fujita, Tomofumi Tada,
   Submitted. [Chapter 5]

Acknowledgements

I would like to begin by thanking Professor Makoto Fujita at the Department of Applied Chemistry, School of Engineering, the University of Tokyo, for his extensive guidance and fruitful discussions throughout this work. Under his direction, the research work presented in this thesis was carried out during April 2009 to March 2015. He also provided me plenty of opportunities to develop my projects and to meet with many chemists. I am also immensely grateful to Associate Professor Takashi Murase (Yamagata University) for his direction, considerable encouragement and continuous support throughout my research life.

I wish to express my sincere gratitude to Professor Kazuyuki Ishii, Associate Professor Kazuma Mawatari, Associate Professor Michito Yoshizawa, and Lecturer Yasuhide Inokuma, for their helpful advice and suggestions for the improvement of this thesis.

Concerning the electron transport study in chapter 5, I am deeply appreciative of the support I have received form Professor Manabu Kiguchi and coworkers, and Associate Professor Tomofumi Tada. Their scientific help made my research more attractive.

I am grateful to the staffs in the Fujita laboratory: Associate Professor Sota Sato (Tohoku University), Lecturer Yasuhide Inokuma, Assistant Professor Tomohisa Sawada, and Assistant Professor Daishi Fujita, for their scientific advice and encouragement. I am also thankful to Ms. Yukari Ara, Ms. Miki Yoshioka, Ms. Ayano Oishi, and Ms. Noriko Yamaguchi for their various help and kindness.

I am greatly indebted to Assistant Professor Kosuke Ono (Tokyo Institute of Technology) for his direction on our chemistry, experiments, and presentation skills. I also really appreciate Dr. Yoshihiro Yamauchi, Dr. Sinnosuke Horiuchi, Mr. Kosuke Otsuka, and Mr. Hayato Tsutsumi for their advice on laboratory life and technical skills concerning self-assembled cages.

I am thankful to Assistant Professor Jeremy Klosterman (Bowling Green State University), Dr. Javier Martí-Rujas, Dr. Kate Harris, Dr. Manabu Hoshino, Dr. Bunnai Saito, Mr. Naoki Okahata, Dr. Jyunji Iwasa, Assistant Professor Yoshihiro Ueda (Kyoto University), Dr. Yuh Kohyama, Assistant Professor Koki Ikemoto (Tohoku University), Dr. Fang Yu, Dr. Ning Guo-Hong, Dr. Vincent Duplan, Dr. Nicolas Zigon, Dr. Bernd Schmidt, Dr. Yuya Domoto, Dr. Rajorshi Das, Mr. Stephane Peschard, Mr. Tatsuhiko Arai, Mr. Hiroki Takezawa, Mr. Shota Yoshioka, Mr. Satoshi Nishiguchi, Ms. Asana Takahashi, Mr. Shitao Wang, Mr. Ryota Tanaka, Ms. Yumi Miyamoto, Ms. Eri Numata, Mr. Yutaka Yoshimasa, Ms. Mayu Yamada, Mr. Yusuke Otsubo, Mr. Shuhei Kamiya, Mr. Kazuyuki Mori, Mr. Hiroyuki Yokoyama, Mr. Shouta Akiba and other members of Fujita's research group for their fruitful suggestions and helpful advice.

I thank to the financial support from Research Fellowship for Young Scientist of Japan Society for the Promotion of Science (JSPS).

Finally, I would like to express my deep appreciation to my family for their consistent assistant and encouragement throughout my research life.

Takafumi Osuga

March 2015